

---

Electronic Thesis and Dissertation Repository

---

4-22-2013 12:00 AM

# An Investigation of Subaxial Cervical Spine Trauma and Surgical Treatment through Biomechanical Simulation and Kinematic Analysis

Stewart D. McLachlin  
*The University of Western Ontario*

Supervisor  
Dr. Cynthia Dunning  
*The University of Western Ontario*

Graduate Program in Mechanical and Materials Engineering  
A thesis submitted in partial fulfillment of the requirements for the degree in Doctor of Philosophy  
© Stewart D. McLachlin 2013

Follow this and additional works at: <https://ir.lib.uwo.ca/etd>



Part of the [Biomechanical Engineering Commons](#), and the [Biomedical Devices and Instrumentation Commons](#)

---

## Recommended Citation

McLachlin, Stewart D., "An Investigation of Subaxial Cervical Spine Trauma and Surgical Treatment through Biomechanical Simulation and Kinematic Analysis" (2013). *Electronic Thesis and Dissertation Repository*. 1216.  
<https://ir.lib.uwo.ca/etd/1216>

This Dissertation/Thesis is brought to you for free and open access by Scholarship@Western. It has been accepted for inclusion in Electronic Thesis and Dissertation Repository by an authorized administrator of Scholarship@Western. For more information, please contact [wlsadmin@uwo.ca](mailto:wlsadmin@uwo.ca).

# AN INVESTIGATION OF SUBAXIAL CERVICAL SPINE TRAUMA AND SURGICAL TREATMENT THROUGH BIOMECHANICAL SIMULATION AND KINEMATIC ANALYSIS

(Thesis format: Integrated Article)

by

Stewart D. McLachlin

Department of Mechanical & Materials Engineering  
Graduate Program in Engineering Science

A thesis submitted in partial fulfillment  
of the requirements for the degree of  
Doctor of Philosophy

The School of Graduate and Postdoctoral Studies  
The University of Western Ontario  
London, Ontario, Canada

© Stewart D. McLachlin 2013

## ABSTRACT

*In vitro* biomechanical investigations can help to identify changes in subaxial cervical spine (C3-C7) stability following injury, and determine the efficacy of surgical treatments through controlled joint simulation experiments and kinematic analyses. However, with the large spectrum of cervical spine trauma, a large fraction of the potential injuries have not been examined biomechanically. This includes a lack of studies investigating prevalent flexion-distraction injuries. Therefore, the overall objective of this thesis was to investigate the changes in subaxial cervical spine kinematic stability with simulated flexion-distraction injuries and current surgical instrumentation approaches using both established and novel biomechanical techniques.

Three *in vitro* experiments were performed with a custom-designed spinal loading simulator. The first evaluated sequential disruption of the posterior ligaments with and without a simulated facet fracture (n=7). In these specimens, posterior lateral mass screw fixation provided more stability than anterior cervical discectomy and fusion with plating (ACDFP). A second study examined a unilateral facet perch injury by reproducing a flexion-distraction injury mechanism with the simulator (n=9). The resulting soft tissue damage was quantified through meticulous dissection of each specimen, which identified the most commonly injured structures across all specimens as both facet capsules,  $\frac{3}{4}$  of the annulus, and  $\frac{1}{2}$  of the ligamentum flavum. This information was used to develop and validate a standardized injury model (SIM) in new specimens (n=10). A final study examined the ACDFP surgical factor of graft size height (bony spacer replacing the intervertebral disc to promote fusion) for the SIM and two other injuries (n=7). Results were motion and injury dependent, which suggests that both these factors must be considered in the surgical decision.

Two additional investigations were completed. The first examined mathematical techniques to generate a large number of accurate finite helical axes from six-DOF rigid body tracker output to describe changes in cervical spine kinematic stability. The second explored the effect of boundary conditions and PID control settings on the ability of the current simulator design to reproduce desired loading techniques.

Ultimately, it is hoped that these results, and the protocols developed for future investigations, will provide valuable biomechanical evidence for standardized treatment algorithms.

**Keywords:** Cervical spine; facet joint; soft tissue injury; spinal instrumentation; biomechanics; kinematics; spinal loading simulator; finite helical axis; loading efficiency.



## CO-AUTHORSHIP STATEMENT

The *in vitro* experiments performed in this thesis required a multi-disciplinary approach with both engineering and surgical personnel. The individual contributions are listed below:

- Chapter 1:     Stewart McLachlin – sole author
- Chapter 2:     Stewart McLachlin – study design, data collection, data analysis, wrote manuscript; Parham Rasoulinejad – study design, performed surgeries, data collection; Christopher Bailey – study design, reviewed manuscript; Cynthia Dunning – study design, reviewed manuscript.
- Chapter 3:     Stewart McLachlin – study design, data collection, data analysis, wrote manuscript; Melissa Nadeau – study design, performed surgeries, data collection; Christopher Bailey – study design, reviewed manuscript; Cynthia Dunning – study design, reviewed manuscript.
- Chapter 4:     Stewart McLachlin – study design, data collection, data analysis, wrote manuscript; Louis Ferreira – study design, reviewed manuscript; Cynthia Dunning – study design, reviewed manuscript.
- Chapter 5:     Stewart McLachlin – study design, data collection, data analysis, wrote manuscript; Reina Yao – study design, performed surgeries, data collection; Christopher Bailey – study design, reviewed manuscript; Cynthia Dunning – study design, reviewed manuscript.
- Chapter 6:     Stewart McLachlin – study design, data collection, data analysis, wrote manuscript; Cynthia Dunning – study design, reviewed manuscript.
- Chapter 7:     Stewart McLachlin – sole author

## ACKNOWLEDGMENTS

My sincerest thanks must first go to the person who took a chance on a slightly above-average undergraduate engineering student almost seven years ago: Dr. Cynthia Dunning. Dr. Dunning has been nothing short of a remarkable supervisor and mentor throughout my graduate studies. Her ability to provide guidance, encourage leadership, add structure to incoherent ideas, and stay positive through adversity are only a small number of her many amazing mentorship capabilities that I hope to carry on in my future career.

A second massive thank you is required for my orthopaedic surgery colleagues, without whom, this multi-disciplinary effort could not have worked. Dr. Chris Bailey's dedication to these studies as a surgical mentor, in addition to his already heavy clinical workload, always provided me with reinforcement that the research had relevance to his practice. I also need to thank the surgical residents who were critical to the success of this work. Drs. Parham Rasoulinejad, Melissa Nadeau, Max McCabe, and Reina Yao – your tireless work ethic in the lab was remarkable.

To my labmates in the BTL, both past and present, thanks for making every day in the lab such a fun and positive place to work throughout the years. It has always felt like a “team effort” in the BTL and it starts by working with a bunch of kind, thoughtful, and mainly brilliant people. I also need to specifically thank Drs. Tim Burkhart, Emily Lalone, Ryan Willing, and Louis Ferreira for their assistance over the past year to help wrap up my PhD research and with answering the difficult question of “How do you finish a PhD?”

It goes without saying that I could not have accomplished this feat without the continued support of my family and friends. Thanks to you all (even if you never read this)!

A final thank you goes to the Natural Sciences and Engineering Research Council of Canada and the Joint Motion Program – A CIHR training program in Musculoskeletal Health Research and Leadership for providing me with financial support to complete this work.

## DEDICATION

*To Marion Copley and Dr. John McLachlin, who instilled  
in me the benefits of life-long learning.*

# TABLE OF CONTENTS

Abstract.....	ii
Co-Authorship Statement .....	iv
Acknowledgments .....	v
Dedication.....	vi
Table of Contents.....	vii
List of Tables .....	xii
List of Figures.....	xiv
Abbreviations, Symbols, and Nomenclature .....	xvii
<b>Chapter 1: Introduction.....</b>	<b>1</b>
1.1 Cervical Spine Anatomy and Mobility .....	1
1.1.1 Osteology .....	2
1.1.2 Soft Tissues .....	6
1.1.3 Cervical Spine Mobility .....	8
1.1.4 Cervical Spine Stability .....	11
1.1.5 Effect of Age on Mobility.....	12
1.2 Cervical Spine Trauma and Surgical Treatment.....	12
1.2.1 Classification of Subaxial Traumatic Injuries.....	13
1.2.2 Surgical Treatment Options .....	16
1.3 <i>In Vitro</i> Biomechanics of the Cervical Spine .....	23
1.3.1 Simulating Spine Motions.....	23
1.3.2 Spinal Stability Measures .....	25
1.3.3 Simulating Traumatic Injury Mechanisms.....	30
1.3.4 Biomechanics of Surgical Fixation.....	31
1.4 Analysis and Interpretation of Cervical Spine Kinematics.....	32
1.4.1 Motion Tracking and Registration .....	32

1.4.2	Spatial Descriptions and Transformation Matrices.....	33
1.4.3	Vertebral Orientation and Euler Angles .....	35
1.4.4	Vertebral Axis of Rotation and the Finite Helical Axis.....	37
1.4.5	Visualization Methods .....	39
1.5	Thesis Rationale.....	39
1.6	Objectives and Hypotheses .....	40
1.7	Thesis Overview .....	42
1.8	References.....	42
<b>Chapter 2: The Kinematic Stability of Stage 1 Flexion-Distractive Injuries of the Cervical Spine Before and After Instrumented Fixation .....</b>		<b>51</b>
2.1	Introduction.....	51
2.2	Materials and Methods.....	53
2.3	Results.....	61
2.3.1	Overall Intact and Injured Kinematics (C2-C5).....	61
2.3.2	Segmental Intact and Injured Kinematics .....	64
2.3.3	Instrumented Kinematics .....	68
2.4	Discussion.....	68
2.5	Summary & Future Directions.....	73
2.6	References.....	73
<b>Chapter 3: In Vitro Simulation and Standardization of the Soft Tissue Damage Sustained in the Cervical Spine Following a Unilateral Facet Perch Injury.....</b>		<b>77</b>
3.1	Introduction.....	77
3.2	Materials and Methods.....	79
3.2.1	General Experimental Setup .....	79
3.2.2	Study 1 – Unilateral Facet Perch Creation.....	82
3.2.3	Study 2 – Standardized Injury Model .....	86
3.2.4	Study 1 & 2 Data Analysis.....	86

3.2.5 Preliminary SIM Usage.....	87
3.3 Results.....	87
3.3.1 Study 1 - Unilateral Facet Perch Creation .....	87
3.3.2 Study 2 – Standardized Injury Model .....	88
3.3.3 Preliminary SIM usage .....	95
3.4 Discussion .....	95
3.5 Summary & Future Directions.....	100
3.6 References.....	101
<b>Chapter 4: A Refined Technique to Calculate Helical Axes from Six-DOF Tracker Output with an Application in Spinal Kinematics.....</b>	<b>104</b>
4.1 Introduction.....	104
4.2 Materials and Methods.....	106
4.2.1 Mathematical Concepts.....	106
4.2.2 Experimental Data Collection.....	107
4.2.3 Jig Data Analysis .....	107
4.2.4 Spine Data Analysis .....	109
4.3 Results.....	110
4.3.1 Jig Results .....	110
4.3.2 Spine Results.....	110
4.4 Discussion .....	113
4.5 Summary & Future Directions.....	122
4.6 References.....	122
<b>Chapter 5: Influence of Graft Size on the Kinematic Stability of Anterior Cervical Plating Following In Vitro Flexion-Distracton Injuries.....</b>	<b>125</b>
5.1 Introduction.....	125
5.2 Materials and Methods.....	126
5.3 Results.....	132

5.4 Discussion .....	134
5.5 Summary & Future Directions .....	146
5.6 References .....	147
<b>Chapter 6: The Effect of Fixed versus Semi-Constrained End Conditions on Bending Moment Efficiency in the Current Spinal Loading Simulator .....</b>	<b>149</b>
6.1 Introduction .....	149
6.2 Materials and Methods .....	151
6.2.1 Current Design Testing .....	151
6.2.2 Modified Design Testing .....	152
6.3 Results .....	154
6.3.1 Current Design Testing .....	154
6.3.2 Modified Design Testing .....	158
6.4 Discussion .....	158
6.5 Summary .....	166
6.6 References .....	166
<b>Chapter 7: Conclusions .....</b>	<b>169</b>
7.1 Summary .....	169
7.2 Strengths and Limitations .....	172
7.3 Future Directions .....	173
7.4 Significance .....	175
7.5 References .....	175
<b>Appendix A – Glossary .....</b>	<b>177</b>
<b>Appendix B – Experimental Testing Protocol .....</b>	<b>182</b>
<b>Appendix C – LabVIEW VIs for Post-hoc Data Analysis .....</b>	<b>190</b>
C.1 Overview of Master Program .....	190
C.2 Screw Matrix Moving Window Analysis and FHA Parameter Extraction VIs ..	192

<b>Appendix D – Specimen Demographics &amp; Tabulated Data.....</b>	<b>195</b>
<b>Appendix E – MATLAB Code for Alpha Shapes .....</b>	<b>203</b>
E.1 Background on Alpha Shapes .....	203
E.2 MATLAB Code for Generating Multiple Alpha Shapes Based on FHA Intercept Data Sets .....	203
<b>Appendix F – Protocol for Creating 3D Bone Models.....</b>	<b>207</b>
<b>Appendix G – Biaxial Bearing Stage Development .....</b>	<b>210</b>
G.1 Project Summary.....	210
G.2 Concept Generation: Linear Bearing Systems .....	210
G.3 Bearing Stage Components.....	212
<b>Appendix H – Copyright Permission .....</b>	<b>214</b>
H.1 Chapter 2 – Copyright Release .....	214
H.2 Chapter 3 – Copyright Release .....	219
<b>Curriculum Vitae.....</b>	<b>220</b>



## LIST OF TABLES

Table 2.1: Average ( $\pm$ SD) C2-C5 ROM ( $^{\circ}$ ) for Each Simulated Motion .....	62
Table 2.2: Average ( $\pm$ SD) C2-C5 NZ ( $^{\circ}$ ) for Each Simulated Motion .....	62
Table 3.1: Specimen Demographics & Facet Perch Results.....	89
Table 3.2: Extent of Soft Tissue Injury Data for All Specimens (n = 9) .....	89
Table 3.3: Average ROM ( $\pm$ SD) Values Pre- and Post-UFP injury (n=9) .....	90
Table 3.4: Average NZ ( $\pm$ SD) Values Pre- and Post-UFP injury (n=9) .....	90
Table 3.5: Percent Change in ROM with Facet Fracture and Instrumentation (n=4) .....	96
Table 4.1: Window Size Effect on X-Y Intercept Standard Deviations .....	111
Table 4.2: Window Size Effect on Average X-Y Intercept and the Direction Cosines.....	111
Table 4.3: Window Size Effect on the FHAs Generated in Intact Spine Data .....	112
Table 4.4: Window Size Effect on the Average FHA Intercepts and Direction Cosines in Intact Spine Data.....	112
Table 5.1: Average ( $\pm$ SD) C5-C6 ROM for the Intact and SIM States .....	133
Table 5.2: Alpha Shape Area for the Intact and SIM States .....	135
Table 5.3: Planar Location of the Average Centroid of the Alpha Shapes .....	135
Table 6.1: Bending Moment Efficiency of Chapter 5 Load Data.....	157
Table 6.2: Caudal Forces Measured in Chapter 5 Load Data .....	159
Table 6.3: Caudal Forces Measured in the Modified Simulator Setup .....	159
Table 6.4: Bending Moment Efficiency in the Modified Simulator Setup.....	161
Table D.1: Specimen Demographics .....	195
Table D.2: Chapter 2 Specimens C3-C4 Range of Motion .....	196
Table D.3: Chapter 2 Specimens C2-C3 Range of Motion .....	197
Table D.4: Chapter 2 Specimens C4-C5 Range of Motion .....	198
Table D.5: Chapter 2 Specimens C2-C5 Neutral Zone.....	199

Table D.6: Chapter 3 – Study 1 Specimens Range of Motion and Neutral Zone.....	200
Table D.7: Chapter 3 – Study 2 Specimens Range of Motion and Neutral Zone.....	201
Table D.8: Chapter 5 Specimens Range of Motion .....	202

## LIST OF FIGURES

Figure 1.1: Subaxial Cervical Vertebrae.....	3
Figure 1.2: Osteology of the Subaxial Cervical Vertebrae .....	4
Figure 1.3: Articulating Joints of the Cervical Spine .....	5
Figure 1.4: Intervertebral Disc in the Cervical Spine .....	7
Figure 1.5: Ligaments of the Cervical Spine .....	9
Figure 1.6: Spine Motions.....	10
Figure 1.7: Cervical Facet Joint Injuries.....	14
Figure 1.8: X-rays of Cervical Instrumentation .....	17
Figure 1.9: Anterior Approach for Spinal Fusion.....	19
Figure 1.10: Posterior Approach for Spinal Fusion.....	21
Figure 1.11: Custom Instron 8874 Materials Testing Machine .....	26
Figure 1.12: Components for UWO Spinal Loading Simulator .....	27
Figure 1.13: UWO Spinal Loading Simulator .....	28
Figure 1.14: Kinematic Stability Measures .....	29
Figure 1.15: Euler Angle Sequence .....	36
Figure 1.16: Finite Helical Axis.....	38
Figure 2.1: Simulator and Tracker Setup for Multi-segment Cervical Spine.....	54
Figure 2.2: Optotrak® Certus and Smart Marker .....	56
Figure 2.3: Simulated Facet Fracture.....	58
Figure 2.4: Posterior and Anterior Instrumentation.....	59
Figure 2.5: Hysteresis Curve for Overall and Segmental Kinematics .....	60
Figure 2.6: Neutral Zone for Simulated Motions with Posterior Injury Progression .....	63
Figure 2.7: C3-C4 Flexion-Extension ROM with Posterior Injury Progression .....	65
Figure 2.8: C3-C4 Axial Rotation ROM with Posterior Injury Progression .....	66

Figure 2.9: C3-C4 Lateral Bend ROM with Posterior Injury Progression .....	67
Figure 2.10: Percent Decrease in C3-C4 ROM with Instrumentation .....	69
Figure 3.1: Potting Screw Insertion .....	80
Figure 3.2: Simulator and Tracker Setup for Single Motion Segment .....	81
Figure 3.3: Simulator Modification to Induce a Unilateral Facet Perch.....	83
Figure 3.4: Identification of Instance of Perch .....	84
Figure 3.5: Tables for Recording Specimen Disruption .....	85
Figure 3.6: Changes in Kinematic Stability of Axial Rotation.....	92
Figure 3.7: Changes in Kinematic Stability of Flexion-Extension.....	93
Figure 3.8: Changes in Kinematic Stability of Lateral Bending.....	94
Figure 4.1: Experimental Tracker Setup on Custom Jig.....	108
Figure 4.2: Quantifying the Axial Rotation FHA Intercepts .....	114
Figure 4.3: Quantifying the Flexion-Extension FHA Intercepts .....	115
Figure 4.4: Quantifying the Lateral Bending FHA Intercepts .....	116
Figure 4.5: 3D FHAs for Intact Axial Rotation .....	117
Figure 4.6: 3D FHAs for Intact Flexion-Extension .....	118
Figure 4.7: 3D FHAs for Intact Lateral Bending.....	119
Figure 5.1: Modifications to Spinal Loading Simulator Setup.....	127
Figure 5.2: Flexibility Testing Stages Flowchart.....	129
Figure 5.3: ACDFP Grafts and Plates.....	130
Figure 5.4: Flexion-Extension Alpha Shapes of FHA Intercepts with Sagittal Plane .....	136
Figure 5.5: Axial Rotation Alpha Shapes of FHA Intercepts with Transverse Plane.....	137
Figure 5.6: Lateral Bending Alpha Shapes of FHA Intercepts with Frontal Plane .....	138
Figure 5.7: Flexion-Extension ROM as a Result of Injury and Graft Size.....	139
Figure 5.8: Axial Rotation ROM as a Result of Injury and Graft Size.....	140
Figure 5.9: Lateral Bending ROM as a Result of Injury and Graft Size .....	141

Figure 5.10: Effect of Disc Space Height on the Uncovertebral Joint.....	143
Figure 6.1: Bending Moment Efficiency .....	153
Figure 6.2: Biaxial Bearing System .....	155
Figure 6.3: Testing of a C4-C5 with Biaxial Bearing System .....	156
Figure 6.4: Caudal Forces & Applied Moment during the Final Loading Cycle .....	160
Figure 6.5: Location of Applied and Caudal Bending Moments .....	163
Figure 6.6: Load Instability in PID Loop Tuning .....	165
Figure B.1: Four-point Potting Alignment Jig .....	184
Figure B.2: Instron WaveMatrix Flexibility Test Method .....	186
Figure B.3: Instron® Actuator Settings .....	187
Figure B.4: NDI First Principles™ Software .....	189
Figure C.1: Back Panel of Master VI for Kinematic Stability.....	191
Figure C.2: Screw Matrix Moving Window Analysis VI.....	193
Figure C.3: MathScript for FHA Parameter Extraction from Screw Matrix .....	194
Figure F.1: Image Segmentation Steps to Isolate Individual Vertebra.....	208
Figure G.1: Guide Blocks and Rails Design Concept.....	211
Figure G.2: Linear Bearing and Shaft Design Concept .....	211

## **ABBREVIATIONS, SYMBOLS, AND NOMENCLATURE**

[P] – position vector  
[R] – rotation matrix  
[S] – screw matrix  
[T] – transformation matrix  
2D – two-dimensional  
3D – three-dimensional  
ACDFP – anterior cervical discectomy and fusion with plating  
A – anterior  
ALL – anterior longitudinal ligament  
AR – axial rotation  
BFD – bilateral facet dislocation  
C1-C7 – first to seventh cervical vertebrae  
Co – contralateral;  
CT – computed tomography  
DOF – degree-of-freedom  
FC – facet capsule  
FE – flexion-extension  
FHA – finite helical axis  
Hz – hertz (unit of frequency)  
I – inferior  
Ip - ipsilateral  
IS - interspinous  
IVD – intervertebral disc  
L – lateral  
LB – lateral bending  
M – medial  
MRI – magnetic resonance imaging  
N – newton (unit of force)  
Nm – newton meter (unit of torsional loading)  
NP – neutral position  
NZ – neutral zone  
OA – osteoarthritis

P – posterior  
 PID – proportion, integral, derivative  
 PLL – posterior longitudinal ligament  
 PLC – posterior ligament complex  
 PMMA - polymethylmethacrylate  
 PVC – polyvinyl chloride  
 rmANOVA – repeated measures analysis of variance  
 ROM – range of motion  
 S – superior  
 s – second (unit of time)  
 SD – standard deviation  
 SS – supraspinous  
 SDA – screw displacement axis  
 SIM – standardized injury model  
 SLIC – Subaxial Injury Classification  
 SNK – Student-Newman-Keuls  
 UFP – unilateral facet perch  
 UF# – unilateral facet fracture  
 ° – degrees  
 $\alpha$  – significance level  
 $\Phi$  – rotation angle about FHA  
 $n$  – FHA direction cosine vector  
 $t$  – translation along FHA  
 $p$  – planar intercept of FHA

## CHAPTER 1: INTRODUCTION

**OVERVIEW:** *This chapter introduces the basic principles of cervical spine biomechanics, beginning with a synopsis of the anatomy and mobility of the subaxial cervical spine. This is followed by a review of common cervical spine trauma. Surgical treatment options for flexion-distraction injuries are explained, along with the current surgical treatment algorithms that are used to direct clinical treatment. A detailed review of the simulation tools and techniques used in laboratory biomechanical investigations of the spine is provided, including an examination of the kinematic approaches that can describe spinal mobility. This chapter concludes with the study rationale and the overall objectives and hypotheses of this body of work.<sup>1</sup>*

### 1.1 CERVICAL SPINE ANATOMY AND MOBILITY

The cervical spine composes the musculoskeletal anatomy within the human neck. It serves three critical functions: 1) to allow motion of the head and neck through complex neuromuscular control; 2) to support the weight and act as a shock absorber for the skull and brain; and 3) to provide protection for the important neurovascular structures including the spinal cord and vertebral artery that run through it (White and Panjabi, 1990).<sup>2</sup> These functions are accomplished via the osseous and soft tissues structures that both stabilize and produce mobility of the cervical spine.

---

<sup>1</sup> Specialized terminology found throughout this thesis is defined in Appendix A

<sup>2</sup> The classic textbook by White and Panjabi on the “*Clinical Biomechanics of the Spine*” explains in great detail the anatomical information presented here and is an invaluable reference for this area of research (White and Panjabi, 1990).



### **1.1.1 OSTEOLOGY**

The osseous structures of the cervical spine are small, irregularly shaped bones known as vertebrae. Of the 24 articulating vertebrae in the human spine, the seven cervical vertebrae (C1-C7) are smallest, yet may be the most diverse from an osteology standpoint (White and Panjabi, 1990) (Figure 1.1). Starting with C1 at the cranial end, the cervical spine articulates with the base of the skull (occiput). Inferiorly, it ends at C7, where it connects to the thoracic vertebrae at the base of the neck. All cervical vertebrae consist of similar components to other bones of the body; a hard, compact outer shell of cortical bone surrounding a lighter, spongy cancellous (or trabecular) bone.

#### **1.1.1.1 SUBAXIAL VERTEBRAE**

Excluding the unique anatomy of the Atlas (C1) and Axis (C2), the vertebrae of the lower, or subaxial, cervical spine (C3-C7) consist of similar geometrical osseous features. Each of these vertebrae contain a vertebral body, along with two pedicles, lateral masses, laminae, and a single spinous process (Figure 1.2). The vertebral body is a large, cylindrical mass making up the anterior half of each vertebra. There are defined curved ridges at the lateral edges (uncinate processes or the uncovertebral joint) from an anterior perspective (Figure 1.3). Extending laterally from the vertebral body are the transverse processes, which surround the transverse foramen within which runs the vertebral artery. The pedicles in the cervical spine are short regions of bone that connect the body to the lateral masses. The latter are large pillars of bone that are referenced in halves as either the superior or inferior articular processes. Extending posteriorly from the masses are the thin sections of bone known as the laminae, which meet in the midline to form the spinous process. The hollow triangular section formed by this bony geometry is referred to as the vertebral foramen, which envelopes the spinal cord.

#### **1.1.1.2 FACET JOINTS**

Of significant interest to this thesis are the bony facet joints, which are more formally known as zygapophyseal joints. These diarthrodial (*i.e.*, flat) synovial joints,

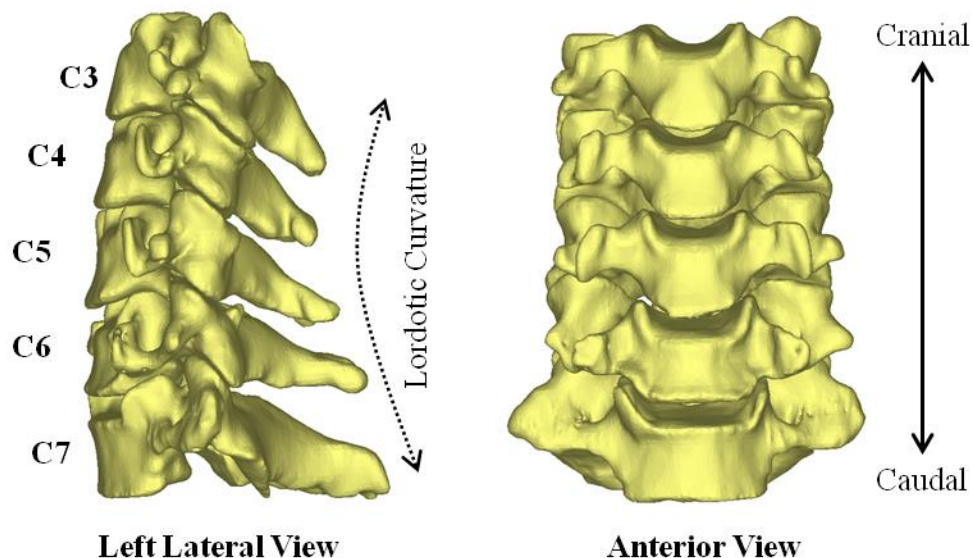


**Figure 1.1: Subaxial Cervical Vertebrae**

The subaxial region of the cervical spine consists of the third (C3) to the seventh (C7) vertebrae. The lateral view (left) shows the lordotic curvature of the cervical spine. The anterior view (right) illustrates the normal joint spacing between the endplates of each vertebral body, which contains the intervertebral disc (not shown). In referring to adjacent vertebrae, the one above would be the “cranial” vertebra, and the one below the “caudal” vertebra.

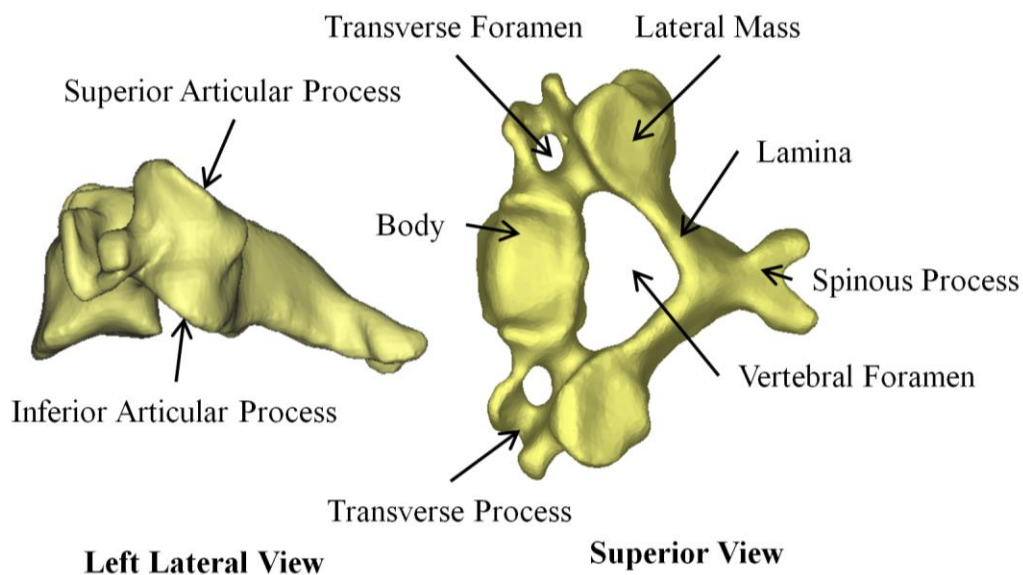


**Figure 1.2: Osteology of the Subaxial Cervical Vertebrae**

Each of the subaxial cervical vertebrae display similar anatomical features. The body is the large cylindrical mass in the anterior region. There are seven processes (*i.e.*, bony protrusions) – two transverse, two superior articular, two inferior articular, and a single spinous process. The superior and inferior articular processes form the lateral masses. These lateral masses connect to the spinous process by the laminae. The foramen protect vitally important structures – the spinal cord with the vertebral foramen and the vertebral artery with the transverse foramen.

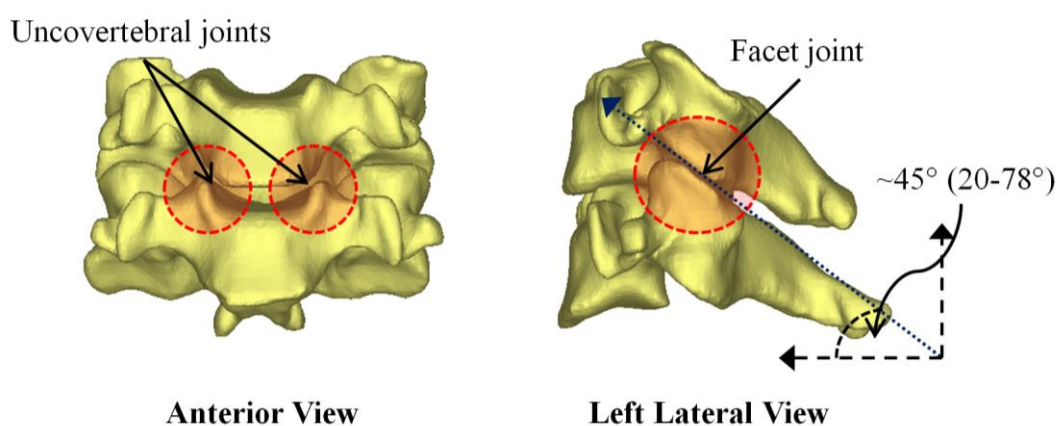


**Figure 1.3: Articulating Joints of the Cervical Spine**

The uncovertebral joints are formed by the curved uncinate processes on the superior surface of the vertebral body. The facet joint is formed by the inferior and superior articular processes of adjacent vertebrae, and angled at approximately  $45^\circ$  in the sagittal plane (range  $20-78^\circ$ ) (Panjabi *et al.*, 1993). The angled facet joint plays a critical role in guiding cervical spine motion, absorbing compressive loads, and limiting anterior translation of the vertebra, protecting the intervertebral disc (Pal and Sherk, 1988).

running bilaterally along the entire spine, are formed by the articulation of the inferior and superior articular processes of adjacent cranial and caudal vertebrae, respectively (Figure 1.3). Each vertebra therefore forms a pair of facet joints with the vertebra above and below it. The elliptical-shaped faces of the adjacent articular processes, along with the synovial fluid and cartilage (about 1mm in height at its maximum point), work together to provide a low-friction sliding type joint. In the subaxial cervical spine, this joint is angled at approximately  $45^{\circ}$  in the sagittal plane, but can range anywhere from  $20-78^{\circ}$  (Figure 1.3) (Pal *et al.*, 2001; Panjabi *et al.*, 1993; White and Panjabi, 1990). This angulation of the facet joint allows it to carry a significant portion of the compressive load on the cervical spine (approximately 30%), along with playing a crucial role in guiding spinal mobility (Pal and Sherk, 1988). Furthermore, the angulation of the facet joint helps to prevent shear or rotational loading damage to the intervertebral disc (see Section 1.1.2) (White and Panjabi, 1990). In addition to their load bearing role, the cervical facet joints play a critical function in regulating the overall health of the cervical spine through mechanotransduction (*i.e.*, cellular response to mechanical loading), which was recently detailed in a thorough review by Jaumard *et al.* (Jaumard *et al.*, 2011).

### 1.1.2 SOFT TISSUES

The soft tissue structures of the cervical spine are critical for the described musculoskeletal functions. Between adjacent vertebral bodies lies the intervertebral disc (IVD). The structure of each IVD is split into two key components: the annulus fibrosus and the nucleus pulposus. In their primary roles, the fibrous ring structure of the annulus fibrosus allows for the IVD to resist high bending and torsional loads, and the gelatinous mass of the nucleus pulposus acts hydrostatically to store energy to distribute compressive loads (White and Panjabi, 1990). In contrast to the “jelly donut” structure of the lumbar IVD, the cervical IVD has more of a “crescent-like” appearance, with a large annulus anterior, but very thin posteriorly (Mercer and Bogduk, 1999) (Figure 1.4). A healthy IVD cervical spine is around 3.5-6.0mm in height, with the nucleus pulposus taking up of 50-70% of the vertebral body surface area (An *et al.*, 1993; Mercer and Bogduk, 1999).

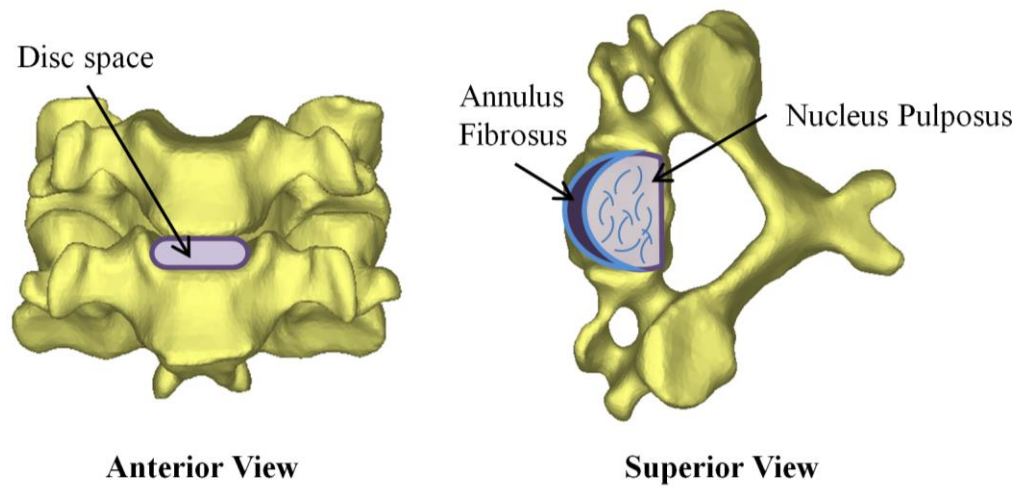


**Figure 1.4: Intervertebral Disc in the Cervical Spine**

The intervertebral disc (IVD) fills the space between adjacent vertebral bodies. The structure of the IVD is composed of the annulus fibrosus, an outer ring of tough laminates, surrounding a central core of soft, gelatinous material called the nucleus pulposus. In the cervical spine, the annulus fibrosus is a crescent-like shape, thicker in the anterior region.

In addition to the IVD, the cervical spine is almost completely surrounded by tensile ligamentous structures (Figure 1.5). The anterior longitudinal ligament (ALL) and posterior longitudinal ligament (PLL) run along the respective faces of the vertebral body. In addition to the PLL, the remaining posterior ligamentous structures are the capsular ligaments, ligamentum flavum, and interspinous and supraspinous ligaments. The capsular ligaments encase the entire facet joint. Most ligaments are largely collagenous in their make-up; however, the ligamentum flavum, which runs along the interior face of the laminae, is primarily elastin and under constant tension in the neutral position (White and Panjabi, 1990). The interspinous and supraspinous ligaments connect adjacent spinous processes. Grouped together, the facet capsules, ligamentum flavum, interspinous, and supraspinous are considered to form the posterior ligamentous complex (Holdsworth, 1970).

The cervical spine also consists of a complex, layered musculature system that allows for significant mobility of the head and neck, while still helping to maintain stability. This system consists of twenty-two superficial and deep muscles with varying origins and insertion points, each of which has a unique function (Goel *et al.*, 1986; White and Panjabi, 1990). The role of the muscles is not directly considered in this work.

### **1.1.3 CERVICAL SPINE MOBILITY**

One of the important functions of the cervical spine is to allow physiologic motions of the head and neck. These motions are defined based on a motion segment, the smallest unit representing the general mechanical behavior of a spinal region. A motion segment is defined by two adjacent vertebral bodies (*i.e.*, C5-C6) and their connecting soft tissues (*i.e.*, the IVD, facet joints, and ligaments) (White and Panjabi, 1990).

The motions are generally defined with a standard six degree-of-freedom (six-DOF) system, consisting of three rotations about and three translations along the Cartesian coordinate system defined for the human body (*i.e.*, sagittal, frontal, and transverse planes) (Figure 1.6) (Panjabi and White, 1971; Wilke *et al.*, 1998). The three standard rotational motions have been defined as flexion-extension, lateral bending, and axial rotation (White and Panjabi, 1990). By definition, flexion-extension is a rotation of

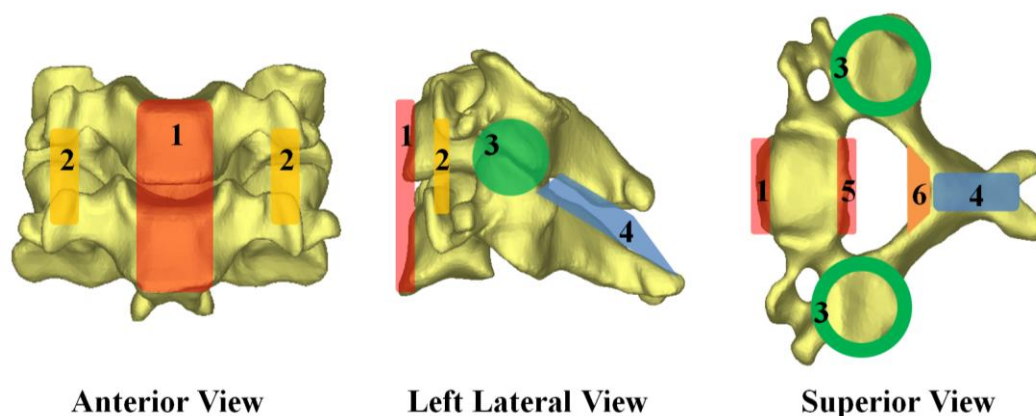


**Figure 1.5: Ligaments of the Cervical Spine**

The cervical spine is stabilized, in part, by numerous ligaments. The anterior longitudinal ligament (1), ALL, runs vertical along the width of the vertebral body. The intertransverse ligament (2) is a small ligament connecting the transverse processes. Surrounding the facet joint is the capsular ligament (3). The interspinous and supraspinous ligaments (4) connect adjacent spinous processes. The posterior longitudinal ligament (5), PLL, runs vertically along the interior wall of the vertebral body. Finally, the ligamentum flavum (6) runs vertically along the opposite side of the vertebral foramen, connecting adjacent laminae.



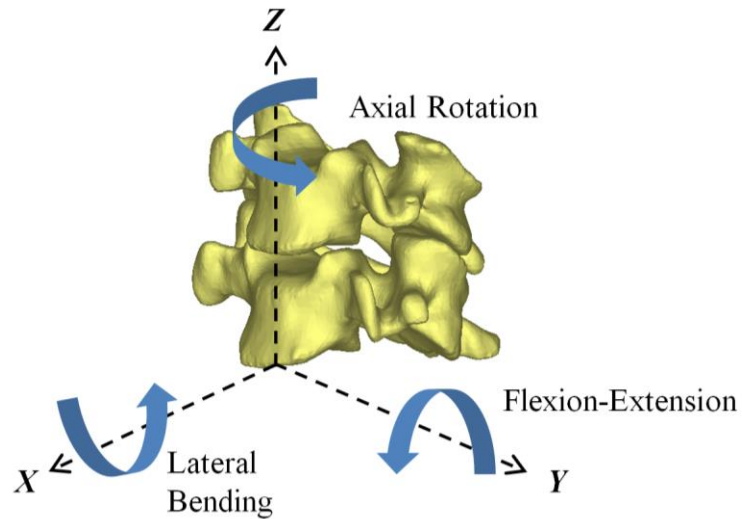


**Figure 1.6: Spine Motions**

The three physiologic rotations of the spine are Flexion-Extension, Lateral Bending, and Axial Rotation. Flexion-Extension rotates the spine in the sagittal plane about the medial-lateral ( $Y$ ) axis; Lateral Bending rotates the motion segment in the frontal plane to left and right sides about the anterior-posterior ( $X$ ) axis; and Axial Rotation, to the left and right, rotates in the transverse plane about the superior-inferior ( $Z$ ) axis. Since the motion segment is a six-DOF system, three translations are also found in the spine in addition to the rotations shown. For clarity purposes, translations have not been included.

the motion segment in the sagittal plane in anterior (flexion) and posterior (extension) directions about the medial-lateral axis; lateral bending is a rotation of the motion segment in the frontal plane to left and right sides about the anterior-posterior axis; and axial rotation, to the left and right, occurs in the transverse plane about the superior-inferior axis. In the healthy cervical spine, there is little translation in the motion segments, largely as result of the geometry of the facet joint (White and Panjabi, 1990).

Due to the anatomy of the cervical spine, some of these motions are intrinsically linked. Flexion-extension is largely an independent motion, but axial rotation and lateral bending occur in combination as a result of the angulation of the facet joint in the sagittal plane. For example, overall motion of the head in axial rotation is actually a combined movement in axial rotation and lateral bending for the cervical spine. A classic anatomical study by Lysell revealed an approximate ratio;  $1^\circ$  of axial rotation for  $7.5^\circ$  of lateral bending at C7, with a larger ratio for superior motion segments, and a ratio of  $0.75^\circ$  of lateral bending for  $1^\circ$  of axial rotation (Lysell, 1969).

#### **1.1.4 CERVICAL SPINE STABILITY**

All joints in the human body are defined by an inherent stability. In the cervical spine, stability relies on the mechanical properties of the IVD and ligamentous structures to provide passive restraint of the motion segment. The surrounding musculature also contributes to stability through active compressive loading of the vertebral articulation. In a healthy spine, the osseous anatomy provides very little intrinsic stability in the cervical spine. When these anatomical structures are all functioning properly, the cervical spine remains stable; however, changes to these structures as a result of aging, degeneration, and trauma can lead to spinal instability.

Instability of the spine can be difficult to define and quantify (Reeves *et al.*, 2007). From a traditional mechanical instability perspective, the cervical spine could be considered “mechanically unstable” when the sum of the forces and moments on the spine does not equal zero (Hibbeler, 2001). This engineering definition would be impossible to apply in the normal clinical situation (*i.e.*, unknown forces and moments). As such, White and Panjabi define clinical instability of the spine as: if, under

physiological loads, there are changes in the patterns of motion which may result in neurologic deficit, excessive deformity and/or pain, acutely or with time (White and Panjabi, 1990). Due to this pain and instability, physiologic motions may become limited or altogether impossible. The altered motion is referred to as pathologic motion, and causes a detrimental effect on a person's ability to perform normal daily activities. White and Panjabi also describe "kinematic instability" as excessive change in physiologic motion, axis of rotation, or in the coupling characteristic of the spine (White and Panjabi, 1990). This biomechanical definition of stability is more applicable to laboratory testing, since concepts such as "pain" cannot be determined through *in vitro* studies. Due to the cadaveric studies performed in this thesis, the later definition of instability is implied.

### **1.1.5 EFFECT OF AGE ON MOBILITY**

In the younger population, the osteoligamentous anatomy of the cervical spine is generally healthier, stronger, and more flexible, leading to increased mobility (Penning, 1978). As the spine ages, disc degeneration and osteoarthritis (OA) begin to occur and mobility decreases (Papadakis *et al.*, 2011; Penning, 1978). With disc degeneration, the IVD loses its water content and begins to harden. OA is a condition that causes decreased joint mobility, often including ossification of the facet joint. Large bony osteophytes can grow from many load bearing regions of the vertebrae, significantly altering mobility or eliminating it altogether (Fujiwara *et al.*, 2000). These conditions significantly stiffen the spinal column which, when combined with osteoporosis, has the unfortunate side effect of increasing fracture risk for low-energy injuries, such as falls from a standing height (Malik *et al.*, 2008).

## **1.2 CERVICAL SPINE TRAUMA AND SURGICAL TREATMENT**

The cervical spine plays a critical role in normal human function, yet this structure is prone to traumatic injuries with relatively little protection for potentially devastating consequences. Cervical spine injuries are present in 3-6% of all emergency room visits, totaling approximately 150 000 incidents per year in North America (Milby *et al.*, 2008). These injuries cover a large spectrum, including minor sprains and strains,

herniated discs (tears in the annulus causing leakage), and subluxations, fractures, and dislocations of the facet joint (without neural deficit) (Figure 1.7) (Allen *et al.*, 1982; Dvorak *et al.*, 2007a; Vaccaro *et al.*, 2007). In general, these traumas are the result of a high-speed injury, such as a motor vehicle or sporting activity accident, and are most common among the younger male population (Dvorak *et al.*, 2007a). Trauma to the lower cervical spine is the most frequent (Kwon *et al.*, 2006). Fortunately, damage to the spinal cord is present in only a small percentage of these injuries (estimated to be around 12 000 per year) (Kwon *et al.*, 2006; Lowery *et al.*, 2001).

### **1.2.1 CLASSIFICATION OF SUBAXIAL TRAUMATIC INJURIES**

With the wide spectrum of traumatic injuries that can occur in the cervical spine, it can be very challenging for the surgeon to discern their management decision without significant experience. In these cases, the surgeon relies on the classifications of traumatic injuries set out by previous surgeons based on their experiences (Allen *et al.*, 1982; Holdsworth, 1970). Early classification systems focused on anatomical, morphological, and mechanistic criteria of the trauma. Sir Francis Holdsworth described his experiences in over 1000 patients with facet fractures and dislocations in one of the most widely referenced historical classification systems (Holdsworth, 1970). More complex classification systems have since been developed, yet an ideal classification system does not yet exist (Allen *et al.*, 1982; Vaccaro *et al.*, 2007). A preferable system

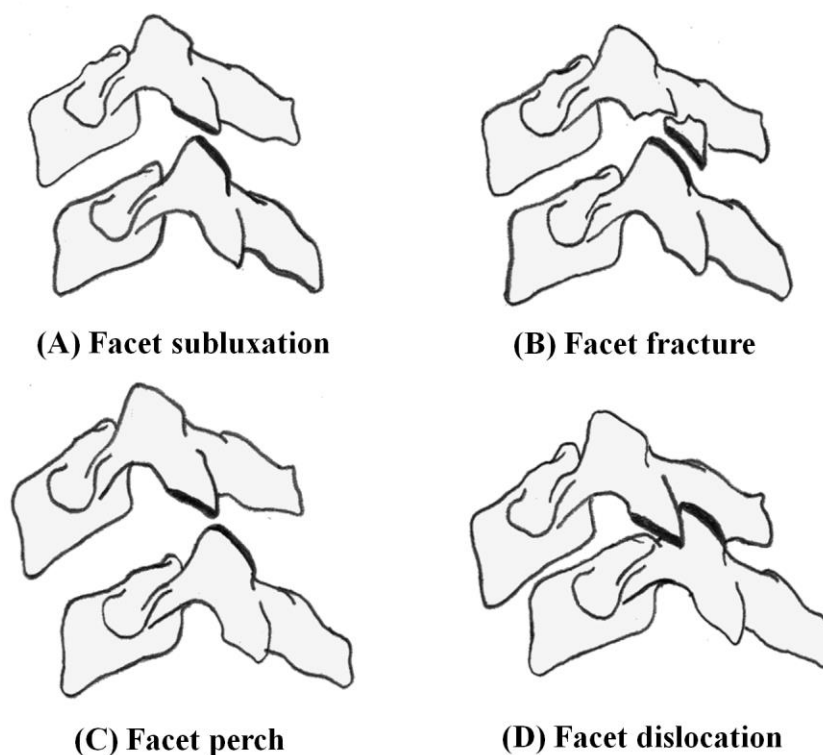


### Figure 1.7: Cervical Facet Joint Injuries

Traumatic cervical facet joint injuries result in a spectrum of soft tissue and bony disruption. **(A)** Facet subluxation describes an injury where the joint has gone beyond its physiologic range of motion. **(B)** Facet fractures can occur in either the inferior articular process of the superior vertebrae (shown), or in the superior articular process of the inferior vertebrae. **(C)** A facet perch is an extreme case of subluxation where the ends of the joint lie atop each other. **(D)** Facet dislocation occurs when the joint surfaces have slid past each other and are locked. Dvorak *et al.* (2007) described the incidence of these injuries in a series of 90 cases. The most common result were facet fractures, with fewer cases involving subluxations and facet perch/dislocations.

would describe the mechanism of injury, spinal alignment, neurological injury, assessment of stability, and fracture pattern (Vaccaro *et al.*, 2007).

The most popular classification system today is the Allen-Ferguson system, based on a mechanistic classification of injury in 162 patients (Allen *et al.*, 1982). This system divided traumatic injuries of the cervical spine into six phylogenies; compressive flexion, vertical compression, distractive flexion, compressive extension, distractive extension, and lateral flexion. Of these, the distractive flexion was the most common. While this has been the most widely adopted classification, its evidence was based solely on lateral radiographs and the details gathered about how the injury occurred. Nevertheless, it has still proven to be an effective diagnostic tool (Nakashima *et al.*, 2011b).

Recently, a new classification system has proposed further clarification of traumatic injuries. The subaxial injury classification (SLIC) system was put forth by a group of expert spine surgeons (Spine Trauma Study Group) (Vaccaro *et al.*, 2007). SLIC is similar to the Allen-Ferguson system in that it is largely based around mechanisms of injury, but provides further evidence on the morphology of fractures, assessment of the discoligamentous complex, and neurologic status (Vaccaro *et al.*, 2007). However, for this system to become the standard, more evidence into its efficacy is required (Bono *et al.*, 2011; Patel *et al.*, 2010).

### **1.2.1.1 FLEXION-DISTRACTION INJURIES**

In the classic study by Allen *et al.* (1982), flexion-distraction (distractive-flexion) type injuries were divided into four stages, based on the severity of post-injury translational displacement (Allen *et al.*, 1982). Stage 1 consists of an isolated posterior ligamentous injury resulting in facet subluxation only in association with post-traumatic flexion. Stage 2 describes a unilateral facet injury, while stages 3 and 4 include bilateral facet dislocation/subluxation. Each stage of this injury can be associated with a variety of injury patterns including facet fractures, facet subluxation/dislocation (pure ligamentous injury), and vertebral body fractures. The more recent SLIC adds some additional consideration to this injury pattern (considered hyper-flexion) for facet subluxations and perched facets (Vaccaro *et al.*, 2007). However, the combination of

fractures and ligamentous injury that can produce the various stages of injury and the resulting instability pattern is poorly understood.

The treatment of subaxial flexion-distraction injuries is complex due to the many variables influencing the treatment decision. Management of flexion-distraction injuries have found that patients treated surgically outperform those treated with conservative management (Beyer *et al.*, 1991; Dvorak *et al.*, 2007a; Rorabeck *et al.*, 1987). However, there is no consensus for an optimal surgical approach (Glaser *et al.*, 1998).

### **1.2.2 SURGICAL TREATMENT OPTIONS**

Spinal fusion (“arthrodesis”) is a surgical treatment method for instability of the spine. This technique involves the use of specialized spinal instrumentation and a reconstituted bone graft (either harvested as an autograft, freeze-dried allograft, or synthetic) to achieve long term bone-on-bone fusion for a stable spinal construct (Zdeblick and Ducker, 1991). As such, the short-term goal of the instrumentation is to provide adequate stability to enable long-term bony fusion. Bony fusion is necessary; otherwise, the instrumentation providing stability will eventually fail.

The first reported case of surgical fixation of the spine was for treatment of a fracture-dislocation injury in the cervical spine, where stability was restored by wiring adjacent spinous processes together (Hadra, 1891). A more reliable wiring technique was eventually described by Rogers in the 1940’s (Rogers, 1942). Subsequently there were only minor advances in surgical fixation innovations for the spine until the 1990’s, when solid metallic constructs such as plate and screw systems were adopted. These were based on a better understanding of biofidelic metals, including stainless steel, titanium, and cobalt-chrome. Today, several approaches have been described for fixation following cervical spine trauma, including flexion-distraction injuries (Kwon *et al.*, 2007).

The available surgical approaches for instrumentation in the cervical spine are anterior, posterior, and combined (White and Panjabi, 1990), as described below (Figure 1.8). Each of these approaches has unique clinical advantages and disadvantages, and

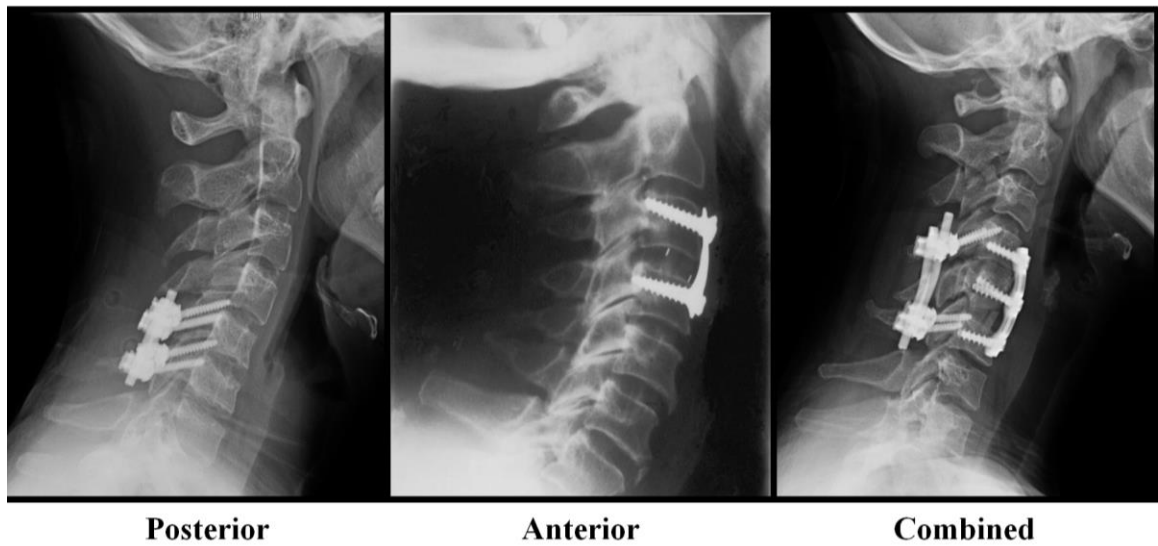


**Figure 1.8: X-rays of Cervical Instrumentation**

**Posterior:** Lateral mass screws and rods shown in the C5-C6 vertebrae. **Anterior:** ACDFP in the C3-C4 vertebrae. **Combined:** Multi-level ACDFP with supplemental lateral mass screws and rods in the C4-C6 vertebrae.



surgeons must consider patient, fracture, and surgical factors when weighing their options. Patient factors include such considerations as age, body habitus, medical comorbidities, and associated injuries (Kwon *et al.*, 2007, 2006). Fracture factors are derived from X-ray and computed tomography (CT) interpretation, including the degree of mal-alignment (both rotational and translational), which is frequently categorized as subluxation, perched, or dislocated, as well as associated facet and vertebral body fractures (Dvorak *et al.*, 2007a). Surgical factors can include the stability imparted by the various approaches, variability with respect to instrumentation options, influence of under or over sizing the anterior column reconstruction, whether a decompression of the neural elements is required, or the associated morbidity to a specific approach (Kwon *et al.*, 2006).

### **1.2.2.1 ANTERIOR APPROACH**

The gold standard anterior approach for cervical spine trauma is referred to as an anterior cervical discectomy and fusion with plating, or ACDFP for short (Aebi *et al.*, 1991; Caspar *et al.*, 1989; Vaccaro and Balderston, 1997). This widely adopted procedure involves a surgical approach through the anterior neck, clearing the musculature anterior to the spine, and removal of the ALL and IVD (*i.e.*, discectomy) at the injured level (Figure 1.9). The empty space left behind following IVD removal is filled with a reconstituted bone graft and/or interbody device, such as a cage or spacer, to reconstruct the anterior column (Smith and Robinson, 1958). The size and shape of the bone graft is based on surgical experience (*i.e.*, surgical factor). A thin metal plate is then placed over the adjacent vertebral bodies, preventing anterior displacement of the graft, and four screws are inserted (two into each vertebral body) to secure the plate and fix the adjacent vertebrae together. The interface between the screws and plate can either be fixed angle or variable angle; variable angle allows more freedom in screw direction but relies on a compressive fit with the plate to keep it rigidly in place (Brodke *et al.*, 2006). To ensure minimal exposure of the plate and maximum compression, the faces of the vertebrae are cleared of any protruding bony osteophytes.

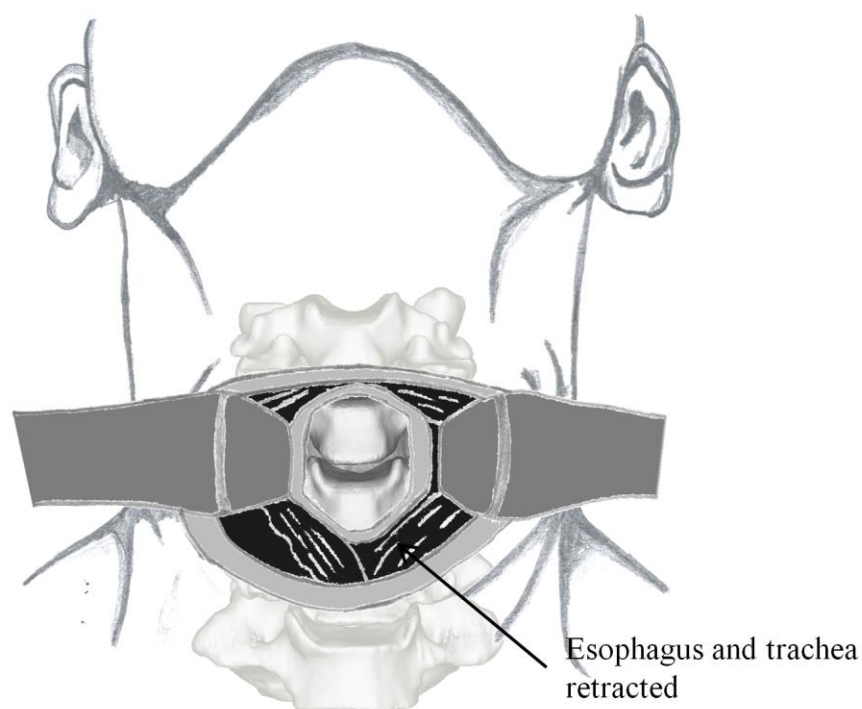


**Figure 1.9: Anterior Approach for Spinal Fusion**

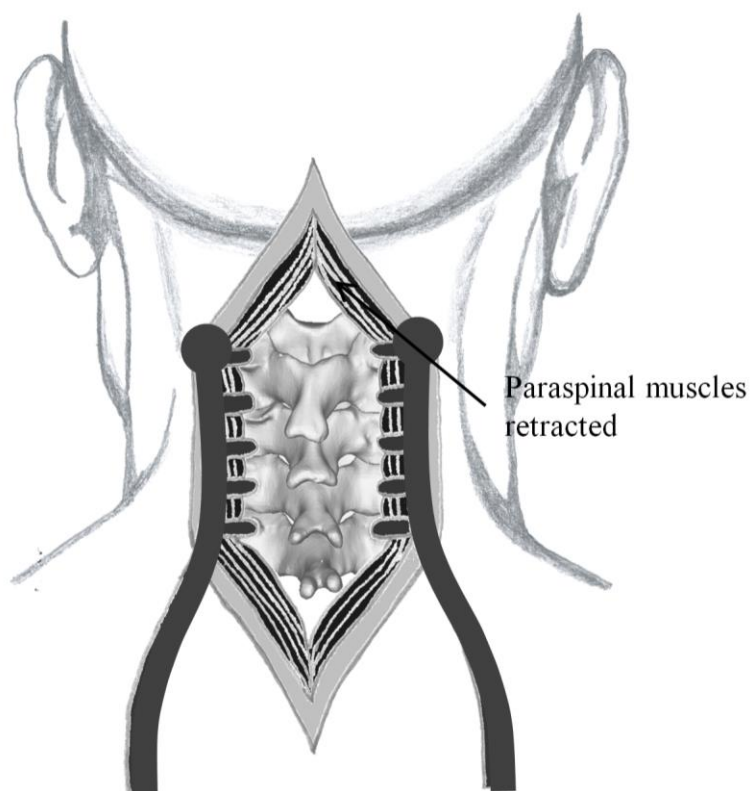
In an anterior surgical approach, the surgeon clears a path to the vertebral body by making an incision on one side of the neck. Metal retractors then hold aside the esophagus and trachea to create a small window to view and perform the ACDFP procedure on the motion segment of interest.

The anterior approach is most common in situations of degeneration causing compression of the spinal cord or nerve roots, where this approach allows direct visualization for the decompression procedure; however, it is also widely used for flexion-distraction traumatic injuries (Kwon *et al.*, 2007). Recent clinical retrospective reviews have found good success of the ACDFP procedure for this type of trauma, producing successful long-term bony fusion (Henriques *et al.*, 2004; Rabb *et al.*, 2007; Woodworth *et al.*, 2009). However, this procedure is not always ideal. Recently, Johnson *et al.* identified a 13% failure rate of ACDFP in the setting of a facet or vertebral body fracture (Johnson *et al.*, 2004). Furthermore, this procedure's success is limited in longer constructs spanning multiple levels of the cervical spine (Kirkpatrick *et al.*, 1999), with the added drawback of reduced neck motion.

The clinical advantages of the anterior approach include better long-term alignment, as well as less musculature dissection to access the spine, making for a quicker recovery from surgery (Caspar *et al.*, 1989; Vaccaro and Balderston, 1997). Also, if there are any disc fragments within the canal, an anterior approach must be initially selected for safe removal (Nakashima *et al.*, 2011b). The main disadvantage to this procedure is a high rate of post-operative swallowing difficulties as a result of the protruding plate construct.

### **1.2.2.2 POSTERIOR APPROACH**

In addition to the anterior approach, the posterior osteology of the cervical spine also provides a viable location for spinal instrumentation (Figure 1.10). Wiring of the spinous process was an early technique for fixation (Rogers, 1942). This eventually evolved to plated constructs over the lateral masses, to the now current gold standard of lateral mass/pedicle screw and rod fixation (Cooper *et al.*, 1988; Roy-Camille *et al.*, 1989). This perhaps mimics the success of the posterior approach used for pedicle screw systems in the lumbar spine, though cervical instrumentation in the pedicle is not currently considered a safe treatment due to the serious anatomical risks (*i.e.*, vertebral artery) with screw placement. In the lateral mass technique, screws are inserted on an angle in a superior-lateral direction (“upward and outward”) to have the most bone



---

**Figure 1.10: Posterior Approach for Spinal Fusion**

With a posterior approach, the surgeon makes an incision along the back of the neck. The paraspinal musculature is then retracted until the posterior vertebral anatomy is reached (laminae and spinous process). Through this window, the lateral mass screw fixation procedure can be performed.

purchase within the lateral mass (An *et al.*, 1991). The heads of most screw designs are polyaxial, allowing for adjustment of the connecting rod angles. Rods are also curved by the surgeon during the procedure to suit the desired curvature of the spine and fixed within screws between adjacent levels.

Clinical literature has supported use of the posterior approach in providing strong, multi-level constructs for bony fusion (Anderson *et al.*, 1991; Nakashima *et al.*, 2011a). However, it is less widely used than the anterior approach due to some of the clinical drawbacks (Kwon *et al.*, 2007). The procedure requires more muscle dissection and the need for a multi-level procedure in the setting of facet fracture. The procedure does have the advantage though of direct (visible) reduction of the facet joint, versus indirect for the anterior approach.

### **1.2.2.3 COMBINED ANTERIOR AND POSTERIOR INSTRUMENTATION**

In the case of severe trauma to the subaxial cervical spine, combined anterior and posterior instrumentation may be required to restore stability (Song and Lee, 2008). As expected, this is a much more substantial operation, where the patient must be flipped between procedures. This combined approach may be unnecessarily invasive in some injury cases (Song and Lee, 2008).

### **1.2.2.4 CURRENT TREATMENT ALGORITHMS**

With the widespread adoption of fusion techniques, treatment algorithms are required to standardize and ultimately improve patient care. Previous treatment algorithms have been relatively simplistic and have not considered the entire injury spectrum (Allen *et al.*, 1982). Based on the recent SLIC classification, Dvorak and his colleagues have developed the most in-depth treatment algorithm to date for subaxial cervical spine trauma (Dvorak *et al.*, 2007b; Vaccaro *et al.*, 2007). This classification weights factors such as the injury morphology, integrity of the discoligamentous complex, and the neurologic status of the patient. This is an improvement over the previous singular experience guidelines in the literature for treatment (Bohlman, 1979; Holdsworth, 1970), especially in the case of rapidly developing technologies and

evidence-based medicine practices. However, most of the supporting information in the Dvorak algorithm comes from expert opinion and retrospective reviews with few randomized clinical trials (Dvorak *et al.*, 2007b). The authors do comment that this population is non-homogeneous, and therefore is difficult to generate a large enough sample size. Some of the evidence in the treatment algorithm does come from biomechanical testing (Do Koh *et al.*, 2001; Ianuzzi *et al.*, 2006), but overall there is currently a lack of studies investigating the biomechanics of flexion-distraction injuries and instrumentation.

### **1.3 IN VITRO BIOMECHANICS OF THE CERVICAL SPINE**

Biomechanical investigations of the cervical spine can help add depth to these classifications or treatment algorithms by providing an understanding of the instability present for specific injuries (Do Koh *et al.*, 2001; Ianuzzi *et al.*, 2006). They are also valuable in the development and evaluation of new techniques and devices for spine surgery. The main goal of many *in vitro* biomechanical studies is to attempt to recreate the *in vivo* motion (Panjabi, 1988); however, this is not possible with individual variability and the complexity of the musculature in the spine (too many muscles to determine individual muscle loading) (Bernhardt *et al.*, 1999). As such, in the spine, these studies attempt to produce a reliable approximation of the physiologic motion of the spine, where the advantage lies in producing repeatable motion (Panjabi, 1988). This enables *in vitro* joint simulation to compare the stability of the intact, injured, and instrumented spine (Goel *et al.*, 1984).

#### **1.3.1 SIMULATING SPINE MOTIONS**

To evaluate the spinal stability and the effects of various treatment procedures including spinal fixation devices, *in vitro* biomechanical investigations are completed through the use of spinal loading simulators - test apparatus in which *in vitro* spinal specimens can be mounted and tested under defined loading conditions (Wilke *et al.*, 1998). The principles behind most spinal loading simulators are the flexibility methods developed by Goel *et al.* (1987) and Panjabi (1988) (Goel *et al.*, 1987; Panjabi, 1988).

Rather than a displacement-based input, the flexibility method uses a load input protocol. A pure bending moment is applied to produce one of the three physiologic motions (*i.e.*, flexion-extension, lateral bending, and axial rotation) and the other five-DOF remain unconstrained (Panjabi, 1988). The concept of applying a pure moment ensures that all segments of the spine are loaded equally, and that this loading remains the same as the spine deforms during testing (Panjabi, 1988). Furthermore, pure moment loading has the advantage of being relatively easy to recreate across separate labs (Wheeler *et al.*, 2011), a critical component for standardized testing of mechanical devices (Panjabi, 1988; Wilke *et al.*, 1998). In regards to the magnitude of the applied moment, the true loading of the spine is unknown. Previous work by others has shown that 1.5Nm to 2.5Nm is a reasonable load target for the flexibility test method in the cervical spine (Dvorak *et al.*, 2005; Wilke *et al.*, 1998).

Spine simulator designs have evolved from simple benchtop models capable of applying simple bending loads to current complex modified materials testing machines (Cheng *et al.*, 2009; Panjabi *et al.*, 1975). Many designs have been employed, including suspending motors (servo or stepper) orthogonally above the specimen (Gay *et al.*, 2006; G  det *et al.*, 2007; Wilke *et al.*, 1994), or in combination with linear bearings and universal joints (Goertzen *et al.*, 2004). Spinal loading simulators can also be built as a modification to an existing servohydraulic materials testing machine. Crawford *et al.* (1995) used the actuator of their MTS<sup>®</sup> testing machine (MTS Systems Corp., Eden Prairie, MN, USA) in combination with a pulley and cable system setup to apply a pure bending moment to a multi-segment spine (Crawford *et al.*, 1995). In a similar setup to the stand alone device of Wilke *et al.* (1994), Cunningham *et al.* (2003) designed a six-DOF spine simulator using stepper motors in a gimbal connected to the actuator of their uni-axial MTS<sup>®</sup> testing machine (Cunningham *et al.*, 2003). Recently, there has also been a push to develop robotic simulators, capable of complex six-DOF motion, though these systems are very costly and require complex programming to achieve desired results (Schulze *et al.*, 2012).

### 1.3.1.1 UWO SPINAL LOADING SIMULATOR

The University of Western Ontario (UWO) spinal loading simulator used for this body of work was designed and developed as a modification to an 8874 Instron® tri-axial servo-hydraulic apparatus in the Jack McBain Biomechanical Testing Laboratory (McLachlin, 2008) (Figure 1.11). The simulator uses the Instron's actuators and control methods to produce repeatable and reproducible segmental spinal motion. The overhead "axial" actuator of the Instron® is capable of applying axial load and torque. Its "off-axis" actuator provides a secondary torque axis. Modification components were designed for the materials testing machine as a system of connecting arms and fixtures using both the axial and off-axis actuators to produce motion (Figures 1.12 & 1.13). Axial rotation is applied via the "axial" actuator, and both flexion-extension and lateral bend are applied with the "off-axis" actuator, with a 90° rotation of the specimen required between these two motions. This design has been used to test the repeatability and reproducibility in a single lumbar spine, showing excellent results (McLachlin, 2008). However, it has not been adapted to the much smaller cervical spine, nor has it incorporated 3D motion analysis.

### 1.3.2 SPINAL STABILITY MEASURES

The outcome measure of interest from spine simulators is spinal motion, necessitating the use of measurement tools and techniques to quantify the resulting kinematics. Spine movement is traditionally quantified by range of motion (ROM). ROM is defined as the maximum physiologic movement (*i.e.*, no plastic deformation) the spine travels through in one loading direction (Figure 1.14) (Panjabi *et al.*, 1975). In addition to ROM, quantifying the laxity around the spine's neutral position is important for defining the physiologic stability. Quasi-static studies described the "neutral zone" (NZ) as the region of the ROM where spine motion is produced with minimal internal resistance (*i.e.*, the laxity of the segment). This is measured as a residual deformation from the neutral position following loading (Oxland and Panjabi, 1992). More recently, new parameters have emerged to describe the laxity of the specimen in studies involving continuous spinal motion, with the width of the hysteresis loop during cyclic continuous



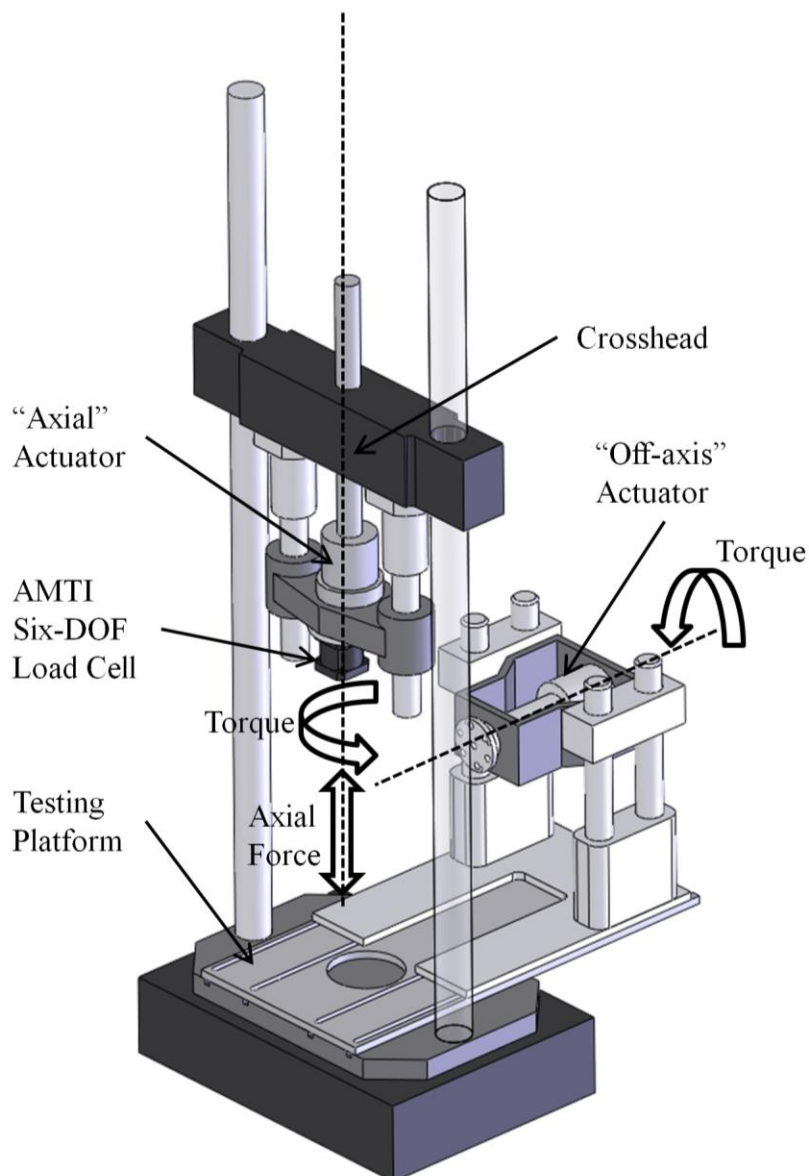


**Figure 1.11: Custom Instron 8874 Materials Testing Machine**

This servo-hydraulic machine is capable of applying load from two different actuators. The “axial” actuator can apply an axial force, as well as a torque. The “off-axis” actuator can apply a torque about its axis. An AMTI six degree-of-freedom (DOF) load cell is used to control the loading of the axial actuator. Two large columns support and position the axial actuator’s crosshead. In addition to the translation available in the axial actuator, the crosshead’s position can be vertically adjusted to account for a variety of specimen lengths. Also, the off-axis torque actuator could be moved horizontally if necessary.

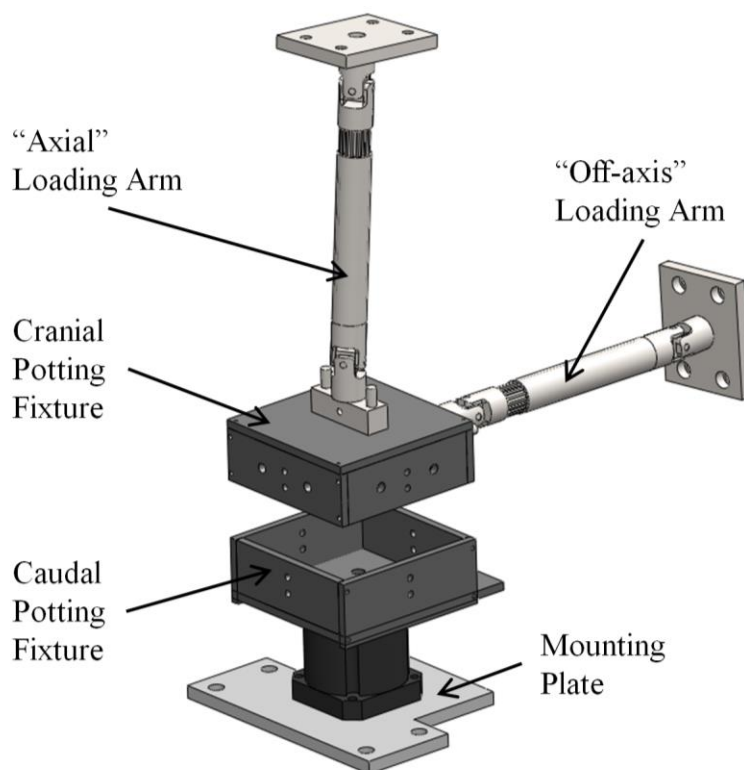


**Figure 1.12: Components for UWO Spinal Loading Simulator**

The main components of the spinal loading simulator are the two loading arms (“axial” and “off-axis”), which are able to translate the bending loads from the respective Instron® torsion actuators to the specimen. These are built with a frictionless linear bearing over a spline shaft, with universal joints at each end. While both arms are telescoping in nature, the axial loading arm is set at a fixed length to prevent it from sliding under its own weight. In this case, the Instron’s axial force actuator is set to hold 0N to achieve the same function. The spine specimen is held at each end within the cranial and caudal potting fixtures. The loading arms connect to the cranial potting fixture to apply bending loads to the spine specimen. The caudal potting fixture is fixed to the testing platform of the Instron® through a mounting plate.

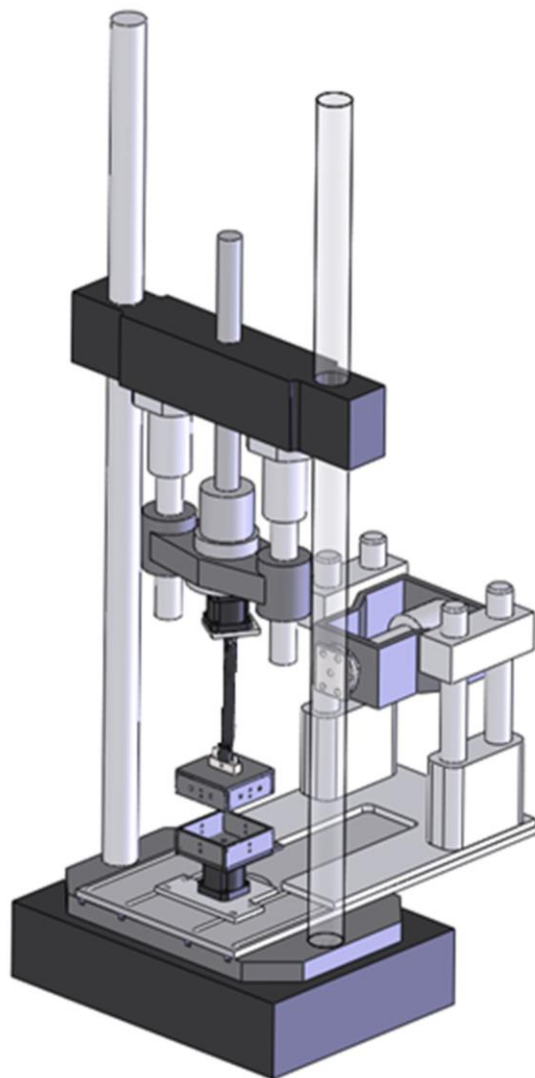


**Figure 1.13: UWO Spinal Loading Simulator**

The modified Instron® materials testing machine provides the loading actuators to create physiologic spine motion. The current simulator makes use of both actuators to apply continuous physiologic motions. Custom-fixturing ensures that unconstrained motions are applied. Flexion-extension and lateral bending are applied through the off-axis loading arm. Axial rotation is applied by the axial loading arm, with the off-axis loading arm removed for these tests (shown).

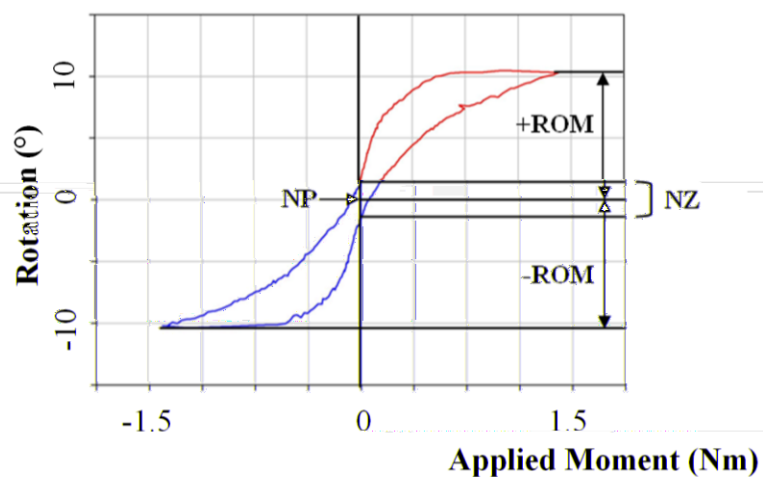


**Figure 1.14: Kinematic Stability Measures**

Range of motion (ROM) is the largest physiologic rotation (*i.e.*, no plastic deformation) the spine moves through in a specified loading direction (+ROM and -ROM). The neutral zone (NZ) exists as a measure of specimen laxity, shown in the figure as the width of the hysteresis loop at 0Nm, which is centered about the neutral position (NP).

loading being most commonly reported as the NZ (Goertzen *et al.*, 2004; Wilke *et al.*, 1998) (Figure 1.14). However, the adequacy of such kinematic parameters for the purpose of defining changes in cervical spine stability still requires further investigation.

### 1.3.3 SIMULATING TRAUMATIC INJURY MECHANISMS

Due to the devastating nature and risk for potential neurologic injury, it is impossible to assess the kinematics of severe cervical spine trauma *in vivo*. However, understanding how the kinematics are affected by injury is important for determining whether the spine is unstable. To better understand these changes, *in vitro* biomechanical tests to recreate injuries and instability are required. This is not a new concept in the cervical spine. Early cadaveric studies of spinal injuries identified the changes in motion that result from simulated traumatic injuries (Bauze and Ardran, 1978; Beatson, 1963; Roaf, 1960). Panjabi and White identified that the spine was considered unstable once all of the posterior elements plus one anterior were disrupted, as well as the visa versa (Panjabi *et al.*, 1975). These data were then used clinically as a diagnosis of instability. They also showed that motion does not incrementally increase with sequential injury to the stabilizing elements, but rather remains physiologic until sudden and complete failure emerges (White *et al.*, 1975).

A number of notable biomechanical studies have attempted to document cervical spine stability, but have either not modelled clinically-relevant mechanisms of injury, have been quasi-static, or represented manual ligament transection studies (Brown *et al.*, 2005; Nowinski *et al.*, 1993; Panjabi *et al.*, 1975; Roaf, 1960; Sim *et al.*, 2001; Zdeblick *et al.*, 1993, 1992). However, whether the surgical resection is valid in terms of reproducing the appropriate injury magnitude and associated spinal instability is unknown. In contrast, dynamically-induced injury mechanisms, using custom loading devices, can provide a better representation of the expected clinical instability but a variable injury pattern. Two potential mechanisms that produce a flexion-distraction injury have been proposed *in vitro*: (1) hyper-flexion and distraction, and (2) flexion, distraction, and rotation (Bauze and Ardran, 1978; Crawford *et al.*, 2002; Ivancic *et al.*, 2008; Panjabi *et al.*, 2007). Crawford *et al.* (2002) successfully utilized the second of

these mechanisms with a spine simulator to dynamically create a unilateral facet injury (Crawford *et al.*, 2002). These dynamic studies would more likely recreate the instability present with *in vivo* injuries; however, the dynamic nature of inducing the injury limits repeatability.

### 1.3.4 BIOMECHANICS OF SURGICAL FIXATION

One of the most common subjects of biomechanical testing is in comparative testing of surgical devices prior to their clinical implementation. Spine simulators have been used for the past 30 years to assess the efficacy of spinal fixation devices in restoring stability (Coe *et al.*, 1989; Goel *et al.*, 1987; Panjabi, 1988). This has provided significant insight into the effectiveness of instrumentation, which is then used as evidence in treatment algorithms. However, the recent recommendation of surgical approach for flexion-distraction injuries of the cervical spine, based on expert opinion and systematic literature review, identified only two biomechanical studies (Dvorak *et al.*, 2007b), both of which tested surgical fixation in a “worst-case” catastrophic scenario, removing the entire vertebral body to simulate a corpectomy model (Do Koh *et al.*, 2001; Ianuzzi *et al.*, 2006).

These are not the only two studies relevant to this injury mechanism. One biomechanical investigation reported on the success of anterior fixation alone for stage 3 flexion-distraction injuries without facet fractures (Paxinos *et al.*, 2009); however, there was no comparison to a posterior approach in the same specimens. In studies comparing the two most common approaches in the cervical spine, all have found posterior instrumentation outperformed anterior fixation in reducing the range of motion of the injured motion segment (Bozkus *et al.*, 2005; Do Koh *et al.*, 2001; Duggal *et al.*, 2005; Kotani *et al.*, 1994; Pitzen *et al.*, 2003). In terms of the effect of facet fracture, Pitzen *et al.* (2003) evaluated the effect of posterior injury, including loss of the facet joint, with use of anterior plating alone and found the capsular ligaments and articular facets were important stabilizing elements (Pitzen *et al.*, 2003). To ultimately improve clinical guidelines, biomechanically relevant surgical and fracture factors need to be fully investigated in the laboratory to understand their influence on cervical spine stability.

Interestingly, while there is a significant amount of literature to support the posterior approach from a biomechanical perspective, there have been recent clinical reports on the effectiveness of the anterior approach alone in treatment of isolated posterior injuries (Henriques *et al.*, 2004; Rabb *et al.*, 2007; Woodworth *et al.*, 2009). This contrast to the biomechanical literature suggests that there is a gap between interpretation of the biomechanical knowledge and the results seen in clinical studies.

## **1.4 ANALYSIS AND INTERPRETATION OF CERVICAL SPINE KINEMATICS**

In addition to creating motion, significant efforts have been directed towards the development and implementation of techniques to quantify cervical spine kinematics. Kinematics is the branch of classical mechanics that deals with the science of motion without regard to the forces that cause motion (Craig, 2005). The cervical spine is a complex 3D structure that allows for complex motions, therefore proper analysis and interpretation of the motion is crucial. This is especially true in its application to knowledge translation. Kinematic data generated by mechanical testing must be clinically relevant and understandable.

### **1.4.1 MOTION TRACKING AND REGISTRATION**

Motion tracking has been a common clinical practice in the spine since the invention of radiography, where lateral radiographs are used to describe static shots of patients in the neutral position and fully flexed or extended. The clinician then interprets how the vertebrae have moved relative to the neutral position (Allen *et al.*, 1982). This crude 2D, though non-invasive, technique has been the backbone of major surgical operations based on detecting a few millimeters of translation (White and Panjabi, 1990). Newer *in vivo* motion analysis technologies, such as the use of radiostereometric analysis, or bi-plane fluoroscopy, are on the horizon, advancing to the point where they are capable of accurately determining the 3D kinematics of the spine *in vivo* (Anderst *et al.*, 2011). However, the use of such technology routinely in the operating room is not yet feasible, and has been largely used for only research purposes.

With *in vitro* testing, the need for non-invasive tracking techniques is removed, and the vertebrae themselves are directly visible. As such, the gold standard has been optical tracking systems to determine 3D spinal kinematics. These multi-camera devices are used to determine segmental motion as they are generally best suited to this type of testing environment. Optical tracking systems, including the Optotrak Certus® (Northern Digital Inc., Waterloo, ON, Canada) are commonly used measurement tools for this purpose. Rigid body trackers are placed on each body of interest (*i.e.*, independent vertebrae), and their motion is tracked relative to a fixed camera system.

Assuming rigid body motion between the trackers and vertebrae, the tracker can be registered to its respective vertebra by digitizing relevant bony landmarks, which are then used to create an anatomical frame of reference on each bone. Cartesian (or orthogonal) coordinate systems are used along the anatomical axes, where positions and orientations of the vertebral body are then described relative to the reference vertebra. Many coordinate systems have been defined for the spine (Panjabi *et al.*, 1981; Wilke *et al.*, 1998). Panjabi initially described that the anatomical axes of the spine should be defined as have the *X* axis running anterior-posterior, *Y* axis as superior-inferior, and the *Z* axis as medial-lateral (Panjabi *et al.*, 1981). Others have described coordinate system for the spine defined as *X* axis running anterior-posterior, *Y* axis as medial-lateral, and the *Z* axis as superior-inferior (see Figure 1.6) (Wilke *et al.*, 1998). With these frames of reference and the use of transformation matrices, motion of the trackers relative to the camera can be converted to relative motion between vertebrae in terms of flexion-extension, lateral bending, and axial rotation. To accomplish these tasks, spatial algebra is required, where mathematical software, such as MATLAB™ (MathWorks, Natick, MA, USA) or LabVIEW™ (National Instruments, Austin, TX, USA), can be used to perform the analysis.

#### **1.4.2 SPATIAL DESCRIPTIONS AND TRANSFORMATION MATRICES**

These anatomic frames of reference within the vertebrae (*i.e.*, “*object*”) define orientation by a set of three orthogonal unit vectors relative to a reference coordinate frame (*i.e.*, “*reference*”) (Small *et al.*, 1992). These vectors are written in terms of a



reference coordinate frame as direction cosines. When stacked together they form what is referred to as a rotation matrix  $[R]$  (Eq. 1.1) (Craig, 2005).

$${}^{Ref}_{Obj}R = \begin{bmatrix} {}^{Ref}\hat{X}_{Obj} & {}^{Ref}\hat{Y}_{Obj} & {}^{Ref}\hat{Z}_{Obj} \end{bmatrix} = \begin{bmatrix} \hat{X}_{Obj} \cdot \hat{X}_{Ref} & \hat{Y}_{Obj} \cdot \hat{X}_{Ref} & \hat{Z}_{Obj} \cdot \hat{X}_{Ref} \\ \hat{X}_{Obj} \cdot \hat{Y}_{Ref} & \hat{Y}_{Obj} \cdot \hat{Y}_{Ref} & \hat{Z}_{Obj} \cdot \hat{Y}_{Ref} \\ \hat{X}_{Obj} \cdot \hat{Z}_{Ref} & \hat{Y}_{Obj} \cdot \hat{Z}_{Ref} & \hat{Z}_{Obj} \cdot \hat{Z}_{Ref} \end{bmatrix} \quad \text{Eq.1.1}$$

Notation for this matrix follows the convention by Craig (Craig, 2005). To fully describe an object in 3D space, a position of the object is also required to define its origin relative to the reference coordinate frame, defined by a position vector  $[P]$ . When the rotation matrix and position vector are combined together, the resulting matrix is referred to as a homogeneous transform or transformation matrix  $[T]$ . To maintain orthogonality, an additional placeholder row is added to the  $[T]$  matrix consisting of  $[0 \ 0 \ 0 \ 1]$  (Eq. 1.2) (Craig, 2005).

$${}^{Ref}_{Obj}[T]_{4 \times 4} = \begin{bmatrix} {}^{Ref}_{Obj}[R]_{3 \times 3} & {}^{Ref}[P]_{Obj,origin} \\ 0 & 0 & 0 & 1 \end{bmatrix} \quad \text{Eq. 1.2}$$

This matrix now contains all of the required information to completely describe an object's orientation and location in a reference frame.

There are a number of mathematical properties of the orthogonal transformation matrix that make it ideal for spinal kinematics. Transformation matrices can be easily manipulated to describe changes in the frame of reference. Multiplication of these matrices can be used to change the frame of reference of an object, essential for describing relative vertebral rotation. For example, to describe the motion of the C4 vertebra relative to the inferior C5 vertebra, where both have rigid body trackers affixed to the bony anatomy and anatomical frames have been defined relative to the respective trackers, the multiplication would be as follows:

$${}^{C5vertebra}_{C4vertebra}[T] = {}^{C5vertebra}_{C5tracker}[T] \ {}^{C5tracker}_{Camera}[T] \ {}^{Camera}_{C4tracker}[T] \ {}^{C4tracker}_{C4vertebra}[T] \quad \text{Eq. 1.3}$$

where  $[T]$  matrices of the tracker relative to the vertebra and vice verse come from the digitizing process.

### 1.4.3 VERTEBRAL ORIENTATION AND EULER ANGLES

To describe the orientation of a vertebra as well as how it changes over time, a set of three rotations can be used, similar to the aircraft dynamics terms of “yaw, pitch, and roll.” In the spine, the use of Euler angles is common for this purpose, providing a set of three sequential rotations where each rotation occurs about the previous axes. For example, Euler ZYX analysis would refer to an initial rotation about the *Z* axis, a subsequent rotation about the *Y* axis, followed by a rotation about the *X* axis (Figure 1.15). In terms of the spine, this could refer to an initial rotation about the flexion-extension axis, then lateral bending, followed by axial rotation to describe the 3D orientation of the vertebra. It should be noted the importance of the angle sequence, and the effect it has on orientation outcome. Crawford *et al.* performed an analysis of 12 permutations of angle sequence and found that the largest rotation should be completed first, with little effect afterwards (Crawford *et al.*, 1996).

The three angles themselves are then subsequently determined from the rotation matrix using basic trigonometry, depending on the sequence of angles used. This provides an easy method of describing the orientation of one vertebra relative to the next with only a single transformation matrix. As the transformation matrix changes over time as the bodies move, the angles can be easily determined (*i.e.*, how flexed is one vertebra compared to the adjacent). These are the standard techniques used to describe the spinal stability measures from Section 1.3.2 (*i.e.*, ROM and NZ).

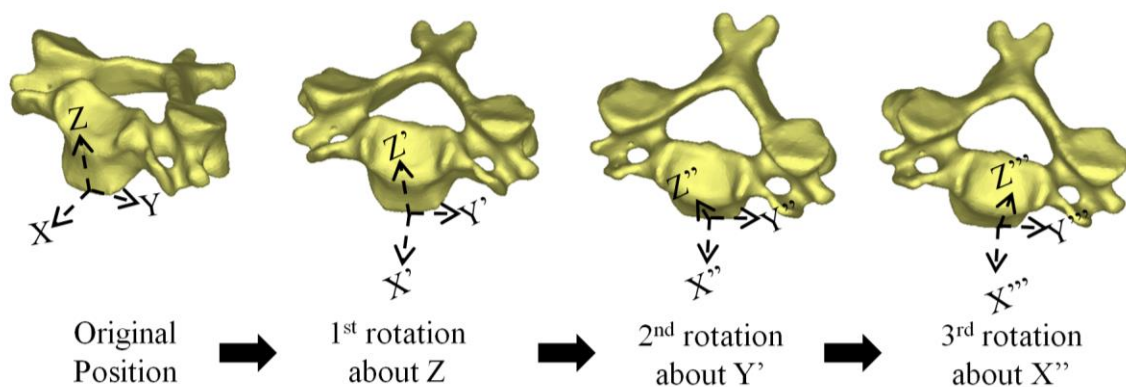


**Figure 1.15: Euler Angle Sequence**

Euler angle analysis considers the 3D orientation of an object, such as a vertebra, relative to a reference frame to occur as three successive rotations. In this case, each subsequent rotation occurs about an axis defined from the previous rotation. In the figure above, the orientation is described as an initial rotation about the Z axis, followed by a rotation about the Y' axis, and a final rotation again about the X'' axis. As such, this would be considered an Euler ZYX sequence.

#### 1.4.4 VERTEBRAL AXIS OF ROTATION AND THE FINITE HELICAL AXIS

When describing spinal kinematics, an important parameter to consider for spinal stability is the axis of rotation – in theory, a stable joint would have little deviation in its axis of rotation. This measure becomes even more important when spinal instrumentation is used and the spinal kinematics are altered. New technologies that attempt to restore intact kinematics, such as disc arthroplasty, need to consider how this parameter changes with *in vivo* implementation (Kowalczyk *et al.*, 2011).

To determine the axis of rotation, two static frames extracted from the motion are required. The most common technique is the use of the finite helical axis (FHA), also known as the screw displacement axis (SDA). These measures describe an axis about which an object rotates and along which it translates (Panjabi *et al.*, 1981). The parameters calculated from FHA algorithms are then the rotation ( $\Phi$ ) about the axis, translation ( $t$ ) along the axis, the axis direction vector ( $n$ ), and its intercept with the orthogonal planes ( $p$ ) (Figure 1.16).

In relation to joint mechanics, use of the finite helical axis has existed for some time (Dimnet *et al.*, 1982; Panjabi and White, 1971; Spoor and Veldpaus, 1980; Woltring *et al.*, 1985). One drawback to this technique identified early on was its susceptibility to stochastic error if calculated for a small rotation (Woltring *et al.*, 1985). The mathematics behind its use involves cosines, which for calculating small angles, can result in large errors if there is noise present. More recent studies identified that filtering could improve the technique to achieve a reasonable set of axes for rotations as small as  $0.5^\circ$  (Duck *et al.*, 2004). In the spine, the technique has been previously used (Panjabi and White, 1971); however, its mathematical implementation can be quite challenging and even more so for the clinical translation of these data. With the advances in computer power and increasing number of collaborations between engineers and surgeons, the FHA may become a crucial tool to describe spine stability in the lab and in the clinic (Kettler *et al.*, 2004; Metzger *et al.*, 2010). Efforts have been undertaken to improve understanding of how the FHA can be implemented in spinal kinematics (Crawford, 2006), while others have investigated the most accurate algorithm for FHA

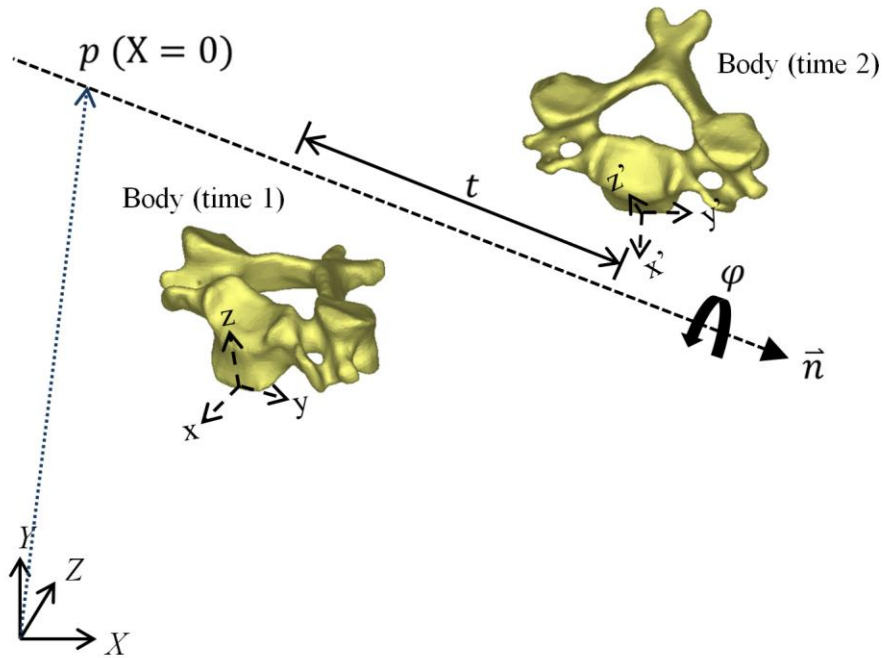


**Figure 1.16: Finite Helical Axis**

The finite helical axis describes a unique axis in space about which an object rotates ( $\Phi$ ) and along which it translates ( $t$ ) between two frames of motion. The axis is defined in space by a vector ( $n$ ) and an intercept ( $p$ ) with a plane of interest (as shown with YZ plane). This intercept is the centre of rotation in that plane.

calculation (Metzger *et al.*, 2010). Some studies have focused on improving the knowledge translation of the FHA through integration of the axis with medical imaging (Kettler *et al.*, 2004). Current implementation of this approach can be cumbersome and streamlining is required that is consistent with current tracking technology, such as six-DOF rigid body trackers. Furthermore, interpretation as a clinical measure for describing changes in kinematic stability requires further investigation to reduce the substantial knowledge of 3D algebra and spatial perception to comprehend its concepts.

### **1.4.5 VISUALIZATION METHODS**

In addition to quantifying cervical spine motion, qualitative description and visualization of the motion pathway of the vertebral body is also important. One method available to better visualize cervical anatomy is through the use of subject-specific, computerized bone models generated from CT scans of each specimen (Coffey *et al.*, 2012; Keefe *et al.*, 2009). Numerous software packages are now available, such as Mimics™ (Materialise, Leuven, Belgium), that are able to threshold standard CT image slices based on known bone densities into a 3D volume of the bony geometry.

## **1.5 THESIS RATIONALE**

The cervical spine relies on a complex interaction of osteoligamentous anatomy to both provide mobility and maintain stability. Unfortunately, these structures are prone to traumatic injury. Flexion-distraction injuries of the cervical spine encompass a range of instability that varies greatly depending on the pattern of injury produced, and only a small portion of this spectrum of this injury has been studied in detail. As surgical treatment is dependent on the severity of instability, the treatment for these injuries is also variable. Treatment algorithms have advanced to evidence-based methods, yet the evidence remains insufficient. Based upon a review of the current state of knowledge, it is clear further biomechanical investigation through dedicated evaluation of each injury mechanism and stage is required. Specifically, there is a lack of biomechanical investigations of injuries to the facet joint, including subluxation, facet perch, and facet fracture.

Biomechanical simulation of the spine has been a useful tool for improving the knowledge base surrounding cervical spine trauma and surgical treatment for the past thirty years, yet with the continued advances in surgical instrumentations, the assortment of surgical factors that are decided within the operating room, and the frequency of the these operations, more investigations are necessary. From a trauma standpoint, biomechanical simulation of traumatic injuries requires valid instability models – a fact that is generally not considered in surgical sectioning studies. Furthermore, the kinematics of the intact, instrumented, and injured spine are complex, yet the majority of studies only describe the most basic extent of motion (*i.e.*, ROM and NZ), where the pathology of the joint axis of rotation is not considered. Tools such as the FHA have only been preliminarily explored for this concept, yet may be challenging to implement and knowledge translation to the clinician remains an issue. Furthermore, the gold standard methodology for testing cervical spine stability has been pure bending moment using spinal loading simulators; however, whether this loading methodology is actually being created in all testing scenarios is poorly described (*i.e.*, what is the efficiency of the “pure” bending moment being applied?). Ultimately, the purpose of *in vitro* biomechanical studies is to provide the clinician with more evidence; as such, better interpretation and knowledge translation strategies may be required.

## 1.6 OBJECTIVES AND HYPOTHESES

The **overall objective** of this thesis was to investigate the changes in subaxial cervical spine kinematic stability with simulated flexion-distraction injuries and current surgical instrumentation techniques using appropriate biomechanical methods. This will be accomplished through the following **specific objectives**:

1. customize the original simulator design and introduce new motion capture tools for producing and tracking 3D cervical spine kinematics;
2. evaluate the change in kinematic stability of stage 1 flexion-distraction injuries in a multi-segment cervical spine before and after surgical fixation;
3. develop an experimental method that reliably produces a unilateral facet perch in cadaveric subaxial spinal segments based on a described dynamic mechanism of injury;

4. identify the associated soft tissue injuries associated with a unilateral facet perch, and use them to create a valid and repeatable standardized injury model;
5. define a simple and effective technique using six-DOF rigid body trackers to generate accurate FHAs that characterize 3D motion with applications in the cervical spine;
6. investigate the application of a mathematical technique combined with image segmentation to visualize and quantify changes in 3D spinal kinematics based on the FHAs generated;
7. examine the surgical factor of graft size height on ACDFP stability in simulated flexion-distraction injuries; and finally
8. further refine the spinal loading simulator by investigating the role of caudal end constraints and actuator control settings in producing pure bending moment loading.

The **hypotheses** of this work were:

1. the spinal loading simulator is capable of producing controlled flexion-extension, axial rotation, and lateral bending in intact, injured, and instrumented cervical motion segments;
2. sequential disruption of the posterior stabilizing structures of the unilateral facet complex will result in progressive increase in range of motion and neutral zone for simulated flexion-extension, axial rotation, and lateral bending;
3. posterior and anterior instrumentation will provide equivalent kinematic stability in the simulated isolated posterior column injury;
4. the spinal loading simulator can be configured to reproduce a described traumatic flexion-distraction injury mechanism for a unilateral facet perch/dislocation in cadaveric cervical motion segments;
5. dissection techniques will be able to ascertain the soft tissue damage present in a unilateral facet perch injury and consistent disruption trends will be observed;
6. a reliable technique can be developed to generate a large number of precise FHAs that describe the general 3D motion of an object;
7. changes in kinematic stability can be quantified by the generated FHAs of spinal motion;



8. in comparison to a graft size equivalent to the height of the disc space, ACDFP with an undersized graft will lead to poor soft tissue tensioning and therefore reduced stability in all motions, while an ACDFP with an oversized graft will be more stable as a result of the increased soft tissue tension; and finally,
9. the shear loads at the caudal end of the spinal motion segment can be eliminated through a combination of translational freedom and actuator control settings to ensure pure moment loading.

## 1.7 THESIS OVERVIEW

In addition to this introductory chapter, there are six additional chapters, five of which are based on experimental studies. Chapter 2 looks at the changes in kinematic stability of stage 1 flexion-distraction injuries and the surgical fixation options used to restore stability for bone-on-bone fusion. Chapter 3 simulates a more advanced unilateral facet perch injury and attempts to develop a standardized soft tissue injury based on a recognized pattern of tissue disruption. Chapter 4 examines the concept of the finite helical axis in detail to improve its accuracy and usability in quantifying changes in kinematic stability. Chapter 5 investigates the surgical factor of graft size height on ACDFP stability in the injury model developed in Chapter 3 and more advanced compounded flexion-distraction injuries. Chapter 6 considers that there is a lack of transparency in custom spinal loading simulators and that the loads at the caudal end need to be investigated and reported to ensure pure bending moment loading. Chapter 7 summarizes the overall outcomes of this body of work, its strengths and limitations, its relevance to the engineering and clinical communities, and potential future directions.

## 1.8 REFERENCES

- Aebi, M., Zuber, K., Marchesi, D., 1991. Treatment of cervical spine injuries with anterior plating. Indications, techniques, and results. *Spine* 16, S38–45.
- Allen, B.L., Ferguson, R.L., Lehmann, T.R., O'Brien, R.P., 1982. A mechanistic classification of closed, indirect fractures and dislocations of the lower cervical spine. *Spine* 7, 1–27.

An, H., Evanich, C., Nowicki, B., Haughton, V., 1993. Ideal thickness of Smith-Robinson graft for anterior cervical fusion: A cadaveric study with computed tomographic correlation. *Spine* 18, 2043–2047.

An, H., Gordin, R., Renner, K., 1991. Anatomic considerations for plate-screw fixation of the cervical spine. *Spine* 16, S548–551.

Anderson, P.A., Henley, M.B., Grady, M.S., Montesano, P.X., Winn, H.R., 1991. Posterior cervical arthrodesis with AO reconstruction plates and bone graft. *Spine* 16, S72–79.

Anderst, W., Baillargeon, E., Donaldson, W., 2011. Validation of a non-invasive technique to precisely measure in vivo three-dimensional cervical spine movement. *Spine* 36, 1–17.

Bauze, R., Ardran, G., 1978. Experimental production of forward dislocation in the human cervical spine. *Journal of Bone & Joint Surgery* 60-B, 239–245.

Beatson, T., 1963. Fractures and dislocations of the cervical spine. *Journal of Bone & Joint Surgery* 45-B, 21–35.

Bernhardt, P., Wilke, H.J., Wenger, K.H., Jungkunz, B., *et al.*, 1999. Multiple muscle force simulation in axial rotation of the cervical spine. *Clinical Biomechanics* 14, 32–40.

Beyer, C.A., Cabanela, M.E., Berquist, T.H., 1991. Unilateral facet dislocations and fracture-dislocations of the cervical spine. *Journal of Bone & Joint Surgery* 73-B, 977–981.

Bohlman, H., 1979. Acute fractures and dislocations of the cervical spine. An analysis of three hundred hospitalized patients and review of the literature. *Journal of Bone & Joint Surgery* 61-A, 1119–1142.

Bono, C.M., Schoenfeld, A., Rampersaud, R., Levi, A., *et al.*, 2011. Reproducibility of radiographic measurements for subaxial cervical spine trauma. *Spine* 36, 1374–1379.

Bozkus, H., Ames, C.P., Chamberlain, R.H., Nottmeier, E.W., *et al.*, 2005. Biomechanical analysis of rigid stabilization techniques for three-column injury in the lower cervical spine. *Spine* 30, 915–922.

Brodke, D.S., Klimo, P., Bachus, K.N., Braun, J.T., Dailey, A.T., 2006. Anterior cervical fixation: analysis of load-sharing and stability with use of static and dynamic plates. *Journal of Bone & Joint Surgery* 88-A, 1566–1573.

Brown, T., Reitman, C.A., Nguyen, L., Hipp, J.A., 2005. Intervertebral motion after incremental damage to the posterior structures of the cervical spine. *Spine* 30, E503–508.

Caspar, W., Barbier, D., Klara, P., 1989. Anterior cervical fusion and Caspar plate stabilization for cervical trauma. *Neurosurgery* 25, 491–502.

Cheng, B.C., Burns, P., Pirris, S., Welch, W.C., 2009. Load sharing and stabilization effects of anterior cervical devices. *Journal of Spinal Disorders & Techniques* 22, 571–577.

Coe, J.D., Warden, K.E., Sutterlin, C.E., McAfee, P.C., 1989. Biomechanical evaluation of cervical spinal stabilization methods in a human cadaveric model. *Spine* 14, 1122–1131.

Coffey, D., Korsakov, F., Ewert, M., Hagh-Shenas, H., *et al.*, 2012. Visualizing motion data in virtual reality: understanding the roles of animation, interaction, and static presentation. *Computer Graphics Forum* 31, 1215–1224.

Cooper, P.R., Cohen, A., Rosiello, A., Koslow, M., 1988. Posterior stabilization of cervical spine fractures and subluxations using plates and screws. *Neurosurgery* 23, 300–306.

Craig, J., 2005. *Introduction to robotics: mechanics and control*, 3rd edition. Pearson Prentice Hall, New Jersey, p. 19–45.

Crawford, N.R., 2006. Technical note: determining and displaying the instantaneous axis of rotation of the spine. *World Spine Journal* 1, 53–56.

Crawford, N.R., Brantley, A.G., Dickman, C.A., Koeneman, E.J., 1995. An apparatus for applying pure nonconstraining moments to spine segments in vitro. *Spine* 20, 2097–2100.

Crawford, N.R., Duggal, N., Chamberlain, R.H., Park, S.C., *et al.*, 2002. Unilateral cervical facet dislocation: injury mechanism and biomechanical consequences. *Spine* 27, 1858–1864.

Crawford, N.R., Yamaguchi, G.T., Dickman, C.A., 1996. Methods for determining spinal flexion/extension, lateral bending, and axial rotation from marker coordinate data: Analysis and refinement. *Human Movement Science* 15, 55–78.

Cunningham, B.W., Gordon, J.D., Dmitriev, A.E., Hu, N., McAfee, P.C., 2003. Biomechanical evaluation of total disc replacement arthroplasty: an in vitro human cadaveric model. *Spine* 28, S110–7.

Dimnet, J., Pasquet, A., Krag, M., Panjabi, M., 1982. Cervical spine motion in the sagittal plane: kinematic and geometric parameters. *Journal of Biomechanics* 15, 959–969.

Do Koh, Y., Lim, T.H., Won You, J., Eck, J., An, H.S., 2001. A biomechanical comparison of modern anterior and posterior plate fixation of the cervical spine. *Spine* 26, 15–21.

Duck, T.R., Ferreira, L.M., King, G.J.W., Johnson, J.A., 2004. Assessment of screw displacement axis accuracy and repeatability for joint kinematic description using an electromagnetic tracking device. *Journal of Biomechanics* 37, 163–167.

Duggal, N., Chamberlain, R.H., Park, S.C., Sonntag, V.K.H., *et al.*, 2005. Unilateral cervical facet dislocation: biomechanics of fixation. *Spine* 30, E164–168.

Dvorak, M.F., Fisher, C.G., Aarabi, B., Harris, M.B., *et al.*, 2007a. Clinical outcomes of 90 isolated unilateral facet fractures, subluxations, and dislocations treated surgically and nonoperatively. *Spine* 32, 3007–3013.

Dvorak, M.F., Fisher, C.G., Fehlings, M.G., Rampersaud, Y.R., *et al.*, 2007b. The surgical approach to subaxial cervical spine injuries: an evidence-based algorithm based on the SLIC classification system. *Spine* 32, 2620–2629.

Dvorak, M.F., Pitzen, T., Zhu, Q., Gordon, J.D., *et al.*, 2005. Anterior cervical plate fixation: a biomechanical study to evaluate the effects of plate design, endplate preparation, and bone mineral density. *Spine* 30, 294–301.

Fujiwara, A., Lim, T.H., An, H.S., Tanaka, N., *et al.*, 2000. The effect of disc degeneration and facet joint osteoarthritis on the segmental flexibility of the lumbar spine. *Spine* 25, 3036–3044.

Gay, R.E., Ilharreborde, B., Zhao, K., Zhao, C., An, K.-N., 2006. Sagittal plane motion in the human lumbar spine: comparison of the in vitro quasistatic neutral zone and dynamic motion parameters. *Clinical Biomechanics* 21, 914–919.

Gédet, P., Thistlethwaite, P.A., Ferguson, S.J., 2007. Minimizing errors during in vitro testing of multisegmental spine specimens: considerations for component selection and kinematic measurement. *Journal of Biomechanics* 40, 1881–1885.

Glaser, J.A., Jaworski, B.A., Cuddy, B.G., Albert, T.J., *et al.*, 1998. Variation in surgical opinion regarding management of selected cervical spine injuries. A preliminary study. *Spine* 23, 975–982.

Goel, V., Clark, C., McGowan, D., Goyal, S., 1984. An in-vitro study of the kinematics of the normal, injured and stabilized cervical spine. *Journal of Biomechanics* 17, 363–376.

Goel, V., Nye, T., Clark, C., Nishiyama, K., Weinstein, J., 1987. A technique to evaluate an internal spinal device by use of the Selspot system: an application to Luque closed loop. *Spine* 12, 150–159.

Goel, V.K., Liu, K., Clark, C.R., 1986. Quantitative geometry of the muscular origins and insertions of the human head and neck. In: In Sances, A. (Ed.), *Mechanisms of Head and Spine Trauma*. Alroy Publishers, New York.

Goertzen, D.J., Lane, C., Oxland, T.R., 2004. Neutral zone and range of motion in the spine are greater with stepwise loading than with a continuous loading protocol. An in vitro porcine investigation. *Journal of Biomechanics* 37, 257–261.

Hadra, B., 1891. Wiring the spinous processes in Pott's disease. *Journal of Bone & Joint Surgery* 207–210.

Henriques, T., Olerud, C., Bergman, A., Jónsson, H., 2004. Distractive flexion injuries of the subaxial cervical spine treated with anterior plate alone. *Journal of Spinal Disorders & Techniques* 17, 1–7.

Hibbeler, R., 2001. *Engineering mechanics. Statics, 9th edition*. Prentice-Hall, New Jersey, p. 193–238.

Holdsworth, F., 1970. Fractures, dislocations, and fracture-dislocations of the spine. *Journal of Bone & Joint Surgery* 45-B, 6–20.

Ianuzzi, A., Zambrano, I., Tataria, J., Ameerally, A., *et al.*, 2006. Biomechanical evaluation of surgical constructs for stabilization of cervical teardrop fractures. *The Spine Journal* 6, 514–523.

Ivancic, P.C., Pearson, A.M., Tominaga, Y., Simpson, A.K., *et al.*, 2008. Biomechanics of cervical facet dislocation. *Traffic injury prevention* 9, 606–611.

Jaumard, N. V., Welch, W.C., Winkelstein, B.A., 2011. Spinal facet joint biomechanics and mechanotransduction in normal, injury and degenerative conditions. *Journal of Biomechanical Engineering* 133, 1–31.

Johnson, M.G., Fisher, C.G., Boyd, M., Pitzen, T., *et al.*, 2004. The radiographic failure of single segment anterior cervical plate fixation in traumatic cervical flexion distraction injuries. *Spine* 29, 2815–2820.

Keefe, D.F., Ewert, M., Ribarsky, W., Chang, R., 2009. Interactive coordinated multiple-view visualization of biomechanical motion data. *IEEE Transactions on Visualization and Computer Graphics* 15, 1383–1390.

Kettler, A., Marin, F., Sattelmayer, G., Mohr, M., *et al.*, 2004. Finite helical axes of motion are a useful tool to describe the three-dimensional in vitro kinematics of the intact, injured and stabilised spine. *European Spine Journal* 13, 553–559.

Kirkpatrick, J.S., Levy, J.A., Carillo, J., Moeini, S.R., 1999. Reconstruction after multilevel corpectomy in the cervical spine. A sagittal plane biomechanical study. *Spine* 24, 1186–1190.

Kotani, Y., Cunningham, B.W., Abumi, K., McAfee, P.C., 1994. Biomechanical analysis of cervical stabilization systems. An assessment of transpedicular screw fixation in the cervical spine. *Spine* 19, 2529–2539.

Kowalczyk, I., Lazaro, B.C.R., Fink, M., Rabin, D., Duggal, N., 2011. Analysis of in vivo kinematics of 3 different cervical devices: Bryan disc, ProDisc-C, and Prestige LP disc. *Journal of Neurosurgery Spine* 15, 630–635.

- Kwon, B.K., Fisher, C.G., Boyd, M.C., Cobb, J., *et al.*, 2007. A prospective randomized controlled trial of anterior compared with posterior stabilization for unilateral facet injuries of the cervical spine. *Journal of Neurosurgery Spine* 7, 1–12.
- Kwon, B.K., Vaccaro, A.R., Grauer, J.N., Fisher, C.G., Dvorak, M.F., 2006. Subaxial cervical spine trauma. *Journal of the American Academy of Orthopaedic Surgeons* 14, 78–89.
- Lowery, D.W., Wald, M.M., Browne, B.J., Tigges, S., *et al.*, 2001. Epidemiology of cervical spine injury victims. *Annals of Emergency Medicine* 38, 12–16.
- Lysell, E., 1969. Motion in the cervical spine. An experimental study on autopsy specimens. *Acta Orthopaedica Scandinavica Suppl.* #123.
- Malik, S.A., Murphy, M., Connolly, P., O’Byrne, J., 2008. Evaluation of morbidity, mortality and outcome following cervical spine injuries in elderly patients. *European Spine Journal* 17, 585–591.
- McLachlin, S.D., 2008. *Design and Development of In Vitro Tools to Assess Fixation and Motion in the Spine*. Master’s Thesis, University of Western Ontario, London, ON, Canada, 1–114.
- Mercer, S., Bogduk, N., 1999. The ligaments and annulus fibrosus of human adult cervical intervertebral discs. *Spine* 24, 619–628.
- Metzger, M.F., Faruk Senan, N.A., O’Reilly, O.M., Lotz, J.C., 2010. Minimizing errors associated with calculating the location of the helical axis for spinal motions. *Journal of Biomechanics* 43, 2822–2829.
- Milby, A.H., Halpern, C.H., Guo, W., Stein, S.C., 2008. Prevalence of cervical spinal injury in trauma. *Neurosurgical Focus* 25, E10.
- Nakashima, H., Yukawa, Y., Ito, K., Machino, M., *et al.*, 2011a. Posterior approach for cervical fracture-dislocations with traumatic disc herniation. *European Spine Journal* 20, 387–394.
- Nakashima, H., Yukawa, Y., Ito, K., Machino, M., Kato, F., 2011b. Mechanical patterns of cervical injury influence postoperative neurological outcome: a verification of the allen system. *Spine* 36, E441–446.
- Nowinski, G.P., Visarius, H., Nolte, L.P., Herkowitz, H.N., 1993. A biomechanical comparison of cervical laminaplasty and cervical laminectomy with progressive facetectomy. *Spine* 18, 1995–2004.
- Oxland, T.R., Panjabi, M.M., 1992. The onset and progression of spinal injury: a demonstration of neutral zone sensitivity. *Journal of Biomechanics* 25, 1165–1172.

- Pal, G., Routal, R., Saggu, S., 2001. The orientation of the articular facets of the zygapophyseal joints at the cervical and upper thoracic region. *Journal of Anatomy* 198, 431–441.
- Pal, G., Sherk, H., 1988. The vertical stability of the cervical spine. *Spine* 13, 447–449.
- Panjabi, M., White, A., Johnson, R., 1975. Cervical spine mechanics as a function of transection of components. *Journal of Biomechanics* 8, 327–336.
- Panjabi, M., White, A.A., 1971. A mathematical approach for three-dimensional analysis of the mechanics of the spine. *Journal of Biomechanics* 4, 203–211.
- Panjabi, M.M., 1988. Biomechanical evaluation of spinal fixation devices: I. A conceptual framework. *Spine* 13, 1129–1134.
- Panjabi, M.M., Krag, M.H., Goel, V.K., 1981. A technique for measurement and description of three-dimensional six degree-of-freedom motion of a body joint with an application to the human spine. *Journal of Biomechanics* 14, 447–460.
- Panjabi, M.M., Oxland, T., Takata, K., Goel, V., *et al.*, 1993. Articular facets of the human spine. Quantitative three-dimensional anatomy. *Spine* 18, 1298–1310.
- Panjabi, M.M., Simpson, A.K., Ivancic, P.C., Pearson, A.M., *et al.*, 2007. Cervical facet joint kinematics during bilateral facet dislocation. *European Spine Journal* 16, 1680–1688.
- Papadakis, M., Sapkas, G., Papadopoulos, E.C., Katonis, P., 2011. Pathophysiology and biomechanics of the aging spine. *The Open Orthopaedics Journal* 5, 335–342.
- Patel, A.A., Hurlbert, R.J., Bono, C.M., Bessey, J.T., *et al.*, 2010. Classification and surgical decision making in acute subaxial cervical spine trauma. *Spine* 35, S228–234.
- Paxinos, O., Ghanayem, A.J., Zindrick, M.R., Voronov, L.I., *et al.*, 2009. Anterior cervical discectomy and fusion with a locked plate and wedged graft effectively stabilizes flexion-distraction stage-3 injury in the lower cervical spine: a biomechanical study. *Spine* 34, E9–15.
- Penning, L., 1978. Normal movements of the cervical spine. *American Journal of Roentgenology* 130, 317–326.
- Pitzen, T., Lane, C., Goertzen, D., Dvorak, M., *et al.*, 2003. Anterior cervical plate fixation: biomechanical effectiveness as a function of posterior element injury. *Journal of Neurosurgery Spine* 99, 84–90.
- Rabb, C.H., Lopez, J., Beauchamp, K., Witt, P., *et al.*, 2007. Unilateral cervical facet fractures with subluxation: injury patterns and treatment. *Journal of Spinal Disorders & Techniques* 20, 416–422.

Reeves, N.P., Narendra, K., Cholewicki, J., 2007. Spine stability: the six blind men and the elephant. *Clinical Biomechanics* 22, 266–274.

Roaf, R., 1960. A study of the mechanics of spinal injuries. *Journal of Bone & Joint Surgery* 42-B, 810–823.

Rogers, W., 1942. Treatment of fracture-dislocation of the cervical spine. *Journal of Bone & Joint Surgery* 24-A, 245–258.

Rorabeck, C., Rock, M., Hawkins, R., Bourne, R., 1987. Unilateral facet dislocation of the cervical spine. An analysis of the results of treatment in 26 patients. *Spine* 12, 23–27.

Roy-Camille, R.R., Sailant, G., Mazel, C., 1989. *Internal fixation of the unstable cervical spine by posterior osteosynthesis with plate and screws. Cervical Spine Research Society, 2nd edition, The Cervical Spine*. Lippincott: Philadelphia, 390–404.

Schulze, M., Hartensuer, R., Gehweiler, D., Hölscher, U., *et al.*, 2012. Evaluation of a robot-assisted testing system for multisegmental spine specimens. *Journal of Biomechanics* 45, 1457–1462.

Sim, E., Vaccaro, A.R., Berzlanovich, A., Schwarz, N., Sim, B., 2001. In vitro genesis of subaxial cervical unilateral facet dislocations through sequential soft tissue ablation. *Spine* 26, 1317–1323.

Small, C.F., Bryant, J.T., Pichora, D.R., 1992. Rationalization of kinematic descriptors for three-dimensional hand and finger motion. *Journal of Biomedical Engineering* 14, 133–141.

Smith, G., Robinson, R., 1958. The treatment of certain cervical-spine disorders by anterior removal of the intervertebral disc and interbody fusion. *Journal of Bone & Joint Surgery* 40-A, 607–624.

Song, K.-J., Lee, K.-B., 2008. Anterior versus combined anterior and posterior fixation/fusion in the treatment of distraction-flexion injury in the lower cervical spine. *Journal of Clinical Neuroscience* 15, 36–42.

Spoor, C., Veldpaus, F., 1980. Rigid body motion calculated from spatial co-ordinates of markers. *Journal of Biomechanics* 13, 391–393.

Vaccaro, A., Balderston, R., 1997. Anterior plate instrumentation for disorders of the subaxial cervical spine. *Clinical Orthopaedics and Related Research* 335, 112–121.

Vaccaro, A.R., Hulbert, R.J., Patel, A.A., Fisher, C., *et al.*, 2007. The subaxial cervical spine injury classification system: a novel approach to recognize the importance of morphology, neurology, and integrity of the disco-ligamentous complex. *Spine* 32, 2365–2374.



Wheeler, D.J., Freeman, A.L., Ellingson, A.M., Nuckley, D.J., *et al.*, 2011. Inter-laboratory variability in in vitro spinal segment flexibility testing. *Journal of Biomechanics* 44, 2383–2387.

White, A.A., Johnson, R.M., Panjabi, M.M., Southwick, W.O., 1975. Biomechanical analysis of clinical stability in the cervical spine. *Clinical Orthopaedics and Related Research* (109), 85–96.

White, A.A., Panjabi, M.M., 1990. *Clinical Biomechanics of the Spine, 2nd edition*. Lippincott Williams & Wilkins, Philadelphia, p. 1–125.

Wilke, H.J., Claes, L., Schmitt, H., Wolf, S., 1994. A universal spine tester for in vitro experiments with muscle force simulation. *European Spine Journal* 3, 91–97.

Wilke, H.J., Wenger, K., Claes, L., 1998. Testing criteria for spinal implants: recommendations for the standardization of in vitro stability testing of spinal implants. *European Spine Journal* 7, 148–154.

Woltring, H., Huiskes, R., De Lange, A., 1985. Finite centroid and helical axis estimation from noisy landmark measurements in the study of human joint kinematics. *Journal of Biomechanics* 18, 379–389.

Woodworth, R.S., Molinari, W.J., Brandenstein, D., Gruhn, W., Molinari, R.W., 2009. Anterior cervical discectomy and fusion with structural allograft and plates for the treatment of unstable posterior cervical spine injuries. *Journal of Neurosurgery Spine* 10, 93–101.

Zdeblick, T., Ducker, T., 1991. The use of freeze-dried allograft bone for anterior cervical fusions. *Spine* 16, 726–729.

Zdeblick, T.A., Abitbol, J.J., Kunz, D.N., McCabe, R.P., Garfin, S., 1993. Cervical stability after sequential capsule resection. *Spine* 18, 2005–2008.

Zdeblick, T.A., Zou, D., Warden, K.E., McCabe, R., *et al.*, 1992. Cervical stability after foraminotomy. A biomechanical in vitro analysis. *Journal of Bone & Joint Surgery* 74-A, 22–27.

## CHAPTER 2: THE KINEMATIC STABILITY OF STAGE 1 FLEXION-DISTRACTION INJURIES OF THE CERVICAL SPINE BEFORE AND AFTER INSTRUMENTED FIXATION

***OVERVIEW:** This chapter is the first in a series of studies investigating the kinematic stability of a spectrum of unilateral facet injuries in the subaxial cervical spine. The initial injury investigated is the most benign of the described stages in the flexion-distraction mechanism, isolated soft tissue disruption of the posterior elements. This was also the first study to use the custom-designed spinal loading simulator, as well as the incorporation of a new Optotrak Certus® tracking system. The format follows a typical manuscript style of Introduction, Methods, Results, and Discussion.*<sup>3</sup>

### 2.1 INTRODUCTION

Within the flexion-distraction mechanism, Allen *et al.* classified the resulting subaxial cervical spine injuries into four stages of increasing injury severity, where a stage 1 injury was defined as failure of the posterior ligamentous complex (Allen *et al.*, 1982). Clinically, these isolated posterior soft tissue injuries may also include minimally displaced facet fractures. Previous biomechanical studies have examined the stability provided by the posterior structures in the subaxial spine in the context of: sectioning studies of the soft tissues, posterior laminectomy, and in advanced stages of flexion-distraction injuries (Brown *et al.*, 2005; Crawford *et al.*, 2002; Goel *et al.*, 1984; Panjabi *et al.*, 1975; Sim *et al.*, 2001; Zdeblick *et al.*, 1993, 1992). While these studies begin to address the stabilizing role of the posterior elements, they are, for the most part, not applicable to the stability present following a traumatic stage 1 flexion-distraction injury.

---

<sup>3</sup> This chapter is adapted from two manuscripts: (1) Rasoulinejad P, McLachlin SD, Bailey SI, Gurr KR, Bailey CS, Dunning CE. The importance of the posterior osteoligamentous complex to subaxial cervical spine stability in relation to a unilateral facet injury. *Spine J.* 2012; 12(7): 590-595 and (2) McLachlin SD, Rasoulinejad P, Bailey SI, Gurr KR, Bailey CS, Dunning CE. Anterior versus Posterior Fixation for an Isolated Posterior Facet Complex Injury in the Subaxial Cervical Spine. In Revision with *Journal of Neurosurgery Spine*, February 2013.

In fact, there is a specific lack of biomechanical understanding of the stability of these injuries under the normal motions of the cervical spine and, as such, has most likely led to the controversy surrounding the most appropriate course of treatment (Nassr *et al.*, 2008).

Despite their relatively benign appearance, it is generally recommended that facet fractures be treated surgically (Allen *et al.*, 1982; Dvorak *et al.*, 2007a; Glaser *et al.*, 1998). Both anterior and posterior internal fixation, as well as a combined approach, have been advocated (Aebi *et al.*, 1991; Anderson *et al.*, 1991; Brodke *et al.*, 2003; Cooper *et al.*, 1988; Henriques *et al.*, 2004; Kwon *et al.*, 2007; McNamara *et al.*, 1991; Rabb *et al.*, 2007; Song and Lee, 2008; Woodworth *et al.*, 2009); however, there has been little biomechanical evidence to date to assist the decision making process (Dvorak *et al.*, 2007b). While numerous retrospective clinical reviews have shown the efficacy of the anterior plating approach in treating isolated posterior injuries (Henriques *et al.*, 2004; Rabb *et al.*, 2007; Woodworth *et al.*, 2009), others have found the fixation to be less successful in cases with associated facet fractures (Johnson *et al.*, 2004). In terms of biomechanical studies, most have generally found posterior instrumentation more effective than anterior fixation at reducing the range of motion of the injured motion segment (Bozkus *et al.*, 2005; Do Koh *et al.*, 2001; Duggal *et al.*, 2005; Kotani *et al.*, 1994; Pitzen *et al.*, 2003). However, to the author's knowledge, no known study has specifically examined the biomechanical stability of anterior versus posterior fixation for an isolated posterior facet complex injury in association with a facet fracture and, as such, has limited the effectiveness of developing an appropriate treatment algorithm for this type of injury.

The purpose of this chapter was two-fold. The first objective was to quantify the increase in motion produced following sequential disruption of the posterior osteoligamentous structures (*i.e.*, stage 1 injury) based on applying simulated flexion-extension, axial rotation, and lateral bending. The second objective was to compare the effectiveness of three instrumentation techniques (anterior, posterior, and combined instrumentation) in reducing ROM from the injured state.

## 2.2 MATERIALS AND METHODS<sup>4</sup>

Eight fresh-frozen cadaveric C2-C5 cervical spines (mean age: 68±9 years) were cleaned of musculature without disruption of ligaments, bones, and disc tissue. Fluoroscopy was utilized to ensure specimen integrity. Each specimen was potted using Denstone™ cement (Heraeus Kulzer Inc., South Bend, IN) within 1” sections of 4” diameter PVC piping. To improve fixation to the cement, additional screws were inserted into the C2 and C5 vertebrae that then extended into the cement (Bozkus *et al.*, 2005; Crawford *et al.*, 2002). Laser levels were used to ensure that the C3-C4 disc spaced remained horizontal as the cement cured (Wilke *et al.*, 1998). Due to the lengthy time required for preparation and potting, the specimens were re-frozen and thawed at a later date for testing. Repeated freezing and thawing has been shown to have little effect on the biomechanical properties of the spine (Hongo *et al.*, 2008).

A custom-developed spinal loading simulator, capable of applying independent flexion-extension, lateral bending, and axial rotation to the spine, was used in this study (see Figure 1.13). Its design was based on an existing materials testing machine (Instron 8874, Canton, MA) that applied non-destructive bending moments to the cranial potting fixture (C2), while the caudal end (C5) remained fixed to the testing platform. The telescoping, ball spline loading arms were connected to the cranial fixture and actuator via universal joints to allow for unconstrained specimen motion (*i.e.*, five-DOF) (Figure 2.1). The axial loading arm (top) was set to hold no load, removing the weight of the metal fixture, loading arm, and counterbalance from the specimen during testing. Furthermore, the original caudal potting fixture was modified from its original metal box design to a more versatile custom-clamping system, which allowed for the curvature of the spine to be adjusted using fixed-angle wedges. The addition of a fixed angle wedge was initially investigated; but, with little effect seen, it was not included in this work.

Upgrading from the original 2D tracking system used to evaluate the original simulator design (see Section 1.3.1.1), 3D spinal kinematics were captured in this study

---

<sup>4</sup> A detailed version of the step-by-step for the general testing protocol is found in Appendix B.

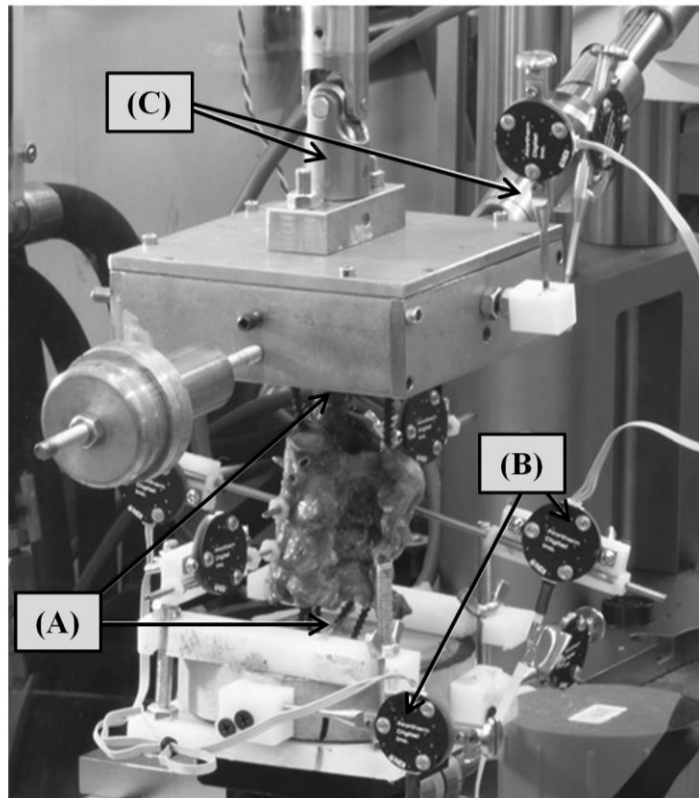


**Figure 2.1: Simulator and Tracker Setup for Multi-segment Cervical Spine**

(A) C2-C5 cadaver specimens were fixed at the cranial and caudal ends in the simulator. (B) Spinal motion was tracked using Optotrak Smart Markers®. (C) Two telescoping ball spline loading arms with universal joints at each end were connected to the cranial fixture to apply bending moments to the specimen.

using a newly-acquired Optotrak® Certus tracking system and First Principles™ software (NDI, Waterloo, ON, Canada) (Figure 2.2A). The rigid body trackers used were Optotrak® Smart Markers, which consist of three infrared markers (Figure 2.2B). Trackers were connected to the vertebrae either along Kirschner (K) wires for the exposed C3 and C4 vertebrae or to the cranial and caudal potting fixtures for the C2 and C5 vertebrae. The original tracker backing and pin (“Orthopaedic Research Pin” style) was found cumbersome and ineffective for the cervical spine. As such, they were modified to custom plastic backings connected to long, threaded Kirschner (K) wires. Due to the limited size and surrounding ligaments of the cervical vertebrae, insertion of the K wire was challenging to achieve adequate fixation to the bone and limit soft tissue disruption. Two successful trajectories were found that maintained marker visibility and accommodated the required 90° orientation change for shifting from flexion-extension to lateral bending: 1) an anterior-posterior direction through the vertebral body, lateral to the anterior longitudinal ligament, and 2) laterally through the vertebral body, just anterior to the posterior longitudinal ligament. Furthermore, the locations of specific anatomic landmarks were digitized relative to the tracker location in order to create a local anatomic coordinate system on each vertebra. Using a custom digitizing wand, the anatomic landmarks recorded were: the superior and inferior points of the anterior midline of the vertebral body and the most lateral points of the left and right transverse processes. Coordinate systems constructed from the points had positive axes directed anterior (X axis), left lateral (Y axis) and superior (Z axis), and an origin at the inferior point of the midline of the vertebral body (Wilke *et al.*, 1998).

For all steps of the protocol, loading was applied at 3°/s up to the target load of  $\pm 1.5\text{Nm}$  for flexion-extension, lateral bending, and axial rotation with tracker data captured at 60Hz. Each motion trial was repeated for three cycles using the final cycle for data analysis (Crawford *et al.*, 2002; Dvorak *et al.*, 2005; Wilke *et al.*, 1998). Initially, kinematic data was collected with all ligamentous, capsular, and bony structures intact as a baseline measure for each of the three movements. Data was then re-captured after each stage of a sequential posterior disruption of the C3-C4 level which occurred in the following order: (1) posterior ligament complex (PLC) disruption (supraspinous, interspinous, and all of ligamentum flavum), (2) facet capsular (FC) disruption,

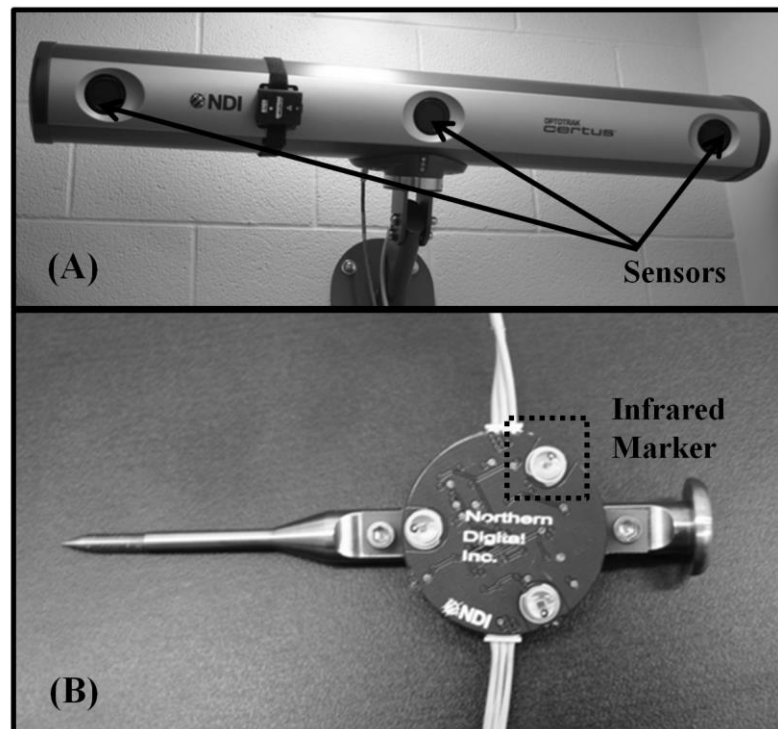


**Figure 2.2: Optotrak® Certus and Smart Marker**

(A) An Optotrak Certus® motion tracking system was used to capture the induced spinal kinematics in this study (and subsequent chapters). The system consists of three camera sensors, which are used to identify the 3D location (*i.e.*, X, Y, and Z positions) of infrared markers in its visible capture volume. (B) The rigid body trackers were the prepackaged Optotrak® Smart Markers, which consist of three infrared markers used to output six-DOF pose information of the tracker (*i.e.*, three rotations and three translations).

(3) progressive resection of the inferior articular process of C3 by one-half, and finally (4) complete resection of the inferior articular process of C3 (Figure 2.3). The resections of the inferior articular process of C3 attempt to simulate a unilateral facet fracture. Capsular and bony injuries were only created in the left facet for all specimens. To maintain hydration, normal saline was applied throughout the testing period.

Following testing of the intact and injured states, the specimen was removed from the simulator to insert instrumentation for the three surgical fixation methods (applied sequentially). Posterior instrumentation, which consisted of a lateral mass screw and rod system (Oasys® posterior cervical system; Stryker Spine, Allendale, NJ, USA), was inserted and tested first since no further specimen disruption was required for this technique (as opposed to a discectomy required for the anterior stabilization). The screws were inserted bilaterally into the lateral masses of C2 and C4, as the C3 facetectomy inhibited local fixation (Figure 2.4A). After testing of this construct was completed, the rods of the posterior instrumentation were removed to disable fixation and the anterior instrumentation (screw and plate system; Atlantis®, Medtronic Sofamor Danek, Minneapolis, MN, USA) followed. Anterior instrumentation always followed the posterior testing, as this anterior approach required the additional injury of a discectomy. The approach spared the posterior longitudinal ligament, and involved the insertion of an appropriately sized and shaped bone graft into the disc space. The anterior cervical plate system was then fixated to the C3 and C4 vertebrae and tested under the three simulated motions (Figure 2.4B). Finally, the combined effect of posterior and anterior instrumentation was examined by reconnecting the posterior rods to the lateral mass screws, and repeating the loading protocol.

Post-hoc analysis of the kinematic data generated was performed using custom-written LabVIEW™ software (National Instruments, Austin, TX, USA) and Euler ZYX angle algorithms (Wilke *et al.*, 1998) (see Appendix C). For the intact and injured states, parameters of interest included the magnitudes of overall (C2-C5) ROM and NZ and the segmental (*i.e.*, C2-C3, C3-C4, and C4-C5) ROM. The NZ measurement for each movement was defined as the width the hysteresis curve at  $\pm 0.2\text{Nm}$  (Figure 2.5) (Dvorak *et al.*, 2003). For ROM, separate analyses were conducted for the three movements



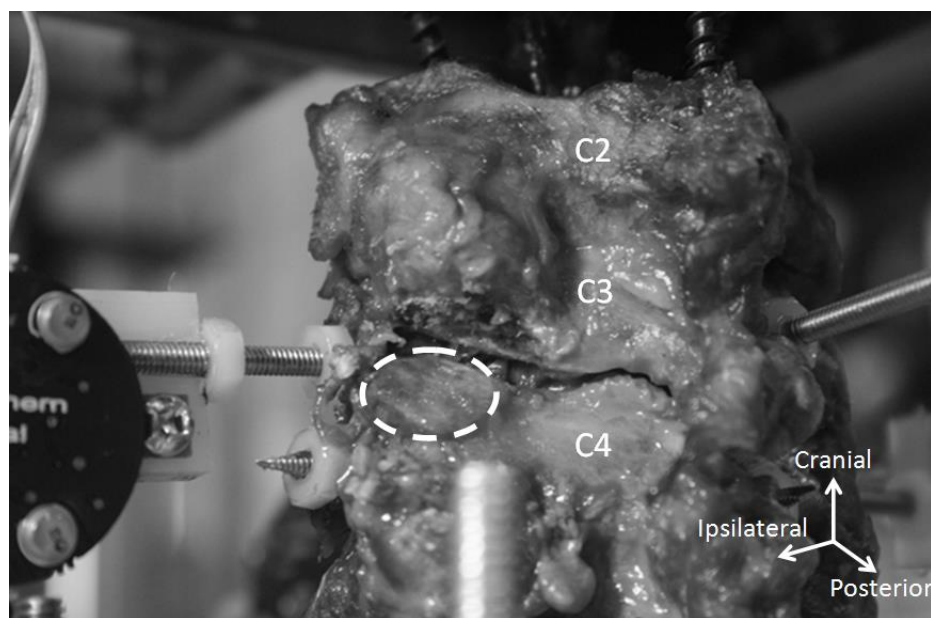


**Figure 2.3: Simulated Facet Fracture**

This photo shows a close-up of the complete bony facet removal injury (inferior articular process of superior vertebrae). This was the final injury step following removal of the posterior ligament complex and facet capsule. All bony facet resections were completed on the left side of each specimen.

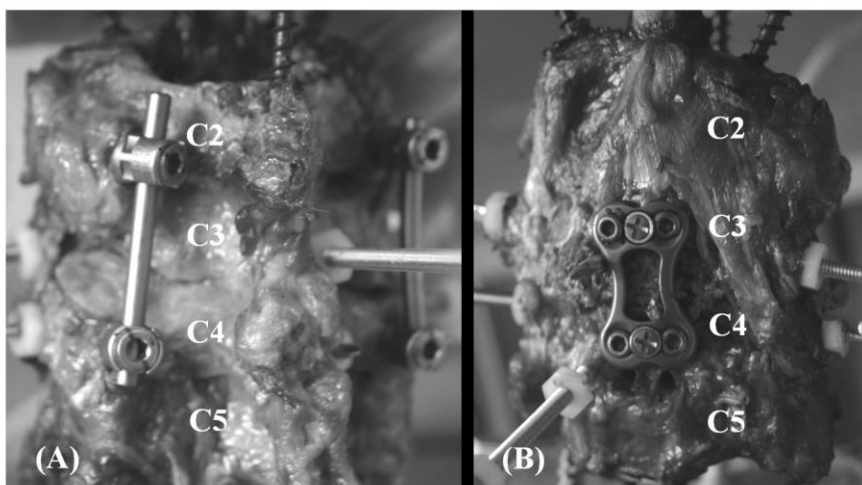


**Figure 2.4: Posterior and Anterior Instrumentation**

(A) Posterior instrumentation (screw/rod) inserted across C2-C4 as a result of the removed C3 left articular process. (B) Anterior instrumentation (screw/plate) inserted across C3-C4 after removal of the anterior longitudinal ligament and insertion of the bone graft into the disc space.

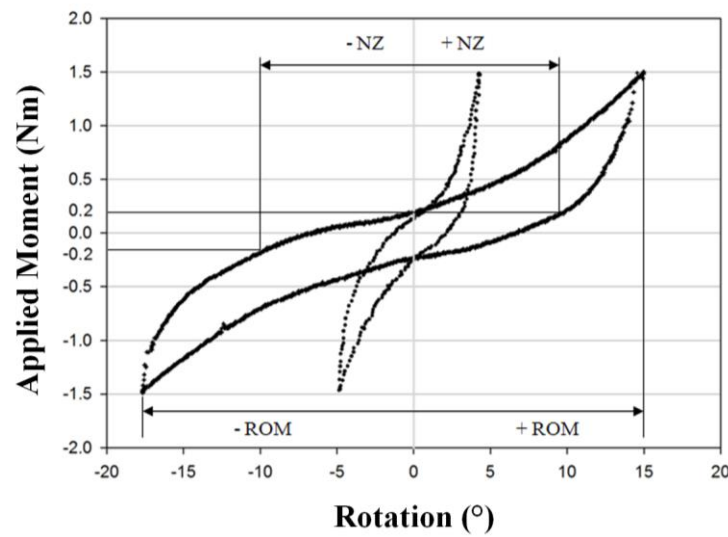


**Figure 2.5: Hysteresis Curve for Overall and Segmental Kinematics**

The kinematic parameters used in this study include range of motion (ROM) and neutral zone (NZ) between  $\pm 0.2\text{Nm}$ . Both of these parameters were collected from the overall motion across multiple segments (C2-C5) (shown in the larger curve for axial rotation). Segmental ROM (*i.e.*, C3-C4) was also analyzed based on the smaller dotted curve.

(flexion-extension, lateral bend, and axial rotation). In each case, two-way repeated measures analyses of variance (rmANOVA) were used to examine the effects of movement direction (*e.g.*, in the axial plane, rotating away (contralateral) or towards (ipsilateral) the injury site) and injury pattern. These were followed by post-hoc Student-Newman-Keuls (SNK) tests ( $\alpha=0.05$ ). Statistical analysis of NZ was performed using one-way rmANOVA with a factor of injury stage alone. This was also followed by pairwise comparisons using post-hoc SNK tests ( $\alpha=0.05$ ). To represent the clinical goal of achieving spinal fusion, the instrumentation was compared based on the percent reduction in C3-C4 ROM from the final injury state for the three instrumentations, where a 100% percent reduction would mean that there was zero ROM at that level and 0% represents no decrease in motion from the injured state. Statistical tests were performed using a one-way repeated measures analyses of variance (factor = fixation method) and post-hoc SNK tests ( $\alpha=0.05$ ).

## 2.3 RESULTS<sup>5</sup>

### 2.3.1 OVERALL INTACT AND INJURED KINEMATICS (C2-C5)

Differences were identified in both the ROM (Table 2.1) and NZ (Table 2.2). There was an effect of injury stage on the magnitude of the NZ for all three movements; flexion-extension ( $p=0.001$ ) and axial rotation ( $p<0.001$ ), and lateral bend ( $p=0.027$ ) (Figure 2.6). Within flexion-extension, the intact state was different from all injury patterns ( $p<0.05$ ); without significant changes between injuries. In axial rotation, the intact and PLC disrupted states were not different from one another ( $p>0.05$ ), but intact was different from all the other injury states ( $p<0.05$ ). While the FC cut was not different from the PLC disruption, bony resection for both the half and full cut increased NZ beyond the PLC value ( $p<0.05$ ). Finally, the complete bony facet removal further increased the NZ compared to the FC cut ( $p<0.05$ ). For the lateral bend NZ, there was only an increase seen when the intact state was compared to the complete bony facet removal ( $p<0.05$ ).

---

<sup>5</sup> Tabulated ROM and NZ data for all tested specimens is found in Appendix D

**Table 2.1: Average ( $\pm$  SD) C2-C5 ROM ( $^{\circ}$ ) for Each Simulated Motion**

<b>Injury Status</b>	<b>Flexion</b>	<b>Extension</b>	<b>Ipsilateral Axial Rotation</b>	<b>Contra. Axial Rotation</b>	<b>Ipsilateral Lateral Bend</b>	<b>Contra. Lateral Bend</b>
Intact	$4.7 \pm 1.2$	$4.3 \pm 1.1$	$9.3 \pm 2.8$	$11.4 \pm 3.2$	$5.5 \pm 1.1$	$4.9 \pm 1.0$
PLC cut	$4.9 \pm 1.3$	$4.6 \pm 1.2$	$10.3 \pm 3.2$	$11.9 \pm 3.7$	$5.6 \pm 1.5$	$5.2 \pm 1.0$
FC cut	$4.9 \pm 1.3$	$4.6 \pm 1.4$	$10.8 \pm 3.4$	$12.7 \pm 4.4$	$6.0 \pm 1.8$	$5.0 \pm 0.8$
1/2 facet	$5.0 \pm 1.4$	$4.8 \pm 1.3$	$11.5 \pm 4.3$	$13.2 \pm 4.2$	$6.2 \pm 1.9$	$5.0 \pm 1.0$
Full facet	$4.9 \pm 1.3$	$4.9 \pm 1.4$	$12.3 \pm 4.5$	$14.5 \pm 4.1$	$5.7 \pm 1.7$	$5.9 \pm 1.3$

***Note:** For axial rotation and lateral bending, motion towards the injured side was considered ipsilateral and towards the opposite side as contralateral (contra).*

**Table 2.2: Average ( $\pm$  SD) C2-C5 NZ ( $^{\circ}$ ) for Each Simulated Motion**

<b>Injury Status</b>	<b>Flexion-Extension</b>	<b>Axial Rotation</b>	<b>Lateral Bend</b>
Intact	$1.3 \pm 0.4$	$9.0 \pm 2.6$	$1.2 \pm 0.3$
PLC cut	$1.3 \pm 0.4$	$9.6 \pm 3.1$	$1.2 \pm 0.3$
FC cut	$1.4 \pm 0.4$	$10.4 \pm 3.8$	$1.2 \pm 0.3$
1/2 facet	$1.4 \pm 0.4$	$10.9 \pm 4.2$	$1.2 \pm 0.3$
Full facet	$1.4 \pm 0.4$	$11.6 \pm 4.1$	$1.3 \pm 0.4$

***Note:** NZ was measured as the width of the hysteresis width at  $\pm 0.2\text{Nm}$ .*

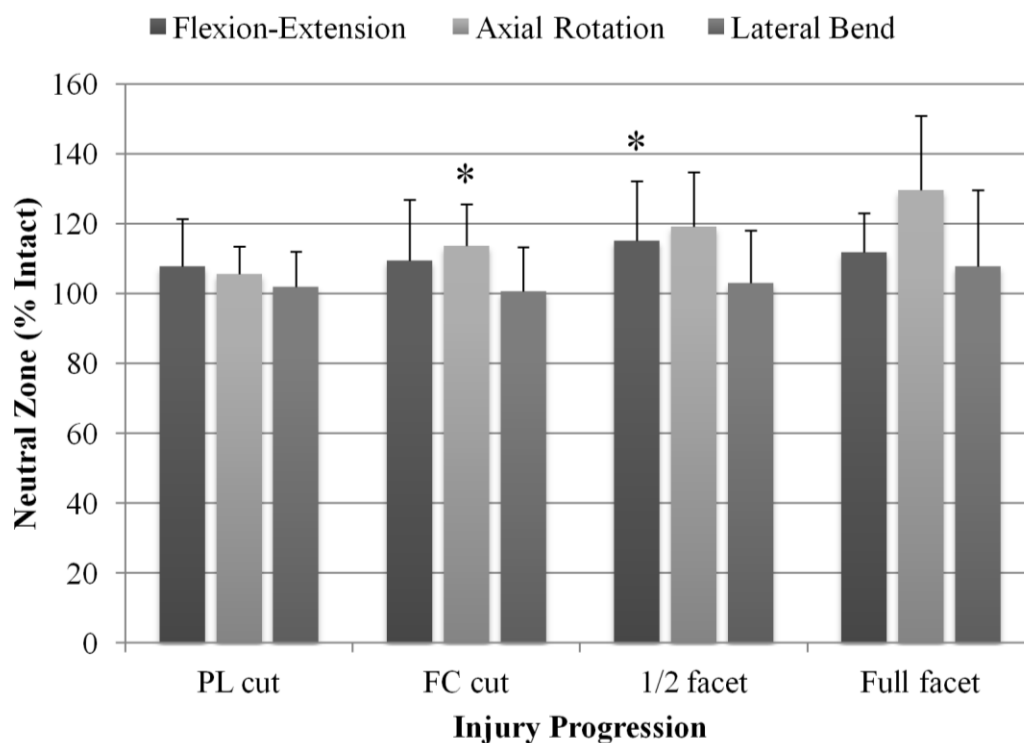


**Figure 2.6: Neutral Zone for Simulated Motions with Posterior Injury Progression**

This graph shows the overall NZ data, for all three simulated motions (*i.e.*, flexion-extension, axial rotation, and lateral bend), averaged over the eight specimens as a percentage of the intact NZ for the progressive injury pattern. There was an increase for flexion-extension following the half bony facet cut and for axial rotation following the facet capsule removal ( $p < 0.05$ ). There was no change in the lateral bend data. The asterisks represent where a significant increase occurred ( $p < 0.05$ ).

For ROM, the two-way repeated measures ANOVA showed a difference for movement direction in axial rotation only ( $p=0.04$ ), with more contralateral rotation than ipsilateral. There was also an effect of the injury state on flexion-extension ( $p<0.001$ ), axial rotation ( $p<0.001$ ) and lateral bend ( $p<0.001$ ). The flexion-extension ROM in the intact state was less than all other stages tested ( $p<0.05$ ). Additional removal of the bony facet increased flexion-extension ROM compared to sectioning of the PLC ( $p<0.05$ ), with complete bony facet removal providing a further increase compared to the FC cut ( $p<0.05$ ). ROM during axial rotation increased following removal of the facet capsule over the intact state ( $p<0.05$ ). With bony facet involvement, further increases in ROM were seen with full facet being different from all other states and half facet resection being different from the intact and PLC cut ( $p<0.05$ ). In terms of the lateral bend ROM, the only states that were not different from one another were sectioning of the PLC and FC ( $p>0.05$ ).

### **2.3.2 SEGMENTAL INTACT AND INJURED KINEMATICS**

For the analysis of the individual motion segments (C2-C3, C3-C4, C4-C5) in isolation, only ROM and not NZ was considered. At the level of the injury (*i.e.*, C3-C4), there was an overall effect of injury state in flexion-extension ( $p<0.001$ ), axial rotation ( $p<0.001$ ) and lateral bend ( $p<0.001$ ), but no difference in movement direction ( $p>0.05$ ). Within flexion-extension, ROM was less for the intact stage compared to all other injury stages ( $p<0.05$ ) without further significant increases between injury stages (Figure 2.7). Identical results were found for applied axial rotation; however, there was also a further increase in ROM following complete inferior articular process removal compared to all other injury states ( $p<0.05$ ) (Figure 2.8). Lateral bend ranges of motion were not different between the intact and PL cut stages ( $p>0.05$ ) and both were less than all other stages ( $p<0.05$ ). With complete inferior articular process removal, there was a further significant increase in ROM when compared to the FC cut and half bony resection stages ( $p<0.05$ ) (Figure 2.9).

For the segments above and below the injury (*i.e.*, C2-C3 and C4-C5) there was no effect of the movement direction performed and an effect of injury pattern for axial rotation only ( $p=0.03$ ). In these cases, the final (full inferior articular process removal)

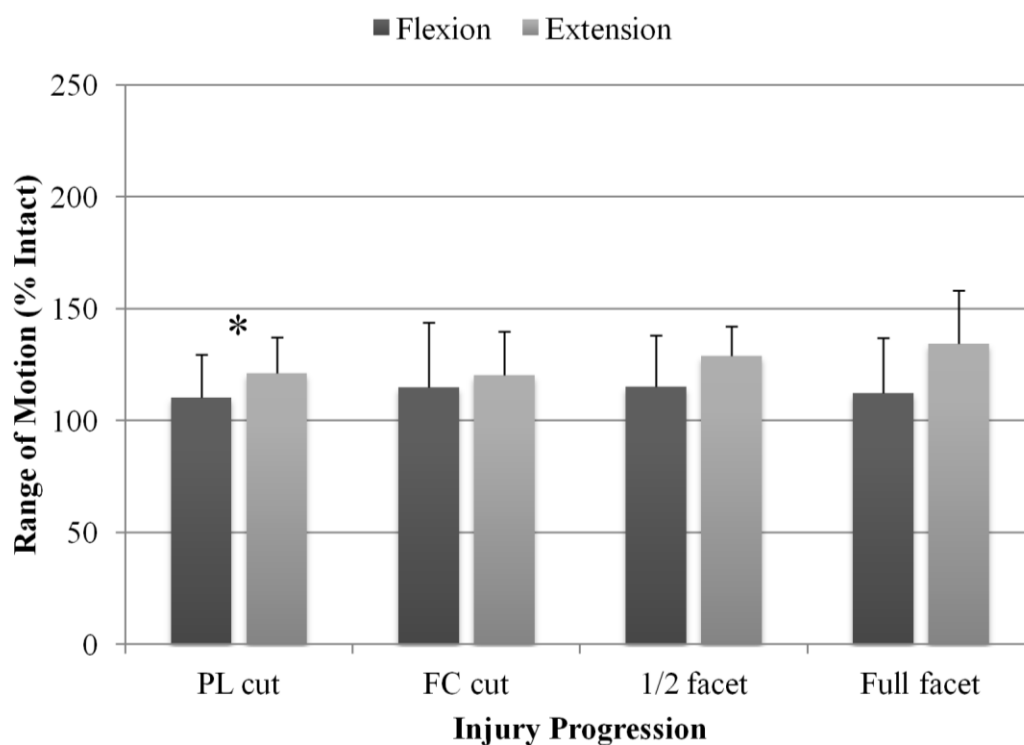


**Figure 2.7: C3-C4 Flexion-Extension ROM with Posterior Injury Progression**

This graph shows the flexion-extension ROM data averaged over the eight specimens as a percentage of the intact ROM for the progressive injury pattern. There was an increase in flexion-extension following the posterior ligament complex removal ( $p < 0.05$ ), with no change with further injury.



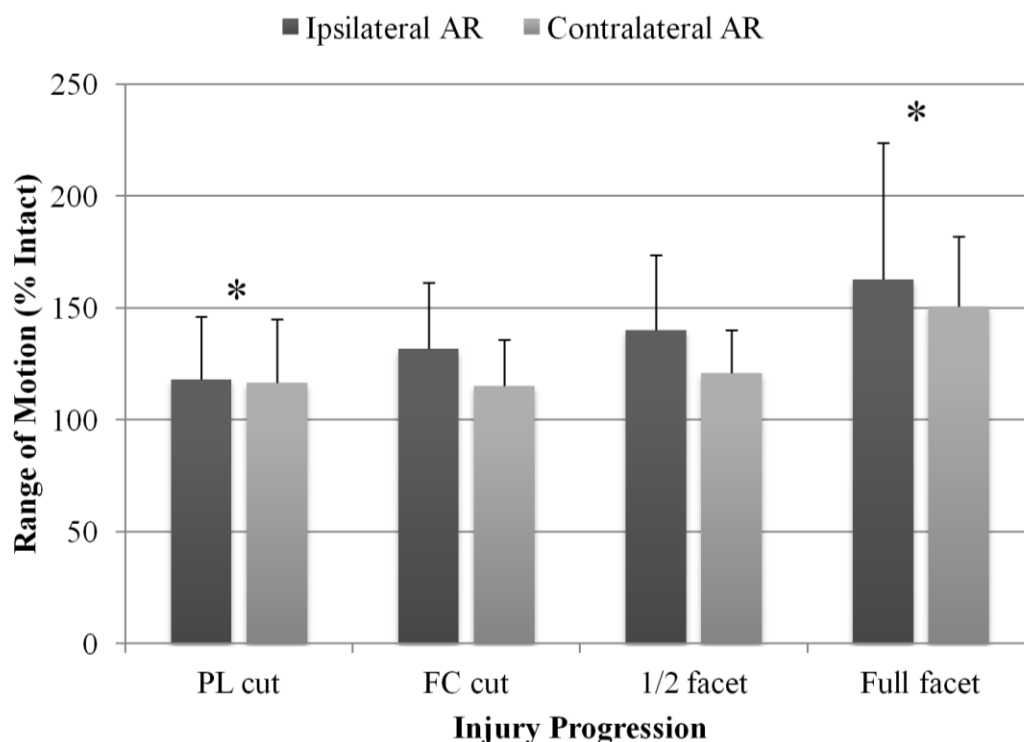


**Figure 2.8: C3-C4 Axial Rotation ROM with Posterior Injury Progression**

This graph shows the axial rotation ROM data to ipsilateral and contralateral sides averaged over the eight specimens as a percentage of the intact ROM for the progressive injury pattern. There was an increase in axial rotation following the posterior ligament complex removal ( $p < 0.05$ ), and a second increase following complete bony facet removal ( $p < 0.05$ ).

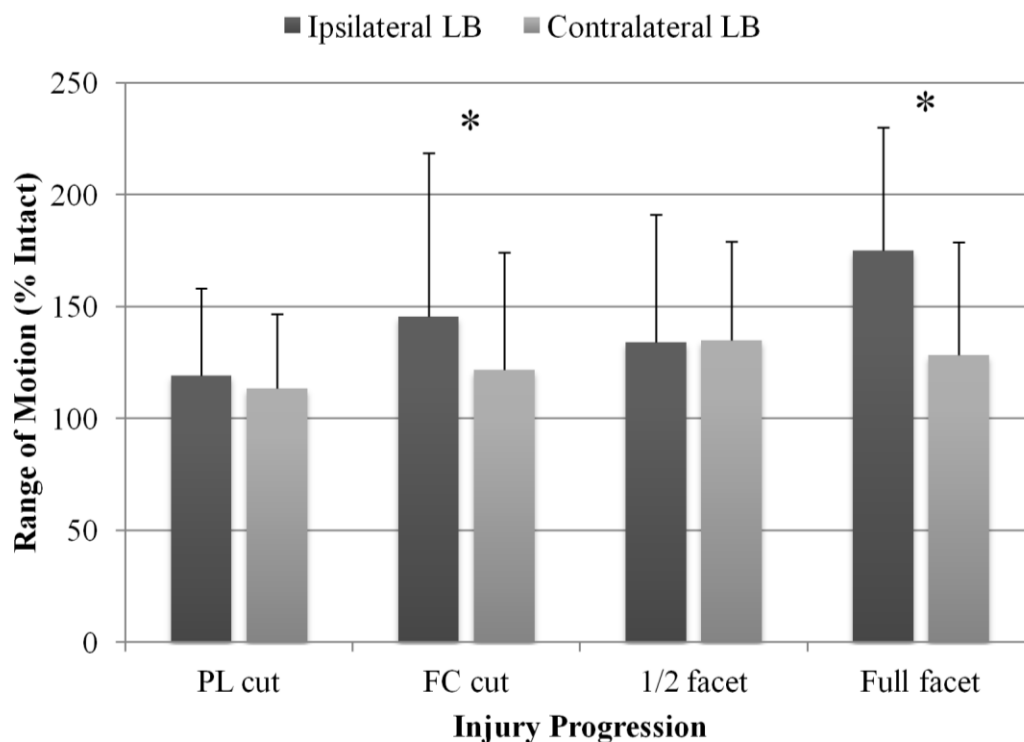


**Figure 2.9: C3-C4 Lateral Bend ROM with Posterior Injury Progression**

This graph shows the lateral bend ROM data to ipsilateral and contralateral sides averaged over the eight specimens as a percentage of the intact ROM for the progressive injury pattern. There was an increase in lateral bend following the facet capsule removal ( $p < 0.05$ ), and a second increase following complete bony facet removal ( $p < 0.05$ ).

stage had a larger ROM compared to the intact stage for both the C2-C3 and C4-C5 ( $p<0.05$ ). There was also an increase in ROM between the final stage and PL cut for the C2-C3 level only ( $p<0.05$ ).

### 2.3.3 INSTRUMENTED KINEMATICS

Instrumentation testing was only completed in seven of the eight specimens tested, due to equipment availability. In flexion-extension, the mean percent change ( $\pm$  standard deviation) in ROM for the instrumented states compared to the injured state was  $-85\pm6\%$ ,  $-53\pm20\%$ , and  $-85\pm24\%$  for the posterior, anterior, and posterior-anterior combined approaches, respectively (Figure 2.10). Statistical analysis found all instrumentations reduced ROM from the injured state ( $p<0.05$ ) and were different from each other ( $p<0.05$ ), apart from the posterior versus combined approach ( $p>0.05$ ).

For axial rotation, all instrumented states lead to a decrease in ROM compared to the injured state ( $p<0.05$ ). Both the posterior and posterior-anterior combined instrumentations lead to large decreases in ROM ( $-77\pm10\%$  and  $-78\pm22\%$ , respectively); whereas, the decrease for anterior fixation was much smaller in magnitude ( $-18\pm24\%$ ). ROM for posterior and posterior-anterior combined, while not found different from each other ( $p>0.05$ ), were both less than the anterior instrumentation ROM ( $p<0.05$ ).

Lateral bend testing found posterior and posterior-anterior combined reduced ROM ( $-90\pm6\%$  and  $-94\pm5\%$ , respectively) compared to the injured state ( $p<0.05$ ); however, in this simulated motion, the ROM of the anterior approach was not different from the injured state ( $-4\pm79\%$ ;  $p>0.05$ ). Data from only six specimens was used for the lateral bend analysis because of a missing data file for one specimen.

## 2.4 DISCUSSION

The passive restraint provided by the posterior osteoligamentous structures to motion of the subaxial spine is not well investigated with respect to flexion-distraction injuries. The current study demonstrated that the effect of progressive sectioning was dependent on the direction of motion. This suggests that certain posterior structures are more relevant restraints to specific motions (*i.e.*, axial rotation or flexion) than others.

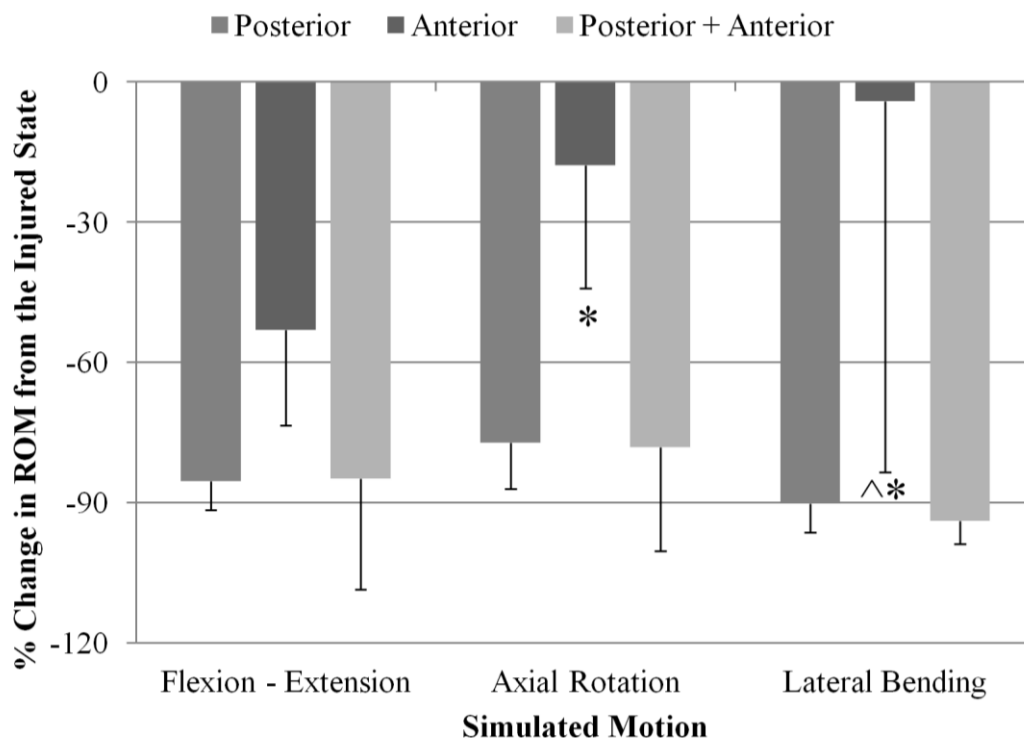


**Figure 2.10: Percent Decrease in C3-C4 ROM with Instrumentation**

Percent change in C3-C4 ROM compared to the final injured state in each of the three motions tested for the three instrumented states. All instrumentations reduced ROM in flexion-extension and axial rotation, but anterior instrumentation did not decrease ROM from the injured state in lateral bending (^ represents  $p>0.05$ ). Furthermore, in axial rotation and lateral bending, anterior instrumentation provided a smaller decrease in ROM compared to both posterior and combined instrumentation (\* represents  $p<0.05$ ).

The dominant restraint for rotation in the sagittal plane (flexion) appears to be the posterior ligamentous complex; which, in this study, represents the supraspinous, interspinous, and ligamentum flavum. This is the only structure that when sacrificed significantly increased segmental flexion-extension motion and neutral zone. For axial rotation, the facet capsule and inferior articular process provide significant restraint to segmental and overall range of motion as well as neutral zone; although, neutral zone and segmental axial rotation also increased with sacrifice of the posterior ligamentous complex. Understandably, the contralateral axial rotation was more significantly affected than was ipsilateral, which relates to the morphology of the facet (the inferior articular process rests posterior to the superior articular process). No specific structure demonstrated as a dominant restraint for lateral bending.

The isolated posterior column injury of this study found increases in ROM between the different states of sectioning were relatively moderate and was limited to a stage 1 flexion-distraction injury (*i.e.*, facet subluxation only) (Allen *et al.*, 1982). This may suggest that the role of the posterior soft tissues and bony facet anatomy is in limiting the range of motion as a secondary stabilizer. In that sense, it is most likely the anterior structures that provide primary stability.

Measuring the “neutral zone” is the most widely reported method for determining the instability of the spine (Dvorak *et al.*, 2005; Kim *et al.*, 2004; Pitzen *et al.*, 2003; Wilke *et al.*, 1998). In the current study, statistical analysis showed that there was an increase in NZ with sectioning of posterior stabilizers for all three planes of rotation. However, the magnitude of the NZ measured for all motions was relatively small despite the statistically significant change. While NZ will increase by two to three times its original size when tested following the reduction of a unilateral subaxial facet dislocation (Crawford *et al.*, 2002), the maximum percentage increase in NZ generated in the current study (without creating a dislocation) was at most approximately 30% in the case of axial rotation. Although the posterior osteoligamentous structures influence NZ stability to some degree, the spine remains relatively stable when they are compromised in isolation from the anterior discoligamentous structures. Interestingly, although NZ is generally used as the measure of stability, it has been recognized as a measure of the laxity or

degeneration of the intervertebral disc (Gay *et al.*, 2006). As such, the isolated posterior osteoligamentous injury states created in this study would not be expected to significantly impact the NZ measure, and help to explain the observations seen in this work.

In regards to fixation, the goal of the current study was to evaluate the effectiveness of anterior plating versus a posterior lateral mass screw and rod system for an isolated posterior soft tissue injury with a unilateral facet fracture, but with a preserved anterior discoligamentous complex. The posterior approach did an excellent job reducing ROM for all motions compared to the injured state. In contrast, the anterior instrumentation alone in this isolated posterior injury model produced less desirable results. While the anterior approach was successful at significantly reducing flexion-extension ROM, and to a lesser extent for axial rotation, it did not alter the ROM beyond the injured state for lateral bending. Furthermore, the posterior system was more effective at stabilizing the injury than the anterior approach for both axial rotation and lateral bend. The addition of the posterior system to the anterior (combined approach) was very effective at re-establishing stability as demonstrated by the reduction in ROM at the injured level to that of the posterior approach. Contrary to the hypothesis that both systems would be equivalent, the necessary disruption of the anterior longitudinal ligament, anterior annulus, and nucleus pulposus required to perform the anterior stabilization, resulted in an increase ROM of the specimens compared to leaving these structures intact despite the addition of the plate. Therefore, in the scenario of an anterior open reduction and internal fixation, this finding suggests the importance of the articular process as a buttress to pathologic motion. These results are supported by the work of Pitzen *et al.* who, in a study evaluating the effect of posterior injury with use of anterior plating, found the capsular ligaments and articular facets were important stabilizing elements with the use of anterior plating alone (Pitzen *et al.*, 2003).

There are inherent limitations related to the *in vitro* nature of the study. There was a large variability in terms of the measured ROM and NZ between specimens, evident by the relatively large standard deviations. This is likely the result of significant specimen variability, in terms of soft tissue quality and disc degeneration; however, the effect of this variability is limited by the repeated-measures design of the study that

allowed for the injury progression to be compared within the same specimen. On the other hand, the repeated-measures design only allowed for one injury progression model to be evaluated for our sample size, which was feasibly limited to testing eight specimens. While a different sequence of injury progression is clinically possible, our sectioning protocol represents a reasonable attempt to model the injury progression of an isolated posterior column injury following a flexion-distraction mechanism. It should be noted that the authors chose to investigate only one injury level (C3-C4) along with one segment above and below the injury; however, different results may have been seen with an injury to a lower motion segment. Furthermore, the facetectomy of C3 required that the posterior instrumentation span from C2 to C4, which differed from the anterior plating of C3 to C4. While both these approaches used only four screws, the longer “two-level” fixation of the posterior instrumentation is not ideal for comparison to the shorter “one-level” anterior plating. However, the results from this study are still clinically valid and generalizable since the same posterior instrumentation strategy would be required clinically in the setting of a facet fracture. Also, the order of insertion for the instrumentation systems could not be randomized as a result of the discectomy of C3-C4 for the anterior approach. While the results of this study found that the posterior versus the posterior-anterior instrumentations were not different from one another, the injury model differed between these instrumentation techniques (due to the discectomy). The authors of the current study chose not to test discectomy state with posterior instrumentation alone, since this treatment method would not be relevant clinically.

In conclusion, disruption of the posterior osteoligamentous structures of the C3-C4 motion segment lead to an increase in ROM for all three planes, as hypothesized. The posterior ligamentous complex and the facet complex are dominant stabilizers for flexion-extension and axial rotation, respectively. The overall changes in both ROM and NZ were relatively small but consistent with an isolated posterior osteoligamentous complex injury of the stage 1 flexion-distraction injury. In terms of instrumentation, the hypothesis of this study was found false, in that the anterior and posterior instrumentations did not provide equivalent stability for this injury pattern. The ineffectiveness of anterior instrumentation in resisting axial rotation and lateral bend suggests that, in the early post-operative period, the sacrifice of anterior discoligamentous

stabilizers inadvertently produces more instability then is re-established by the current anterior fusion technique.

## 2.5 SUMMARY & FUTURE DIRECTIONS

This initial study with the custom spinal loading simulator and Optotrak Certus® tracking system established a successful protocol for testing cadaveric motion segments. However, there were some issues with testing multi-segment spine, in terms of tracker visibility and measuring the NZ of entire specimen, which would not have been an issue in testing a single motion segment. As well, to further understand the entire “spectrum of instability” surrounding unilateral facet fracture/dislocations, future studies should be performed to understand the elastic/plastic deformation of the anterior discoligamentous complex with and without an associated posterior osteoligamentous injury.

## 2.6 REFERENCES

- Aebi, M., Zuber, K., Marchesi, D., 1991. Treatment of cervical spine injuries with anterior plating. Indications, techniques, and results. *Spine* 16, S38–45.
- Allen, B.L., Ferguson, R.L., Lehmann, T.R., O’Brien, R.P., 1982. A mechanistic classification of closed, indirect fractures and dislocations of the lower cervical spine. *Spine* 7, 1–27.
- Anderson, P.A., Henley, M.B., Grady, M.S., Montesano, P.X., Winn, H.R., 1991. Posterior cervical arthrodesis with AO reconstruction plates and bone graft. *Spine* 16, S72–79.
- Bozkus, H., Ames, C.P., Chamberlain, R.H., Nottmeier, E.W., *et al.*, 2005. Biomechanical analysis of rigid stabilization techniques for three-column injury in the lower cervical spine. *Spine* 30, 915–922.
- Brodke, D.S., Anderson, P.A., Newell, D.W., Grady, M.S., Chapman, J.R., 2003. Comparison of anterior and posterior approaches in cervical spinal cord injuries. *Journal of Spinal Disorders & Techniques* 16, 229–235.
- Brown, T., Reitman, C.A., Nguyen, L., Hipp, J.A., 2005. Intervertebral motion after incremental damage to the posterior structures of the cervical spine. *Spine* 30, E503–508.
- Cooper, P.R., Cohen, A., Rosiello, A., Koslow, M., 1988. Posterior stabilization of cervical spine fractures and subluxations using plates and screws. *Neurosurgery* 23, 300–306.



- Crawford, N.R., Duggal, N., Chamberlain, R.H., Park, S.C., *et al.*, 2002. Unilateral cervical facet dislocation: injury mechanism and biomechanical consequences. *Spine* 27, 1858–1864.
- Do Koh, Y., Lim, T.H., Won You, J., Eck, J., An, H.S., 2001. A biomechanical comparison of modern anterior and posterior plate fixation of the cervical spine. *Spine* 26, 15–21.
- Duggal, N., Chamberlain, R.H., Park, S.C., Sonntag, V.K.H., *et al.*, 2005. Unilateral cervical facet dislocation: biomechanics of fixation. *Spine* 30, E164–168.
- Dvorak, M.F., Fisher, C.G., Aarabi, B., Harris, M.B., *et al.*, 2007a. Clinical outcomes of 90 isolated unilateral facet fractures, subluxations, and dislocations treated surgically and nonoperatively. *Spine* 32, 3007–3013.
- Dvorak, M.F., Fisher, C.G., Fehlings, M.G., Rampersaud, Y.R., *et al.*, 2007b. The surgical approach to subaxial cervical spine injuries: an evidence-based algorithm based on the SLIC classification system. *Spine* 32, 2620–2629.
- Dvorak, M.F., Pitzen, T., Zhu, Q., Gordon, J.D., *et al.*, 2005. Anterior cervical plate fixation: a biomechanical study to evaluate the effects of plate design, endplate preparation, and bone mineral density. *Spine* 30, 294–301.
- Dvorak, M.F., Sekeramayi, F., Zhu, Q., Hoekema, J., *et al.*, 2003. Anterior occiput to axis screw fixation: part II: a biomechanical comparison with posterior fixation techniques. *Spine* 28, 239–245.
- Gay, R.E., Ilharreborde, B., Zhao, K., Zhao, C., An, K.-N., 2006. Sagittal plane motion in the human lumbar spine: comparison of the in vitro quasistatic neutral zone and dynamic motion parameters. *Clinical Biomechanics* 21, 914–919.
- Glaser, J.A., Jaworski, B.A., Cuddy, B.G., Albert, T.J., *et al.*, 1998. Variation in surgical opinion regarding management of selected cervical spine injuries. A preliminary study. *Spine* 23, 975–982.
- Goel, V., Clark, C., McGowan, D., Goyal, S., 1984. An in-vitro study of the kinematics of the normal, injured and stabilized cervical spine. *Journal of Biomechanics* 17, 363–376.
- Henriques, T., Olerud, C., Bergman, A., Jónsson, H., 2004. Distractive flexion injuries of the subaxial cervical spine treated with anterior plate alone. *Journal of Spinal Disorders & Techniques* 17, 1–7.
- Hongo, M., Gay, R.E., Hsu, J.-T., Zhao, K.D., *et al.*, 2008. Effect of multiple freeze-thaw cycles on intervertebral dynamic motion characteristics in the porcine lumbar spine. *Journal of Biomechanics* 41, 916–20.

Johnson, M.G., Fisher, C.G., Boyd, M., Pitzen, T., *et al.*, 2004. The radiographic failure of single segment anterior cervical plate fixation in traumatic cervical flexion distraction injuries. *Spine* 29, 2815–2820.

Kim, S.-M., Lim, T.J., Paterno, J., Park, J., Kim, D.H., 2004. A biomechanical comparison of three surgical approaches in bilateral subaxial cervical facet dislocation. *Journal of Neurosurgery Spine* 1, 108–115.

Kotani, Y., Cunningham, B.W., Abumi, K., McAfee, P.C., 1994. Biomechanical analysis of cervical stabilization systems. An assessment of transpedicular screw fixation in the cervical spine. *Spine* 19, 2529–2539.

Kwon, B.K., Fisher, C.G., Boyd, M.C., Cobb, J., *et al.*, 2007. A prospective randomized controlled trial of anterior compared with posterior stabilization for unilateral facet injuries of the cervical spine. *Journal of Neurosurgery Spine* 7, 1–12.

McNamara, M., Devito, D.P., Spengler, D.M., 1991. Circumferential fusion for the management of acute cervical spine trauma. *Journal of Spinal Disorders & Techniques* 4, 467–471.

Nassr, A., Lee, J.Y., Dvorak, M.F., Harrop, J.S., *et al.*, 2008. Variations in surgical treatment of cervical facet dislocations. *Spine* 33, E188–193.

Panjabi, M., White, A., Johnson, R., 1975. Cervical spine mechanics as a function of transection of components. *Journal of Biomechanics* 8, 327–336.

Pitzen, T., Lane, C., Goertzen, D., Dvorak, M., *et al.*, 2003. Anterior cervical plate fixation: biomechanical effectiveness as a function of posterior element injury. *Journal of Neurosurgery Spine* 99, 84–90.

Rabb, C.H., Lopez, J., Beauchamp, K., Witt, P., *et al.*, 2007. Unilateral cervical facet fractures with subluxation: injury patterns and treatment. *Journal of Spinal Disorders & Techniques* 20, 416–422.

Sim, E., Vaccaro, A.R., Berzlanovich, A., Schwarz, N., Sim, B., 2001. In vitro genesis of subaxial cervical unilateral facet dislocations through sequential soft tissue ablation. *Spine* 26, 1317–1323.

Song, K.-J., Lee, K.-B., 2008. Anterior versus combined anterior and posterior fixation/fusion in the treatment of distraction-flexion injury in the lower cervical spine. *Journal of Clinical Neuroscience* 15, 36–42.

Wilke, H.J., Wenger, K., Claes, L., 1998. Testing criteria for spinal implants: recommendations for the standardization of in vitro stability testing of spinal implants. *European Spine Journal* 7, 148–154.

Woodworth, R.S., Molinari, W.J., Brandenstein, D., Gruhn, W., Molinari, R.W., 2009. Anterior cervical discectomy and fusion with structural allograft and plates for the

treatment of unstable posterior cervical spine injuries. *Journal of Neurosurgery Spine* 10, 93–101.

Zdeblick, T.A., Abitbol, J.J., Kunz, D.N., McCabe, R.P., Garfin, S., 1993. Cervical stability after sequential capsule resection. *Spine* 18, 2005–2008.

Zdeblick, T.A., Zou, D., Warden, K.E., McCabe, R., *et al.*, 1992. Cervical stability after foraminotomy. A biomechanical in vitro analysis. *Journal of Bone & Joint Surgery* 74-A, 22–27.

## CHAPTER 3: IN VITRO SIMULATION AND STANDARDIZATION OF THE SOFT TISSUE DAMAGE SUSTAINED IN THE CERVICAL SPINE FOLLOWING A UNILATERAL FACET PERCH INJURY

***OVERVIEW:** This chapter expands on the investigation of Chapter 2 moving further into the spectrum of flexion-distraction injuries in the cervical spine (i.e., stages 2 & 3). While simple injuries such as an isolated posterior soft tissue injury can be readily created and examined, more advanced stages require further consideration of the injury mechanism to create valid results. As such, this chapter explores the concept of inducing a unilateral facet perch injury in vitro using a describe mechanism of injury in single motion segments. The soft tissue injuries were then examined and tabulated. These data were expanded to develop a valid and reliable standardized model of this injury pattern for further studies.<sup>6</sup>*

### 3.1 INTRODUCTION

The varying dynamics of cervical spine trauma causes a large spectrum of bony and soft tissue injuries (Allen *et al.*, 1982; Dvorak *et al.*, 2007a). On the extreme end of this spectrum, significant soft tissue injuries leave the cervical spine very unstable (Kwon *et al.*, 2006). However, a large majority of these injuries will cause a lesser degree of osteoligamentous damage and resulting instability, which includes the unilateral facet perch injury (Allen *et al.*, 1982; Dvorak *et al.*, 2007a; Kwon *et al.*, 2006). Thought to be caused by a flexion-distraction mechanism, the perch injury is defined as excessive subluxation of the facet joint, immediately prior to a dislocation (Allen *et al.*, 1982; Benzel, 2001). While expert surgical opinions suggest treating these injuries operatively

---

<sup>6</sup> This chapter is adapted from two manuscripts: (1) Nadeau M, McLachlin SD, Bailey SI, Gurr KR, Dunning CE, Bailey CS. A biomechanical assessment of soft tissue damage in the cervical spine following a unilateral facet injury. J Bone Joint Surg Am. 2012;94:e156(1-6) and (2) McLachlin SD, Nadeau M, Yao R, Gurr KR, Bailey CS, Dunning CE. Standardized In Vitro Model for Conducting Biomechanical Investigations of a Unilateral Facet Perch Injury in the Cervical Spine. Submitted to The Spine Journal, Jan 2013.

(Dvorak *et al.*, 2007a, 2007b; Vaccaro *et al.*, 2007), a consensus on the optimal surgical approach for treatment of a unilateral facet perch has not yet been achieved.

*In vitro* biomechanical comparisons of the surgical treatment options for cervical spine trauma add important data to the literature (Do Koh *et al.*, 2001; Duggal *et al.*, 2005; Paxinos *et al.*, 2009; Pitzen *et al.*, 2003; Traynelis *et al.*, 1993); however, these require *a priori* development of soft tissue injury models that are both valid and reliable. That is, the soft tissue damage that the model induces must demonstrate the appropriate level of biomechanical instability as measured by changes in flexibility (*i.e.*, valid) and be readily created in multiple specimens to provide for reliable comparison (*i.e.*, repeatable). Traditionally, *in vitro* methods to reproduce precise injury patterns involve surgical sectioning of the structures thought to be involved in the specific mechanism of injury being tested, such as the technique used in Chapter 2 and in numerous other studies (Arand *et al.*, 2002; Brown *et al.*, 2005; Do Koh *et al.*, 2001; Lehmann *et al.*, 2004; Panjabi *et al.*, 1975; Paxinos *et al.*, 2009; Pitzen *et al.*, 2003; Rasoulinejad *et al.*, 2012; Samartzis *et al.*, 2010; Shea *et al.*, 1992; Sim *et al.*, 2001; Traynelis *et al.*, 1993). Whether these surgical resections are valid in terms of reproducing the appropriate extent of the injury magnitude and associated spinal instability is often unknown. Furthermore, few studies have actually attempted to identify the extent of anatomical disruption secondary to unilateral facet injury and also quantify the associated kinematics (Crawford *et al.*, 2002; Sim *et al.*, 2001; Vaccaro *et al.*, 2001). Inducing the injury using custom loading devices may provide a better representation of the clinical injury mechanism and associated instability (as measured by altered kinematics) (Crawford *et al.*, 2002; Panjabi *et al.*, 2007). However, this “dynamic” approach inevitably produces variability in the injury pattern, which negatively affects the injury model’s repeatability (Panjabi *et al.*, 2007).

Therefore, the aims of this study were: (1) to develop an experimental method that reliably produces a unilateral facet perch in cadaveric subaxial spinal segments, (2) to quantify the resulting change in kinematic stability, (3) to identify the associated soft tissue injuries, and finally (4) to validate and investigate the preliminary application of a standardized injury model (SIM) for this injury, where validation was based on achieving

equivalent kinematic instability (*i.e.*, similar increases in flexibility as measured by ROM and NZ).

## 3.2 MATERIALS AND METHODS

### 3.2.1 GENERAL EXPERIMENTAL SETUP

Nineteen fresh-frozen single motion segments (nine C4-C5, five C5-C6, five C6-C7; mean age  $68 \pm 13$ ) were used for this study. Prior to experimental testing, each specimen was scanned using computed tomography (CT) to ensure that there was no underlying bony abnormality or pathology present. Specimens were then carefully dissected of existing musculature to leave only the passive stabilizing soft tissue structures intact (*i.e.*, capsule, disc, ligaments, etc.). The cranial and caudal vertebrae of the motion segment were fixed using Denstone® dental cement (Heraeus Kulzer Inc., South Bend, IN, USA) within 10cm diameter rings of polyvinyl chloride (PVC) pipe, cut to a 2.5cm thickness. To improve fixation to the cement, a modified additional screw insertion technique for the single segment was devised to increase resistance to rotation torque. Four screws with bi-cortical purchase placed in each vertebral body: two entering the end plate and exiting at the posterior vertebral body cortex, and two penetrating each lamina and going into the posterior vertebral body cortex (Figure 3.1). Specimens were supported during the cementing process so that their alignment remained anatomic and neutral.

Each specimen was mounted in the custom-developed spinal loading simulator (Figure 3.2). Specimens were first tested in the intact state in flexion-extension, lateral bending, and axial rotation using the flexibility testing methodology (Panjabi, 1988; Wilke *et al.*, 1998). Briefly, loading was applied at a rate of  $3^\circ/\text{s}$  up to a target load of  $\pm 1.5\text{Nm}$  (Dvorak *et al.*, 2005; Pitzen *et al.*, 2003). The upper loading arm was also used to remove the weight of the metal fixture from the spine, using the actuator's load control to maintain a load of 0N. Spine motion was measured using an Optotrak Certus™ tracking system (NDI, Waterloo, ON, Canada). Optotrak Smart Markers were rigidly attached to the cranial and caudal fixtures and relative rotations in the anatomic planes



**Figure 3.1: Potting Screw Insertion**

Images showing the insertion locations of four 1.5” drywall screws used to achieve additional fixation between the cranial and caudal vertebrae and the Denstone™ cement in potting fixture. The ends of the screws were submerged into “wet” cement during the potting process, with the specimen held in a desired alignment. This configuration was designed to resist the large axial rotation torques required to produce the unilateral facet perch injury, but were also positioned to avoid disturbing any critical osteoligamentous structures.

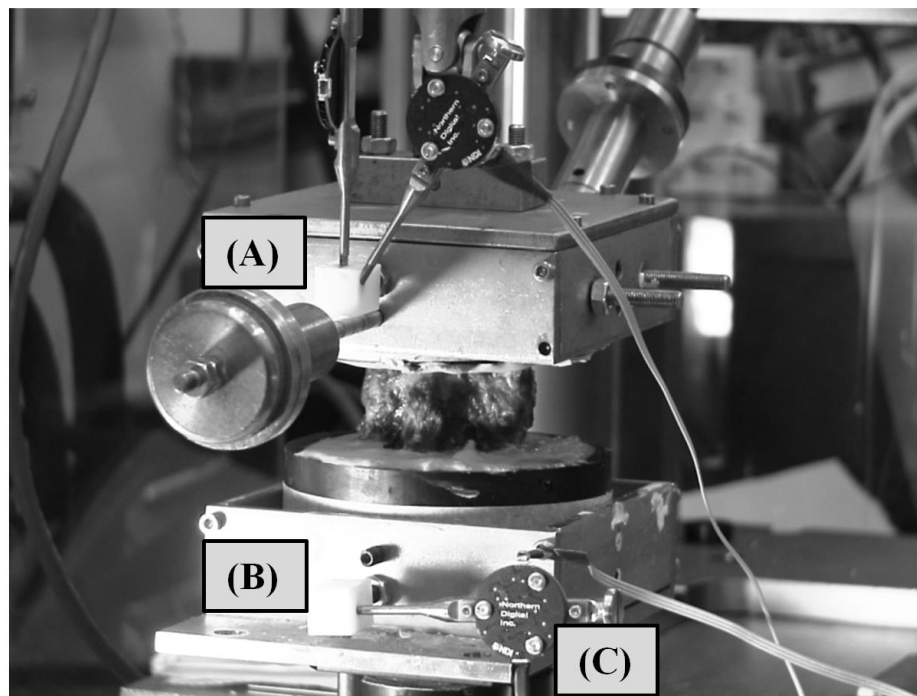


**Figure 3.2: Simulator and Tracker Setup for Single Motion Segment**

Cadaveric cervical spine segments were mounted in the cranial (A) and caudal (B) loading fixtures of the spinal loading simulator, with Optotrak® Smart Markers (C) attached to each fixture for motion tracking. This ensured no unnecessary disruption of the anatomy, prior to creating the injury.



between the two vertebrae were determined by digitizing anatomic landmarks to create local bone coordinate systems (see Section 2.2) (Wilke *et al.*, 1998). Kinematic data collected for left lateral bend and left axial rotation motions were considered as ipsilateral (side of injury) rotations and, oppositely, rotations to the right side were described as contralateral (opposite side of injury). Throughout testing, the specimens were kept moist with normal saline (Wilke *et al.*, 1998).

### **3.2.2 STUDY 1 – UNILATERAL FACET PERCH CREATION**

In nine specimens (four C4-C5 and five C6-C7, mean age:  $61 \pm 6$  years), a unilateral facet perch was induced in the left facet joint of each specimen. The simulated mechanism of injury of a unilateral facet dislocation has been described in the literature as being a combination of flexion, contralateral bending, and axial rotation (Allen *et al.*, 1982; Argenson *et al.*, 1988; Braakman and Vinken, 1967; Crawford *et al.*, 2002; Kaye and Nance, 1990; Norton, 1962; Roaf, 1960; Young *et al.*, 1989). Initially, the potting fixture of the rostral vertebra was loaded with deadweights to position the specimen in flexion and contralateral bend, necessary to moderately distract the facet joint of interest (Figure 3.3). A contralateral axial rotational torque was then applied via the spinal loading simulator at a rate of  $0.5^\circ/\text{s}$ , until impending dislocation (*i.e.*, facet perch) was achieved in the left facet joint. Direct visualization of the facet perch was possible by virtue of a small lateral capsular split performed during specimen preparation (Fig. 3.4A). Following the facet perch (Fig. 3.4B), the rostral vertebra was rotated back into a reduced position, and post-injury flexibility testing was performed using the same protocol as in the intact state.

Each specimen was then removed from the simulator and systematically inspected by a single observer using gross dissection techniques. Specifically, the integrity of the facet capsules, supraspinous and interspinous ligaments, ligamentum flavum, anterior and posterior longitudinal ligaments, annulus and nucleus pulposus were assessed. All structures were evaluated ipsilaterally (side of the facet injury) and contralaterally (side opposite to the facet injury). The disc included independent assessment of the annulus and the nucleus pulposus. A standardized data sheet was used to record whether the structures were intact, stretched (but in continuity), or disrupted (Figure 3.5A).

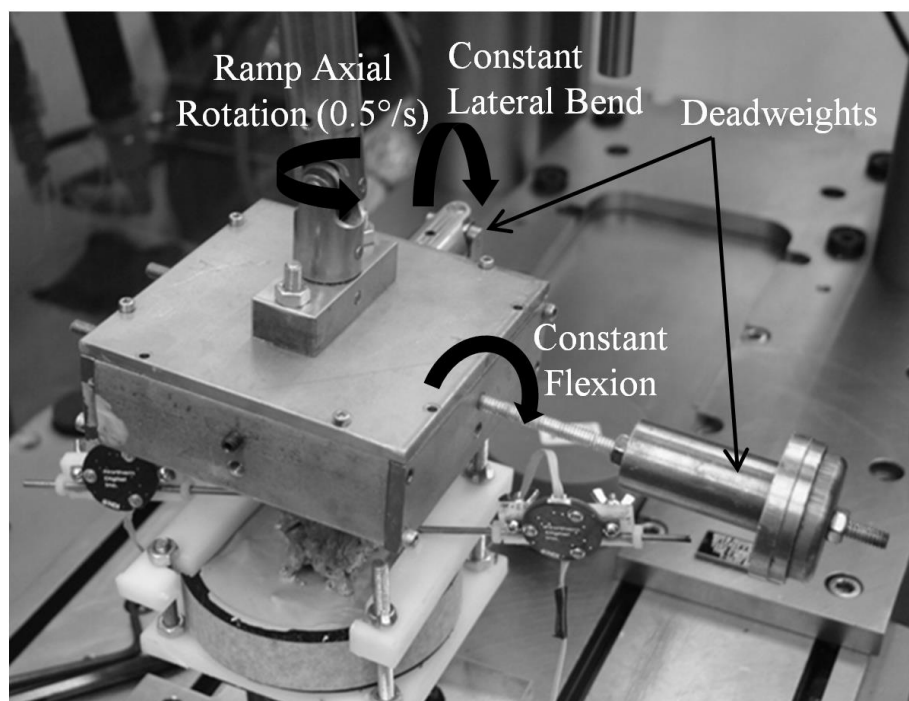


**Figure 3.3: Simulator Modification to Induce a Unilateral Facet Perch**

To induce the unilateral facet perch, deadweights were applied to the sides of the cranial potting fixture to induce maximum physiologic flexion and lateral bend on the contralateral side (to distract the ipsilateral facet). The injury, and subsequent soft tissue disruption, was then created via increasing axial rotation at  $0.5^\circ/\text{s}$  until the perched position was reached.

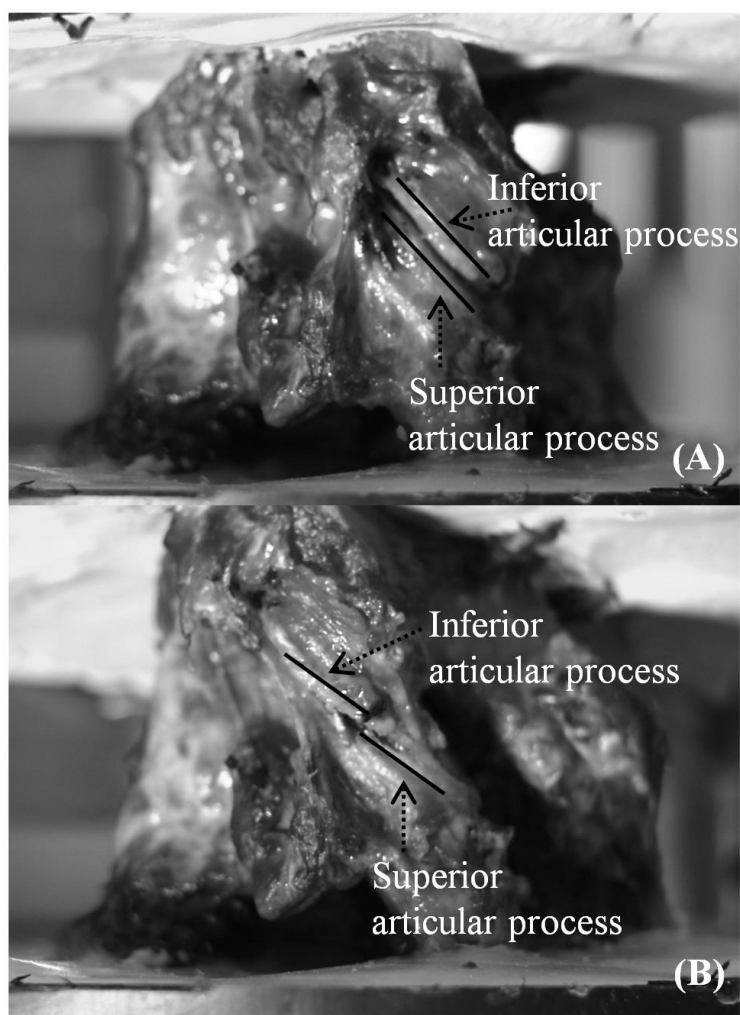


**Figure 3.4: Identification of Instance of Perch**

(A) Image shows the approach to gain direct visualization of facet to be injured prior to testing, by virtue of lateral capsular surgical slit. Small marks were defined on the anterior and posterior aspects of the articular processes to assist with identifying the instance of facet perch. (B) When this position was achieved (as identified by the solid black lines), the mechanism of injury was interrupted (axial torque component) and rotated back into a reduced position.

**(A)**

SPECIMEN:		DATE:	
STRUCTURE	SIDE	STATUS	
<b>PLL</b>	Contralateral		
<b>Lig. Flavum</b>	Contralateral		
<b>Capsule</b>	Contralateral	Anterior:	
		Lateral:	
		Posterior:	
<b>Disc</b>	Contralateral	Anterior:	
		Posterior:	
<b>Annulus</b>	Contralateral	Anterior:	
		Lateral:	
		Posterior:	
<b>ALL</b>	Contralateral		
<b>ALL</b>	Ipsilateral		
<b>Annulus</b>	Ipsilateral	Anterior:	
		Lateral:	
		Posterior:	
<b>Disc</b>	Ipsilateral	Anterior:	
		Posterior:	
<b>Capsule</b>	Ipsilateral	Anterior:	
		Lateral:	
<b>Lig. Flavum</b>	Ipsilateral		
<b>PLL</b>	Ipsilateral		
<b>IS</b>	Midline		
<b>SS</b>	Midline		

**(B)**

	Annulus						Disc				Lig Flavum		Capsule				ALL		PLL		IS	SS
	Ip			Co			Ip		Co		Ip	Co	Ip		Co		Ip	Co	Ip	Co	-	-
	A	L	P	A	L	P	A	P	A	P	-	-	A	P	A	P	-	-	-	-	-	-
Specimen 1																						
Specimen 2																						
Specimen 3																						
Specimen 4																						

**Figure 3.5: Tables for Recording Specimen Disruption**

(A) The specimen dissection chart was used to record the integrity of each soft tissue structure as being intact, stretched or disrupted based on a careful inspection of the specimen following the application of injury-inducing loading in the spine simulator. (B) The chart data are tabulated in Excel to have a status for each soft tissue structure, shown for four pilot specimens (intact-white, stretched-grey, disrupted-black). Structures are broken down into location relative to injury (ipsilateral (Ip) or contralateral (Co)) and in some cases whether the injury exists in the anterior (A), lateral (L), or posterior (P) region of the structure.

Structures that were stretched or disrupted were grouped as “injured structures” for purposes of data analysis.

### **3.2.3 STUDY 2 – STANDARDIZED INJURY MODEL**

Data from the nine specimens of Study 1 were tabulated and the most consistently injured structures were identified to extrapolate a common pattern of injury. This soft tissue disruption was then induced by surgical sectioning in the remaining ten specimens (five C4-C5 and five C5-C6; mean age  $74 \pm 10$  years). In the initial pilot specimen this caused only a small motion increase compared to the intact kinematics. As such, a second step was added to the protocol, in which each sectioned specimen was rotated to a perched position using the simulator (to stretch the remaining soft tissues). The combination of sectioning plus rotation is herein referred to as the standard injury model (SIM). All ten specimens received the SIM; however, in the first five specimens, the protocol performed involved the two steps described above (surgical sectioning alone then testing, followed by the rotation and testing); while, in the last five specimens, the separate testing step of surgical sectioning alone was not conducted.

### **3.2.4 STUDY 1 & 2 DATA ANALYSIS**

Kinematic data from both Study 1 and 2 were analyzed using a custom-written LabVIEW software (National Instruments, Austin, TX, USA) to determine the magnitude of ROM and NZ for each simulated movement (see Appendix C). The NZ was defined as the change in hysteresis at 0Nm (Wilke *et al.*, 1998). To validate the SIM, intact and injured states were compared using a two State (intact vs. injured) by two Study (1 vs. 2) mixed repeated measures analysis of variance (rmANOVA). Data from Study 2 were grouped into the two separate injury steps: Study 2A represented the intact and initial surgical sectioning injury of the first five specimens and Study 2B included the data for the intact and SIM states in all ten specimens. Therefore, two mixed rmANOVAs were performed such that Study 1 was compared to Study 2A and Study 2B separately. Post-hoc testing was conducted using Tukey’s honest significant difference with a correction for unequal sample sizes. Independent t-tests were also run to examine any potential differences between the two studies based on specimen age and the torque required to

achieve a unilateral facet perch. All statistical testing was conducted using SPSS Version 20 (IBM, New York, NY, USA) and alpha was set at 0.05.

### **3.2.5 PRELIMINARY SIM USAGE**

The validated SIM was then used in a preliminary investigation involving four specimens to demonstrate the model's efficacy. First, the effect of adding a unilateral facet fracture to the SIM was examined. The facet fracture was created in two stages: the first stage removed 50% of the inferior articular process on the injured side, followed by complete removal of the joint. Comparisons of the stabilization provided by posterior, anterior and combined instrumentation were then investigated in these same specimens. The posterior stabilization consisted of a lateral mass screw and rod system (Oasys® posterior cervical system; Stryker Spine, Allendale, NJ, USA), while the anterior was a standard anterior cervical discectomy, fusion and plating for the single injured level (Atlantis®, Medtronic Sofamor Danek, Minneapolis, MN, USA). Instrumentation insertion followed the same insertion techniques described in Section 2.2, except that with only a single motion segment tested in the current study, posterior instrumentation spanned only this single level (rather than two). Due to the preliminary nature of this additional testing, data were not subjected to statistical analysis.

## **3.3 RESULTS<sup>7</sup>**

### **3.3.1 STUDY 1 - UNILATERAL FACET PERCH CREATION**

An impending unilateral facet dislocation (*i.e.*, perched facet) was achieved in all nine specimens, without creating any dislocations. Three specimens also sustained a facet fracture, with two of these fractures occurring at 90% subluxation of the facets. The third fracture occurred at 50% subluxation, but involved the posterior 10% of the superior articular process only and was undisplaced. Between the non-fractured and fractured specimens, there were similar injuries to the soft tissue structures. Therefore, these specimens were included in data analysis. Specimen data for all nine specimens,

---

<sup>7</sup> Tabulated ROM and NZ data for all tested specimens is found in Appendix D.

including age, level, presence of fracture, and the maximum torque and rotation achieved during the facet perch injury mechanism was tabulated (Table 3.1).

Post-injury dissections results are shown in Table 3.2. These dissections revealed that the capsules and annulus fibrosus were the most commonly damaged structures. All specimens demonstrated capsular injury, with eight being bilateral. All specimens sustained disruptions of the annulus fibrosis, which extended into the nucleus pulposus to involve over 50% the disc substance in seven specimens. Most commonly, the injured portion of the disc was contralateral to the facet perch, spanning this entire portion from anterior to posterior. Eight of the nine specimens had at least 50% of the ligamentum flavum injured, with the ipsilateral side the most often affected (66%). The interspinous and supraspinous ligaments were never completely torn, but were stretched in three and four specimens, respectively. The anterior and posterior longitudinal ligaments (ALL and PLL) sustained a partial intra-substance tear in only two and one specimens, respectively. These were associated with injuries to the outer disc where the fibers of the longitudinal ligaments blend with those of the annulus.

Both ROM (Table 3.3) and NZ (Table 3.4) for all three motions simulated increased following the unilateral facet injury (Table 3.3). The largest change was seen in axial rotation, with a near three-fold increase in NZ and contralateral axial ROM (*i.e.*, right axial rotation following a left facet injury) ( $p < 0.05$ ). In contrast, the increase in ipsilateral axial ROM (rotation towards the injured facet) was smaller (32%) and not significant ( $p > 0.05$ ). In lateral bending, a 100% increase was seen in the NZ ( $p < 0.05$ ) with an 87% increase in ipsilateral (left) ROM ( $p < 0.05$ ). In the opposing direction, contralateral bending showed an increase of 63%, but was not significant ( $p > 0.05$ ). Flexion-extension data analysis revealed an increase in flexion only (52% increase,  $p < 0.05$ ).

### **3.3.2 STUDY 2 – STANDARDIZED INJURY MODEL**

Based on the highest frequency of soft tissue disruptions in Study 1, creation of the SIM required surgical sectioning of both facet capsules,  $\frac{3}{4}$  of the annulus (entire right

**Table 3.1: Specimen Demographics & Facet Perch Results**

Specimen	Age (Yrs)	Level	Facet Fracture	Torque to Perch (Nm)	Rotation to Perch (°)
1	65	C6-C7	No	17.8	29.4
2	64	C6-C7	No	16.1	27.6
3	65	C6-C7	No	12.5	19.9
4	57	C6-C7	No	12.7	32.1
5	60	C6-C7	Yes	18.6	18.8
<i>Average of C6-C7s</i>	$62 \pm 4$	-	-	$15.5 \pm 2.9$	$25.6 \pm 5.9$
6	81	C4-C5	No	9.7	24.3
7	48	C4-C5	No	21.1	30.7
8	65	C4-C5	Yes	23.5	21.3
9	60	C4-C5	Yes	18.9	27.1
<i>Average of C4-C5s</i>	$64 \pm 14$	-	-	$18.3 \pm 6.0$	$25.8 \pm 4.0$
<i>All Specimens</i>	$63 \pm 9$	-	-	$16.8 \pm 4.4$	$25.7 \pm 4.8$

**Table 3.2: Extent of Soft Tissue Injury Data for All Specimens (n = 9)**

Structure	Intact	Unilateral Injury	Bilateral Injury	Side of Injury (Ipsilateral/Contralateral)
Facet Capsules	0	9	8	(8/9)
Annulus Fibrosus	0	9	3	(6/6)
Nucleus Pulposus	2	7	4	(5/6)
Ligamentum Flavum	1	8	2	(6/4)
ALL	7	2	0	(2/0)
PLL	8	1	0	(0/1)
Interspinous Ligament	6	3	N/A	N/A
Supraspinous Ligament	5	4	N/A	N/A



**Table 3.3: Average ROM ( $\pm$  SD) Values Pre- and Post-UFP injury (n=9)**

<b>Motion</b>	<b>ROM Pre-Injury</b>	<b>ROM Post-Injury</b>	<b>% Change</b>	<b>p-value</b>
Flexion	5.6 $\pm$ 2.1	8.5 $\pm$ 3.1	52	0.02
Extension	3.3 $\pm$ 0.6	3.9 $\pm$ 1.4	18	0.13
Ipsilateral Axial Rot.	3.1 $\pm$ 0.9	4.1 $\pm$ 3.4	32	0.37
Contralateral Axial Rot.	3.5 $\pm$ 1.2	13.8 $\pm$ 4.2	294	<0.001
Ipsilateral Lateral Bend	3.9 $\pm$ 2.3	7.3 $\pm$ 4.9	87	0.04
Contralateral Lateral Bend	4.1 $\pm$ 1.1	6.7 $\pm$ 4.0	63	0.12

**Table 3.4: Average NZ ( $\pm$  SD) Values Pre- and Post-UFP injury (n=9)**

<b>Motion</b>	<b>NZ Pre-Injury</b>	<b>NZ Post-Injury</b>	<b>% Change</b>	<b>p-value</b>
Flexion- Extension	2.0 $\pm$ 1.4	3.8 $\pm$ 3.6	90	0.18
Axial Rotation	2.5 $\pm$ 1.2	8.9 $\pm$ 3.3	256	<0.001
Lateral Bend	1.7 $\pm$ 0.7	3.4 $\pm$ 1.1	100	<0.001

half along with the anterior region of the left side), and  $\frac{1}{2}$  of the ligamentum flavum (always the left half) based on the subluxation of the left facet joint. For an injury of the right facet joint, the injury was mirrored to the opposing side. Injuries to the right or left facet were split evenly among the ten specimens tested.

No differences in specimen age were found between the Study 1 and Study 2 ( $p>0.05$ ); however, the additional five specimens of 2B were older (mean age = 84 years) than the first five specimens of 2A (mean age = 64 years). With regards to rotating to the perched position for the standard injury (*i.e.*, Study 2B), less torque ( $p<0.05$ ) was required to achieve a unilateral facet perch ( $9.9\pm4.1\text{Nm}$  vs.  $16.8\pm4.4\text{Nm}$ ) than Study 1.

Overall, there was effect of State ( $p<0.05$ ), such that the intact had a smaller ROM than the injured state for all motions across studies. For the effect of Study, there was no identified difference ( $p>0.05$ ) overall between Study 1 and Study 2A & 2B independent of injury, except for Study 2B lateral bending. However, there were significant interactions which required further investigation.

Specific to Study 2A, there were no differences ( $p>0.05$ ) in ROM and NZ between the intact and injured states for all three motions for surgical sectioning alone. In the Study 2B injury (*i.e.*, standard injury model), an increase ( $p<0.05$ ) was identified in ROM and NZ for all motions except lateral bending NZ.

Comparison of the intact kinematics between Studies 1 and 2 found no difference ( $p>0.05$ ) in the ROM and NZ for Study 1 versus either Study 2A or 2B (Figures 3.6, 3.7, and 3.8), except in the case of lateral bending ROM between Study 1 and Study 2B, where the latter had reduced motion ( $p<0.05$ ) (Figure 3.8B).

In regards to the comparison of UFP injury kinematics, both the ROM and NZ in axial rotation of the sectioned specimens of Study 2A were less than that of the injury control specimens of Study 1 ( $p<0.05$ ) (Figure 3.6A). However, once the sectioned specimens were rotated to induce additional soft tissue attenuation, there was no difference in either ROM or NZ between the standard injury of Study 2B and the Study 1 injury control (Figure 3.6B). In the flexion-extension motion, injured ROM and NZ data

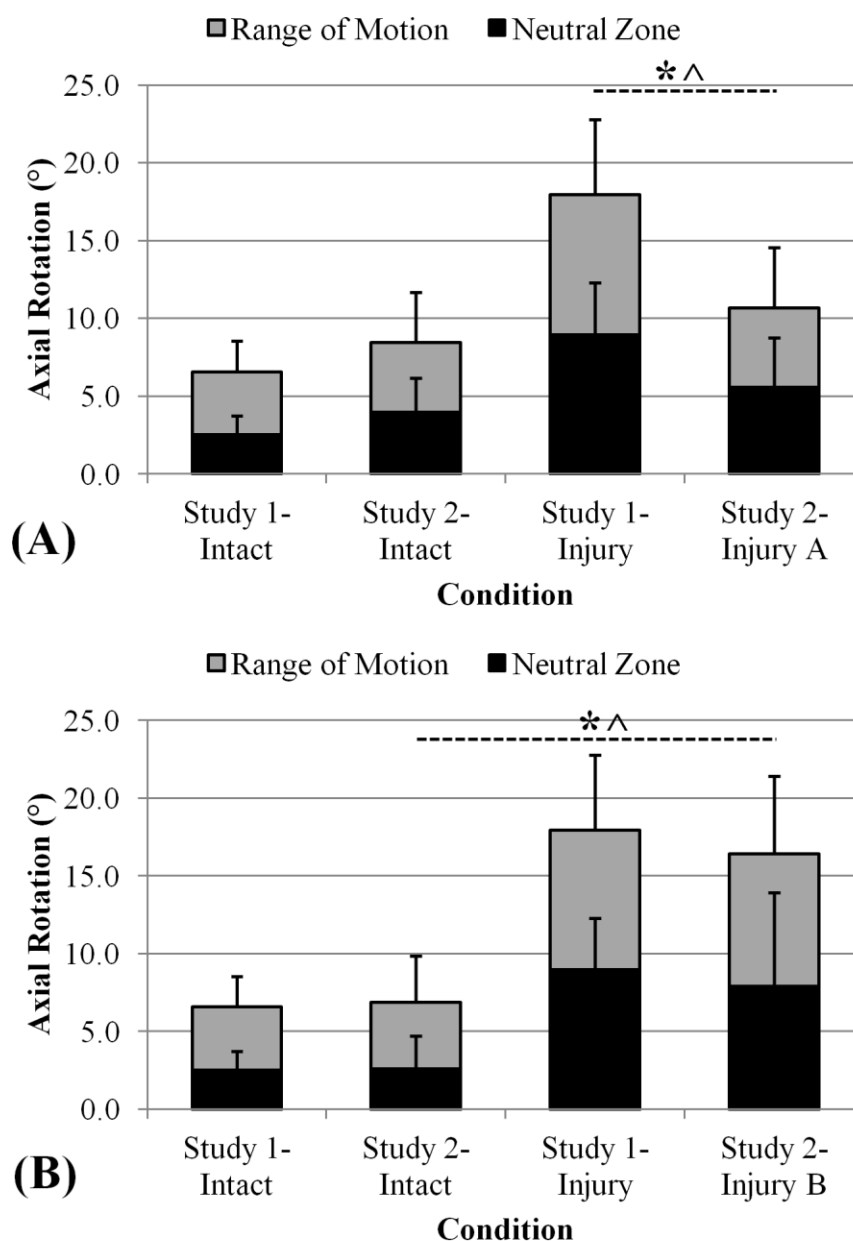


**Figure 3.6: Changes in Kinematic Stability of Axial Rotation**

Axial rotation ROM and NZ results for the previous dynamic unilateral facet perch injury (Study 1) and the current standardized injury model (Study 2) are shown. **(A)** Intact and injury data for Study 1 (n=9) and the first five specimens from Study 2, where Injury 2A represents the isolated surgical sectioning injury. **(B)** Intact and injury data for Study 1 and all specimens from Study 2 (n=10), with all specimens in Injury 2B sustaining the standard injury (sectioning plus perch). Statistical differences ( $p < 0.05$ ) are highlighted between groups via the dashed line and symbol representing ROM (\*) and NZ (^).

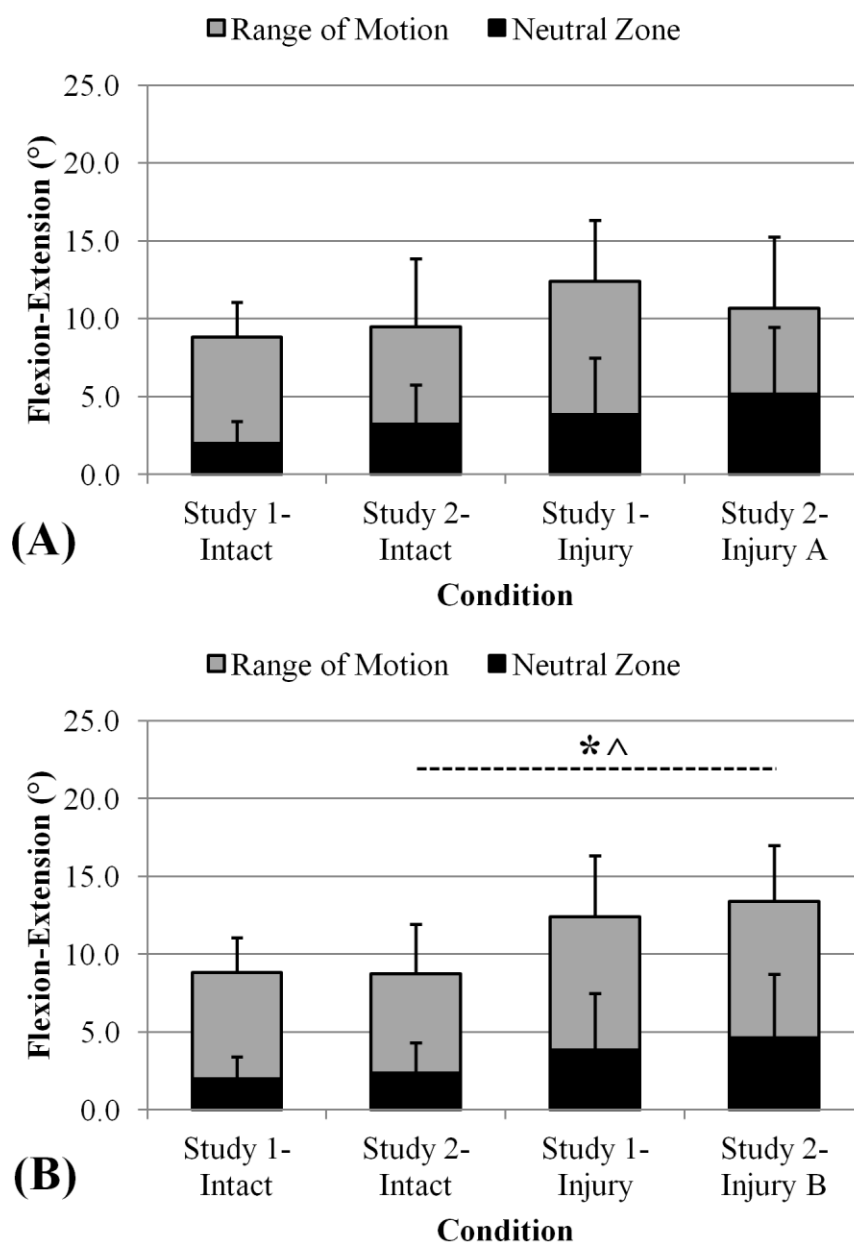


**Figure 3.7: Changes in Kinematic Stability of Flexion-Extension**

Flexion-extension ROM and NZ results for the previous dynamic unilateral facet perch injury (Study 1) and the current standardized injury model (Study 2) are shown. **(A)** Intact and injury data for Study 1 (n=9) and the first five specimens from Study 2, where Injury 2A represents the isolated surgical sectioning injury. **(B)** Intact and injury data for Study 1 and all specimens from Study 2 (n=10), with all specimens in Injury 2B sustaining the standard injury (sectioning plus perch). Statistical differences ( $p<0.05$ ) are highlighted between groups via the dashed line and symbol representing ROM (\*) and NZ (^).

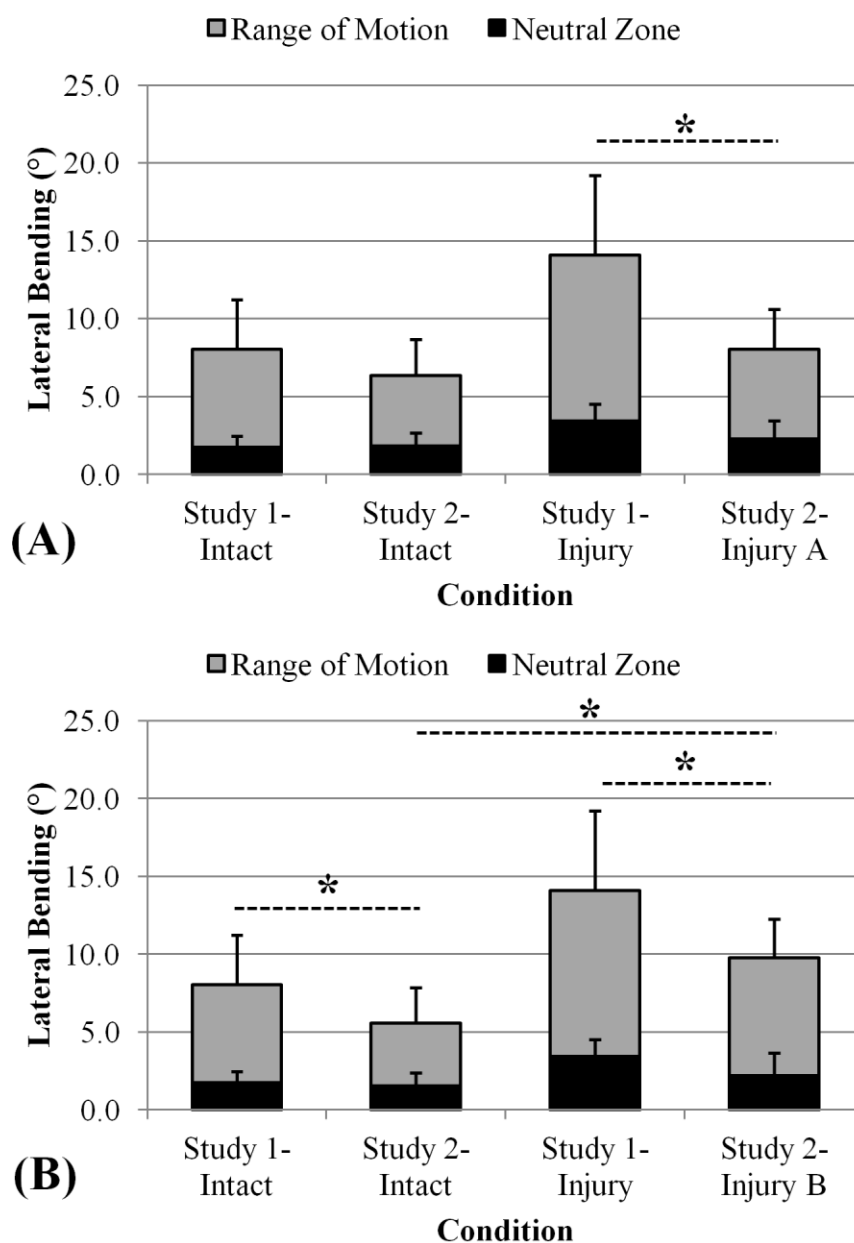


**Figure 3.8: Changes in Kinematic Stability of Lateral Bending**

Lateral bending ROM and NZ results for the previous dynamic unilateral facet perch injury (Study 1) and the current standardized injury model (Study 2) are shown. **(A)** Intact and injury data for Study 1 ( $n=9$ ) and the first five specimens from Study 2, where Injury 2A represents the isolated surgical sectioning injury. **(B)** Intact and injury data for Study 1 and all specimens from Study 2 ( $n=10$ ), with all specimens in Injury 2B sustaining the standard injury (sectioning plus perch). Statistical differences ( $p<0.05$ ) are highlighted between groups via the dashed line and symbol representing ROM (\*).

from both Study 2A & 2B were statistically equivalent ( $p > 0.05$ ) to the data from Study 1 (Figure 3.7A & 3.7B). Similar to the axial rotation data, the Study 2A sectioning injury alone did not achieve the same ROM as the Study 1 injury control ( $p < 0.05$ ) in lateral bending, but neither did the Study 2B SIM ROM (Figure 3.8A & 3.8B). However, for the Study 2B data set, the intact lateral bending was different from the Study 1 intact data ( $p < 0.05$ ). In this isolated case, with dissimilar intact ROM, the percent increase in the average lateral bending ROM from intact to injury was compared between Study 1 and 2B and it was found that both studies had a 75% increase in ROM.

### **3.3.3 PRELIMINARY SIM USAGE**

For the preliminary investigation into the SIM's applicability, both stages of the unilateral facet fracture were successfully created in four specimens. Both fracture levels had minimal effect on the ROM in all three simulated motions (Table 3.5). Subsequent comparison of the three instrumentation approaches, however, provided large decreases in ROM for all, with the largest decreases seen for posterior and combined instrumentation (Table 3.5).

## **3.4 DISCUSSION**

The unilateral facet perch injury is a well-defined injury pattern, yet the treatment strategy for this injury pattern is largely based on surgeons' expert opinion with no quantitative biomechanical evidence utilized in support of this decision (Dvorak *et al.*, 2007b; Vaccaro *et al.*, 2007). This study tried to address the lack of biomechanical knowledge by examining the soft tissue injuries from a unilateral facet perch in cadaver models and validated an appropriate SIM. The rationale for this was that a soft tissue injury model for a unilateral facet perch that was both reliable and valid would be the most relevant starting point for further *in vitro* testing. This testing could analyze instrumentation modalities as well as associated bony injuries, such as facet fractures. Furthermore, this study briefly examined potential applications of the injury model including the addition of a unilateral facet fracture and common instrumentation approaches.

**Table 3.5: Percent Change in ROM with Facet Fracture and Instrumentation (n=4)**

Condition	Axial Rotation % Change	Flexion-Extension % Change	Lateral Bend % Change
50% Facet Fracture	$1 \pm 4$	$3 \pm 8$	$-2 \pm 6$
100% Facet Fracture	$7 \pm 5$	$4 \pm 9$	$10 \pm 11$
Anterior Instrumentation	$-69 \pm 17$	$-83 \pm 8$	$-69 \pm 20$
Posterior Instrumentation	$-94 \pm 2$	$-85 \pm 5$	$-88 \pm 5$
Combined Instrumentation	$-97 \pm 1$	$-95 \pm 1$	$-89 \pm 5$

**Note:** (1) Percent change for the facet fractures refer to change from ROM of standard injury. (2) Instrumentations are relative to the change from standard injury plus 100% facet fracture.

This investigation was successful in utilizing an *in vitro* model to produce a unilateral perched facet. The most common soft tissue injury pattern observed consisted of disruptions of the facet capsules bilaterally, the ipsilateral ligamentum flavum, and greater than 50% of the contralateral annulus and nucleus pulposus. These findings are similar to those of Vaccaro *et al.* who identified the ligamentum flavum, nucleus pulposus, and facet capsules as the most commonly disrupted structures seen on MRI, with the interspinous and supraspinous ligament also disrupted in 60% and 40% of their specimens, respectively (Vaccaro *et al.*, 2001). In the current investigation, the authors observed the interspinous and supraspinous as stretched in only a small portion of the specimens tested. This difference may be attributed to the poor specificity associated with the ability of MRI to diagnosis cervical spine soft tissue injury (Rihn *et al.*, 2010). A cadaveric study by Sim *et al.* and a subsequent study by Ebraheim *et al.* identified the ipsilateral facet capsule, ipsilateral ligamentum flavum, and more than 50% of the ipsilateral annulus as structures requiring resection to produce a unilateral facet dislocation (Ebraheim *et al.*, 2009; Sim *et al.*, 2001). This further demonstrates the importance of the anterior discoligamentous complex as a passive restraint to unilateral facet subluxation or dislocation.

The current results also identified bilateral facet capsular disruption commonly attributed to unilateral facet injuries, while Sim *et al.* demonstrated only a unilateral facet capsular injury (Sim *et al.*, 2001). Again, the explanation for this disparity could be based on the difference in injury mechanisms; their model of lateral distraction followed by sequential ablation of taut soft tissues implies the contralateral side would never experience distraction forces. In agreement with the present findings, Vaccaro *et al.* identified bilateral facet capsule injury in their MRI observations (Vaccaro *et al.*, 2001). The results of the current study therefore reinforce and further demonstrate the important concept that although referred to as *unilateral* facet injuries, there is in fact injury to the facets bilaterally.

Surgical sectioning alone did not produce a valid injury model for a unilateral facet perch, which potentially calls into question the validity of previous studies utilizing sectioning techniques to recreate traumatic injuries. While measured flexion-extension



was found equivalent to the control data for both Study 2A and 2B injuries, this was not the case in axial rotation and lateral bending. For the latter two motions, rotating the spine to the unilaterally perched position following surgical sectioning (to create the SIM) showed excellent validity in terms of reproducing the increases in ROM and NZ compared to the injury control. Furthermore, the SIM provided a more reliable and consistent injury pattern than the previous mechanism of injury method. Therefore, the original hypothesis is accepted that the instability of a unilateral facet perch could not be reproduced through surgical sectioning alone, and that some attenuation of the remaining soft tissues was required.

To the authors' knowledge, this is the first study of its kind to attempt to validate a standardized soft tissue injury model for a specific injury pattern based on previously collected dynamic injury data. The large majority of biomechanical studies evaluating traumatic cervical spine injuries or the effectiveness of various treatment options have modeled the *in vitro* injuries using a stepwise surgical sectioning approach (Arand *et al.*, 2002; Brown *et al.*, 2005; Do Koh *et al.*, 2001; Lehmann *et al.*, 2004; Panjabi *et al.*, 1975; Paxinos *et al.*, 2009; Pitzen *et al.*, 2003; Rasoulinejad *et al.*, 2012; Samartzis *et al.*, 2010; Shea *et al.*, 1992; Sim *et al.*, 2001; Traynelis *et al.*, 1993). Whether these *in vitro* biomechanics studies have adequately captured the expected instability of the clinical injury mechanism is unknown although the results of this study question the validity of that approach. This study demonstrates that, the remaining intact soft tissues, as well as the intact portions of partially disrupted tissues, provide a large contribution to the stability of the UFP injured spine. Furthermore, the majority of these previous studies evaluated treatment modalities using a model consisting of a substantial greater soft tissue disruption than the model of the current study. These larger injuries have subsequently been generalized to less severe injury patterns during the development of treatment algorithms (Do Koh *et al.*, 2001; Dvorak *et al.*, 2007b; Iannuzzi *et al.*, 2006; Pitzen *et al.*, 2003; Vaccaro *et al.*, 2007).

A brief investigation of the applicability of the SIM as a validated starting point for further injury and instrumentation comparisons was undertaken in four specimens. With this small a sample size, no statistical analysis was performed but trends in results

were similar to other studies investigating the biomechanical effects of cervical spine instrumentation (Do Koh *et al.*, 2001). Interestingly, the effect of the additional facet fracture states had almost a negligible effect on the ROM of the SIM. Previous data from Chapter 2 indicated that facet fractures can increase flexibility over an isolated posterior soft tissue injury, yet with this particular SIM for a UFP no large changes were identified. This is potentially the result of the lost stabilizing effect on ROM provided by the facet joint once the joint has been pathologically subluxed to the perched position and attenuated the stabilizing ligaments.

A number of limitations of UFP injury creation have been identified. The destructive nature of the experimental protocol in Study 1 allowed for only a single mechanism of injury to be studied. Although this injury mechanism was chosen based on previous literature (Allen *et al.*, 1982; Argenson *et al.*, 1988; Braakman and Vinken, 1967; Burke and Berryman, 1971; Crawford *et al.*, 2002; Kaye and Nance, 1990; Norton, 1962; Roaf, 1960; Young *et al.*, 1989), it is almost certain that other injury mechanisms occur *in vivo*, to which the current results may not be applicable. Furthermore, this mechanism was induced at a much slower rate than could generally be expected to occur with traumatic forces, which may alter the nature and/or extent of soft tissue damage. However, the soft tissue injury pattern identified did coincide with previous literature. While a high-speed mechanism of injury may have been more clinically relevant, it was necessary to apply rotation at a slower rate to consistently stop the rotation at the moment of facet perch.

Limitations of the SIM are also evident. First, the authors used previously collected *in vitro* flexibility data to validate the SIM for a unilateral facet perch. However, there is no available *in vivo* data describing changes in spinal kinematics with this injury. In this case, the dynamic mechanism of injury simulated in the lab then served as the next best “control” data for biomechanical instability as measured by changes in ROM and NZ. Additionally, it was found that some weakening or attenuation of the remaining tissues was required to achieve the desired increases in flexibility, but unfortunately there was no direct way to determine how much each structure was plastically deformed. By rotating the sectioned specimen to the perched position, the

authors have attempted to induce the best estimate for how much soft tissue stretching would likely occur. There may have been, however, some inherent variability in how much the remaining soft tissues were stretched depending on a number of factors including applied torque, soft tissue integrity and specimen age (*i.e.*, an older population was used).

In conclusion, the dissection results from this work demonstrated that a substantial injury occurs to the anterior discoligamentous complex following a unilateral rotary subluxation to a perched position, and that the capsular injury occurs bilaterally. Furthermore, the ALL and PLL are not important passive restraints to a perched unilateral facet injury. Kinematic data collected found a large increase in both ROM and NZ following the unilateral facet injury, especially in axial rotation. In regards to the SIM, two steps were required to produce a valid and reliable soft tissue injury model for a unilateral facet perch. The consistent ligament sectioning, step one, provided the reliability and the second step of rotation ensured the validity. The fact that sectioning alone was insufficient and that some degree of attenuation in the remaining soft tissues was required suggests that in the clinical scenario of a traumatic flexion-distraction injury there is most likely some amount of plastic deformation in all of the surrounding tissues, even if not visually disrupted.

### **3.5 SUMMARY & FUTURE DIRECTIONS**

This investigation showed that the spinal loading simulator can be an effective tool for inducing clinically-relevant injury mechanisms in cadaver spine specimens. However, the visualization of the injury was challenging (*i.e.*, to see the precise moment of perched facets) and may have been slightly variable between specimens. One method to improve this would be visualization of the motion segment anatomy using computer bone models, to recreate the kinematics of the perched facet joint. Furthermore, this study found that the additional facet fracture injury had little outcome on the ROM once the specimen had already been perched. The loss of this joint may, however, effect the axis of rotation and needs to be further investigated. Finally, this study again found anterior instrumentation was less stable compared to posterior instrumentation. However,

with the clinical success of the anterior approach, this data may suggest that other important factors need to be considered.

### 3.6 REFERENCES

Allen, B.L., Ferguson, R.L., Lehmann, T.R., O'Brien, R.P., 1982. A mechanistic classification of closed, indirect fractures and dislocations of the lower cervical spine. *Spine* 7, 1–27.

Arand, M., Neller, S., Kinzl, L., Claes, L., Wilke, H.J., 2002. The traumatic spondylolisthesis of the axis. A biomechanical in vitro evaluation of an instability model and clinical relevant constructs for stabilization. *Clinical Biomechanics* 17, 432–8.

Argenson, C., Lovet, J., Sanouiller, J., Peretti, F. De, 1988. Traumatic rotatory displacement of the lower cervical spine. *Spine* 13, 767–773.

Benzel, E.C., 2001. *Biomechanics of Spine Stabilization, 2nd edition*. Thieme, New York, p. 79.

Braakman, R., Vinken, P., 1967. Unilateral facet interlocking in the lower cervical spine. *Journal of Bone & Joint Surgery* 49-B, 249–257.

Brown, T., Reitman, C.A., Nguyen, L., Hipp, J.A., 2005. Intervertebral motion after incremental damage to the posterior structures of the cervical spine. *Spine* 30, E503–508.

Burke, D., Berryman, D., 1971. The place of closed manipulation in the management of flexion-rotation dislocations of the cervical spine. *Journal of Bone & Joint Surgery* 53-B, 165–182.

Crawford, N.R., Duggal, N., Chamberlain, R.H., Park, S.C., *et al.*, 2002. Unilateral cervical facet dislocation: injury mechanism and biomechanical consequences. *Spine* 27, 1858–1864.

Do Koh, Y., Lim, T.H., Won You, J., Eck, J., An, H.S., 2001. A biomechanical comparison of modern anterior and posterior plate fixation of the cervical spine. *Spine* 26, 15–21.

Duggal, N., Chamberlain, R.H., Park, S.C., Sonntag, V.K.H., *et al.*, 2005. Unilateral cervical facet dislocation: biomechanics of fixation. *Spine* 30, E164–168.

Dvorak, M.F., Fisher, C.G., Aarabi, B., Harris, M.B., *et al.*, 2007a. Clinical outcomes of 90 isolated unilateral facet fractures, subluxations, and dislocations treated surgically and nonoperatively. *Spine* 32, 3007–3013.

Dvorak, M.F., Fisher, C.G., Fehlings, M.G., Rampersaud, Y.R., *et al.*, 2007b. The surgical approach to subaxial cervical spine injuries: an evidence-based algorithm based on the SLIC classification system. *Spine* 32, 2620–2629.

Dvorak, M.F., Pitzen, T., Zhu, Q., Gordon, J.D., *et al.*, 2005. Anterior cervical plate fixation: a biomechanical study to evaluate the effects of plate design, endplate preparation, and bone mineral density. *Spine* 30, 294–301.

Ebraheim, N.A., Liu, J., Ramineni, S.K., Liu, X., *et al.*, 2009. Morphological changes in the cervical intervertebral foramen dimensions with unilateral facet joint dislocation. *Injury* 40, 1157–1160.

Ianuzzi, A., Zambrano, I., Tataria, J., Ameerally, A., *et al.*, 2006. Biomechanical evaluation of surgical constructs for stabilization of cervical teardrop fractures. *The Spine Journal* 16, 514–523.

Kaye, J.J., Nance, E.P., 1990. Cervical spine trauma. *Orthopaedic Clinics of North America* 21, 449–462.

Kwon, B.K., Vaccaro, A.R., Grauer, J.N., Fisher, C.G., Dvorak, M.F., 2006. Subaxial cervical spine trauma. *Journal of the American Academy of Orthopaedic Surgeons* 14, 78–89.

Lehmann, W., Blauth, M., Briem, D., Schmidt, U., 2004. Biomechanical analysis of anterior cervical spine plate fixation systems with unicortical and bicortical screw purchase. *European Spine Journal* 13, 69–75.

Norton, W.L., 1962. Fractures and dislocations of the cervical spine. *Journal of Bone & Joint Surgery* 44-A, 115–139.

Panjabi, M., White, A., Johnson, R., 1975. Cervical spine mechanics as a function of transection of components. *Journal of Biomechanics* 8, 327–336.

Panjabi, M.M., 1988. Biomechanical evaluation of spinal fixation devices: I. A conceptual framework. *Spine* 13, 1129–1134.

Panjabi, M.M., Simpson, A.K., Ivancic, P.C., Pearson, A.M., *et al.*, 2007. Cervical facet joint kinematics during bilateral facet dislocation. *European Spine Journal* 16, 1680–1688.

Paxinos, O., Ghanayem, A.J., Zindrick, M.R., Voronov, L.I., *et al.*, 2009. Anterior cervical discectomy and fusion with a locked plate and wedged graft effectively stabilizes flexion-distraction stage-3 injury in the lower cervical spine: a biomechanical study. *Spine* 34, E9–15.

Pitzen, T., Lane, C., Goertzen, D., Dvorak, M., *et al.*, 2003. Anterior cervical plate fixation: biomechanical effectiveness as a function of posterior element injury. *Journal of Neurosurgery* 99, 84–90.

Rasoulinejad, P., McLachlin, S.D., Bailey, S.I., Gurr, K.R., *et al.*, 2012. The importance of the posterior osteoligamentous complex to subaxial cervical spine stability in relation to a unilateral facet injury. *The Spine Journal* 22, 590–595.

Rihn, J.A., Fisher, C., Harrop, J., Morrison, W., *et al.*, 2010. Assessment of the posterior ligamentous complex following acute cervical spine trauma. *Journal of Bone & Joint Surgery* 92-A, 583–589.

Roaf, R., 1960. A study of the mechanics of spinal injuries. *Journal of Bone & Joint Surgery* 42-B, 810–823.

Samartzis, D., Wein, S.M., Shen, F.H., Beazell, J., *et al.*, 2010. A revisitation of distractive-extension injuries of the subaxial cervical spine: a cadaveric and radiographic soft tissue analysis. *Spine* 35, 395–402.

Shea, M., Wittenberg, R.H., Edwards, W.T., A, W.A., Hayes, W.C., 1992. In vitro hyperextension injuries in the human cadaveric cervical spine. *Journal of Orthopaedic Research* 10, 911–916.

Sim, E., Vaccaro, A.R., Berzlanovich, A., Schwarz, N., Sim, B., 2001. In vitro genesis of subaxial cervical unilateral facet dislocations through sequential soft tissue ablation. *Spine* 26, 1317–1323.

Traynelis, V., Donaher, P., Roach, R., Kojimoto, H., Goel, V., 1993. Biomechanical comparison of anterior Caspar plate and three-level posterior fixation techniques in a human cadaveric model. *Journal of Neurosurgery* 79, 96–103.

Vaccaro, A.R., Hulbert, R.J., Patel, A.A., Fisher, C., *et al.*, 2007. The subaxial cervical spine injury classification system: a novel approach to recognize the importance of morphology, neurology, and integrity of the disco-ligamentous complex. *Spine* 32, 2365–2374.

Vaccaro, A.R., Madigan, L., Schweitzer, M.E., Flanders, A.E., *et al.*, 2001. Magnetic resonance imaging analysis of soft tissue disruption after flexion-distraction injuries of the subaxial cervical spine. *Spine* 26, 1866–1872.

Wilke, H.J., Wenger, K., Claes, L., 1998. Testing criteria for spinal implants: recommendations for the standardization of in vitro stability testing of spinal implants. *European Spine Journal* 7, 148–154.

Young, J.W., Resnik, C.S., DeCandido, P., Mirvis, S.E., 1989. The laminar space in the diagnosis of rotational flexion injuries of the cervical spine. *American Journal of Roentgenology* 152, 103–107.

## CHAPTER 4: A REFINED TECHNIQUE TO CALCULATE HELICAL AXES FROM SIX-DOF TRACKER OUTPUT WITH AN APPLICATION IN SPINAL KINEMATICS

***OVERVIEW:** The kinematic data presented so far in this thesis has only considered neutral zone and range of motion calculations based on Euler angle analyses; it would be of interest to consider other techniques that describe the entire motion pathway of a spine motion segment before and after injury or surgical intervention. This chapter explores a simple, refined technique to readily produce FHAs from an Optotrak Certus® based tracking system with minimal error, and display the results using freeware available in the public domain. The efficacy of the technique is demonstrated for the spine in particular, but is applicable to all joint motion studies that capture kinematics using six-DOF rigid body trackers.*

### 4.1 INTRODUCTION

Tracking systems and associated kinematic algorithms are essential tools for understanding joint motion, as well as assessing the effects of pathologies and their related treatments on joint function and stability. One such technique, known as the finite helical axis (FHA) or screw displacement axis, defines the pose of an object in terms of a unique axis vector, coupled with a rotation about and a translation along the axis. These FHA parameters have been widely used to describe motion in the knee (Blankevoort *et al.*, 1990), spine (Kettler *et al.*, 2004), elbow (Duck *et al.*, 2003), ankle (Graf *et al.*, 2012), and wrist (Woltring *et al.*, 1985). Specific to the spine, the most common application of the FHA technique has been to quantify the location of instantaneous centre of rotation of a motion segment while the spine completes a prescribed range of motion (*e.g.*, flexion-extension trial) (Grip *et al.*, 2008; Rousseau *et al.*, 2006). This measure can be sensitive to alterations in the kinematics of the motion segment resulting from trauma, degeneration, or the application of instrumentation (Crawford *et al.*, 2002). Furthermore, with the development of many motion restoring (*i.e.*, dynamic stabilization) devices, this measure is frequently reported as a parameter of interest for evaluating the device efficacy (Kowalczyk *et al.*, 2011; Niosi *et al.*, 2006).

Most reported techniques to determine the FHA require a set of non-collinear markers affixed to an object, or a set of observable features on the object; however, these require complex vector algorithms and significant mathematical efforts to determine the optimal FHA parameters (Kinzel *et al.*, 1972; Metzger *et al.*, 2010; Spoor and Veldpaus, 1980; Woltring *et al.*, 1985). These methods are categorized as ‘vector observation’ algorithms (Markley, 1988), which ultimately develop a screw  $[S]$  matrix from which the FHA parameters are extracted (Beggs, 1983; Spoor and Veldpaus, 1980).

Over the last decade, there has been an increasing prevalence of tracking systems using prepackaged rigid body trackers that natively output six degrees-of-freedom (six-DOF) pose information (*i.e.*, position and orientation) in the form of a  $4 \times 4$  transformation  $[T]$  matrix. Generally, tracker pose is output relative to the tracker’s global coordinate frame; however, with simple matrix multiplications, the  $[T]$  matrices of sequential poses can be transformed to represent the displacement of a tracker relative to itself. This  $[T]$  matrix is consistent with the  $[S]$  matrix produced by an FHA algorithm (Beggs, 1983). The nature of the  $[S]$  matrix and its simple derivation from  $[T]$  matrix output are salient concepts that have not been elucidated in the biomechanics literature. This has led to a common practice among investigators, where  $[T]$  matrix output is converted into sets of simulated marker locations in order to make native tracker output compatible with available FHA ‘vector observation’ algorithms (Duck *et al.*, 2004; Ferreira *et al.*, 2011).

Challenges still remain in determining accurate FHAs for investigations of joint kinematics due to inherent tracker error and vibration (Metzger *et al.*, 2010). One available technique to improve the calculated FHAs is the use of a “moving window” analysis (Crawford, 2006; Ferreira *et al.*, 2011). Crawford suggested an arbitrary window size of  $\pm 10$  data points between calculations for each FHA would reduce the error; however, this may be ineffective for rapid movements or those that have inconsistent angular velocity (Crawford, 2006). A more effective solution may be to traverse the data stream, while evaluating the rotational displacement, in order to achieve a prescribed minimum rotation before an FHA is calculated (Ferreira *et al.*, 2011). This method guarantees the desired window size and maximizes the number of FHAs created.



The purposes of this study were: (1) to define a simple and effective technique to calculate the  $[S]$  matrix directly from six-DOF rigid body trackers; (2) to investigate a “moving window” calculation technique to generate the largest possible number of FHAs that accurately characterize the motion; and (3) to demonstrate the applicability of these techniques to spinal kinematic data.

## 4.2 MATERIALS AND METHODS

### 4.2.1 MATHEMATICAL CONCEPTS

The matrix algebra syntax in this work follows the notation of Craig as previously used in Section 1.4.2 (Craig, 2005), where the leading sub- and super-scripts indicate, respectively, the coordinate frame of an object with respect to a frame of reference, while the trailing sub-script indicates qualifying information (*i.e.*, description, time point, matrix dimensions, *etc.*). To reiterate, the position and orientation of an object *Body1* at an instant in time with respect to a reference frame *Body2* can be defined by a  $4 \times 4$   $[T]$  matrix, which is made up of a  $3 \times 3$  direction cosine rotation  $[R]$  matrix and a  $3 \times 1$   $xyz$  position vector  $[P]$  (Eq. 4.1).

$${}_{Body1}^{Body2}[T]_{4 \times 4} = \begin{bmatrix} {}_{Body1}^{Body2}[R]_{3 \times 3} & {}_{Body1,origin}^{Body2}[P] \\ 0 & 0 & 0 & 1 \end{bmatrix} \quad \text{Eq. 4.1}$$

As *Body1* moves, a sequence of  $[T]$  matrices is defined. However, if the interest is in defining a series of FHAs, then displacement of *Body1* through two time points is required. Though not widely reported in the literature, Beggs defines the relationship between the  $[S]$  and  $[T]$  matrices as (Beggs, 1983):

$${}_{Body1}^{Body2}[T]_{time\ 2} = {}_{Body1}^{Body2}[T]_{time\ 1}[S]^{-1} \quad \text{Eq. 4.2}$$

or rearranged for  $[S]$  as:

$$[S] = {}_{Body2}^{Body1}[T]_{time\ 1} {}_{Body1}^{Body2}[T]_{time\ 2} = {}_{Body1,time2}^{Body1,time1}[T] \quad \text{Eq. 4.3}$$

Therefore, without any complex numerical algorithms, the  $[S]$  matrix can be determined by simple matrix multiplication. The FHA parameters relative to *Body1* were then

calculated using the formulas described in Spoor and Veldpaus (see Appendix C) (Spoor and Veldpaus, 1980).

#### 4.2.2 EXPERIMENTAL DATA COLLECTION

Similar to previous chapters, an Optotrak Certus® motion capture system (NDI, Waterloo, ON, Canada) was used. The rigid body trackers were the Optotrak® Smart Markers, which contain a triad non-collinear infrared light emitting diodes (reported accuracy of 0.1mm). Data were captured using NDI First Principles™ software, recording the six-DOF information of the rigid bodies in transformation matrix format.

A custom jig (CNC machined) that was capable of fixed planar rotations as small as  $0.5^\circ$  about a hinge joint (considered the  $Z$  axis) was used for this study. Two trackers were rigidly attached to the moving portion of the jig and two more to a fixed portion (Figure 4.1). The two moving trackers (referred to as “*Body1\_close*” and “*Body1\_far*”) were positioned approximately 6cm and 10cm away from the hinge axis, respectively. The fixed trackers were also positioned so that one was closer to the hinge axis (*i.e.*, “*Body2\_close*” and “*Body2\_far*”). The camera was rigidly mounted to the wall during testing, approximately 4m away from the trackers. Tracker data were recorded at 60Hz and averaged over 2s in 51 different static positions, generated as the jig planar rotated from  $0^\circ$  (neutral) to  $25^\circ$  in  $0.5^\circ$  increments. In each position, three different sets of  $[T]$  matrices were generated for each of the two moving markers: the moving tracker relative to “*Body2\_close*”, “*Body2\_far*”, and the camera (*i.e.*, global reference frame).

#### 4.2.3 JIG DATA ANALYSIS

The  $[S]$  matrices were calculated directly from  $[T]$  matrices using custom LabVIEW™ software (National Instruments, Austin, TX, USA) (see Appendix C). From

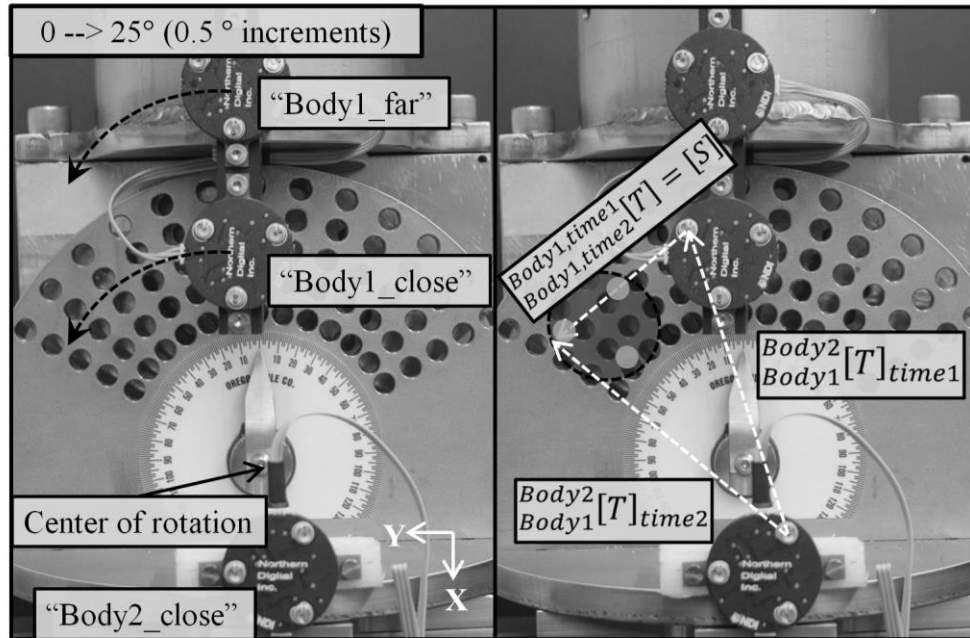


**Figure 4.1: Experimental Tracker Setup on Custom Jig**

**Left:** A custom machined jig that was capable of incremental planer rotations of  $0.5^\circ$  about a fixed hinge joint was used. Four Optotrak® Smart Markers (rigid body trackers) were attached, two to the moving portion and two to the fixed portion (“Body2\_far” not shown). **Right:** Transformation  $[T]$  matrices of a moving tracker “Body1” with respect a reference “Body2” (either a fixed tracker or the camera) were determined by the Optotrak® software. The screw  $[S]$  matrix was then calculated for varying displacements (i.e.,  $1 \rightarrow 2$ ).

these, the FHA direction cosines, rotation about the FHA (which should match the induced rotation), and the location of the centre of rotation (as measured by the *XY* intercept of the FHA with the *Z*=0 plane) were calculated. No data filtering was performed.

Data were initially evaluated as displacement from the neutral 0° position (*i.e.*, 0-0.5°, 0-1°, etc.). Subsequent evaluation explored the concept of “moving window” analysis. With the understanding that FHA calculations are error-prone for small rotations, this technique defined a minimum rotation that needed to be achieved before the calculated FHA was considered acceptable. For example, with this data set, if the minimum rotation were set to 5°, the FHA between 0-5° would be the first accepted. The starting point would then be incremented to the next row of data, such that the next FHA generated in this case would be for 0.5-5.5°. The effect of window size was evaluated for minimum rotations of 0-10°, where a 0° window size would calculate FHAs between adjacent time points regardless of the rotation between them.

#### 4.2.4 SPINE DATA ANALYSIS

In addition to evaluating the jig data, the effectiveness of this technique to calculate FHAs was examined using the intact spinal kinematics data from a single C4-C5 specimen previously tested in Chapter 3. In this case, the coordinate frame nomenclature becomes *Body2* → *C5* and *Body1* → *C4*, such that the FHA of the upper “moving” vertebrae is expressed in the lower vertebrae’s anatomic coordinate frame (*X*: Anterior-Posterior, *Y*: Medial-Lateral, *Z*: Superior-Inferior). Moving window sizes of 2-5° were investigated for each motion based on the previously calculated total ROM of the motion segment (~13°, 12°, 8.5° in axial rotation, flexion-extension, and lateral bending, respectively). The outcome measures of interest were the centre of rotation with the anatomic plane most normal to the axis of rotation (*i.e.*, flexion-extension axis would intersect with the sagittal plane) and the direction cosines of the FHAs generated. In contrast to the known fixed axis of rotation for the custom jig, the FHAs of the motion segment were expected to have significant scatter based on previous studies (Crawford *et al.*, 2002; Kettler *et al.*, 2004). As such, in addition to reporting the average and standard deviation of all FHAs generated, a new technique developed for computation geometry

was considered to quantify this scatter. This involved the use of an alpha shape, which can define a unique polygon that envelops the finite set of points representing the centres of rotation. As the scatter of the FHA changes, the area of the defined alpha shape will as well. Therefore, using a freely available MATLAB (R2012a; Mathworks, Natick, MA, USA) function (see Appendix E), alpha shapes and their areas were calculated for all window sizes for each motion.

## 4.3 RESULTS

### 4.3.1 JIG RESULTS

The rotations calculated about the FHA for the jig were within  $0.15^\circ$  of the prescribed rotation ( $0-25^\circ$  in  $0.5^\circ$  increments) for all 50 rotations, with an average absolute difference between the calculated and prescribed rotations of  $0.06 \pm 0.04^\circ$ . Without the moving window approach, the center of rotation position (which should be constant) demonstrated large standard deviations depending on the trackers used (Table 4.1). The most stable (*i.e.*, smallest standard deviation) FHA intercept was obtained using the two “close” trackers.

Moving window analysis improved the axis direction and center of rotation accuracy with increasing window size (Table 4.2). For FHAs calculated using the “close” trackers, a window size of  $2^\circ$  or greater decreased standard deviation ( $<1\text{mm}$ ) and revealed an average center of rotation at 20.5, 65.8mm in the XY plane. Further increases in the window size did not improve the average location, but did further shrink the standard deviation. Similar improvements were also seen in the direction cosines, where larger window sizes revealed the FHA was nearly identical to the Z axis (Table 4.2).

### 4.3.2 SPINE RESULTS

As expected, the “moving window” technique applied to the spinal kinematics data generated a large number of FHAs for all window sizes investigated, with increased precision with increasing window size (Table 4.3 & 4.4). The effect of each window size on the generated intercept points (*i.e.*, centres of rotation) for the intact kinematics is

**Table 4.1: Window Size Effect on X-Y Intercept Standard Deviations**

Trackers Used	X-Y Intercept Standard Deviations (mm)			
	Relative to Fixed Tracker		Relative to Camera	
	X	Y	X	Y
<i>Body2_far, Body1_close</i>	6.6	24.9	5.9	29.1
<i>Body2_far, Body1_far</i>	12.5	26.5	9.5	30.9
<i>Body2_close, Body1_close</i>	8.4	7.9	N/A	N/A
<i>Body2_close, Body1_far</i>	12.3	11.7	N/A	N/A

**Note:** Non-applicable (N/A) represents the “relative to camera” calculation, which depends only on the moving tracker, “Body1”, and is therefore equivalent to the first two rows.

**Table 4.2: Window Size Effect on Average X-Y Intercept and the Direction Cosines**

Moving Window Size (°)	FHAs Created	Average X Intercept (mm)	Average Y Intercept (mm)	Average X Direction Cosine	Average Y Direction Cosine	Average Z Direction Cosine
0	50	20.2 ± 8.4	63.3 ± 7.9	0.019 ± 0.365	-0.005 ± 0.279	-0.895 ± 0.076
1	48	20.4 ± 1.6	65.0 ± 1.8	0.008 ± 0.130	0.000 ± 0.082	-0.987 ± 0.014
2	46	20.6 ± 0.9	65.5 ± 0.9	0.018 ± 0.088	-0.005 ± 0.052	-0.994 ± 0.006
3	44	20.4 ± 0.7	65.7 ± 0.5	0.029 ± 0.055	-0.005 ± 0.043	-0.997 ± 0.003
4	43	20.5 ± 0.5	65.8 ± 0.5	0.027 ± 0.045	-0.008 ± 0.034	-0.998 ± 0.002
5	40	20.5 ± 0.4	65.8 ± 0.4	0.028 ± 0.037	-0.005 ± 0.026	-0.999 ± 0.001
6	38	20.5 ± 0.4	65.8 ± 0.3	0.027 ± 0.027	-0.010 ± 0.017	-0.999 ± 0.001
7	36	20.5 ± 0.3	65.8 ± 0.2	0.028 ± 0.026	-0.009 ± 0.014	-0.999 ± 0.001
8	34	20.5 ± 0.3	65.8 ± 0.2	0.027 ± 0.023	-0.008 ± 0.015	-0.999 ± 0.001
9	33	20.5 ± 0.3	65.8 ± 0.2	0.027 ± 0.019	-0.007 ± 0.014	-0.999 ± 0.001
10	30	20.5 ± 0.2	65.8 ± 0.2	0.027 ± 0.020	-0.005 ± 0.013	-0.999 ± 0.001

**Note:** (1) The ‘moving window size’ represents the minimum rotation that must be observed prior to a FHA being generated. In the case of 0°, this means that no minimum is imposed and thus all potential FHAs are considered. (2) All data are reported relative to the “Body1\_close” tracker, where the standard deviation reported is based on the number of FHAs generated.

**Table 4.3: Window Size Effect on the FHAs Generated in Intact Spine Data**

Motion	Data Points in Final Cycle	Maximum ROM (°)	Window Size (°)	# of FHAs generated	Alpha Shape Area (mm <sup>2</sup> )
Axial Rotation	588	13.4	2	542	282.3
			3	525	170.8
			4	508	119.7
			5	492	89.5
Flexion-Extension	618	12.3	2	565	78.7
			3	534	34.6
			4	509	19.1
			5	466	13.3
Lateral Bending	454	8.5	2	388	291.0
			3	358	180.2
			4	274	88.6
			5*	191	58.8

**Note:** \*A 5° window size was used here to be consistent across motions even though it exceeds 50% of the maximum ROM. The “data skipping” effect this has is evident with the reduction in the number of FHAs generated.

**Table 4.4: Window Size Effect on the Average FHA Intercepts and Direction Cosines in Intact Spine Data**

Motion	WS (°)	Average X Intercept (mm)	Average Y Intercept (mm)	Average Z Intercept (mm)	Average X Direction Cosine	Average Y Direction Cosine	Average Z Direction Cosine
AR	2	10.1 ± 5.3	2.8 ± 4.5	0	0.563 ± 0.103	0.158 ± 0.104	0.796 ± 0.054
	3	10.7 ± 3.9	2.7 ± 4.0	0	0.578 ± 0.078	0.149 ± 0.099	0.791 ± 0.041
	4	11.1 ± 3.3	2.7 ± 3.6	0	0.588 ± 0.063	0.137 ± 0.095	0.789 ± 0.032
	5	11.2 ± 2.7	2.4 ± 3.2	0	0.593 ± 0.052	0.130 ± 0.088	0.788 ± 0.026
FE	2	-11.3 ± 1.8	0	8.5 ± 1.6	0.033 ± 0.027	0.998 ± 0.004	0.040 ± 0.037
	3	-11.2 ± 1.4	0	8.4 ± 1.1	0.023 ± 0.020	0.999 ± 0.003	0.034 ± 0.030
	4	-11.1 ± 1.1	0	8.2 ± 0.8	0.020 ± 0.015	0.999 ± 0.001	0.030 ± 0.025
	5	-11.2 ± 0.9	0	8.2 ± 0.7	0.021 ± 0.016	0.999 ± 0.001	0.029 ± 0.024
LB	2	0	-5.3 ± 3.8	12.0 ± 5.5	0.847 ± 0.111	0.092 ± 0.063	0.450 ± 0.235
	3	0	-5.6 ± 2.7	11.4 ± 4.3	0.826 ± 0.092	0.083 ± 0.052	0.521 ± 0.167
	4	0	-5.7 ± 2.0	11.8 ± 3.6	0.829 ± 0.069	0.074 ± 0.040	0.536 ± 0.112
	5	0	-5.4 ± 1.4	12.0 ± 3.2	0.839 ± 0.043	0.079 ± 0.028	0.531 ± 0.071

**Note:** Intercepts are displayed for the X, Y, or Z = 0 plane normal to the FHA. The number of FHAs used to calculate these averages and standard deviations are shown in Table 4.3.

shown for axial rotation (Figure 4.2A), flexion-extension (Figure 4.3A), and lateral bending (Figure 4.4A).

Similar to the jig results, the centre of rotation scatter was reduced with larger window sizes for all motions, as quantified with the alpha shape analysis (Figures 4.2B-4.4B). That is, with the decrease in scatter for smaller window sizes, the area of the alpha shape also decreased (Table 4.3)

From a qualitative evaluation of these data sets, it appeared that a window size based on a minimum rotation of  $4^\circ$  reduced some of the scatter present in the smaller window sizes, with little further change as the window size increased. Thus, using a window size of  $4^\circ$ , the FHAs generated from the spinal kinematic data were then plotted on 3D models of the vertebrae to show the deviation in the direction cosines of the FHA vector (Figures 4.5-4.7) (see Appendix F for the 3D bone model development).

## 4.4 DISCUSSION

FHAs are a valuable tool in joint kinematic analysis. This study presented a refined technique to calculate accurate FHAs, and is useful as a guide to expedite the work of investigators using six-DOF rigid body trackers. Using the screw matrix and a common FHA parameter extraction technique, the Optotrak® Smart Markers were very effective for determining FHA rotations as small as  $0.5^\circ$  about the jig's hinge to within  $0.15^\circ$  (Spoor and Veldpaus, 1980). When calculating the center of rotation of the hinge, small rotations ( $<2^\circ$ ) were very error-prone, but improved with application of the moving window technique, such that a standard deviation of less than 1mm for a minimum rotation of  $2^\circ$  or larger was achieved. As this window size was increased, there was a limited benefit to the accuracy, suggesting that a window size of  $2\text{-}5^\circ$  or higher would be appropriate for most biomechanical investigations, though joints with significantly larger ranges of motion could explore increased window sizes. For applications where the total range of motion is less than  $2^\circ$ , the current data suggests it would be challenging to recommend the FHA as a suitable technique, except for calculating an average FHA only. Furthermore, positioning trackers closer to the center of rotation, for both the moving and



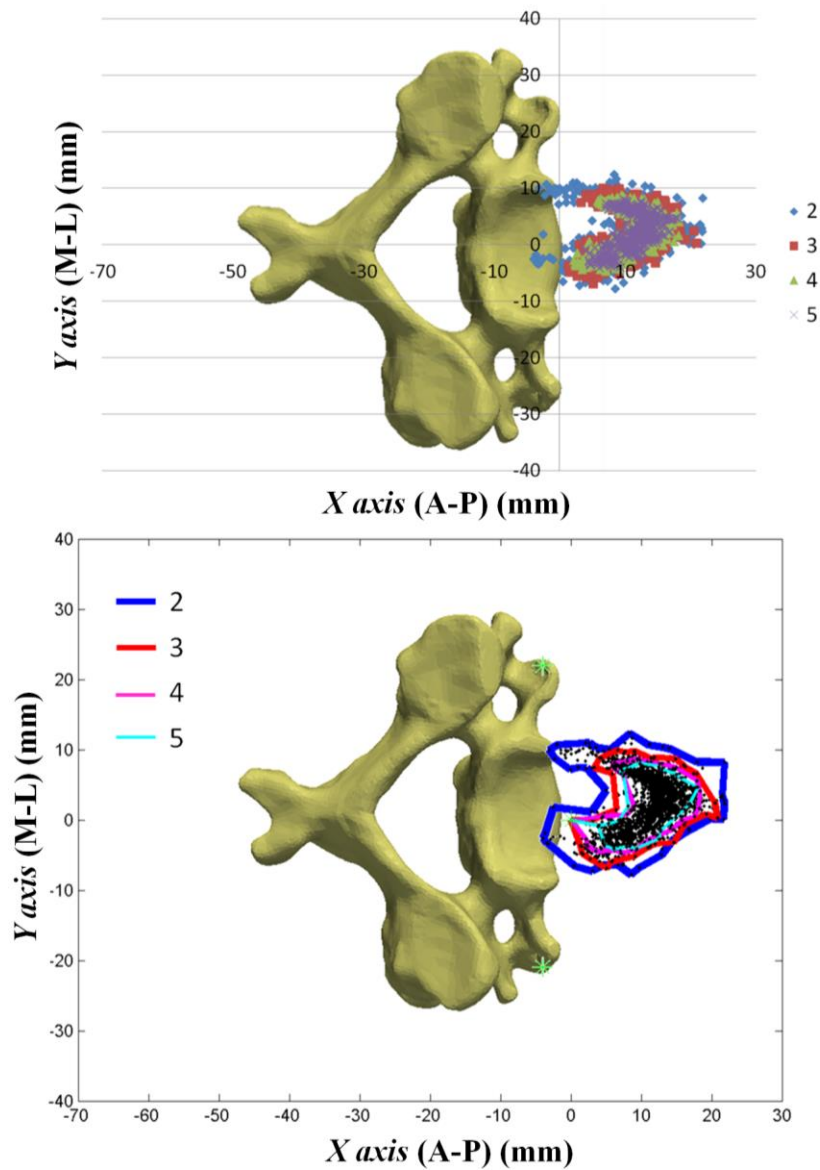


**Figure 4.2: Quantifying the Axial Rotation FHA Intercepts**

The axial rotation intercepts of the FHAs with the transverse plane ( $Z=0$ ) of the lower C5 vertebra were calculated as a function of window size (2-5 degrees). (A) In Microsoft Excel, a scatter plot displays the intercepts relative to the bony anatomy, but is difficult to quantify. (B) Using MATLAB, the same data can be quantified by calculating an alpha shape that envelops the intercepts for each window size. *Note: there is only a small change between the shapes generated for 3, 4, and 5 degrees, respectively, suggesting that a form of convergence is being reached.*

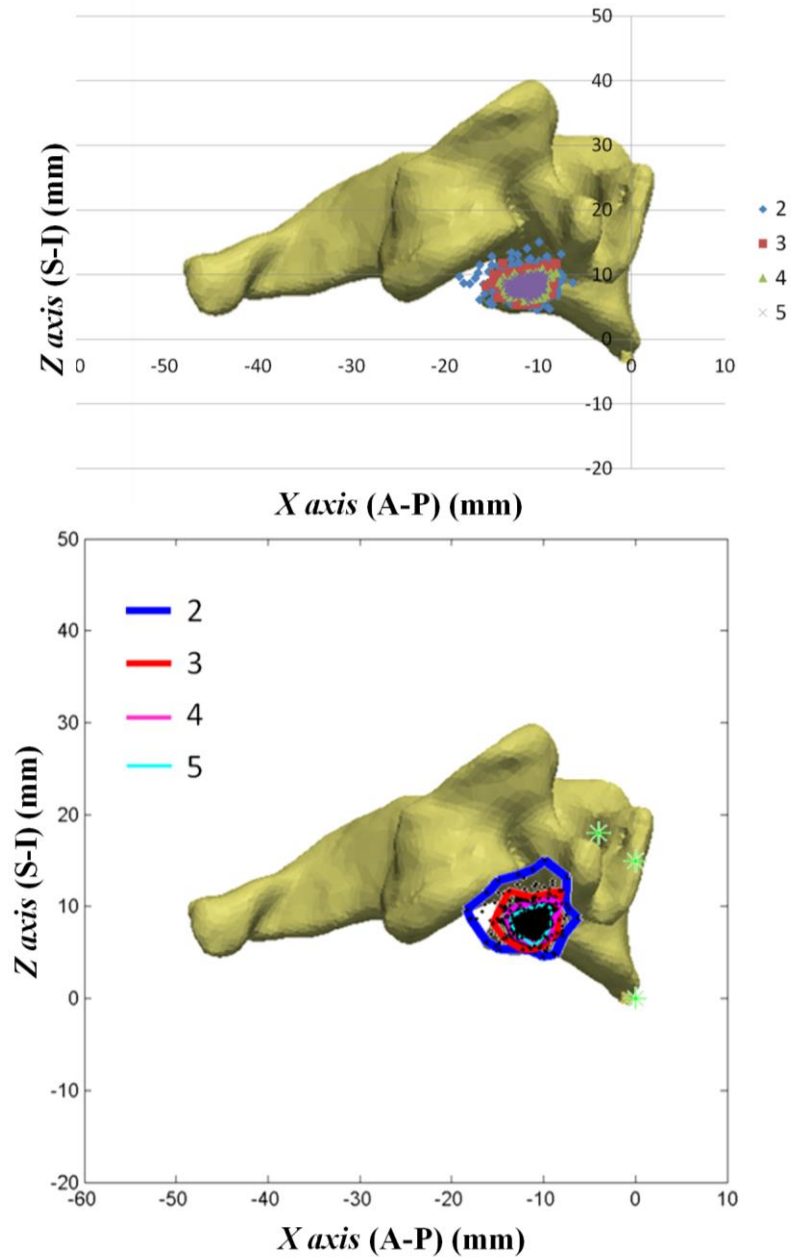


**Figure 4.3: Quantifying the Flexion-Extension FHA Intercepts**

The flexion-extension intercepts of the finite helical axes with the sagittal plane ( $Y=0$ ) of the lower C5 vertebra as a function of window size (2-5 degrees). **(A)** In Microsoft Excel, a scatter plot displays the intercepts relative to the bony anatomy, but is difficult to quantify. **(B)** Using MATLAB, the same data can be quantified by calculating an alpha shape that envelops the intercepts for each window size. *Note: there is only a small change between the shapes generated for 3, 4, and 5 degrees, respectively, suggesting that a form of convergence is being reached.*

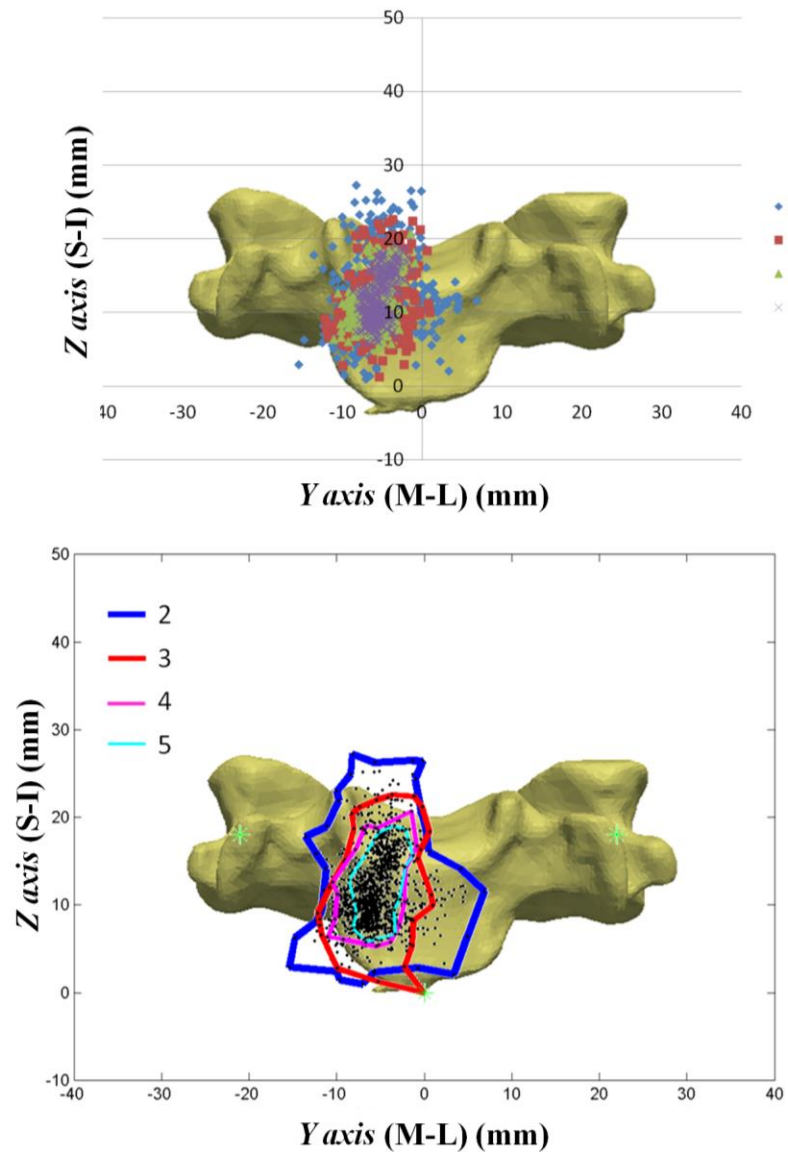


**Figure 4.4: Quantifying the Lateral Bending FHA Intercepts**

The lateral bending intercepts of the finite helical axes with the frontal plane ( $X=0$ ) of the lower C5 vertebra as a function of window size (2-5 degrees). (A) In Microsoft Excel, a scatter plot displays the intercepts relative to the bony anatomy, but is difficult to quantify. (B) Using MATLAB, the same data can be quantified by calculating an alpha shape that envelops the intercepts for each window size. *Note: there is only a small change between the shapes generated for 4 and 5 degrees, respectively, suggesting that a form of convergence is being reached.*



**Figure 4.5: 3D FHAs for Intact Axial Rotation**

The axial rotation FHAs of the upper C4 vertebra with respect to the lower C5 vertebra for a window size of 4 degrees. Due to the large amount of FHAs generated (>300), data were reduced to show only 5% (every 20<sup>th</sup> FHA) of the FHAs to reduce the graphics memory.

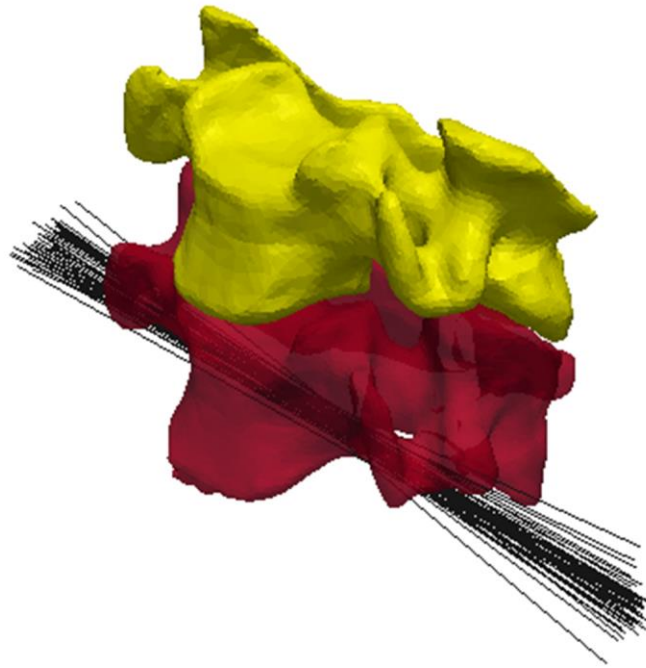


**Figure 4.6: 3D FHAs for Intact Flexion-Extension**

The flexion-extension FHAs of the upper C4 vertebra with respect to the lower C5 vertebra for a window size of 4 degrees. Due to the large amount of FHAs generated (>300), data were reduced to show only 5% (every 20<sup>th</sup> FHA) of the FHAs to reduce the graphics memory.

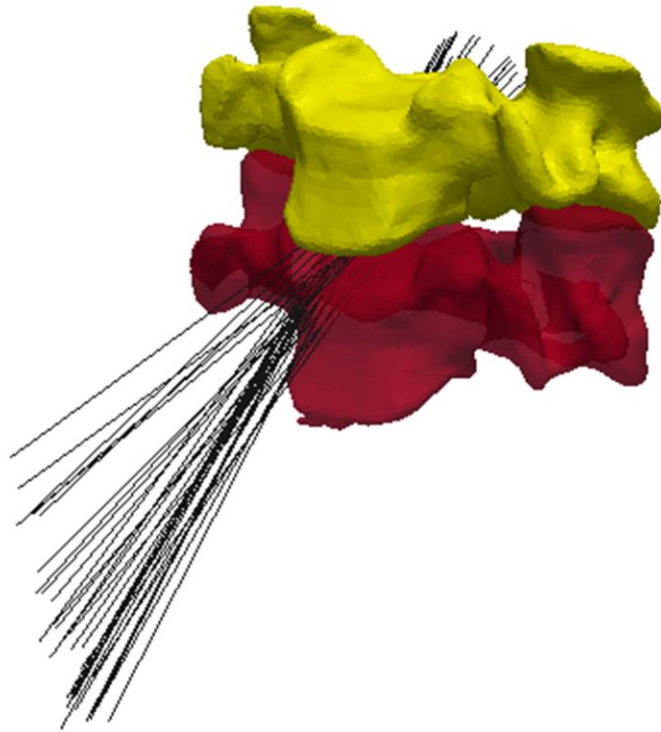


**Figure 4.7: 3D FHAs for Intact Lateral Bending**

The lateral bending FHAs of the upper C4 vertebra with respect to the lower C5 vertebra for a window size of 4 degrees. Due to the large amount of FHAs generated (>300), data were reduced to show only 5% (every 20<sup>th</sup> FHA) of the FHAs to reduce the graphics memory.

fixed trackers, improved the intercept stability, which agrees with previous investigations (Metzger *et al.*, 2010).

This study found that FHAs were more stable when calculated relative to a body reference tracker, as opposed to the camera. This is opposite to the findings of Duck *et al.* who, using the Flock of Birds® system (Ascension Technology, Milton, VT, USA), concluded that measurement error stack-up was reduced by avoiding a reference tracker, and instead fixing the reference body segment to the tracker's global coordinate frame (Duck *et al.*, 2004). This setup is not practical with the Optotrak Certus® since its working volume begins at 1.5m from the camera. Over this distance, vibration and building sway introduce relative movements between the camera and trackers on the specimen (Schmidt *et al.*, 2009). Although the base of the jig used in this study was fixed to ground and relative to the camera, the algorithm is compatible with a joint system that moves relative to the camera. Use of the reference tracker on the specimen cancels out gross movements of the specimen relative to the camera, thus isolating the joint motion. This was achieved by a simple coordinate transformation to set the reference tracker as the *Body1* frame for all the pose  $[T]$  matrices.

Based on the FHAs generated for the sample spinal kinematics data, it was found that  $4^\circ$  was an effective window size to reduce some of the FHA scatter. This matches the value reported by Metzger *et al.* for sufficient error reduction in a study comparing intercept error versus rotation angle, though not in a moving window analysis (Metzger *et al.*, 2010). It should be noted, however, that this minimum window size is also dependent on the total ROM experienced by the motion segment. For example, if the total ROM was less than  $4^\circ$ , zero FHAs would be generated with a window sized based on a  $4^\circ$  minimum rotation. In such cases, a smaller window size would have to be chosen, but with the caveat that more error would be present. One might ask, if it is known that larger window sizes reduce the error present, why not select the largest rotation possible? Selecting too large a window size will cause data to be skipped. To balance these competing goals of reducing error while still capturing sufficient FHAs to describe the entire ROM, the maximum window should not exceed more than half of the total ROM. Furthermore, the selected window size should be consistent across comparisons (within-

specimen or between specimens) to standardize the error present. This, however, is an advantage to the moving window technique, compared to calculations at varying displacements from some neutral position where the error would be inconsistent. A final consideration for use of the FHA as a comparison between specimens is variability in the intercept as a function of specimen size. As others have noted, FHA parameters should then be normalized to specimen size (Crawford, 2006).

One of the long standing problems with the use of FHAs to describe kinematics is that it has largely been used as a qualitative, visualization tool only. In this study, the calculated FHAs were displayed upon 3D models of the vertebrae to give a better representation of the axes themselves versus a single intercept point. A drawback to this approach is the labour-intensive development the 3D bone models from CT scans (see Appendix F). Even with this extensive visualization development, it is still difficult to quantify and relate FHAs between injury states and specimens. In contrast, the alpha shape measure that was introduced in this study presents a relatively simple technique to quantify the scatter of the FHAs in a relevant anatomic plane. Compared to reporting the average and standard deviation of the intercept, the alpha shape and its area present a quantitative measure that gives an increased sense of the deviation in the FHA throughout the entire loading cycle. While the implications of the change in alpha shape area for multiple window sizes is limited, it does present an interesting technique that could be used in future studies where the window size was constant, but the injury state is altered.

The topic of filtering was not included in this investigation, as the focus of this work was evaluating the FHA parameters generated from native tracker output. Filtering kinematic data has been shown by some to improve FHA accuracy for joint biomechanics and should be considered as an additional technique to reduce FHA error (Bottlang *et al.*, 1998; Duck *et al.*, 2004). Furthermore, a limitation of algorithm validation with the jig is that only static measurements were made. However, this was done to control known tracker positions and the number of time points. The hinge motion of the jig is also likely not representative of most biomechanics studies, yet for the preliminary evaluation of the moving window technique, it provided a reliable and stable axis of rotation. Furthermore, to account for hinge's potential biomechanical irrelevancy, the technique



was validated in experimentally collected spinal kinematic data, though with the understanding that a constant axis of rotation would not be found.

In conclusion, this work presented a simple but effective starting point for researchers looking to readily calculate FHAs from rigid body trackers. Furthermore, the accuracy of the FHA parameters produced showed improvement with moving window analysis based on a minimum rotation. For spinal kinematic data, a window size that uses a minimum  $4^\circ$  rotation would appear to be a reasonable starting point, unless this exceeds 50% of the total ROM for that motion. Furthermore, any comparisons using calculated FHA parameters should use an equivalent window size when reporting alpha shape area.

## 4.5 SUMMARY & FUTURE DIRECTIONS

Use of the FHA to date in the spine has been as a visualization tool for understanding how the centre of rotation changes over time; however, there is little evidence to show how it can quantitatively be used as a comparative measure between states and specimens. Use of the average intercept location is a possible option, but may grossly understate large deviations. As such, further investigation is required of the alpha shape area to detect changes in kinematics between injury states.

## 4.6 REFERENCES

- Beggs, J.S., 1983. *Kinematics*. Hemisphere, Washington, DC, p. 33–51.
- Blankevoort, L., Huiskes, R., De Lange, A., 1990. Helical axes of passive knee joint motions. *Journal of Biomechanics* 23, 1219–1229.
- Bottlang, M., Marsh, J.L., Brown, T.D., 1998. Factors influencing accuracy of screw displacement axis detection with a DC-based electromagnetic tracking system. *Journal of Biomechanical Engineering* 120, 431–435.
- Craig, J., 2005. *Introduction to robotics: mechanics and control, 3rd edition*. Pearson Prentice Hall, New Jersey, p. 19–45.
- Crawford, N.R., 2006. Technical note: determining and displaying the instantaneous axis of rotation of the spine. *World Spine Journal* 1, 53–56.

- Crawford, N.R., Duggal, N., Chamberlain, R.H., Park, S.C., *et al.*, 2002. Unilateral cervical facet dislocation: injury mechanism and biomechanical consequences. *Spine* 27, 1858–1864.
- Duck, T.R., Dunning, C.E., Armstrong, A.D., Johnson, J.A., King, G.J., 2003. Application of screw displacement axes to quantify elbow instability. *Clinical Biomechanics* 18, 303–310.
- Duck, T.R., Ferreira, L.M., King, G.J.W., Johnson, J.A., 2004. Assessment of screw displacement axis accuracy and repeatability for joint kinematic description using an electromagnetic tracking device. *Journal of Biomechanics* 37, 163–167.
- Ferreira, L.M., King, G.J.W., Johnson, J.A., 2011. Motion-derived coordinate systems reduce inter-subject variability of elbow flexion kinematics. *Journal of Orthopaedic Research* 29, 596–601.
- Graf, E.S., Wright, I.C., Stefanyshyn, D.J., 2012. Effect of relative marker movement on the calculation of the foot torsion axis using a combined Cardan angle and helical axis approach. *Computational and Mathematical Methods in Medicine* 2012, 1–6.
- Grip, H., Sundelin, G., Gerdle, B., Stefan Karlsson, J., 2008. Cervical helical axis characteristics and its center of rotation during active head and upper arm movements—comparisons of whiplash-associated disorders, non-specific neck pain and asymptomatic individuals. *Journal of Biomechanics* 41, 2799–2805.
- Kettler, A., Marin, F., Sattelmayer, G., Mohr, M., *et al.*, 2004. Finite helical axes of motion are a useful tool to describe the three-dimensional in vitro kinematics of the intact, injured and stabilised spine. *European Spine Journal* 13, 553–559.
- Kinzel, G., Hall, A., Hillberry, B., 1972. Measurement of the total motion between two body segments—I. Analytical development. *Journal of Biomechanics* 5, 93–105.
- Kowalczyk, I., Lazaro, B.C.R., Fink, M., Rabin, D., Duggal, N., 2011. Analysis of in vivo kinematics of 3 different cervical devices: Bryan disc, ProDisc-C, and Prestige LP disc. *Journal of Neurosurgery Spine* 15, 630–635.
- Markley, F., 1988. Attitude determination using vector observations and the singular value decomposition. *The Journal of the Astronautical Sciences* 36, 245–258.
- Metzger, M.F., Faruk Senan, N.A., O'Reilly, O.M., Lotz, J.C., 2010. Minimizing errors associated with calculating the location of the helical axis for spinal motions. *Journal of Biomechanics* 43, 2822–2829.
- Niosi, C.A., Zhu, Q.A., Wilson, D.C., Keynan, O., *et al.*, 2006. Biomechanical characterization of the three-dimensional kinematic behaviour of the Dynesys dynamic stabilization system: an in vitro study. *European Spine Journal* 15, 913–922.

Rousseau, M.-A., Bradford, D.S., Hadi, T.M., Pedersen, K.L., Lotz, J.C., 2006. The instant axis of rotation influences facet forces at L5/S1 during flexion/extension and lateral bending. *European Spine Journal* 15, 299–307.

Schmidt, J., Berg, D., Ploeg, H., Ploeg, L., 2009. Precision, repeatability and accuracy of Optotrak® optical motion tracking systems. *International Journal of Experimental and Computational Biomechanics* 1, 114–127.

Spoor, C., Veldpaus, F., 1980. Rigid body motion calculated from spatial co-ordinates of markers. *Journal of Biomechanics* 13, 391–393.

Woltring, H., Huiskes, R., De Lange, A., 1985. Finite centroid and helical axis estimation from noisy landmark measurements in the study of human joint kinematics. *Journal of Biomechanics* 18, 379–389.

## CHAPTER 5: INFLUENCE OF GRAFT SIZE ON THE KINEMATIC STABILITY OF ANTERIOR CERVICAL PLATING FOLLOWING IN VITRO FLEXION-DISTRACTION INJURIES

***OVERVIEW:** The biomechanical comparison of cervical spine instrumentation presented in earlier chapters suggested that anterior plating is less stable than posterior instrumentation for stages 1 and 2 flexion-distraction injuries, yet clinical reports examining anterior cervical discectomy and fusion with plating (ACDFP) have identified this as a successful treatment option for similar injuries. This leads to speculation that there are other clinically-relevant factors influencing stability that require investigation, including the surgeon's selection of an appropriate graft height for use with this procedure. As such, this chapter details a study conducted to examine the effect of varying graft height on ACDFP stability in multiple injury states, and provides some additional evidence for surgical management of these injuries. In addition to the traditional range of motion measures, the kinematic techniques developed in Chapter 4 were applied to determine their effectiveness in quantifying changes in stability between injury states.*

### 5.1 INTRODUCTION

Successful instrumented fusion of the cervical spine requires consideration of not only the clinical and basic science evidence gathered to date, in addition to the surgeon's own preferences and experiences, but also other patient and surgical factors (Brodke *et al.*, 2003; Kwon *et al.*, 2007). Patient factors can be considered as inherent traits, such as age and associated co-morbidities. Surgical factors are largely choices made by the surgeon; for example, the instrumentation type, size, shape, or other manufacturer options (Kwon *et al.*, 2006). For all ACDFP procedures, one such surgical factor is the surgeon's selection of an appropriate graft size to fit in the disc space. The purpose of the graft, in addition to promoting bone-on-bone fusion, is to restore disc space height, soft tissue tensioning, and normal spine curvature. Selecting a larger graft may increase stability as a result of restored tension in the ligaments, yet too much distraction decreases the load

carried by the facet joint. Olsewski *et al.* noted that a distraction of 3mm or greater over baseline height significantly reduced the ratio of posterior element to graft loading (Olsewski *et al.*, 1994). This would also decrease the buttress effect of the facet joint during rotation or translation. Too small a graft, on the other hand, can result in pathologic changes to spinal alignment, poor soft tissue tensioning, and the potential for graft prolapse (An *et al.*, 1993). Most of the evidence to date has come from cadaveric imaging studies or retrospective clinical reviews (An *et al.*, 1993; Caspar *et al.*, 1989; Tippetts and Apfelbaum, 1988). While graft size is clearly an important surgical factor, it has not been thoroughly investigated from a biomechanical perspective in the context of subaxial cervical trauma.

Therefore, the two main objectives of this study were: (1) to determine if graft height significantly alters the kinematic stability of ACDFP for a simulated unilateral facet perch based on the standardized injury model (SIM) developed in Chapter 3; and (2) to examine further changes in ACDFP stability following additional simulated unilateral facet fracture and bilateral facet dislocation injuries. In addition to these primary objectives, a tertiary objective was to examine the efficacy of the techniques developed in Chapter 4 to quantify changes in kinematic stability between injury states.

## 5.2 MATERIALS AND METHODS

Seven fresh-frozen cadaveric cervical spine segments were used for this study (mean age:  $76 \pm 5$  years). Prior to testing, specimens were imaged with CT scanning to rule out any existing fractures. Based upon the challenges faced and the experience gained with potting the small vertebrae of the specimens used in Chapters 2 and 3, a new technique was employed that used the additional motion segments above and below for cementing purposes only (Duggal *et al.*, 2005). With an interest in testing instrumentation in the C5-C6, the vertebrae spanning C4-C7 were isolated and screws placed through C4 into the superior endplate of C5 and through C7 into the inferior endplate of C6 to pin the C4-C5 and C6-C7 motion segments (Figure 5.1). Each specimen was then potted in 2.5cm thick, 10cm diameter PVC piping using Denstone™ cement (Heraeus Kulzer Inc., South Bend, IN, USA) to hold the C4 and C7 vertebrae.

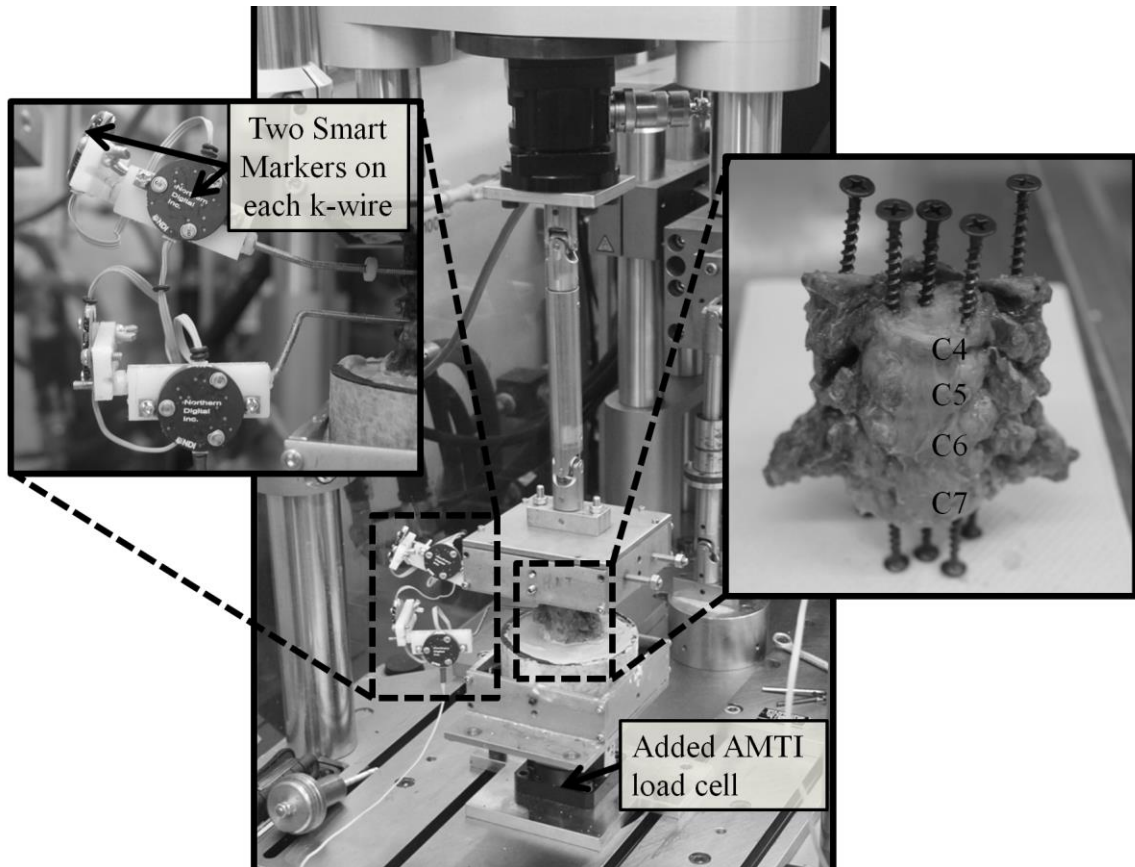


**Figure 5.1: Modifications to Spinal Loading Simulator Setup**

Spinal loading simulator setup (previously shown in Figure 1.13) in this study had an added AMTI load cell beneath the specimen. **Right Inset:** To reduce potential interference in the vertebral body between the screws used for potting and the screws used for spinal instrumentation, a multiple segment C4-C7 spine was “pinned” across the C4-C5 and C6-C7 motions segments as shown. **Left Inset:** A new tracker technique was devised that placed trackers for flexion-extension/axial rotation and lateral bending on the same K-wire. With two sets of trackers required to capture all three motions, this reduced the number of wires that passed through the vertebrae. A small bend in the lower K-wire was also added to eliminate potential interference between the upper and lower trackers.

In terms of the experimental setup, flexibility testing was performed on each specimen using the previously described spinal loading simulator (see Section 1.3.1.1) and loading protocol (see Appendix B). The only addition in this case was a six-DOF AMTI load cell (MC3-6-1000, AMTI, Watertown, MA, USA) placed between the fixed caudal end and the testing platform (to provide data that will not be presented until Chapter 6) (Figure 5.1). Kinematics were captured using the Optotrak Certus® motion capture system (NDI, Waterloo, ON, Canada), with Optotrak® Smart Markers rigidly attached to the C5 and C6 vertebrae, rather than to the potting fixtures themselves as had been done in Chapter 3. To limit additional intrusion of the bony anatomy, Smart Markers for flexion-extension/axial rotation and lateral bending were connected along the same K-wire, rather than two, which had been done previously for visualization purposes (Figure 5.1). Following the same digitization procedure described in Section 2.2, a local bone coordinate system for each of C5 and C6 was defined (*X* axis: anterior-posterior, *Y* axis: medial-lateral, *Z* axis: superior-inferior).

A flexibility testing protocol was designed to assess the kinematic stability of the intact, injured, and instrumented states (Figure 5.2). First, the intact kinematics were collected for flexion-extension, axial rotation, and lateral bending. Subsequently, the SIM that was developed in Chapter 3 for a unilateral facet perch was then induced in the right facet joint at C5-C6 of each specimen. Following flexibility testing of the SIM, the intervertebral disc between C5 and C6 was removed and the disc space completely cleaned with a curette in preparation for ACDFP testing. To explore the effect of graft size, the ACDFP testing condition was repeated for three different sizes grafts (and correspondingly sized plates) in the following order: (1) measured disc space height taken from the pre-injured CT, (2) measured disc space height less 2.5mm (*i.e.*, undersized), (3) measured disc space height plus 2.5mm (*i.e.*, oversized). To ensure repeatability between tests, grafts were machined from Delrin™ plastic into rectangular blocks (12mm wide x 10mm deep) of various heights (as opposed to bone blocks that would generally be used clinically, but may degrade with repeated testing in this model). Plate sizes for the measured disc space height ACDFP were selected to suit the particular anatomy of each specimen, with plate sizes increased and decreased by 2.5mm for the smaller and larger grafts, respectively (Figure 5.3A). Anterior plates (Atlantis; Medtronic, Memphis, TN,

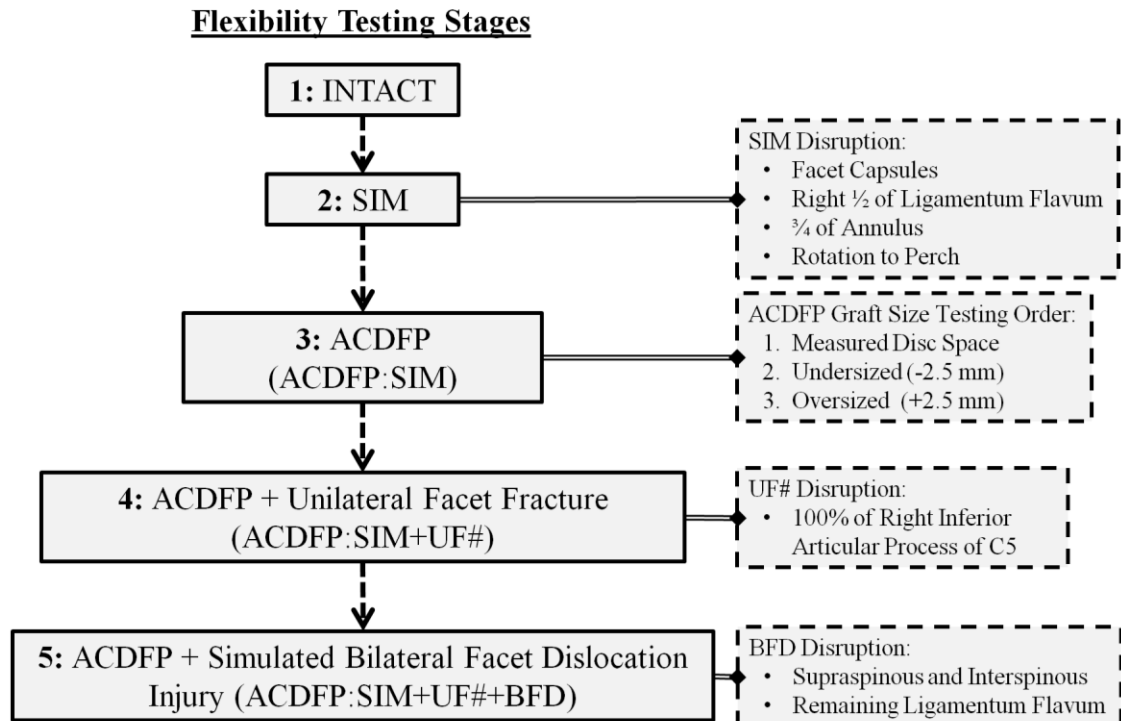


**Figure 5.2: Flexibility Testing Stages Flowchart**

Following intact and SIM testing, the ACDFP with three graft sizes (measured, undersized, and oversized) were compared in three injury states: the SIM alone, the SIM with a unilateral facet fracture (ACDFP:SIM+UF#), and the SIM and fracture with the soft tissue disruption associated with a bilateral facet dislocation (ACDFP:SIM+UF#+BFD).



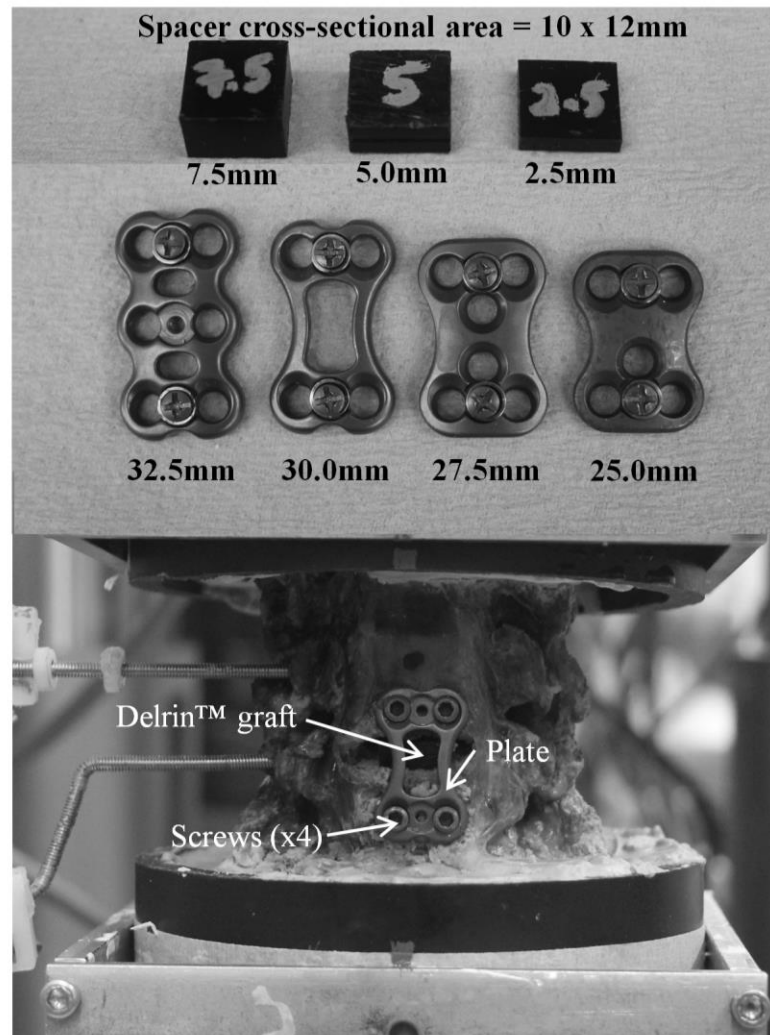


**Figure 5.3: ACDFP Grafts and Plates**

(A) Multiple graft (above) and plate (below) sizes were used for the ACDFP constructs. Grafts were machined from Delrin™ plastic to allow for repeatability of testing without degradation (set based on the measured 5mm graft shown). Plates were selected to suit specimen anatomy with plate size increased and decreased by 2.5mm for the undersized and oversized grafts. (B) With the disc space cleaned, the graft was inserted to lie flush with the anterior wall of the vertebral body. The plate was then fixated with four dynamic angle screws (to maintain screw trajectory between graft sizes).

USA) were secured using 4.0mm diameter and 13.0mm long dynamic angle screws (Figure 5.3B). To prevent loosening of the bone-screw interface due to repeated screw insertion and removal, the screw holes were cemented with approximately 0.5mL of PMMA (Simplex P, Stryker Inc., Kalamazoo, MI, USA) at the time of initial screw insertion. To maintain consistency between tests and specimens, a constant insertional torque of 0.3Nm was used as measured by a torque-limiting screwdriver (Ryken *et al.*, 1995).

After testing the kinematic stability of the ACDFP with the three graft sizes in the SIM, the same three graft sizes were compared for two additional injury states. First, an additional unilateral facet fracture (ACDFP:SIM+UF#) was simulated, using a rongeur to remove the entire inferior articular process of C5 (see Figure 2.3). Second, a bilateral facet dislocation (ACDFP:SIM+UF#+BFD) was simulated based on previous evidence for this injury pattern, which required sectioning the remaining supraspinous ligament, interspinous ligament, and ligamentum flavum (Panjabi *et al.*, 2007).

Kinematic data analyses were performed post-hoc using custom-written LabVIEW™ software (National Instruments, Austin, TX, USA). Parameters generated from the flexibility testing included the magnitude of C5-C6 range of motion (ROM) for the five states (intact, SIM, ACDFP:SIM, ACDFP:SIM+UF#, and ACDFP:SIM+UF#+BFD) for each of the three motions simulated (flexion-extension, axial rotation, and lateral bending). In addition to the standard ROM analyses, finite helical axes (FHAs) were calculated for both the intact and SIM cases using a constant moving window size. The window size (in degrees) had to be determined post-hoc, as it was taken to be half of the smallest ROM from the intact data for each motion (see Section 4.4). Due to the limited ROM of the instrumented states, FHAs were not generated for any of the ACDFP data. From the FHAs calculated, the direction cosine vectors and corresponding alpha shapes enveloping the intercepts in a selected plane (*i.e.*,  $X$ ,  $Y$ , or  $Z = 0$  of the C6 frame for lateral bending, flexion-extension, and axial rotation, respectively) were generated using MATLAB software (R2012; Mathworks, Natick, MA, USA) (see Appendix E). Alpha shapes were quantified by determining their area and

centroid location, and visualized over specimen-specific 3D bone models (see Appendix F).

Statistical analyses were performed using SigmaStat software (Systat Software Inc., Chicago, IL, USA). Intact versus SIM ROM and alpha shape area were initially compared in a paired t-test ( $\alpha=0.05$ ). For analysis of the ACDFP comparison, ROM data were normalized to a percent decrease from the SIM ROM, where a 100% decrease represented complete stabilization with zero ROM and 0% decrease represented the same ROM as the SIM. These data were analyzed using two-way rmANOVA (factors = graft size and injury state) with post-hoc SNK tests ( $\alpha=0.05$ ).

### 5.3 RESULTS<sup>8</sup>

Testing for all seven specimens was completed without incident; there were no cases of specimen loosening within the potting cement and no graft/plate/screw failure. The modified potting technique, with a fixed motion segment above and below worked well, providing rigid fixation to the testing setup and excellent Smart Marker visibility. The measured graft height used was 5mm for six specimens, and 6mm for the remaining one. Insertion of the oversized graft required a distracting load in the range of 100-200N, which was applied with the axial actuator of the Instron<sup>®</sup>.

In terms of the kinematics stability between the intact and injured states, a larger ROM was measured for the SIM compared to the intact state for all applied motions ( $p<0.05$ ) (Table 5.1). The largest increase seen was in axial rotation ROM, with an average percent increase of 286% between intact and SIM. The SIM also more than doubled intact ROM in the other two motions, with a 123% in flexion-extension and a 159% increase in lateral bending.

Based on the calculated intact ROM, a moving window size of 2°, 3°, and 2° was used for flexion-extension, axial rotation, and lateral bending, respectively (See Appendix D). In addition, two specimens were excluded from the FHA analysis since the

---

<sup>8</sup> Tabulated ROM data for all tested specimens is found in Appendix D.

**Table 5.1: Average ( $\pm$ SD) C5-C6 ROM for the Intact and SIM States**

<b>Motion</b>	<b>Intact ROM (°)</b>	<b>SIM ROM (°)</b>	<b>Average % Increase</b>
Axial Rotation	$4.6 \pm 1.8$	$15.4 \pm 3.9$	$286.8 \pm 167.9$
Flexion-Extension	$8.2 \pm 3.2$	$16.2 \pm 4.6$	$123.0 \pm 81.1$
Lateral Bending	$4.7 \pm 2.1$	$10.7 \pm 3.1$	$158.5 \pm 100.4$

intact ROM was less than this window size. In terms of the alpha shapes generated from the FHAs for each specimen, there was an increase in area for all motions ( $p < 0.05$ ) (Table 5.2). The average centroid locations of the alpha shapes are shown in Table 5.3. Between the intact and SIM states, the largest shifts in the centroid location were a 9mm posterior shift for axial rotation, and 5mm superior and posterior shifts in flexion-extension. The alpha shapes, centroids, and average direction cosine vectors are shown for each specimen between the intact and SIM states in Figures 5.4-5.6.

ROM analysis of the injury states and graft sizes revealed, in flexion-extension, that there was an effect of both injury ( $p = 0.015$ ) and graft size ( $p = 0.013$ ) (Figure 5.7). For this motion, the ACDFP:SIM+UF#+BFD had a smaller decrease in ROM compared to the other injury states ( $p < 0.05$ ). Further, the oversized graft had a larger decrease in ROM than the other two graft sizes ( $p < 0.05$ ). For axial rotation, there were no overall effects of either injury state ( $p = 0.072$ ) or graft sizes ( $p = 0.135$ ), but there was a significant interaction between these two main effects ( $p = 0.004$ ) (Figure 5.8). One-way ANOVAs were therefore performed and found that in the ACDFP:SIM+UF#+BFD state only, the undersized graft had a larger decrease in ROM compared to the other grafts ( $p < 0.05$ ). In lateral bending, there was an effect of injury ( $p = 0.008$ ) and graft size ( $p = 0.006$ ), as well as significant interactions ( $p = 0.028$ ) that required the use of additional one-way ANOVAs (Figure 5.9). These extra analyses found that within the SIM state, there was no difference between graft sizes ( $p > 0.05$ ). In the ACDFP:SIM+UF# state, the measured graft had a smaller decrease in ROM than both the undersized and oversized grafts ( $p < 0.05$ ). In the final injury state (ACDFP:SIM+UF#+BFD), the undersized provided a larger decrease than both the measured and oversized grafts ( $p < 0.05$ ).

## 5.4 DISCUSSION

ACDFP is a well accepted mode of treatment for flexion-distraction injuries (Brodke *et al.*, 2003; Dvorak *et al.*, 2007; Kwon *et al.*, 2007); however, there has been little effort to examine the surgical factor of graft size on the kinematic stability of the instrumented construct. This study was designed to compare the stability provided by ACDFP in the context of three simulated facet injuries with three different graft sizes: measured disc space height, undersized, and oversized. Based on the kinematic stability

**Table 5.2: Alpha Shape Area for the Intact and SIM States**

Alpha shape areas were calculated from the intercepts with the plane most normal to the finite helical axes generated. This was Z, Y, X = 0 for axial rotation, flexion-extension, and lateral bending, respectively.

Motion	Intact Area (mm <sup>2</sup> )	SIM Area (mm <sup>2</sup> )	% Increase	Average (±SD) % Increase
Axial Rotation	133.8	365.9	173.5	230.4 ± 185.8
	99.4	618.8	522.5	
	629.0	930.6	47.9	
	220.3	480.0	117.9	
	137.3	535.6	290.1	
Flexion-Extension	770.8	974.0	26.4	93.7 ± 77.4
	199.1	445.6	123.8	
	299.4	679.8	127.1	
	236.7	242.2	2.3	
	173.8	502.2	189.0	
Lateral Bending	96.5	440.1	356.1	381.0 ± 286.0
	100.4	942.6	838.8	
	100.9	489.7	385.3	
	276.8	440.2	59.0	
	59.4	217.1	265.5	

**Table 5.3: Planar Location of the Average Centroid of the Alpha Shapes**

Motion	FHA Reference Plane	Positive Directions	Intact Centroid Location (mm)	SIM Centroid Location (mm)	Average Location Difference (mm)
Axial Rotation	Transverse	Anterior (X)	4.6 ± 5.0	-4.4 ± 5.0	-9.1 ± 3.8
		Left Lateral (Y)	-5.5 ± 3.7	-6.8 ± 9.5	-1.3 ± 4.3
Flexion-Extension	Sagittal	Anterior (X)	-13.6 ± 3.6	-18.5 ± 7.1	-5.0 ± 2.8
		Superior (Z)	8.2 ± 5.2	12.9 ± 6.0	4.7 ± 2.5
Lateral Bend	Frontal	Left Lateral (Y)	-5.2 ± 3.0	-8.1 ± 8.1	-2.9 ± 3.0
		Superior (Z)	25.0 ± 3.2	23.2 ± 7.2	-1.8 ± 7.7

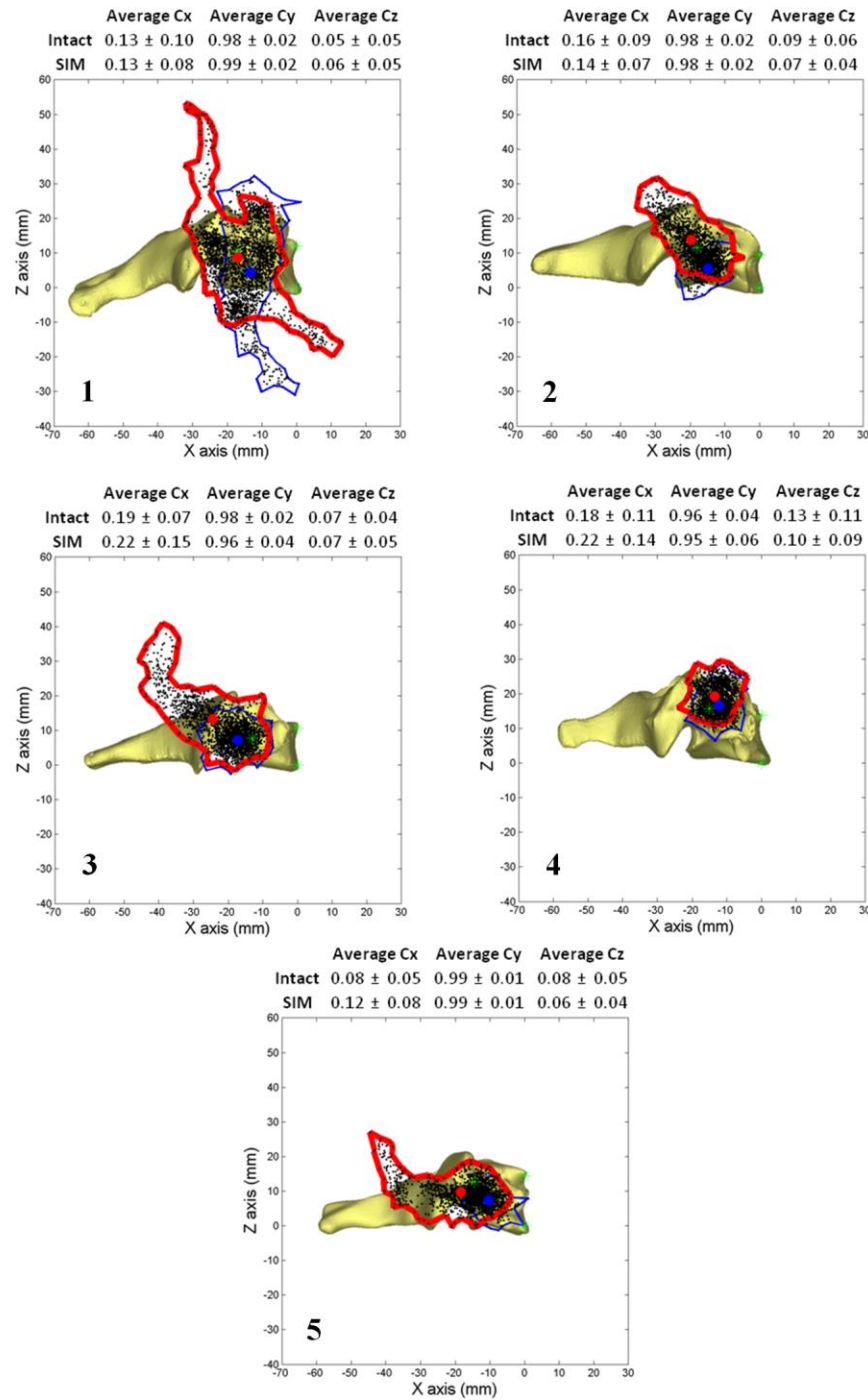


**Figure 5.4: Flexion-Extension Alpha Shapes of FHA Intercepts with Sagittal Plane** Blue (thinner line) represents the intact state, with Red (thicker line) as the SIM. It appears that the simulated UFP tended to shift the shape posteriorly, as evidenced by the change in position of the centroid (intact = circle; SIM = square). Average direction cosines (Cx, Cy, Cz) of the FHAs are shown above each graph for both states (Note: Cy=1 would represent a line coming directly out of the page).

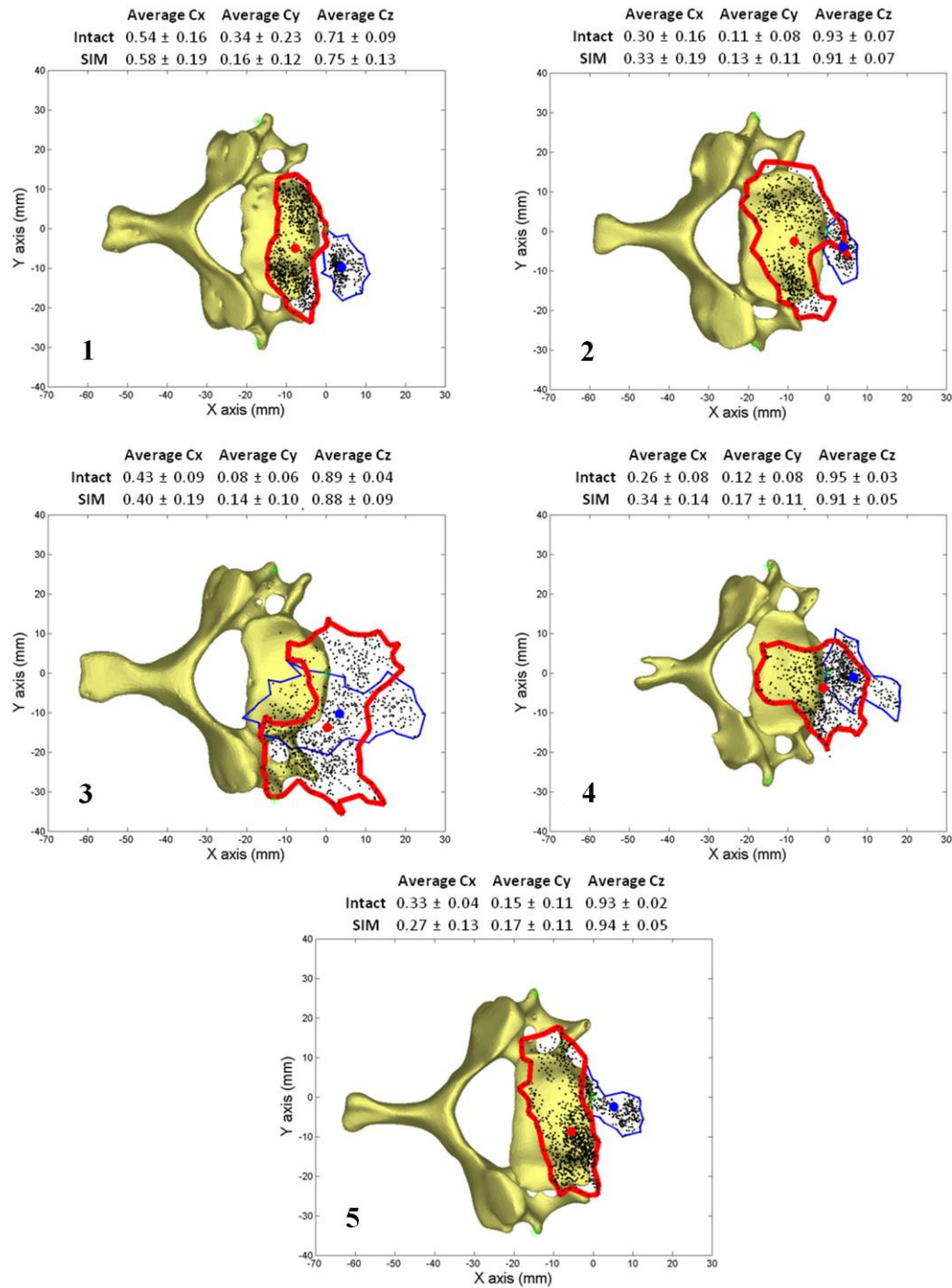


**Figure 5.5: Axial Rotation Alpha Shapes of FHA Intercepts with Transverse Plane** Blue (thinner line) represents the intact state, with Red (thicker line) as the SIM. It appears that the SIM tended to shift the shape posteriorly, as well as laterally. Average direction cosines (Cx, Cy, Cz) of the FHAs are shown above each graph for both states (Note: Cz=1 would represent a line coming directly out of the page).



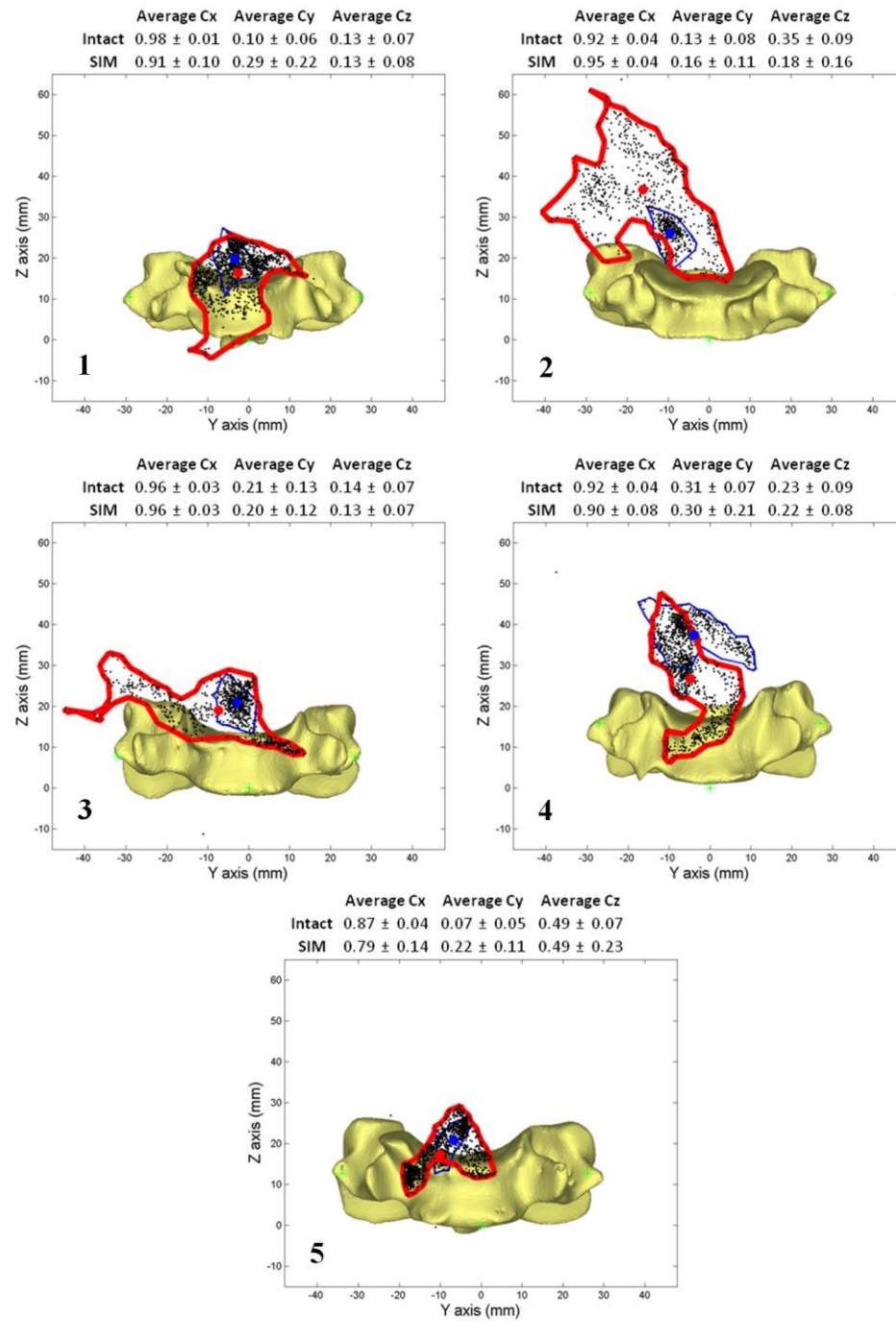


**Figure 5.6: Lateral Bending Alpha Shapes of FHA Intercepts with Frontal Plane** Blue (thinner line) represents the intact state, with Red (thicker line) as the SIM. Based on these five images, there was no distinct trend other than a larger area in the SIM case. Average direction cosines ( $C_x$ ,  $C_y$ ,  $C_z$ ) of the FHAs are shown above each graph for both states (Note:  $C_x=1$  would represent a line coming directly out of the page).

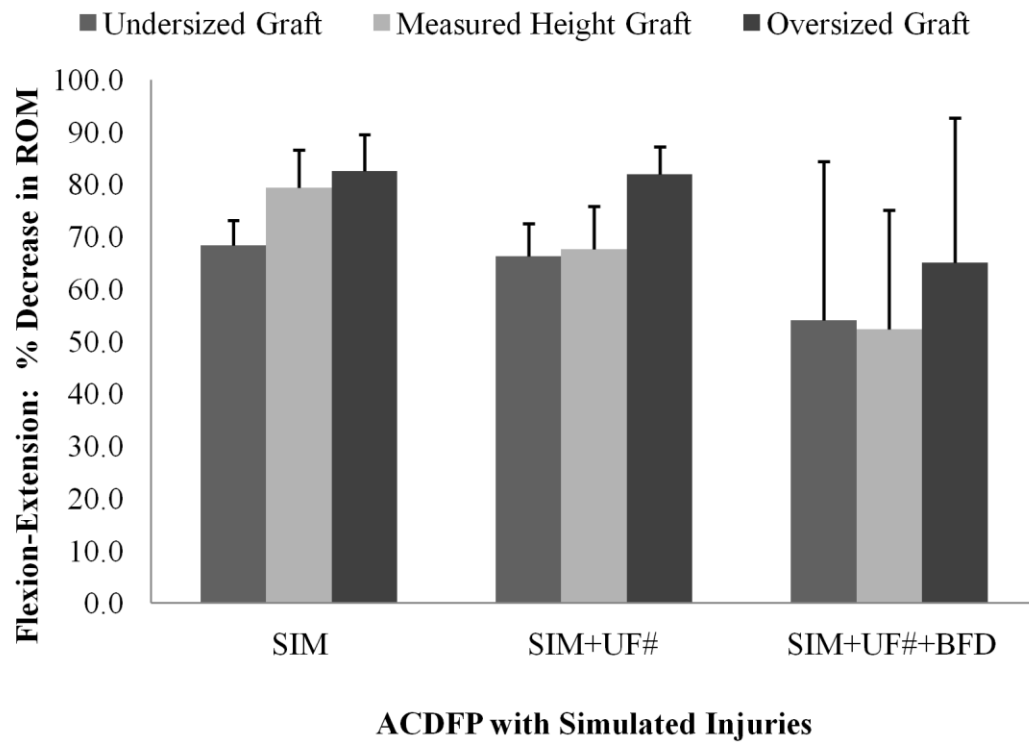


**Figure 5.7: Flexion-Extension ROM as a Result of Injury and Graft Size**

Percent change in C5-C6 ROM compared to the initial injured state in flexion-extension with ACDFP using the three graft sizes after the initial SIM, after adding a unilateral facet fracture (SIM+UF#), and including the simulated soft tissue disruption for a bilateral facet dislocation (SIM+UF#+BFD).

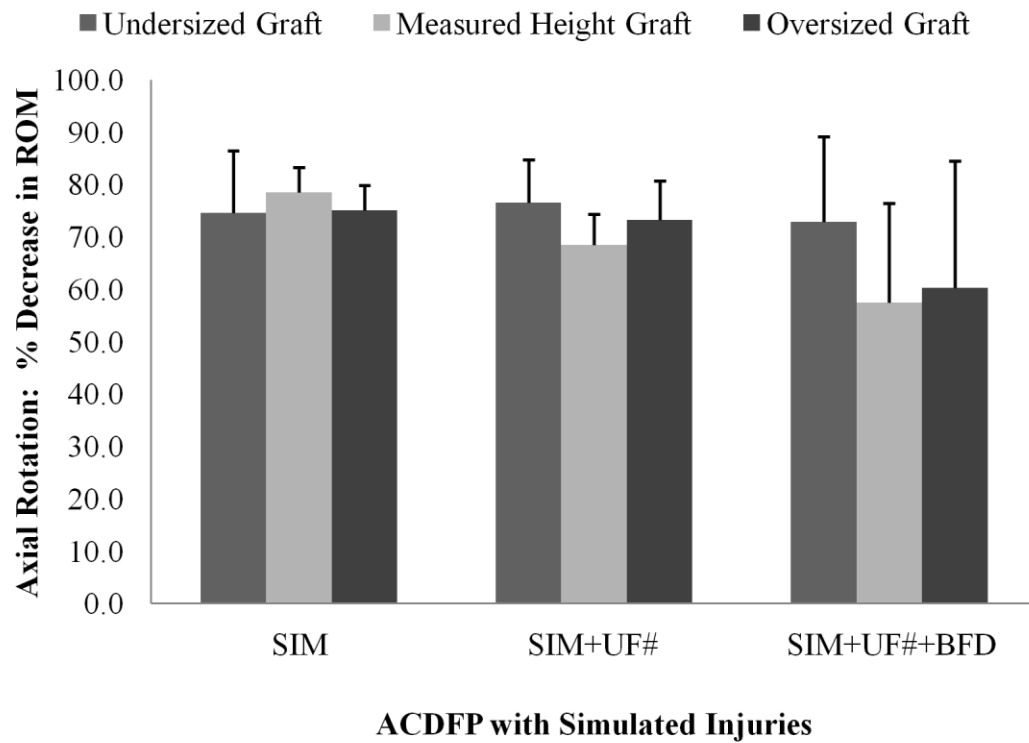


**Figure 5.8: Axial Rotation ROM as a Result of Injury and Graft Size**

Percent change in C5-C6 ROM compared to the initial injured state in axial rotation with ACDFP using the three graft sizes after the initial SIM, after adding a unilateral facet fracture (SIM+UF#), and including the simulated soft tissue disruption for a bilateral facet dislocation (SIM+UF#+BFD).

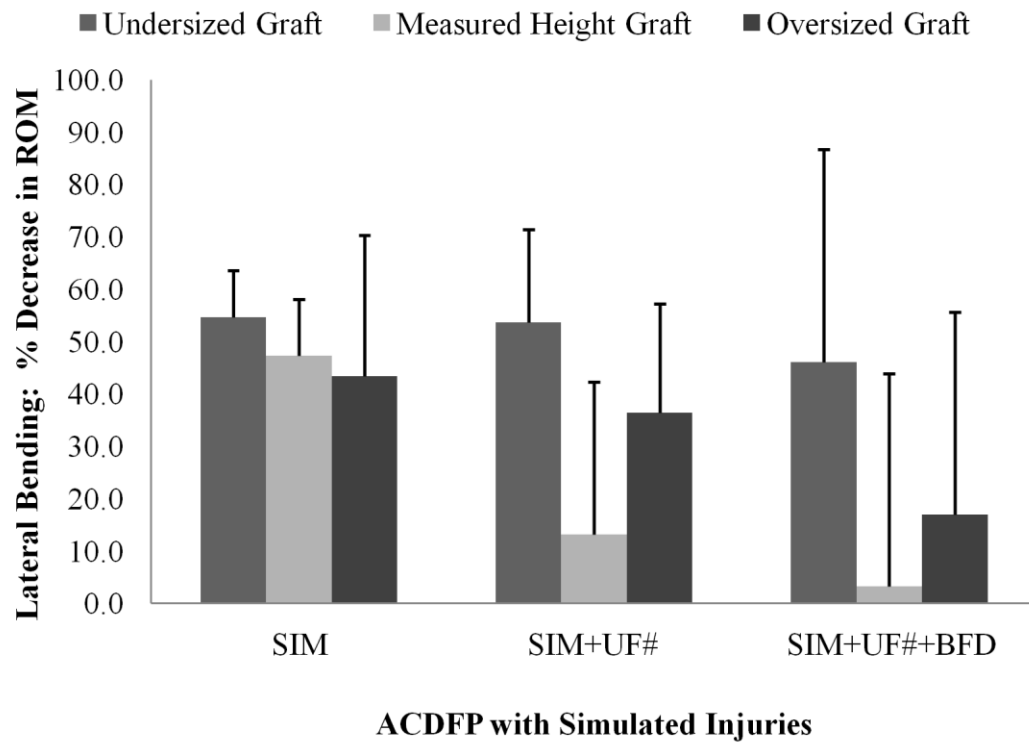


**Figure 5.9: Lateral Bending ROM as a Result of Injury and Graft Size**

Percent change in C5-C6 ROM compared to the initial injured state in lateral bending with ACDFP using the three graft sizes after the initial SIM, after adding a unilateral facet fracture (SIM+UF#), and including the simulated soft tissue disruption for a bilateral facet dislocation (SIM+UF#+BFD).

of the ACDFP, interactions observed between the graft sizes and injuries and the variability between the motions suggest that the selection of graft size should consider all these factors. This is evident in the fact that the undersized graft outperformed both the measured height and oversized grafts in lateral bending, while the oversized graft performed better in flexion-extension. These findings are relevant in combination with the results of Chapter 2, which found ACDFP less stable than posterior instrumentation in stabilizing lateral bending and axial rotation motions. Furthermore, the knowledge translation of these results could extend to the use of cervical orthoses, which are often used postoperatively to supplement cervical spine immobilization. Previous studies have found orthoses are less effective at limiting axial rotation and lateral bending compared to flexion-extension (Agabegi *et al.*, 2010; Ivancic, 2013), suggesting that an oversized graft may not be advantageous in these situations.

One possible explanation for the superior performance of the undersized graft in axial rotation and lateral bending is that, in addition to facet interaction, there was greater uncovertebral joint overlap (*i.e.*, increased contact between adjacent uncinate processes) (Figure 5.10). This would have provided a second bony stabilizer against motion that was not engaged in the measured and oversized grafts. This is not the first study to detail the importance of the uncovertebral joints in increasing the stability of the subaxial cervical motion segments. Penning *et al.* noted that the uncovertebral joints function in the coupling of axial rotation with lateral bending to increase stability (Penning and Wilmink, 1987). Similarly, biomechanical studies have shown that uncinate process resection significantly reduces stiffness and increases axial rotation and lateral bending ROM (Kotani *et al.*, 1998; Snyder *et al.*, 2007).

In terms of flexion-extension, the greater stability with the oversized graft was not surprising. The combination of the graft acting as a strut limiting flexion and a larger plate in the bending direction (as a result of the larger graft) would intuitively suggest more stability would be present. However, with these same aspects, it would have been expected that the measured height graft would have outperformed the undersized graft in flexion-extension; however, this was not the case. The lack of difference found in testing between the two sizes may be mitigated again by the interaction of the uncovertebral

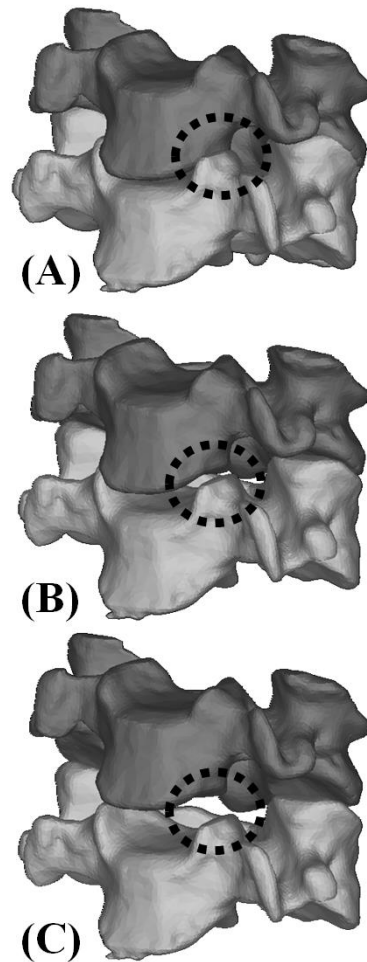


**Figure 5.10: Effect of Disc Space Height on the Uncovertebral Joint**

Disc space height effect on the uncovertebral joint (shown in the dashed circle) is demonstrated using computer bone models of cervical vertebrae. For the undersized graft (A), there is a large overlap of this joint, potentially increasing the level of stability it provides. With the measured graft height (B), there is a small gap between this joint, which is then further increased with the oversized graft (C).

joints with the undersized graft. Both Chen *et al.* and Kotani *et al.* have previously noted the contribution of the uncovertebral joints to flexion-extension stability (Chen *et al.*, 2001; Kotani *et al.*, 1998).

While this study attempted to add clarity to the surgical factor of ideal graft size, there remains no consensus, particularly in the context of injury. Only one previous study has looked at graft size in the context of biomechanical stability for an anterior cervical discectomy and fusion (ACDF) (*i.e.*, with no additional plating). Yin *et al.* concluded that a graft height of 140% baseline disc space height was ideal for immediate ACDF biomechanical stability, while larger grafts were more difficult to insert and risked ligament injury (Yin *et al.*, 2011). However, the additional stability provided by anterior plating was not considered and the specimens were kept in the intact state. Other studies have looked at the impact of graft height on foraminal area (*i.e.*, size of the space containing the spinal cord) (An *et al.*, 1993), on compressive graft loads (Truumees *et al.*, 2002), and load distribution between anterior and posterior elements (Olsewski *et al.*, 1994). An *et al.* suggested that a graft height 2mm above baseline height was optimal for disc heights of 3.5-6.0 mm based on maximal change in foraminal height and area (An *et al.*, 1993). Olsewski *et al.* and Truumees *et al.* both noted that increased disc space distraction results in increased graft loads, suggesting a graft height no greater than 3mm of baseline height or under an absolute height of 10mm respectively (Olsewski *et al.*, 1994; Truumees *et al.*, 2002). Clinically, over-distraction has been shown to result in graft failure, with Brower *et al.* describing an increased rate of collapse or non-union with distraction greater than 4mm (Brower *et al.*, 1992). Other recommendations for graft height have been reported, but without basis in biomechanical studies (Caspar *et al.*, 1989; Smith and Robinson, 1958). No studies evaluated graft size effect in an injured spine.

A new technique was utilized in this study to quantify kinematic stability based on the scatter of the generated FHAs, using the area of an alpha shape that enveloped the intercept points with the anatomic planes of the reference C6 vertebra. Similar to ROM, this area measure increased with injury. There are potential benefits to this approach. While the ROM considers only the extreme ends of motion in a single plane (*i.e.*, how

much rotation in the transverse plane occurs during simulated axial rotation), the area of alpha shape quantifies the FHAs generated throughout the entire loading cycle. Furthermore, since the scatter of the intercept points are based on the 3D FHA, it gives a much more complete view of the kinematic stability (*i.e.*, it considers rotation in all planes during a single simulated movement). To the authors' knowledge, this is the first study to report on the changes in kinematic stability using the alpha shape area. One drawback is that FHAs were only generated for motions exceeding two degrees to reduce the error present in this measure (see Section 4.4). As such, alpha shapes could not be created for the semi-rigid instrumentation comparison of this study. In the case of a more dynamic instrumentation, such as disc replacement, it may prove to be an effective tool for quantifying changes in stability.

The repeated-measures design of this study, comparing multiple graft sizes in the same specimen, strengthened the outcome results; however, this forced some other potential surgical factors. In this case, the use of dynamic angle screws was necessitated to maintain the same screw hole trajectory, due to the changes in sagittal alignment as graft size increased. This required the use of a rotationally dynamic plate, as such the current results may have differed from ACDFP using a static or translationally dynamic plate. However, a prospective randomized single-blinded study of ACDFP using static versus dynamic plates by Nunley *et al.* found no significant difference in clinico-radiological success in single level fusions (Nunley *et al.*, 2009). Similarly, Brodke *et al.* found no significant difference in ROM with use of static, rotationally dynamic, or translationally dynamic plates in a single-level corpectomy model (Brodke *et al.*, 2006).

Similar to the previous *in vitro* biomechanical studies of this thesis, there are inherent limitations (see Section 2.4). The grafts that were used in this study were machined from a hard Delrin plastic, rather than a true bone graft that would be used clinically. This was done to limit degradation of the graft between tests and to standardize the shape. Regarding the shape itself, the grafts were machined as rectangular cubes. In the clinical scenario, the grafts are shaped to fit with the vertebral anatomy; however, this was not feasible with the current plastic designs. In addition, due to the irreversible nature of the simulated facet injuries, it was necessary to test in order



of least to most severe, with the latter two injuries compounded on the SIM. While the SIM had been validated in Chapter 3, these more severe injuries were included to highlight potential differences in graft sizes that would be present with further soft tissue disruption. Furthermore, these injuries on their own were very unstable without the ACDFP, so testing of the uninstrumented state was not considered for these injuries. Finally, insertion of the oversized graft required a mean axial distraction in the range of 100-200N on the specimens. This degree of distraction could have resulted in further soft tissue damage, thereby influencing all testing following the oversized graft. As such, the oversized graft was always tested following the undersized and measured graft sizes.

In conclusion, results from this study demonstrate that graft size does affect the biomechanical stability of ACDFP in a unilateral facet injury model; undersizing the graft results in both facet overlap and locking of the uncovertebral joints, providing greater stability in lateral bending and axial rotation, while oversizing the graft provides greater stability in flexion-extension. Given this, use of an undersized graft, or a graft that engages the uncovertebral joint, may be more advantageous in providing a rigid environment for fusion, especially if an external collar is being used to limit flexion-extension motion. In the clinical scenario, multiple factors must be considered in graft selection for the stabilization of unilateral facet injuries, including curvature restoration, foramen patency, and construct stability.

## **5.5 SUMMARY & FUTURE DIRECTIONS**

This chapter found that graft size did influence the overall kinematic stability of the ACDFP surgical instrumentation; however, the variability in the results suggests that other surgical factors relevant to ACDFP will need to be evaluated in future testing. In regards to future studies, the design of the simulator in the studies performed in Chapters 2, 3, and 5 has considered only a fixed caudal end of the specimen. The effect of additional translational freedom to this end, and the effect on the caudal shear forces require investigation. The additional six-DOF load cell added to the caudal end in the current study will help to identify these changes.

## 5.6 REFERENCES

- Agabegi, S.S., Asghar, F.A., Herkowitz, H.N., 2010. Spinal orthoses. *Journal of the American Academy of Orthopaedic Surgeons* 18, 657–667.
- An, H., Evanich, C., Nowicki, B., Haughton, V., 1993. Ideal thickness of Smith-Robinson graft for anterior cervical fusion: A cadaveric study with computed tomographic correlation. *Spine* 18, 2043–2047.
- Brodke, D.S., Anderson, P.A., Newell, D.W., Grady, M.S., Chapman, J.R., 2003. Comparison of anterior and posterior approaches in cervical spinal cord injuries. *Journal of Spinal Disorders & Techniques* 16, 229–235.
- Brodke, D.S., Klimo, P., Bachus, K.N., Braun, J.T., Dailey, A.T., 2006. Anterior cervical fixation: analysis of load-sharing and stability with use of static and dynamic plates. *Journal of Bone & Joint Surgery* 88-A, 1566–1573.
- Brower, R., Herkowitz, H.N., Kurz, I., 1992. Effect of distraction on union rate of Smith-Robinson type anterior cervical discectomy and fusion. In: *20th Annual Meeting of the Cervical Spine Research Society. Palm Desert, CA*.
- Caspar, W., Barbier, D., Klara, P., 1989. Anterior cervical fusion and Caspar plate stabilization for cervical trauma. *Neurosurgery* 25, 491–502.
- Chen, T.Y., Crawford, N.R., Sonntag, V.K., Dickman, C.A., 2001. Biomechanical effects of progressive anterior cervical decompression. *Spine* 26, 6–14.
- Duggal, N., Chamberlain, R.H., Park, S.C., Sonntag, V.K.H., *et al.*, 2005. Unilateral cervical facet dislocation: biomechanics of fixation. *Spine* 30, E164–168.
- Dvorak, M.F., Fisher, C.G., Fehlings, M.G., Rampersaud, Y.R., *et al.*, 2007. The surgical approach to subaxial cervical spine injuries: an evidence-based algorithm based on the SLIC classification system. *Spine* 32, 2620–2629.
- Ivancic, P.C., 2013. Effects of orthoses on three-dimensional load-displacement properties of the cervical spine. *European Spine Journal* 22, 169–177.
- Kotani, Y., McNulty, P.S., Abumi, K., Cunningham, B.W., *et al.*, 1998. The role of anteromedial foraminotomy and the uncovertebral joints in the stability of the cervical spine: A biomechanical study. *Spine* 23, 1559–1565.
- Kwon, B.K., Fisher, C.G., Boyd, M.C., Cobb, J., *et al.*, 2007. A prospective randomized controlled trial of anterior compared with posterior stabilization for unilateral facet injuries of the cervical spine. *Journal of Neurosurgery Spine* 7, 1–12.
- Kwon, B.K., Vaccaro, A.R., Grauer, J.N., Fisher, C.G., Dvorak, M.F., 2006. Subaxial cervical spine trauma. *Journal of the American Academy of Orthopaedic Surgeons* 14, 78–89.

- Nunley, P.D., Jawahar, A., Kerr, E.J., Cavanaugh, D.A., *et al.*, 2009. Choice of plate may affect outcomes for single versus multilevel ACDF: results of a prospective randomized single-blind trial. *The Spine Journal* 9, 121–127.
- Olsewski, J.M., Garvey, T.A., Schendel, M.J., 1994. Biomechanical analysis of facet and graft loading in a Smith-Robinson type cervical spine model. *Spine* 19, 2540–2544.
- Panjabi, M.M., Simpson, A.K., Ivancic, P.C., Pearson, A.M., *et al.*, 2007. Cervical facet joint kinematics during bilateral facet dislocation. *European Spine Journal* 16, 1680–1688.
- Penning, L., Wilmink, J.T., 1987. Rotation of the cervical spine. A CT study in normal subjects. *Spine* 12, 732–738.
- Ryken, T.C., Clausen, J.D., Traynelis, V.C., Goel, V.K., 1995. Biomechanical analysis of bone mineral density, insertion technique, screw torque, and holding strength of anterior cervical plate screws. *Journal of Neurosurgery* 83, 325–329.
- Smith, G., Robinson, R., 1958. The treatment of certain cervical-spine disorders by anterior removal of the intervertebral disc and interbody fusion. *Journal of Bone & Joint Surgery* 40-A, 607–624.
- Snyder, J.T., Tzermiadianos, M.N., Ghanayem, A.J., Voronov, L.I., *et al.*, 2007. Effect of uncovertebral joint excision on the motion response of the cervical spine after total disc replacement. *Spine* 32, 2965–2969.
- Tippets, R., Apfelbaum, R., 1988. Anterior cervical fusion with the Caspar instrumentation system. *Neurosurgery* 22, 1008–1013.
- Truumees, E., Demetropoulos, C.K., Yang, K.H., Herkowitz, H.N., 2002. Effects of disc height and distractive forces on graft compression in an anterior cervical discectomy model. *Spine* 27, 2441–2445.
- Yin, D., Xin, X., Yang, R., Shi, Y., Shen, H., 2011. Biomechanical stability of lower cervical spine immediately after discectomy with grafting. *Orthopaedic Surgery* 3, 113–118.

## CHAPTER 6: THE EFFECT OF FIXED VERSUS SEMI-CONSTRAINED END CONDITIONS ON BENDING MOMENT EFFICIENCY IN THE CURRENT SPINAL LOADING SIMULATOR

**OVERVIEW:** *Enhancements to the custom-developed spinal loading simulator used in Chapters 2, 3 and 5 have evolved during the course of its use (i.e., better potting techniques, improvements to kinematic marker attachments, etc.). This chapter explores another potential area for refinement, by examining the role that caudal end conditions play in achieving the desired pure bending moment loading and transferring load through the specimen. A new concept of “bending moment efficiency” is introduced, and a preliminary investigation is conducted to illustrate its utility.*

### 6.1 INTRODUCTION

The development of spinal loading simulators has given engineers and surgeons the ability to quantify the efficacy of emerging surgical treatments in an *in vitro* setting, but with *in vivo* relevance. The majority of these simulators have been custom-built in individual research laboratories to apply physiologic-like loading to cadaver spines (Crawford *et al.*, 1995; Gédet *et al.*, 2007; Goertzen *et al.*, 2004; Ilharreborde *et al.*, 2010; Lysack *et al.*, 2000). As such, a key concern is standardization in testing methodologies across institutions (Buckley, 2011; Goel *et al.*, 2006; Wheeler *et al.*, 2011). For this reason, Panjabi and colleagues developed the concept of using pure bending moment loading as a reliable and repeatable technique to simulate spinal motion (Panjabi, 1988), which has subsequently been identified as a physiologic-relevant loading technique (Wilke *et al.*, 2001). Furthermore, a critical review of standards for spinal testing cited the pure bending moment technique as the most appropriate loading method (Wilke *et al.*, 1998). Different approaches have been taken to achieve this loading, including directly applying the moment to the cranial end of the specimen (Goertzen *et al.*, 2004; McLachlin, 2008; Wilke *et al.*, 1994) or creating a bending moment by generating a force couple (Crawford *et al.*, 1995; Lysack *et al.*, 2000). While this pure

bending moment loading method is often cited, the ability of various simulator designs to actually achieve this loading is rarely verified.

One consideration to improve the transparency of this technique would be to report the bending moment efficiency (*i.e.*, output/input moment) and the recorded forces at the caudal end for actual tests. This would simply require an additional six-DOF load cell placed below the test specimen during testing, which in many cases is already present (Goertzen *et al.*, 2004). In the case of a “pure bending moment,” it would be expected that the efficiency value would equal 100% with zero caudal shear force; however, in practice this may be difficult to achieve due to factors such as friction and specimen abnormalities (Cripton *et al.*, 2000; G  det *et al.*, 2007). A similar concept to efficiency was recently presented by Eguizabal *et al.*, looking at the intended versus actual bending moment for two simulator configurations, but the authors only examined this in a surrogate model of a lumbar spine (Eguizabal *et al.*, 2010). This same study also called into question the loading techniques of simulator designs using a “force-couple” to generate bending, which lead to an interesting and timely discussion on these loading principles (Buckley, 2011; Crawford, 2011).

Recreating the physiological DOF of the spine using experimental, *in vitro* approaches is very challenging, so some assumptions must be taken in simulator development. One design feature that seems inconsistent across various institutions is the degree of constraint in the end conditions applied to the cadaver test specimen (*i.e.*, how the specimen is held at each end). At the “loaded end” (*i.e.*, cranial end) of the spine, the pure bending moment methodology describes applying load in one plane, leaving the remaining five-DOF free (Panjabi, 1988; Wilke *et al.*, 1998). Unfortunately, little guidelines are provided for the other end (*i.e.*, caudal). In most cases, including the current simulator design, the caudal end of the specimen is fixed to the testing platform (Crawford *et al.*, 1995; Goertzen *et al.*, 2004; Lysack *et al.*, 2000; McLachlin, 2008). Others have considered that, to induce a pure bending load, shear loading on the specimen needs to be eliminated (Eguizabal *et al.*, 2010; Ilharreborde *et al.*, 2010; Tang *et al.*, 2012). As such, in some designs the caudal end is less constrained, by adding translational (Ilharreborde *et al.*, 2010; Tang *et al.*, 2012) or rotational degrees-of-

freedom (DiAngelo and Foley, 2004). The shear forces at the caudal end present during experimental testing in the current simulator design have not been quantified.

Another source of variability among simulator designs is the axial loading along the spine. While some designs try to recreate compressive loading along the cervical spine, this is of more concern in the lumbar spine, and easier to implement in the larger vertebrae (Miura *et al.*, 2002; Patwardhan *et al.*, 1999). Instead, the custom designed simulator used throughout this thesis uses the axial actuator, operating in load control, to remove or “unload” the weight of the cranial fixture and loading arms on the specimen. This is accomplished by setting the actuator to hold a value of 0N, which requires the actuator’s proportion, integral, and derivative (PID) control settings to be properly tuned to the specimen stiffness. However, the spine deforms and its stiffness varies through the loading cycle; therefore, maintaining the desired “zero load” is challenging. In the testing completed so far in this thesis, the system’s ability to do so has not been examined in detail.

Therefore, the objectives of this chapter were: (1) to quantify the bending moment efficiency and caudal forces values for the current simulator design from previously collected data (*i.e.*, Chapter 5 specimens), and (2) to examine how these values are affected by adding translational freedom to the previously fixed caudal end and modifying the actuator PID control settings in one additional test specimen.

## **6.2 MATERIALS AND METHODS**

### **6.2.1 CURRENT DESIGN TESTING**

In Chapter 5, tuning of the axial actuator was accomplished in one representative specimen, using the “loop tuning” tool in the Instron<sup>®</sup> Console software (Instron, Norwood, MA, USA) with an input compressive square wave set to cycle the axial force between -10N and -30N at 0.5Hz. PID values were then adjusted so that the measured force closely matched the input wave. Values of 4.4, 1.0, and 0.0 for P, I and D, respectively, were selected and used for all specimens tested.

As noted in Chapter 5 (see Section 5.2), these specimens were tested with a second six-DOF load cell (MC3-1000, AMTI, Watertown, MA, USA) placed beneath the caudal potting fixture to monitor the loads at this fixed end (see Figure 5.1). In the present chapter, the load data generated from this additional load cell was analyzed to determine the maximum and minimum axial ( $Z$ ) and shear forces ( $X$  and  $Y$ ) at the caudal end during the final loading cycle for each motion in the intact and SIM states. This also enabled the concept of a bending moment efficiency value for each applied motion to be explored.

Efficiency is generally considered as:

$$\text{Efficiency} = \frac{\text{Output}}{\text{Input}} \times 100\% \quad \text{Eq. 6.1}$$

In the case of the spinal loading simulator's applied bending moment, this could be interpreted as:

$$\text{Bending Moment Efficiency} = \frac{\text{Caudal Bending Moment}}{\text{Applied Bending Moment}} \times 100\% \quad \text{Eq. 6.2}$$

Thus, Equation 6.2 was used to calculate the moment efficiency for each motion (*i.e.*, flexion-extension, axial rotation, and lateral bending) for the intact and SIM conditions only. The calculation was based on the maximum recorded positive caudal and applied bending moments (and similarly for the two largest negative bending moments) during the final loading cycle for each motion (Figure 6.1).

Differences between the intact and SIM states for moment efficiency, axial and shear forces were evaluated using a one-way rmANOVA and post-hoc SNK tests ( $\alpha=0.05$ ) with SigmaStat software (Systat Software Inc., Chicago, IL, USA).

## 6.2.2 MODIFIED DESIGN TESTING

To reduce any potential shear loading, a custom  $XY$  stage was designed and built to add translational freedom to the caudal end of the test specimen (for details on  $XY$

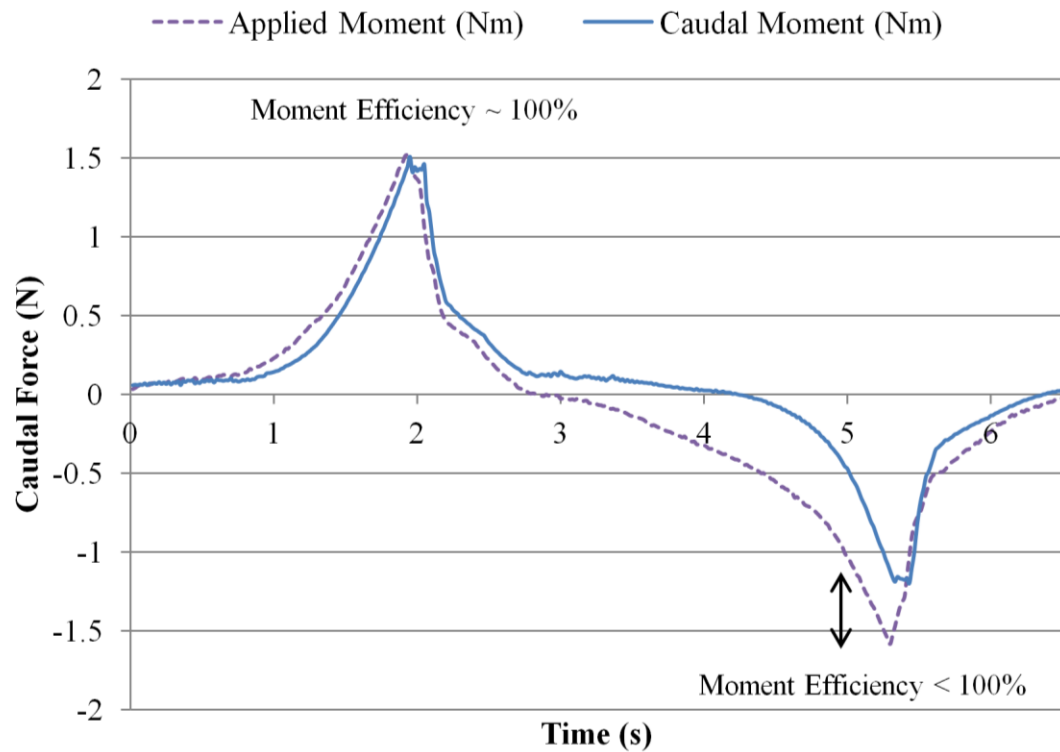


**Figure 6.1: Bending Moment Efficiency**

The concept of bending moment efficiency is calculated as the maximum positive or negative recorded Caudal Moment (output) divided by the maximum positive or negative Applied Moment (input) multiplied by 100%. In the sample graph above, the positive bending moment efficiency is nearly 100%, where the negative moment efficiency is less than 100%.



stage design, see Appendix G).<sup>9</sup> Briefly, this was a biaxial bearing design that had four linear bearings running along two round shafts in both the *X* and *Y* directions (Figure 6.2), providing approximately 57mm of travel along each shaft. This *XY* stage was designed to fit between the testing platform and the caudal six-DOF load cell. Further, locking collars were added to each shaft to allow for the option of fixing the specimen in place.

A single C4-C5 motion segment was used to evaluate the effect of adding this biaxial bearing system, placed between the testing platform and the caudal end of the specimen (Figure 6.3). The motion segment was isolated to leave the ligaments and disc intact, and potted using the technique described in Section 3.2. To examine the impact of “aggressive”, specimen-specific tuning aimed at minimizing error in the desired 0N axial load, tuning for this specimen was achieved using a target input wave switched to a tensile-compression sine wave set to cycle the axial force between  $\pm 30\text{N}$ .

Two specimen states (intact and SIM) were tested using the same loading protocol described in Section 3.2 (*i.e.*, target load of  $\pm 1.5\text{Nm}$ ) for all three simulated motions. For each testing state, the biaxial bearing system was tested in both the “free” state and in the “fixed” state, with the locking collars in place. The axial load was set to hold 0N throughout testing. Data analysis examined the bending moment efficiency and measured caudal forces from the final loading cycle for each motion in both the intact and SIM and for the fixed versus free stage conditions.

## 6.3 RESULTS

### 6.3.1 CURRENT DESIGN TESTING

Data analysis of the previously collected Chapter 5 specimens found that, in axial rotation, there was an average bending moment efficiency of 100% (Table 6.1), with no difference between the intact and injured states ( $p > 0.05$ ). In flexion-extension and lateral

---

<sup>9</sup> The design and development of this testing stage was undertaken by a group of undergraduate students for their 4<sup>th</sup> year design project. A number of potential options were explored, with the final design chosen as the biaxial bearing system.

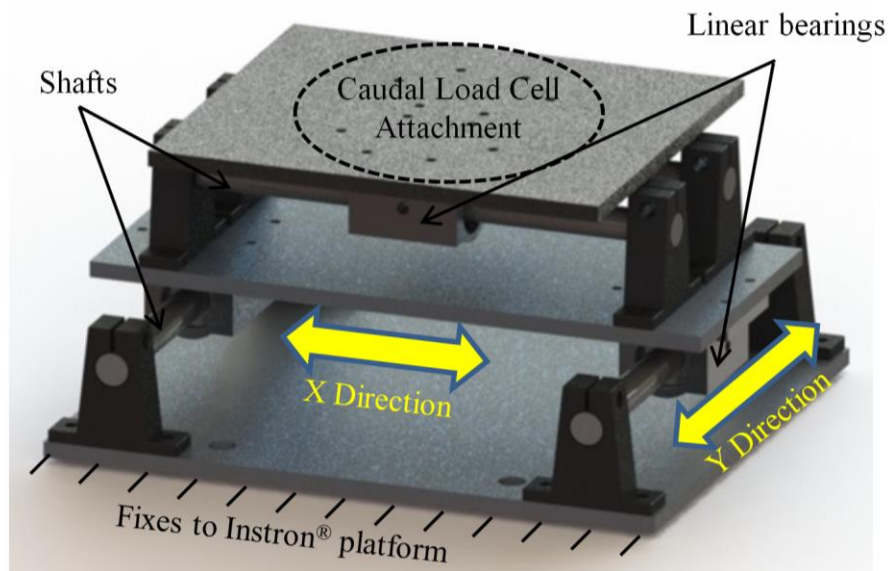


**Figure 6.2: Biaxial Bearing System**

A rendering of the biaxial bearing XY stage design is shown. There are two shafts running in perpendicular directions. Along each shaft are two linear bearings (only one shown in current figure). These bearings should allow for “free” XY translation of the caudal end of the specimen.

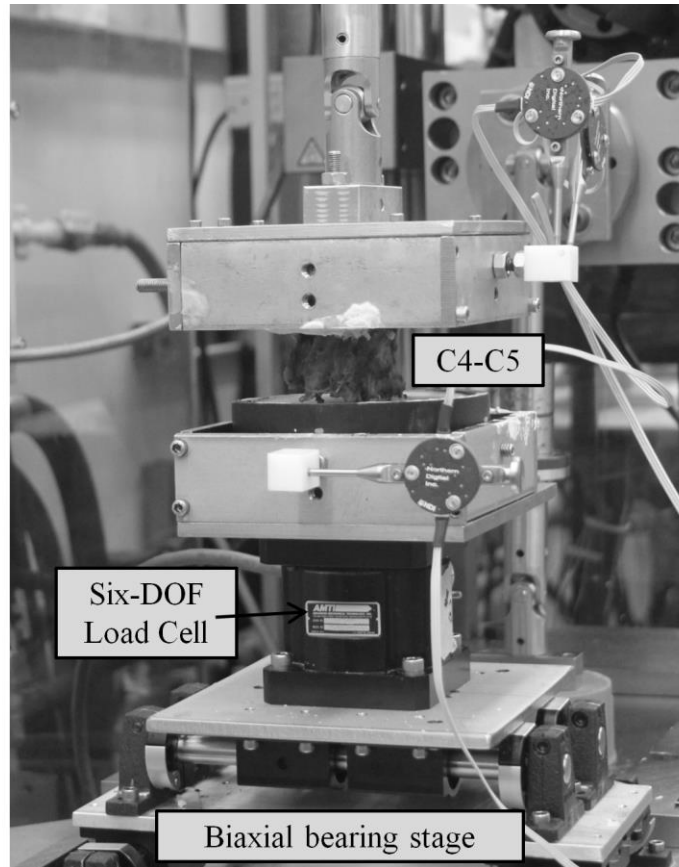


**Figure 6.3: Testing of a C4-C5 with Biaxial Bearing System**

A single C4-C5 motion segment was tested in the modified simulator design, with the addition of the biaxial bearing system and more aggressive, specimen-specific axial actuator tuning. Output loads at the caudal end were measured with a six-DOF load cell.

**Table 6.1: Bending Moment Efficiency of Chapter 5 Load Data**

The average  $\pm$  standard deviation (SD) positive and negative bending moment efficiencies (%) based on the maximum measured applied (input) and caudal (output) bending loads (n=7).

Motion	State	Average $\pm$ S.D. Positive Moment Efficiency (%)	Average $\pm$ S.D. Negative Moment Efficiency (%)
Axial Rotation	Intact	100 $\pm$ 2	101 $\pm$ 3
	SIM	100 $\pm$ 2	101 $\pm$ 3
Flexion- Extension	Intact	112 $\pm$ 19	105 $\pm$ 23
	SIM	101 $\pm$ 16*	41 $\pm$ 34*
Lateral Bending	Intact	138 $\pm$ 18	154 $\pm$ 15
	SIM	110 $\pm$ 23*	125 $\pm$ 20*

**Note:** Since cyclic testing was completed to  $\pm 1.5\text{Nm}$ , both a positive and negative moment efficiency calculation were considered. Positive efficiency represents loading inducing flexion, ipsilateral axial rotation, and ipsilateral lateral bending. The asterisk symbol represents significant differences between the intact and SIM states for a given motion.

bending, the average bending moment efficiency was generally larger than 100% (Table 6.1). Furthermore, in comparing the intact and injured states, moment efficiency was found to decrease with injury for both flexion-extension ( $p < 0.05$ ) and lateral bending ( $p < 0.05$ ).

The calculated shear forces in the  $X$  and  $Y$  directions at the caudal end in these specimens were consistently less than  $\pm 6\text{N}$  (Table 6.2). Axial forces were larger, with the highest loads seen in compression ( $\sim 10\text{-}30\text{ N}$ ). There were no differences between intact and SIM states for axial and shear forces ( $p > 0.05$ ).

### **6.3.2 MODIFIED DESIGN TESTING**

The new loop tuning protocol determined specimen-specific PID settings of 12.7, 1.7, and 0.4. With these new settings, the average axial force during the final loading cycle was approximately 0N for all testing states, with a peak difference of less than 20N (Table 6.3). Average shear forces were approximately 1N or less for all testing states, and did not exceed 4N (Table 6.3). The largest changes in force were measured immediately following a change in loading direction (Figure 6.4). Between the free and fixed  $XY$  stage conditions, there were no changes in the average measured forces, and no visible stage movements observed. Bending moment efficiency for axial rotation was again approximately 100%, with smaller and larger efficiencies measured for flexion-extension and lateral bending, respectively (Table 6.4). With injury, both flexion-extension and lateral bending efficiencies decreased, whereas axial rotation efficiency did not change.

## **6.4 DISCUSSION**

The pure bending moment technique has become the standard protocol for use in custom spinal loading simulators, but its implementation is rarely validated or reported (Panjabi, 1988; Wilke *et al.*, 1998). To improve the transparency of this loading technique, this study examined two measures to describe how well the simulator was creating a pure bending moment: the concept of “bending moment efficiency” and the measurement of forces at the caudal end of the test specimen. These measures were quantified while the degree of caudal end constraint was varied and the actuator control

**Table 6.2: Caudal Forces Measured in Chapter 5 Load Data**

The average  $\pm$  standard deviation (largest value) maximum and minimum caudal forces measured during the final loading cycle (n=7).

		Shear X Force (N)		Shear 'Y' Force (N)		Axial 'Z' Force (N)	
Motion	State	Maximum	Minimum	Maximum	Minimum	Maximum	Minimum
Flexion-Extension	Intact	$1 \pm 1$ (3)	$-3 \pm 1$ (-5)	$4 \pm 0$ (5)	$-5 \pm 1$ (-7)	$7 \pm 8$ (18)	$-23 \pm 5$ (-31)
	SIM	$3 \pm 1$ (4)	$-3 \pm 1$ (-4)	$4 \pm 1$ (5)	$-5 \pm 1$ (-7)	$2 \pm 5$ (9)	$-25 \pm 6$ (-34)
Axial Rotation	Intact	$0 \pm 0$ (0)	$-1 \pm 0$ (2)	$0 \pm 0$ (0)	$-1 \pm 0$ (-2)	$2 \pm 5$ (9)	$-9 \pm 7$ (-18)
	SIM	$0 \pm 0$ (0)	$-1 \pm 0$ (-1)	$1 \pm 1$ (2)	$-1 \pm 1$ (-2)	$5 \pm 6$ (11)	$-11 \pm 6$ (-19)
Lateral Bending	Intact	$2 \pm 0$ (2)	$-2 \pm 1$ (-3)	$4 \pm 1$ (5)	$-4 \pm 1$ (-5)	$4 \pm 6$ (12)	$-13 \pm 6$ (-19)
	SIM	$1 \pm 1$ (3)	$-2 \pm 0$ (-2)	$4 \pm 1$ (6)	$-4 \pm 2$ (-6)	$3 \pm 5$ (10)	$-15 \pm 7$ (-25)

**Note:** The positive directions are approximately anterior (X), left lateral (Y), and superior (Z).

**Table 6.3: Caudal Forces Measured in the Modified Simulator Setup**

The maximum and minimum caudal forces measured during the final loading cycle in a single C4-C5 specimen.

		Shear 'X' Force (N)		Shear 'Y' Force (N)		Axial 'Z' Force (N)	
Motion	State	Max.	Min.	Max.	Min.	Max.	Min.
Flexion-Extension	Intact	1	-1	2	-1	7	-19
	SIM	3	-1	3	-1	6	-19
Axial Rotation	Intact	0	0	0	-2	9	-12
	SIM	1	0	0	-1	7	-8
Lateral Bending	Intact	0	-2	0	-3	6	-12
	SIM	1	-1	4	-3	10	-11

**Note:** The positive directions are approximately anterior (X), left lateral (Y), and superior (Z).

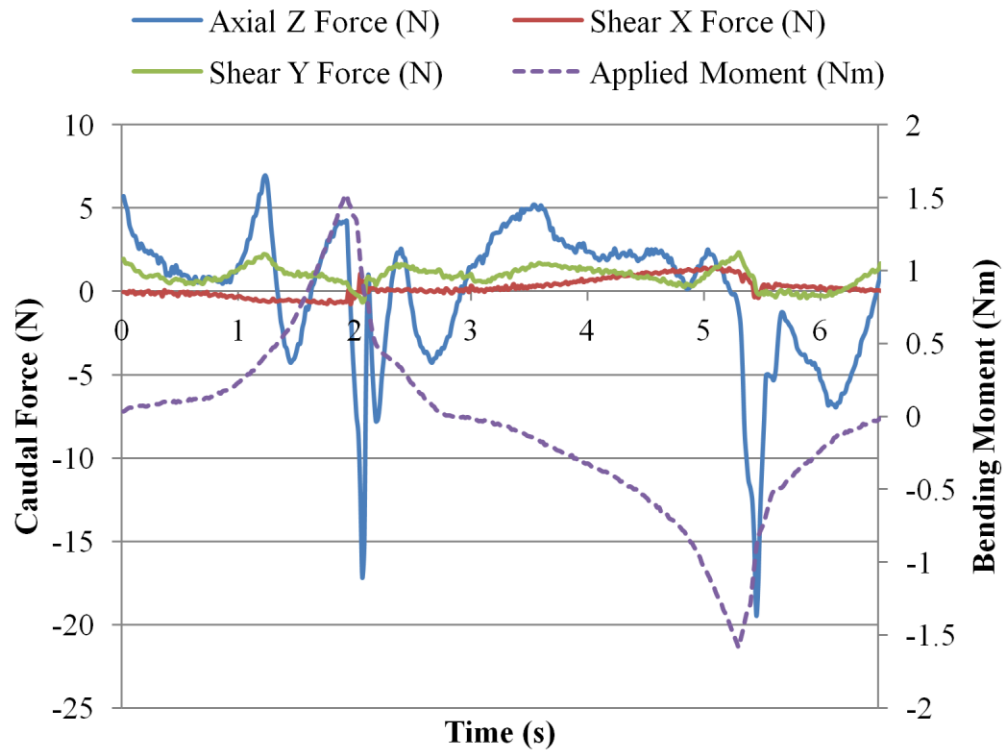


**Figure 6.4: Caudal Forces & Applied Moment during the Final Loading Cycle**

This graph shows a representative sample of the axial and shear forces recorded in the final loading cycle (intact Flexion-Extension with “free” caudal end shown). The axial and shear forces were quite small throughout the majority of the final loading cycle. Peaks in the axial force were seen once the applied moment was reversed and the specimen changed direction.

**Table 6.4: Bending Moment Efficiency in the Modified Simulator Setup**

The positive and negative bending moment efficiency (%) based on the maximum measured applied (input) and caudal (output) bending loads.

Motion	State	Positive Moment Efficiency (%)	Negative Moment Efficiency (%)
Flexion-Extension	Intact	95	76
	SIM	97	41
Axial Rotation	Intact	101	102
	SIM	101	103
Lateral Bending	Intact	95	124
	SIM	100	94

**Note:** Since cyclic testing was completed to  $\pm 1.5\text{Nm}$ , both a positive and negative moment efficiency calculation were considered. Positive efficiency represents loading inducing flexion, ipsilateral axial rotation, and ipsilateral lateral bending.



settings were aggressively tuned for the specific specimen being tested, showing the importance of these design parameters on overall simulator loading performance.

An initial examination of the current simulator design re-investigated data collected in Chapter 5. In all cases, the measured shear forces at the caudal end were small (less than 6N). In terms of bending moment efficiency, the custom spinal loading simulator was very effective in applying a “pure” bending moment in axial rotation, with a measured efficiency of 100% between the cranial and caudal load cells. In flexion-extension and lateral bending, the measured efficiency was not 100%, with cases of both higher and lower efficiencies. This may suggest that, while only bending loads are being generated, the bending moment changes along the length of the spine as the motion segment deforms under flexion-extension and lateral bending loading. This change could be the result of many specimen factors, including shifting in the centre of mass, very stiff or unstable motion segments, or degeneration in the vertebral or disc anatomy causing abnormal internal forces. The fact that these issues were not seen in axial rotation, however, suggests that the simulator design was also a factor. In axial rotation, the bending moment is applied directly above the specimen and caudal load cell (Figure 6.5A). In flexion-extension and lateral bend, the applied bending moment is measured at a different location in the loading plane (Figure 6.5B). Moreover, for these motions that are driven by the “off-axis” actuator, the axial actuator is still working to hold a load of 0N. Even small deviations from this target value would slightly increase or decrease the measured caudal bending moment in these planes.

One significant advantage of the current simulator design was that bending moments were applied directly to the specimen using torsional actuators. This is opposed to an approach that uses linear actuators to create bending load through force couples (Crawford *et al.*, 1995; Lysack *et al.*, 2000; Tang *et al.*, 2012), where extensive manual adjustments are required to ensure a bending moment is created. This alternate approach requires quasi-static testing, and has the potential for generating large shear forces at the caudal end if not monitored (Crawford, 2011). With the current simulator design, the potential for creating shear loads is minimized since no shear forces are actually applied. Nonetheless, it was of interest to quantify the caudal axial and shear forces, and to devise

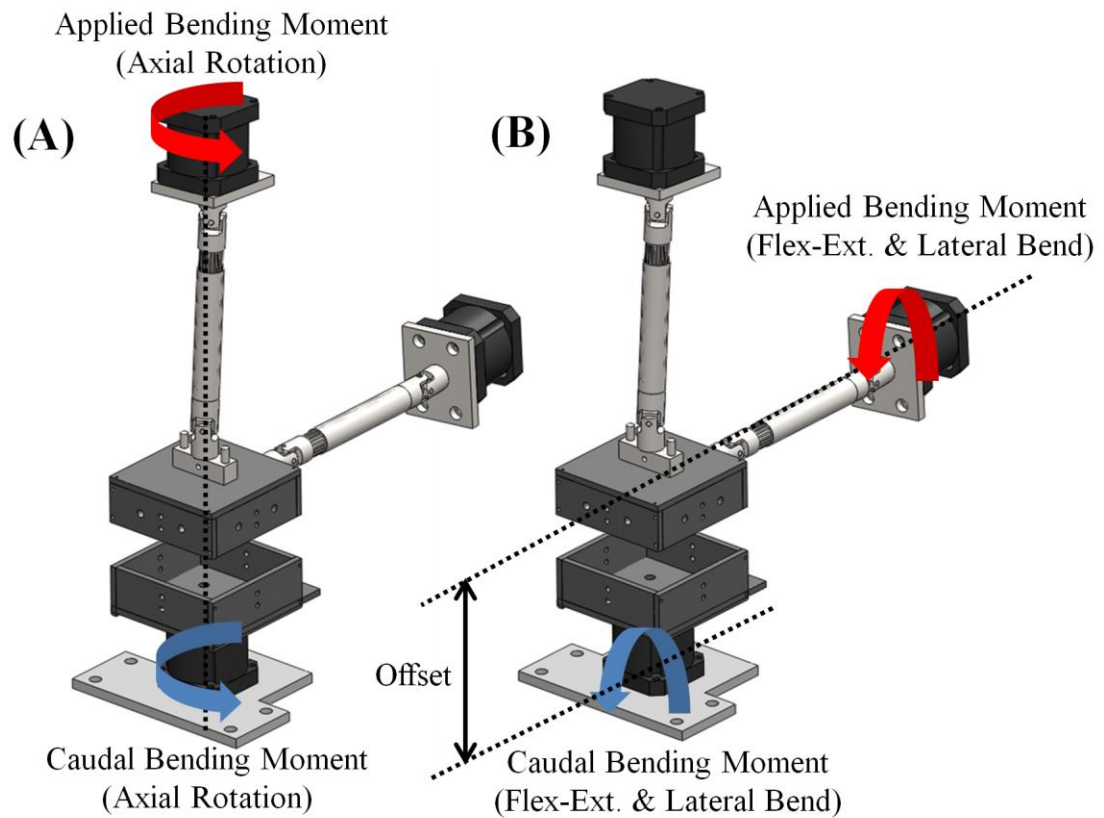


**Figure 6.5: Location of Applied and Caudal Bending Moments**

(A) In axial rotation, the locations of the applied and measured caudal bending moments are directly in line with each other. (B) In flexion-extension and lateral bending, the load cells are not directly in line, leading to potential discrepancies between the applied and measured caudal bending moments (*i.e.*, influenced by specimen deformation, axial loading on the cranial end, *etc.*).

a method to further reduce them, if possible. This led to the desire to compare fixed versus partially-free caudal end conditions.

Using a biaxial bearing system and improved actuator control, the shear loads were slightly reduced between the Chapter 5 data and the single specimen tested in the modified design. However, by comparing the “free” and “fixed” data in the modified design, it would appear that the differences observed in shear load were entirely due to the improved axial control rather than the change in end constraint. Furthermore, it must be noted that there is an inherent amount of friction with the bearing system itself, so completely eliminating shear forces with this bearing system is, in practice, unrealistic. With more aggressive PID settings, not only were the shear loads on the specimen slightly reduced, but larger reductions in the axial force error were observed. A critical comment though is that loop tuning in load control can have potentially devastating consequences if the PID settings are pushed too aggressively and become unstable (Figure 6.6). This actuator instability shows up as large oscillations in the output waveform, which could potentially induce permanent damage in the test specimen. As such, tuning should be approached cautiously. Nonetheless, the improved results with specimen-specific tuning suggest that PID settings should be adjusted for each tested specimen individually, in the intact state only.

There are a number of limitations to the current study. First, only a single specimen was used to compare the effect of the caudal end conditions. Given the small shear loads observed in Chapter 5 data, and the level of agreement observed in efficiency values between these specimens and the one tested for the modified design, testing of more specimens did not seem to be justified, especially considering the extensive costs and preparation required for each cadaver specimen. The single specimen was able to highlight the differences in the fixed versus partially-free end conditions and these end conditions will be continue to be compared in future studies. Furthermore, while there was no effect of the bearing stage identified in these tests, it will continue to be used in future tests, in case larger shear forces are generated, or in the case where controlled translation of the caudal end may be desired (see Section 7.3). A second limitation of this work is that there were only a limited number of load cells available for this testing. In

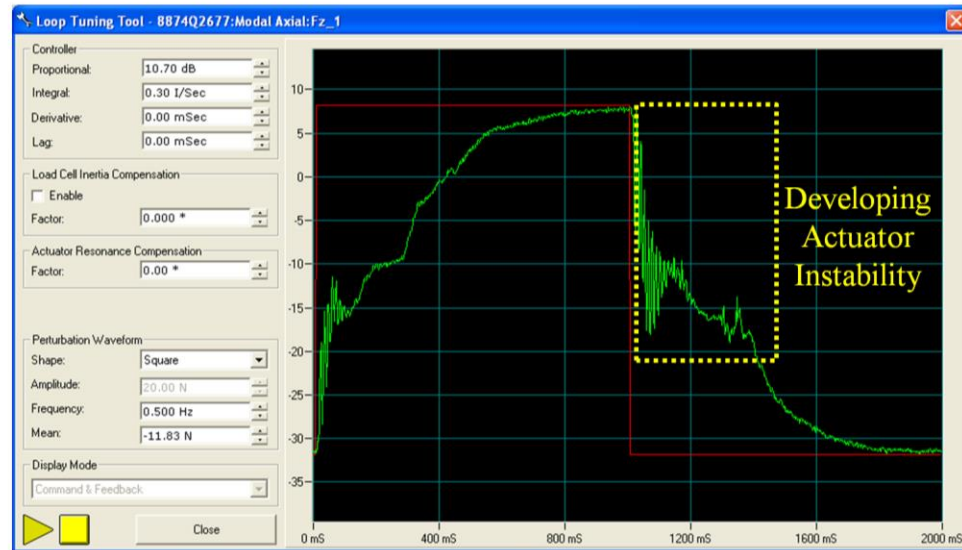


**Figure 6.6: Load Instability in PID Loop Tuning**

PID values were adjusted until the load targets were met, or until there was developing actuator instability (oscillations in the waveform shown) and then slightly reduced. Prior testing to this chapter used a square input wave (shown), but further investigation found a sine wave more effective for spine testing.

an ideal scenario, six-DOF load cells would be located directly on the cranial and caudal ends of the specimen to minimize any friction effects; however, this was not possible in the current simulator design due to the limited number of available load cells. While one AMTI load cell was added to the caudal end, the loads measured on the cranial end of the specimen are measured by Instron<sup>®</sup> load cells at the opposing ends of the loading arms (see Figure 5.1). As such, future testing should attempt to investigate the loads applied directly at the cranial end of the specimen as well (see Section 7.3).

In conclusion, the results from this study found that the design of spinal loading simulator was effective at applying only bending loads to the test specimen. Further investigation of the design suggests that the actuator control settings were an important factor in reducing axial and shear forces at the caudal end. As such, all future tests with the simulator should use a tensile-compressive sine wave to tune the actuator for cervical spine testing.

## 6.5 SUMMARY

This chapter presented metrics of bending moment efficiency and measured caudal forces to validate the effectiveness of the spinal loading simulator to recreate the pure bending moment loading technique. These were relatively simple measures to calculate and should be reported in future tests with the simulator, though further investigation of the efficiency in flexion-extension and lateral bending may be required. In general, these metrics would improve the transparency of studies performed with custom spinal loading simulators. Finally, use of the biaxial bearing system did not have an effect on the shear loading of the specimen test, but should be used in future tests in case larger forces are present.

## 6.6 REFERENCES

- Buckley, J.M., 2011. Response to letter to the editor regarding fixed ring and floating ring pure moment apparatus. *Journal of Biomechanics* 44, 1426–1427; Author Reply 1426–1427.
- Crawford, N.R., 2011. Regarding fixed ring and floating ring pure moment application. *Journal of Biomechanics* 44, 1423–1426; Author Reply 1426–1427.

- Crawford, N.R., Brantley, A.G., Dickman, C.A., Koeneman, E.J., 1995. An apparatus for applying pure nonconstraining moments to spine segments in vitro. *Spine* 20, 2097–2100.
- Cripton, P.A., Bruehlmann, S.B., Orr, T.E., Oxland, T.R., Nolte, L.P., 2000. In vitro axial preload application during spine flexibility testing: towards reduced apparatus-related artefacts. *Journal of Biomechanics* 33, 1559–1568.
- DiAngelo, D.J., Foley, K.T., 2004. An improved biomechanical testing protocol for evaluating spinal arthroplasty and motion preservation devices in a multilevel human cadaveric cervical model. *Neurosurgical Focus* 17, E4.
- Eguizabal, J., Tufaga, M., Scheer, J.K., Ames, C., *et al.*, 2010. Pure moment testing for spinal biomechanics applications: Fixed versus sliding ring cable-driven test designs. *Journal of Biomechanics* 43, 1422–1425.
- Gédet, P., Thistlethwaite, P.A., Ferguson, S.J., 2007. Minimizing errors during in vitro testing of multisegmental spine specimens: considerations for component selection and kinematic measurement. *Journal of Biomechanics* 40, 1881–1885.
- Goel, V.K., Panjabi, M.M., Patwardhan, A.G., Dooris, A.P., Serhan, H., 2006. Test protocols for evaluation of spinal implants. *Journal of Bone & Joint Surgery* 88-A, 103–109.
- Goertzen, D.J., Lane, C., Oxland, T.R., 2004. Neutral zone and range of motion in the spine are greater with stepwise loading than with a continuous loading protocol. An in vitro porcine investigation. *Journal of Biomechanics* 37, 257–261.
- Ilharreborde, B., Zhao, K., Boumediene, E., Gay, R., *et al.*, 2010. A dynamic method for in vitro multisegment spine testing. *Orthopaedics & Traumatology, Surgery & Research* 96, 456–461.
- Lysack, J.T., Dickey, J.P., Dumas, G. a, Yen, D., 2000. A continuous pure moment loading apparatus for biomechanical testing of multi-segment spine specimens. *Journal of Biomechanics* 33, 765–770.
- McLachlin, S.D., 2008. *Design and Development of In Vitro Tools to Assess Fixation and Motion in the Spine*. Master's Thesis, University of Western Ontario, London, ON, Canada, 1–114.
- Miura, T., Panjabi, M.M., Cripton, P.A., 2002. A method to simulate in vivo cervical spine kinematics using in vitro compressive preload. *Spine* 27, 43–48.
- Panjabi, M.M., 1988. Biomechanical evaluation of spinal fixation devices: I. A conceptual framework. *Spine* 13, 1129–1134.
- Patwardhan, A.G., Havey, R.M., Meade, K.P., Lee, B., Dunlap, B., 1999. A follower load increases the load-carrying capacity of the lumbar spine in compression. *Spine* 24, 1003–1009.

Tang, J.A., Scheer, J.K., Ames, C.P., Buckley, J.M., 2012. Pure moment testing for spinal biomechanics applications: fixed versus 3D floating ring cable-driven test designs. *Journal of Biomechanics* 45, 706–710.

Wheeler, D.J., Freeman, A.L., Ellingson, A.M., Nuckley, D.J., *et al.*, 2011. Inter-laboratory variability in in vitro spinal segment flexibility testing. *Journal of Biomechanics* 44, 2383–2387.

Wilke, H.J., Claes, L., Schmitt, H., Wolf, S., 1994. A universal spine tester for in vitro experiments with muscle force simulation. *European Spine Journal* 3, 91–97.

Wilke, H.J., Rohlmann, A., Neller, S., Schultheiss, M., *et al.*, 2001. Is it possible to simulate physiologic loading conditions by applying pure moments? A comparison of in vivo and in vitro load components in an internal fixator. *Spine* 26, 636–642.

Wilke, H.J., Wenger, K., Claes, L., 1998. Testing criteria for spinal implants: recommendations for the standardization of in vitro stability testing of spinal implants. *European Spine Journal* 7, 148–154.

## CHAPTER 7: CONCLUSIONS

**OVERVIEW:** *This chapter summarizes the efforts and outcomes of the studies performed in this thesis, revisiting their abilities to meet the original set of objectives and proposed hypotheses. Overall strengths and limitations of this body of work are discussed, and possible future directions for this line of research are explored. Finally, the overall potential impact and significance of this work are highlighted.*

### 7.1 SUMMARY

*In vitro* biomechanical simulations can help to elucidate information that is not often feasible to obtain through *in vivo* research, such as the instability of a traumatic neck injury or the comparable effectiveness of varying a surgical fixation decision. The main goal of this thesis was to use the principles of biomechanical simulation to investigate changes in the kinematic stability of the subaxial cervical spine with relevant injury patterns and commonly used surgical fixation techniques. Overall, this objective was met through a series of clinically-relevant biomechanical studies and other investigations relevant to the simulator design and kinematic outcome measures.

In Chapter 1, the background concepts and knowledge to date in the areas of cervical spine trauma and surgical management, as well as the principles of, and tools available for, biomechanical simulations and kinematic analysis were detailed, culminating in eight specific objectives and ten hypotheses. Chapter 2 was the first study to use the custom designed and developed spinal loading simulator (McLachlin *et al.*, 2008), and also introduced a new Optotrak Certus® motion capture system (NDI, Waterloo, ON, Canada) (*i.e.*, Objective #1). Using a combination of surgical know-how, the spinal loading simulator, and computer software, a testing protocol and post-hoc data analysis program were devised to take a cadaver specimen from initial musculature dissection through to kinematic analysis of the flexion-extension, axial rotation and lateral bending between adjacent vertebrae (Hypothesis #1 is accepted). These relative vertebral motions were determined using Optotrak® Smart Markers attached to long K-wires, which could be inserted into the small vertebrae with minimal soft tissue



disruption. The study completed in this chapter investigated the kinematic stability of an isolated posterior injury (*i.e.*, Stage I flexion-distraction injury) in the C3-C4 motion segment of a C2-C5 spine before and after common surgical fixation techniques (*i.e.*, Objective #2). Results from this testing found that sequential disruption of the posterior soft tissues along with resection of a single articular process had at least one significant increase over the intact ROM in each motion, but overall did not generate any considerable increase in the overall ROM of the spine (Hypothesis #2 is accepted). Comparison of three common surgical fixation techniques, posterior lateral mass screw fixation, ACDFP and the procedures combined, revealed that for this injury pattern, the anterior approach was significantly less stable from a kinematic perspective (Hypothesis #3 is rejected).

In Chapter 3, the spinal loading simulator was adapted to induce a clinically-relevant traumatic injury mechanism for a unilateral facet perch (*i.e.*, Objective #3). This setup was able to reliably producing an impending dislocation in C4-C5 and C6-C7 motion segments using a combination of deadweights and increasing axial rotation (Hypothesis #4 is accepted). The interest in performing this testing was to determine the extent of soft tissue disruption most commonly associated with this injury pattern (*i.e.*, Objective #4). Using a consistent dissection technique and visual soft tissue disruption scale, the most commonly injured soft tissues were found to include both capsules, and a significant portion of the annulus and ligamentum flavum (Hypothesis #5 is accepted). These injuries were subsequently used to define the SIM.

The focus of Chapter 4 was to generate FHAs in addition to ROM and NZ kinematic stability measures. However, the FHA was not immediately available from the output six-DOF pose data of the NDI First Principles™ software. This led to the desire to define a simple and effective technique using six-DOF rigid body trackers to generate accurate FHAs that characterize 3D motion with applications in the cervical spine (*i.e.*, Objective #5). A method to generate a large number of accurate FHAs was developed based on the concept of using a moving window technique to calculate screw matrices (used to calculate the FHA parameters) based on two transformation matrices in the data set separated by a minimum rotation size (Hypothesis #6 is accepted). The caveat to this

method, though, was that for reasonably accurate FHAs to be produced, a minimum “window size” of 2-5° was necessary, with smaller rotations containing significant error. For movements with a ROM smaller than this value, it appeared only the average FHA could reliably be reported. Furthermore, previous investigations using the FHA had shown it largely as a visualization tool; however, there was additional interest in using the generated FHAs to quantify changes in the 3D kinematic stability of each planar motion (*i.e.*, Objective #6). An advanced mathematical technique called an “alpha shape” was explored to calculate a wrapped boundary around the intercept points of the FHAs with a respective anatomical plane. By defining the centroid and alpha shape area of these points, changes in 3D kinematic stability were identified between the intact and SIM states (Hypothesis #7 is accepted). The potential use of the FHAs to quantify changes in kinematic stability was only preliminarily investigated in Chapter 5.

The majority of Chapter 5 was focused on examining the effect of varying the surgical factor of graft size height in ACDFP fixation of three simulated flexion-distraction injuries (*i.e.*, Objective #7). In this study, a graft height equal to the measured disc space height was compared to grafts undersized and oversized by 2.5mm, with plate sizes adjusted to accommodate changes in graft size. Each graft was initially compared in the SIM state, with further comparison in compounded injuries of a simulated unilateral facet fracture and additional soft tissues injuries associated with a bilateral facet dislocation. Data analysis revealed unexpected results. While the oversized graft provided the most kinematic stability in flexion-extension, the undersized graft was more stable in axial rotation and lateral bending (Hypothesis #8 rejected). It was felt that the undersized graft results were explained by the increased bony stability provided by the overlapping uncovertebral joint, which was not engaged with the larger grafts.

In the studies performed in Chapters 2, 3 and 5, the simulator design was continually enhanced through small changes to improve testing of cervical motion segments; yet, larger design modifications were considered. These included the caudal end conditions and actuator control settings, and specifically, their role in the effectiveness of achieving pure bending moment loading (*i.e.*, Objective #8). In Chapter 6, the concept of bending moment efficiency and the forces measured at the caudal end

were examined, initially for the intact and SIM data generated in the Chapter 5 specimens. Additional testing was performed in a single specimen to examine the effect of a biaxial bearing system positioned beneath the specimen, to add partial translational freedom to the caudal end, and improved actuator load control settings achieved through more aggressive PID tuning. In both the Chapter 5 specimens and the single specimen tested in the modified setup, the measured shear forces were consistently under 7N, yet could not be eliminated entirely (Hypothesis #9 rejected). However, the effect of these very small loads would have on the overall kinematics of the motion segments would expect to be very minimal. Finally, the ability of the simulator to apply a pure bending moment was evident in axial rotation, with a measured moment efficiency of 100%; however, the efficiency in flexion-extension and lateral bending varied and decreased with injury. In testing of biaxial bearing system, there were no identified differences between the free and fixed states in a single motion segment, yet there was almost no shear load measured for this specimen so no effect would be expected. It was suggested then that this system be incorporated in all future simulator testing.

## **7.2 STRENGTHS AND LIMITATIONS**

There are a number of strengths and limitations in this body of work. Specific limitations have already been identified within each chapter which will not be reiterated here; instead this section will focus on overall general limitations of this work. The studies performed in this thesis were the first to make use of the custom spinal loading simulator, designed within the testing frame of a tri-axial Instron® 8874 materials testing machine (Instron, Norwood, MA, USA). In general, this simulator was very effective in applying consistent and reliable loading to the cadaver specimens. Its design also allowed bending moments to be applied directly to the specimen, limiting potentially shear loads. Furthermore, the complexity of the Instron® software easily allowed for flexion-extension and lateral bending loading to be applied with the off-axis actuator, while holding a near-zero load with the axial actuator to remove the weight of the loading arms and potting fixture. In addition to flexibility testing, the considerable loading range of the Instron® torsion actuators allowed for the simulator to be adapted to induce a clinically-relevant injury mechanism for a unilateral facet perch, with torques reaching

almost 30Nm required. This large load range may not have been ideal for the relatively small loads required for cervical spine flexibility testing (*i.e.*,  $\pm 1.5\text{Nm}$ ), yet the output was consistent and repeatable for all testing performed.

Integration of the Optotrak® Certus motion capture system was a dramatic upgrade over the original 2D optical tracking techniques used (McLachlin, 2008). This tracking system also provided very accurate six-DOF measurement with the pre-packaged Optotrak® Smart Markers. There were some reoccurring issues in each study with respect to the attachment of the markers to the vertebrae with minimal soft tissue disruption, especially in tests where bony integrity was required for surgical instrumentation. In some cases, this required attaching the trackers to the potting fixtures themselves, such as in Chapter 3. In Chapter 5, additional segments above and below were included and pinned to accommodate the screws used for potting, leaving space for the tracker's k-wires and surgical instrumentation. In all studies performed to date, no ideal setup has been identified, suggesting a study-by-study approach is still required.

With any *in vitro* testing, there are always general limitations to the results such as: feasibility in testing a large number of specimens, reproducing physiologic loading with and without muscle force replication, inherent specimen variability, and degeneration in the older specimens used. This work made several attempts to reduce these effects; using validated injury models, clinically-relevant instrumentations, improving techniques to generate accurate kinematics, and examining the loading produced in detail. It would be hoped that these results are considered in future surgical management guidelines considering biomechanical evidence. An auxiliary benefit to this research is that the results may highlight potential limitations of the instrumentation, which could be addressed in future implant development.

### **7.3 FUTURE DIRECTIONS**

The three cadaveric studies performed in this thesis only examine a fraction of the spectrum of soft tissue injuries present in cervical spine trauma. The SIM developed in Chapter 3 represented a single flexion-distraction injury mechanism, with numerous other known mechanisms (Allen *et al.*, 1982), which could each have similar injury models

developed. One similar flexion-distraction injury mechanism that could now be investigated would be hyper-flexion/distraction, where a combination of the simulator actuators and biaxial bearing stage could be used to generate this injury. Furthermore, there are additional surgical factors, and combinations of factors, worth investigating. A study currently being conducted examines the effect of plate length in combination with graft size height to further answers questions posed in Chapter 5 – would use of a longer plate in conjunction with an undersized graft provided increased stability in flexion-extension and axial rotation/lateral bend?

Testing in Chapter 6 found that the simulator was very effective in producing very small forces at the caudal end of the specimen, yet only a “pure” bending moment was found in simulated axial rotation. This difference in the flexion-extension and lateral bending moment efficiency may be due to additional gains or losses in the system (or may potentially be a factor in the specimen itself). With a limited number of load cells available for control and measurement, it was not possible to measure loads in all desired locations in the current testing setup. With additional load cell acquisitions and slight simulator adjustments, future testing could examine the loads measured directly above and below the specimen to quantify bending moment efficiency. Also, the biaxial bearing system tested in Chapter 6 found no effect in the specimen tested, due to the small shear loads presents. Additional testing with the bearing system found that approximately 5N of shear force was required to induce translation of the XY stage. Therefore, future testing should continue to use this system as a safety net in case larger forces are somehow generated. Additionally, one future consideration would be to adapt this XY stage for inducing shear loading, where a system of motors and cable could be added to test these types of loads. Furthermore, the addition of motors to induce shear could also be used to reproduce other defined injury mechanisms for cervical spine trauma requiring large shear loads (Allen *et al.*, 1982).

Future testing should also continue to explore the value of using the generated FHAs and resulting alpha shapes to explain changes in kinematic stability with injury, and possibly instrumentation. It is probable that these measures will highlight small changes in 3D motion not present in traditional ROM parameters. These techniques also

made use of anatomical visualization techniques using generated 3D anatomical models from CT images. The same technique could be further explored in future testing to display post-hoc kinematics or with further effort real-time visualization of the simulated motions.

A final consideration for future research would be to build on the knowledge gained of the strengths and weaknesses of specific instrumentation through new or modified implant development. The development of spinal instrumentations has come a long way since the designs by early pioneers in this field (Hadra, 1891; Rogers, 1942), yet there is still considerable room for improvement. Furthermore, with current advancements in 3D printing and novel biomaterials, it can be reasonably assumed that the field of spinal instrumentation could be considerably different within the next decade.

## 7.4 SIGNIFICANCE

In conclusion, this body of work provides valuable information to both the engineering and clinical spine communities with respects to the surgical treatment of flexion-distraction injuries of the subaxial cervical spine. From a clinical perspective, this collective work will aid in the continued establishment of better guidelines for the surgical treatment of flexion-distraction injuries of the cervical spine. In terms of significance to the engineering and scientific communities, the kinematic techniques assessed and potential metrics developed to evaluate simulator performance will provide additional tools to improve the clinical relevance of biomechanical testing. Furthermore, the testing protocols established in this thesis will also significantly streamline future simulator testing in areas such as evaluating surgical fixation efficacy.

## 7.5 REFERENCES

- Allen, B.L., Ferguson, R.L., Lehmann, T.R., O'Brien, R.P., 1982. A mechanistic classification of closed, indirect fractures and dislocations of the lower cervical spine. *Spine* 7, 1–27.
- Hadra, B., 1891. Wiring the spinous processes in Pott's disease. *Journal of Bone & Joint Surgery* 207–210.

McLachlin, S.D., 2008. *Design and Development of In Vitro Tools to Assess Fixation and Motion in the Spine*. Master's Thesis, University of Western Ontario, London, ON, Canada, 1–114.

Rogers, W., 1942. Treatment of fracture-dislocation of the cervical spine. *Journal of Bone & Joint Surgery* 24-A, 245–258.

## APPENDIX A – GLOSSARY<sup>10</sup>

**Allen-Ferguson System:** a classification system for cervical spine trauma based on the describe mechanism of injury

**Allograft:** a tissue graft from a donor of the same species as the recipient but not genetically identical

**Annulus Fibrosus:** ring of fibrous tissue in the intervertebral disc

**Anterior:** situated at or directed toward the front; opposite of posterior; refers to the front of the body when in the anatomical position

**Arthrodesis:** surgical immobilization of a joint so that the bones grow solidly together

**Articular:** pertaining to a joint, or a joint surface

**Atlas:** first vertebra of the cervical spine

**Autograft:** a tissue or organ that is transplanted from one part to another part of the same body

**Axial Rotation:** act of rotating the spine about the superior-inferior axis

**Axis:** second vertebra of the neck

**Caudal:** situated in or directed towards the hind part of the body; inferior to another structure, in the sense of being below it

**Cervical Spine:** the seven vertebrae of the neck

**Collagenous:** naturally occurring fibrous protein; main component of connective tissue

**Comorbid:** existing simultaneously with and usually independently of another medical condition

**Corpectomy:** surgical procedure that removes part of the vertebral body

**Cranial:** directed toward the skull, superior to another structure, in the sense of being above it

**Diarthrodial:** articulation that permits free movement

**Discectomy:** removal of the intervertebral disc

**Discoligamentous:** both the intervertebral disc and surrounding ligaments combined

---

<sup>10</sup> Most anatomical definitions found using Merriam-Webster's Medical Dictionary, Bethesda, MD, <http://www.nlm.nih.gov/medlineplus/medlineplusdictionary.html>. Other definitions have been found using the "define" tool in Google Search.



**Disc Degeneration:** deterioration of the physical structure of the intervertebral disc

**Direction Cosines:** the cosines of the angles between the vector and the three coordinate axes of a reference frame

**Dislocation:** displacement of one or more bones at a joint

**Distraction:** excessive separation.

**Euler Angles:** three independent angles used to uniquely describe the orientation of a rigid body in a frame of reference

**Extension:** rotation of the spine about the medial-lateral axis in a posterior direction

**Facet Joints:** a synovial joint between the superior articular process of one vertebra and the inferior articular process of the vertebra directly above it

**Finite Helical Axis:** a vector that defines the axis of rotation of a moving object

**Flexion:** rotation of the spine about the medial-lateral axis in an anterior direction

**Flexibility Testing:** load-based input for simulating spine motion

**Foramen:** an opening through a bone which nerves, arteries, veins, *etc.* pass through

**Fracture:** the act or process of breaking or the state of being broken

**Frame of Reference:** a system of geometric axes in relation to which measurements of size, position, or motion can be made

**Frontal Plane:** a vertical plane that divides the body into anterior and posterior portions

**Fusion:** surgical immobilization of a joint (see arthodesis)

**Graft:** to implant tissue surgically

**Hysteresis:** the phenomenon in which the value of a physical property lags behind changes in the effect causing it

**Inferior:** in anatomy, used in reference to the lower surface of a structure, or to the lower of two (or more) similar structures

**In Vitro:** in an artificial environment outside the living organism

**In Vivo:** within the living organism

**Intervertebral Disc:** tough elastic discs that are interposed between adjacent vertebrae

**Kinematics:** the study of motion of one body with respect to another

**Laminae:** two thin plates extending from the lateral mass of each vertebra converging at the spinal process

**Lateral:** denoting a position farther from the median plane or mid-line of the body or a structure; refers to being away from the mid-line of the body when in the anatomical position

**Lateral Bending:** rotation of the spine about the anterior-posterior axis to left or right sides

**Lateral Mass:** large pillars of bone on the sides of the cervical vertebrae defined by a superior and inferior articular process

**Laxity:** state of being non-rigid

**Ligament:** band of fibrous tissue connecting bones or cartilages, serving to support and strengthen joints

**Mechanotransduction:** mechanism which converts mechanical stimulus into chemical activity

**Medial:** situated towards the mid-line of the body or a structure

**Morphological:** Of, relating to, or concerned with form or structure

**Motion Segment:** a unit of the spine used to describe the general mechanical behaviour of a region of the spine; consists to adjacent vertebrae, as well as the intervertebral disc and connecting ligaments

**Musculoskeletal:** of, relating to, or involving both musculature and skeleton

**Neurologic:** relating to neurology; the branch of medicine concerning the structure, functions, and diseases of the nervous system

**Neurovascular:** involving both nerves and blood vessels

**Neutral Zone:** a kinematic stability measure traditionally used to define *in vitro* spinal laxity

**Nucleus Pulposes:** an elastic mass lying in the center of each intervertebral disc

**Occiput:** back part of the skull

**Orthogonal:** relating to or composed of right angles

**Osseous:** consisting of bone

**Osteoarthritis:** a non-inflammatory degenerative joint disease of the skeletal system, its articulations, and associated structures

**Osteoligamentous:** both the bone (osseous) and ligaments structures combined

**Osteophyte:** a pathologic bone outgrowth

**Pedicles:** two short pieces of bone that form the lateral sides of the vertebral arch connecting the arch to the vertebral body

**Perched facet:** excessive subluxation of inferior articular process on the superior articular process of the adjacent vertebra below immediately prior to dislocation

**Physiologic:** in accordance with or characteristic of the normal functioning of a living organism

**Posterior:** directed toward or situated at the back; opposite of anterior; refers to the back of the body when in the anatomical position

**Process:** a prominent or projecting part of an organism or organic structure

**Proximal:** situated next to or near the point of attachment or origin

**Quasi-static:** process that occurs very slowly

**Radiograph:** an image produced on a sensitive film by X-rays, gamma rays, or similar radiation, and typically used in medical examination

**Range of Motion:** overall magnitude of motion attained during an activity

**Rigid Body:** an idealization of a solid body in which deformation is neglected

**Sagittal Plane:** the vertical, median plane that divides the body into left and right lateral sides

**Screw Displacement Axis:** see Finite Helical Axis

**Segmentation:** the process of partitioning an image into multiple regions in order to simplify or change the representation of the image

**Servohydraulic:** use of hydraulics (*i.e.*, oil pressure & related electronics) to control mechanical position

**Six Degree-of-Freedom (Loading):** three forces directed along a set of three orthogonal axes, and the bending moments about each axis

**Six Degree-of-Freedom (Motion):** three translations and three rotations in a defined orthogonal reference frame

**Spinous Process:** dorsal process of the neural arch of a vertebra

**Subaxial:** cervical vertebrae below the Axis (C2)

**Subaxial Injury Classification (SLIC):** a proposed classification system for cervical spine trauma based on the describe mechanism of injury, as well as fracture morphology, discoligamentous health, and neurologic status

**Subluxation:** partial dislocation (as of one of the bones in a joint)

**Superior:** situated above, or directed upward

**Synovial Joint:** a joint surrounded by a capsule that is filled with a lubricating fluid

**Transverse Plane:** a horizontal plane that divides the body into superior and inferior portions

**Trauma:** a body wound or shock produced by a sudden physical injury

**Tubercle:** small bony protrusion

**Unilateral:** occurring on, performed on, or affecting one side of the body or one of its parts

**Unit Vector:** an axis directed in space with a length of one

**Vertebra(e):** individual, irregular bones that make up the spinal column

## APPENDIX B – EXPERIMENTAL TESTING PROTOCOL

The following steps outline in detail the complete testing procedure used to set-up and test cadaveric cervical spines with the customized Instron® Materials Testing Machine (*i.e.*, spinal loading simulator) and to track motion with the Optotrak Certus® and NDI First Principles™ software. The level of detail included is such that another operator, given access to the required software tools, could follow these steps to reproduce the *in vitro* studies presented in Chapters 2, 3 and 5 of this thesis. In most cases, pictures describing these components and steps have been included in the thesis; otherwise, pictures are included here.

### A. Materials Required

1. Fresh-frozen cervical spine specimen
2. Cranial and caudal potting fixtures
3. Four-point alignment jig
4. Loading arms and counterbalance weight
5. Two 1” cut pieces of 4” PVC pipe
6. Denstone™ dental cement (2-3 cups required)
7. Extra screws (*i.e.*, drywall screws) for additional fixation
8. Surgical tools (*i.e.*, scalpels, rongeur, curette, pickups, etc.)
9. Optotrak® Smart Markers and K-wires for optical motion tracking
10. Spinal instrumentation (if required)

### B. Pre-testing

1. Keep specimen frozen until night before testing day (thaw overnight)
2. Remove remaining musculature from specimen (requires surgical expertise)
3. Isolate desired motion segments
4. Ensure ligaments and discs are intact
5. Insert two drywall screws into the vertebral endplates and another two through either the lamina or articular process of the cranial and caudal vertebrae (see Figure 3.1) (**Note:** *ensure motion segments of interest have not been fixed*)
6. Add molding clay to screw ends to allow for adjustment of potting alignment

### C. Simulator Setup Within Instron® 8874 Materials Testing Machine

1. Turn ON Instron® pump and 8874 power (low power first – Console software must be running on Instron® computer)
2. Connect the loading arms to axial (fixed-length arm) and off-axis (sliding arm) actuators

3. Ensure that the rotary position of the Instron® is set to 30° (with axial loading arm attached, connection piece to fixture should be parallel to the wall – otherwise may have to connection between AMTI load cell and loading arm)
4. Fix biaxial bearing stage with connected AMTI load cell and caudal potting fixture to the Instron® testing platform, beneath the axial actuator
5. Connect the off-axis loading arm and counterbalance to the cranial potting fixture
6. Insert cemented PVCs (without specimen) as weighted spacers into cranial and caudal fixtures
7. In this setup, tare all Instron® and AMTI load channels to zero load to remove the machine weight from their readings

#### **D. Potting Cranial End Within PVC**

1. Place folded sheets of paper towel and the 1” section of PVC pipe to the bottom of the cranial potting fixture; ensure all screw of the fixture are tightened once the PVC has been inserted
2. Set cranial end of specimen within the cranial potting fixture, with four-point alignment jig in position (Figure B.1)
3. Adjust specimen orientation using the alignment jig such that: the disc space of the tested motion segment is horizontal, the anterior-posterior and medial-lateral axes align with the appropriate loading pegs of the fixture, and so that the most posterior point on the mid-line of the vertebral body lies in the centre of the fixture
4. Mix approximately two cups of Denstone™ dental cement (Heraeus Kulzer, South Bend, IL, USA) with 120mL of water in a sealed plastic bag (adjust as necessary – mixed cement should be in a liquid phase)
5. Tear off one corner of the bag to pour the liquid cement
6. Slowly add wet cement around specimen and screws
7. Fill to height required (should just reach the endplate of the vertebral body)
8. Allow 20-30 minutes for the cement to fully harden

#### **E. Potting Caudal End Within PVC**

1. Connect the cranial potting fixture, with specimen attached, to the axial loading arm of the spinal loading simulator (Instron® must be ON to adjust arm height).
2. Place paper towel and 1” PVC tube in caudal fixture
3. Lower the specimen using the Instron® axial actuator to the height required (screw ends and molding clay should be entirely submerged with the inferior endplate of caudal vertebra just submerged)
4. Adjust the bearing stage so that the specimen is centered in the caudal fixture and then fix in position
5. Follow the same cementing technique as the cranial end (Steps E.4-8)

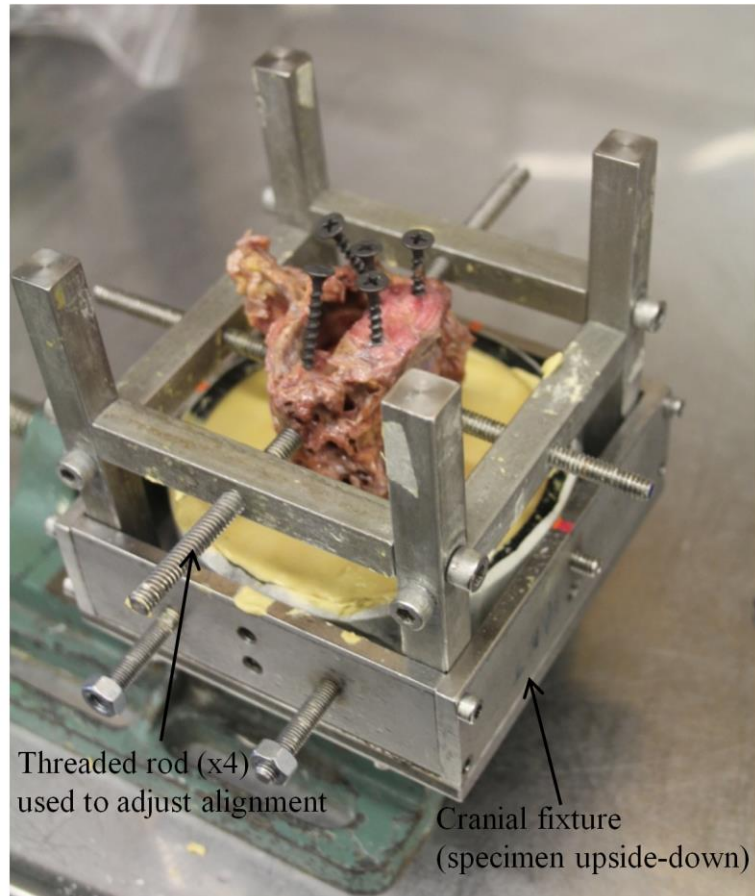


**Figure B.1: Four-point Potting Alignment Jig**

To control specimen alignment during the cementing process, a four-point alignment jig was used. The jig consists of four threaded rods, which can be adjusted to hold the specimen in position. The bolts on the corners of the jig, once tightened, create a rigid structure.

## **F. Tuning Load Control of Axial Actuator using Instron® Console Software**

1. Spine specimen (or other test material) must be connected to axial actuator (*i.e.*, load control requires connection to test frame – cannot run in “air”)
2. Set Fz\_1 channel to load control
3. Ensure reasonable position limits are set (action: system stop)
4. Set load limits at  $\pm 100\text{N}$  (action: unload)
5. Set starting Proportion, Integral, and Derivative control to small values ( $P=0$ ,  $I=0$ ,  $D=0$ )
6. Use loop tuning tool provided with the Instron® software
7. Set a target sine wave signal at 1Hz with an amplitude of  $\pm 30\text{N}$  with a mean load of 0 N
8. Increase the proportional gain (P) of the actuator until the actuator’s response can achieve a close match to the target shape desired (CAUTION: watch for increasing oscillations in the output waveform as a sign of actuator instability)
9. Alter the Integral (I) and Derivative (D) as necessary

## **G. Software Protocol**

1. Open “Method” loading protocol using the WaveMatrix™ program for desired motion (*i.e.*, “flex-ex\_c spine\_1.5Nm”) (Figure B.2)
2. Current method starts by ramping Fz\_1 to hold 0 N and to the desired rotation position for the loading mode (confirm against current rotation position of the actuator)
3. Each loading mode (Axial Rotation: Rotary, Flex-Ex & Lateral Bend: Elbow) consists of three full rotation cycles in a triangular waveform at  $3^\circ/\text{s}$  up to some exaggerated end position; an EVENT is used to achieve the desired applied moment (*i.e.*,  $\pm 1.5\text{ Nm}$ )
4. Make any required changes to load target, loading rate, etc. (Always double check – the actuator will do exactly what its told including complete specimen destruction)
5. Set the acquisition rate (60 Hz)
6. Save the Method
7. Set the required “Analog Output” scale values for desired load & position channels (*i.e.*, Elbow Torque, Caudal Load Cell Moments & Forces) (Figure B.3)

## **H. Optotrak Certus® Setup**

1. Turn ON the Optotrak Certus®, Control Unit, and ODAU power supply
2. Connect the Smart Markers serially to the Wireless Strober
3. Connect the analog output channels of the Instron® to the ODAU box using BNC cables

## **I. NDI First Principles™ Software**

1. Start a new experiment (or Open an existing one)



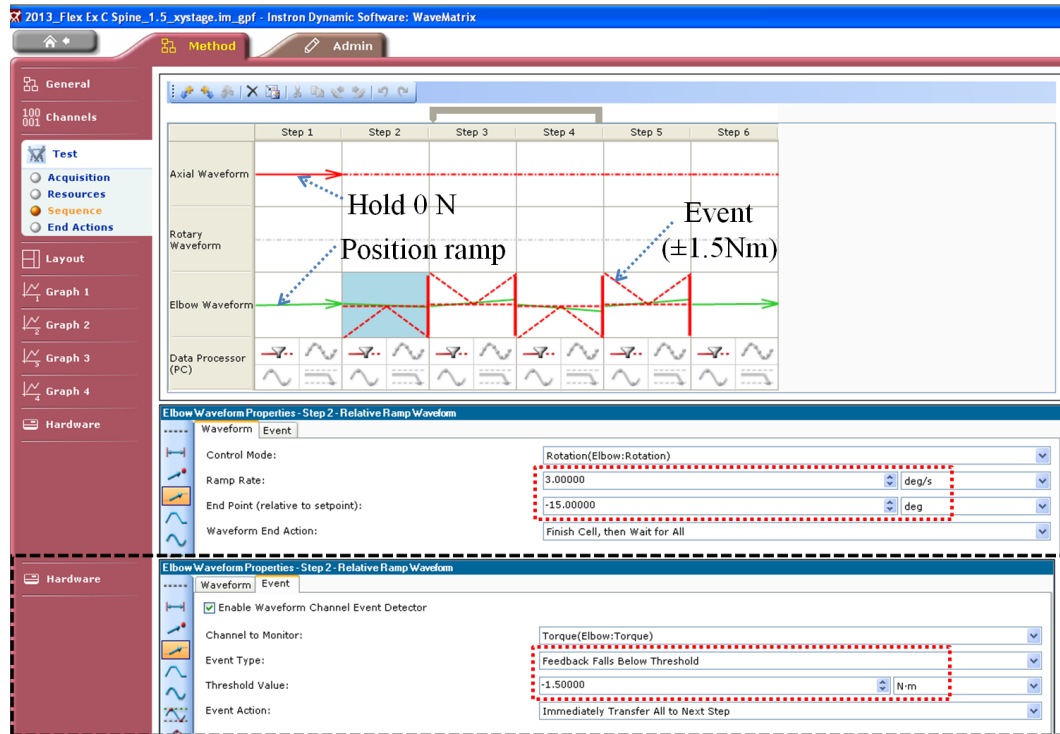


**Figure B.2: Instron WaveMatrix Flexibility Test Method**

The “Method” for flexibility testing protocol cycles relative ramp waveform (Green Lines) at 3°/s until the load target is reached ( $\pm 1.5$  Nm). To ensure this Event is reached, the end point of the relative ramp is set beyond this load target (needs to be manually found prior to testing). In flexion-extension and lateral bending, these waveforms are run on the Elbow channel (shown), or in the case of axial rotation, with the Rotary channel. In all tests, the Axial channel holds a load of 0 N.

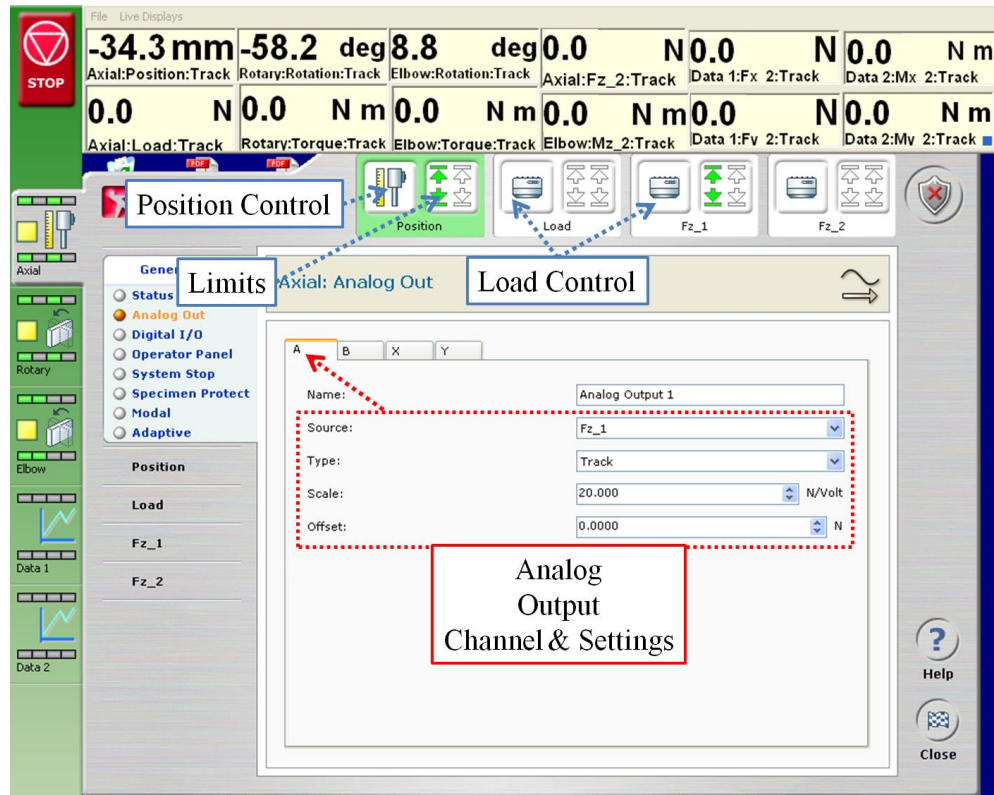


**Figure B.3: Instron® Actuator Settings**

The Instron® 8874 Materials Testing Machine can operate in both position and load control (currently shown operating in position control). For safe operation of the machine, limits should be set in both position and load (when ON they are highlighted by the green arrows). To sync the Instron® channels with the Optotrak data®, data is output through analog voltage signals, which can be scaled to fit the channel range between  $\pm 10$  V (*i.e.*, for a range of  $\pm 200$  N, the scale should be 20 N/V).

2. Make sure all Smart Markers are attached and seen by the software (correct number of markers reported)
3. Change collection frame frequency to 60Hz
4. Under the Rigid Body Setup tab, add a “smart\_02.rig” file for each Smart Marker attached (as well as a “smart\_02\_dig.rig” if digitizing)
5. Add four points to digitize for each Smart Marker
6. Label each tracker and digitized point
7. Under the ODAU Setup tab, change frame frequency to match the collection frame frequency and input the number of analog input channels
8. If digitizing, use the digitizing wand with Smart Marker attached to select physical anatomical landmark locations on each vertebrae (press the F5 key to select) in a standardized order
9. Select “No” for wireless option
10. Enter a “Session Name” and storage location, once done click “Finish”
11. Once the program is running, under Settings→Auto export..., ensure that the NDI 3D, 6D, ODAU and All to ASCII boxes are selected with Rotation Matrix Output
12. Change the duration to an exaggerated amount of time to complete the cyclic loading test (*i.e.*, 180s)
13. Ensure all markers of interest are visible to the Certus (Green circles) (Figure B.4)

#### **J. Starting the Loading Protocol**

1. Start a new Test in WaveMatrix™ and run the Method created for the current motion
2. Click the red “Record” button in First Principles software
3. Click OK to start loading in the WaveMatrix™

#### **K. Finishing the Protocol**

1. The WaveMatrix™ test finishes after the loading cycles are complete
2. Click stop button in First Principles to stop collecting tracker data

#### **L. Further Flexibility Testing**

1. Run the protocol for the three different motion types (*i.e.*, flexion-extension, lateral bending, and axial rotation) (*i.e.*, re-run Steps F – M2)
2. Reconfigure the simulator and specimen for each motion
3. Requires a 90° rotation of axial loading arm (two known positions that work are 30° and -60° (must be within  $\pm 70^\circ$  to avoid actuator posts)
4. Unlock PVC from caudal fixture, apply rotation with Instron, re-lock specimen in caudal fixture
5. Run additional tests for injured and instrumented states as required

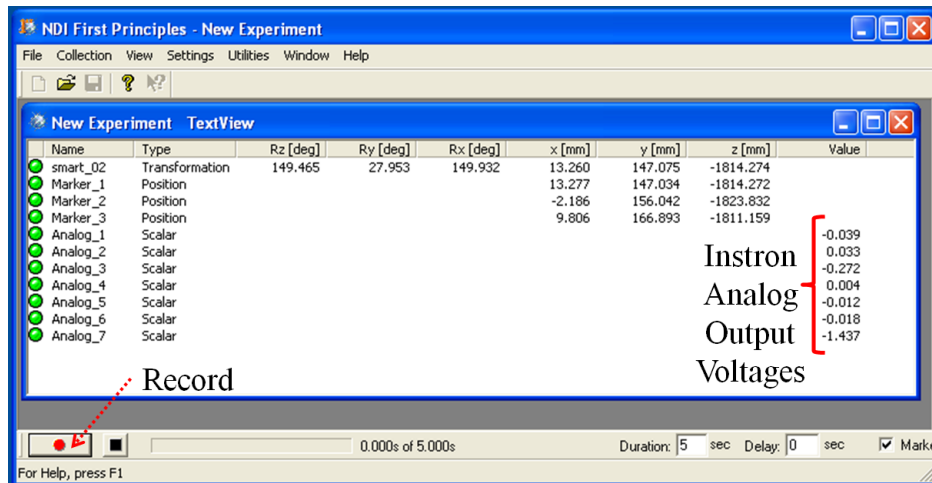


**Figure B.4: NDI First Principles™ Software**

This screenshot shows a test running for a single Smart Marker rigid body (“smart\_02”). Marker\_1 to Marker\_3 represent the individual infrared-light emitting diodes that define the rigid body. Seven analog inputs are being collected, with the voltage displayed on the right of the image. To collect data, the record button must be pressed, which runs for a set duration of time, but can be stopped at any time (saving data in either case).

## APPENDIX C – LABVIEW VIs FOR POST-HOC DATA ANALYSIS

### C.1 OVERVIEW OF MASTER PROGRAM

The kinematic data output by the NDI First Principles™ software from a test is output in two files: the six-DOF rigid body data of the Smart Marker (referred to as the 6D file) and the X, Y, and Z positions of the markers and digitized anatomic landmarks in the camera's reference frame (referred to as the 3D file). An additional file contains the load information from the synced analog voltage data from the Instron® (referred to as the ODAU file). However, to obtain the kinematic stability measures (*i.e.*, ROM, NZ, and FHAs), post-hoc data analysis is required. As such, a series of custom LabVIEW™ virtual instruments (VIs) were coded to take the generated Optotrak® kinematic data and Instron® load data to calculate and output these desired stability measures.

The “master” VI is a semi-automated program that is able to calculate data for all testing states for each induced motion separately (Figure C.1). Optotrak® data files (6D & ODAU) must be sorted into folders specific to each motion. When the master program is run, after choosing the specific study parameters (*i.e.*, motion, specimen name, etc.) on the front panel, the specific folder for these parameters is then selected analyzing all the files sequentially in the folder in a loop. A file containing the digitizing information is required as well. This is generated in another program, which relates the  $[T]$  matrices of the vertebrae to its respective Smart Marker. The final output of the master program (which can be altered) generates the ROM, NZ, and FHAs for the motion segments tested. In the interest of space and relevancy, only the back panel for the master program is shown, with important sub-VIs highlighted.

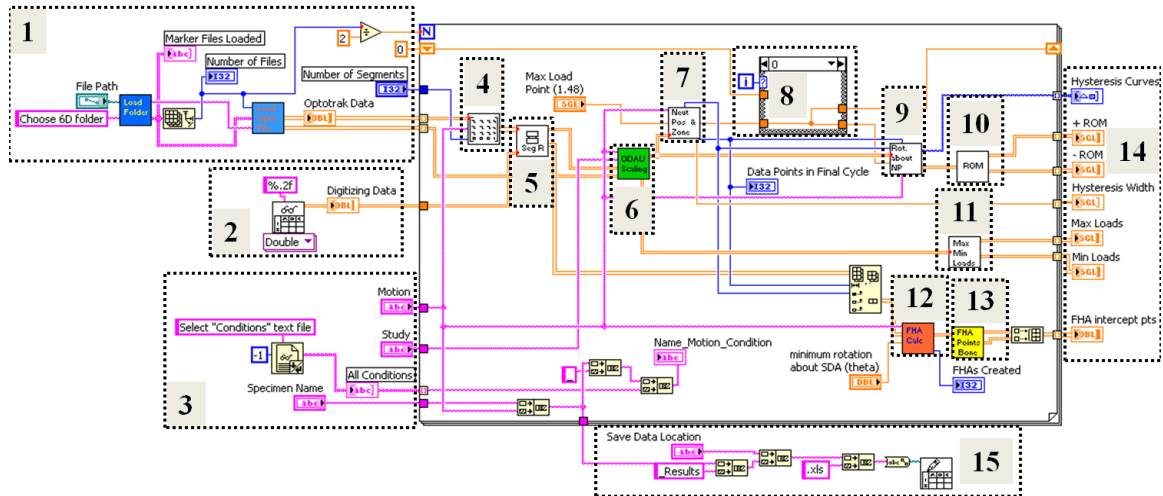


**Figure C.1: Back Panel of Master VI for Kinematic Stability**

(1) Optotrak® 6D and ODAU files are loaded from a folder; (2) digitizing file containing the  $[T]$  matrices of the vertebrae with respect to the trackers; (3) Analysis details (*i.e.*, specimen name, motion, study (for tracker setup information), testing conditions); (4) generate  $4 \times 4$   $[T]$  matrices from Optotrak® row data; (5) calculate six-DOF segmental rotations and translations of motion segments; (6) scale and add load data to six-DOF data; (7) determine the indices of the final cycle and calculates neutral zone (*i.e.*, hysteresis width at 0Nm) and neutral rotation (centre of neutral zone); (8) case structure to pass neutral rotation from intact state only (first trial); (9) shifts ROM data to centre around intact neutral rotation (*i.e.*, decide difference between flexion versus extension); (10) calculate maximum and minimum ROM; (11) calculate maximum and minimum loads; (12) generate FHAs using moving window technique from final loading cycle; (13) calculate the anatomical planar intercept from generated FHAs; (14) output data; and (15) saved data location.

## **C.2 SCREW MATRIX MOVING WINDOW ANALYSIS AND FHA PARAMETER EXTRACTION VIs**

Within the master kinematic program, a sub-VI (12 in Figure C.1) takes the  $[T]$  matrices of relative vertebral pose information during the final loading cycle, generates acceptable  $[S]$  matrices based on a minimum rotation size, then calculates the FHAs parameters from the  $[S]$  matrices using a MathScript LabVIEW™ function. The moving window analysis sub-VI within that program is shown and described in Figure C.2. The MathScript function to calculate FHA parameters from  $[S]$  matrix input is shown and described in Figure C.3.

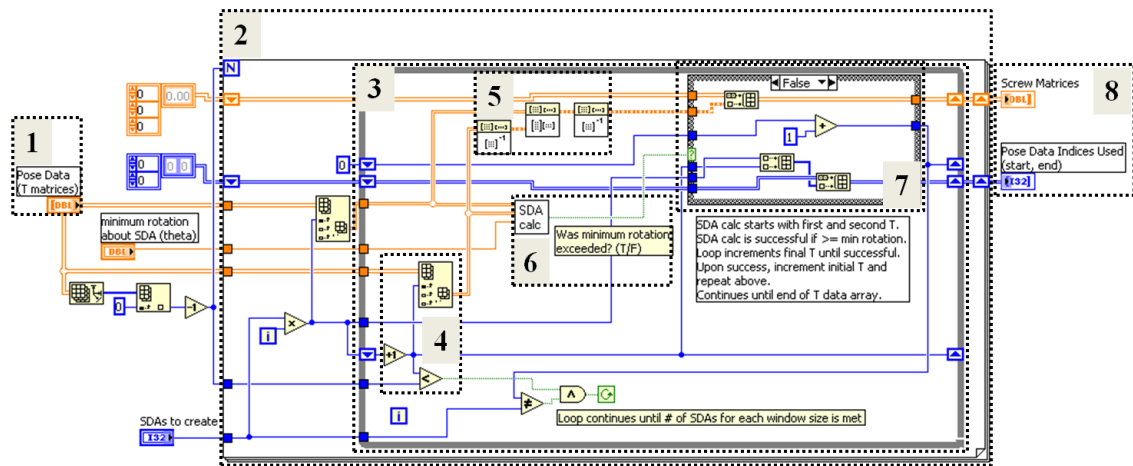


**Figure C.2: Screw Matrix Moving Window Analysis VI**

(1) The input to this VI is a 3D matrix of indexed  $4 \times 4$   $[T]$  matrices, consisting of relative vertebral motion. (2) An outer FOR loop runs for a pre-defined number of loops (number of  $[T]$  matrices  $- 1$ ). (3) An inner WHILE loop takes two  $[T]$  matrices ( $[T]_i$  and  $[T]_{i+n}$ , where  $n$  is the current WHILE loop number). (4) Increments second  $[T]$  matrix ( $T_{i+n}$ ) until the end of the data set is reached. (5) Matrix multiplication to calculate the Screw matrix from the two  $[T]$  matrices (see Eq. 4.3). (6) Calculates the rotation about the FHA from the input  $[T]$  matrices and determines whether it exceeds the minimum rotation. (7) Case structure either adds calculated  $[S]$  matrix to acceptable data set if minimum rotation exceeded, or passes a null value if not. (8) Output data including acceptable  $[S]$  matrices and index locations of  $[T]$  matrices used.



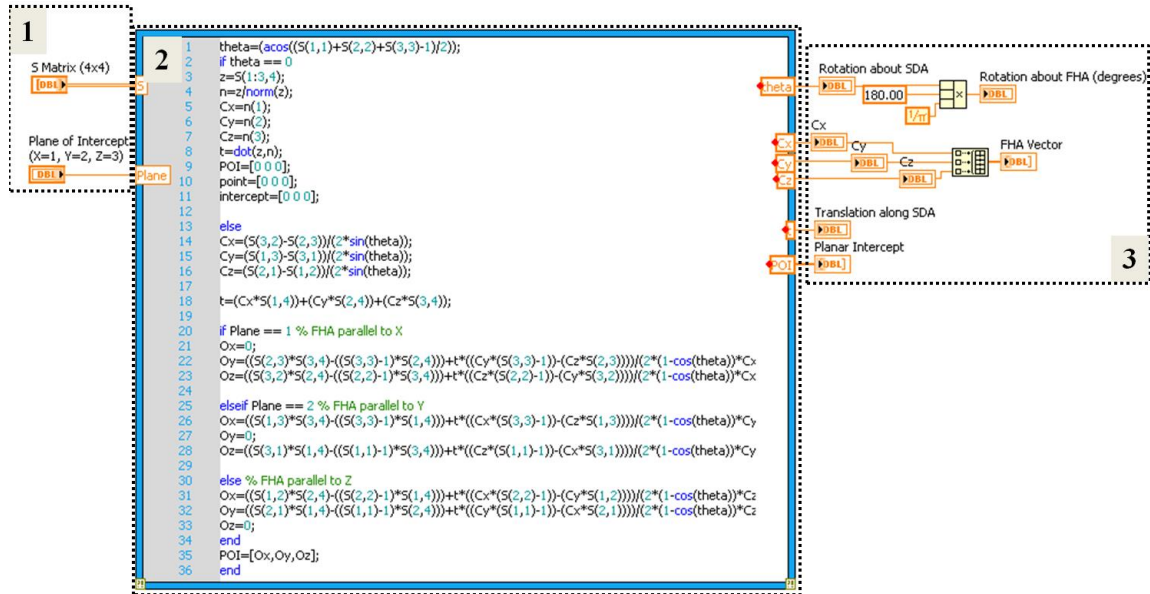


**Figure C.3: MathScript for FHA Parameter Extraction from Screw Matrix**

(1) Inputs to the MathScript are a single  $[S]$  matrix and the appropriate plane of intercept for the FHA. (2) MathScript (similar to MATLAB™ notation) for generating the rotation about the FHA ( $\theta$ ), translation along the FHA ( $t$ ), direction cosines ( $C_x$ ,  $C_y$ ,  $C_z$ ), and planar intercept ( $POI$ ). (3) Output data.

## APPENDIX D – SPECIMEN DEMOGRAPHICS & TABULATED DATA

**Table D.1: Specimen Demographics**

Specimen Number	Supplier Number*	Age	Sex	Motion Segments
Chapter 2				
1	09-02048	64	F	C2-C5 (Injury at C3-C4)
2	09-03016	81	M	
3	09-02030	64	M	
4	09-03038	71	M	
5	09-02025	57	F	
6	09-02042	65	F	
7	09-03058	62	F	
8	09-03052	52	M	
Chapter 3 - Study 1				
1	09-02042	65	F	C6-C7
2	09-02030	64	M	C6-C7
3	09-02038	65	F	C6-C7
4	09-02025	57	F	C6-C7
5	09-03020	60	M	C6-C7
6	09-03016	81	M	C4-C5
7	09-12041	48	M	C4-C5
8	09-03060	65	M	C4-C5
9	09-03020	60	M	C4-C5
Chapter 3 - Study 2				
1	09-12040	44	F	C4-C5
2	09-12055	73	M	C4-C5
3	09-12056	68	M	C4-C5
4	09-12034	58	M	C4-C5
5	09-12032	77	M	C4-C5
6	10-12042	91	F	C5-C6
7	09-10010	78	F	C5-C6
8	08-04095	84	M	C5-C6
9	10-06010	75	F	C5-C6
10	10-12023	90	M	C5-C6
Chapter 5				
1	10-12019	82	M	C5-C6 (C4-C5, C6-C7 pinned)
2	10-12038	77	M	
3	10-12016	78	M	
4	10-12020	77	F	
5	09-10032	79	F	
6	10-12009	68	F	
7	09-10016	70	F	

**\*Note:** All specimens were supplied by The LifeLegacy Foundation (Tucson, AZ).

**Table D.2: Chapter 2 Specimens C3-C4 Range of Motion**

ROM data (degrees) presented for intact, injured, and instrumented states

Motion	Direction	Condition	Specimen Number							
			1	2	3	4	5	6	7	8
Flexion-Extension	Flexion	Intact	1.1	1.4	3.7	2.0	1.1	1.5	1.0	1.4
		PL cut	1.1	1.4	3.6	2.3	1.2	1.6	1.5	1.3
		FC cut	1.0	1.6	3.1	2.6	1.2	1.7	1.7	1.3
		1/2 facet	1.1	1.5	3.6	2.6	1.2	1.8	1.6	1.2
		Full facet	1.2	1.5	3.2	1.9	1.3	1.9	1.6	1.2
		Posterior	0.1	0.2	0.7	0.4	0.1	0.2	0.1	
		Anterior	0.2	2.0	0.2	0.5	0.5	0.6	0.8	
		Combined	0.1	0.2	0.1	0.1	0.1	0.1	0.0	
	Extension	Intact	-1.1	-0.7	-4.0	-1.4	-0.8	-0.9	-0.8	-1.3
		PL cut	-1.1	-1.0	-5.2	-1.6	-0.9	-1.0	-1.1	-1.3
		FC cut	-1.3	-0.8	-5.9	-1.5	-0.8	-1.0	-1.2	-1.3
		1/2 facet	-1.2	-0.9	-5.8	-1.6	-0.9	-1.2	-1.2	-1.7
		Full facet	-1.1	-0.8	-6.0	-2.3	-0.9	-1.3	-1.2	-1.5
		Posterior	-0.1	-0.1	-1.0	-0.5	-0.0	-0.3	-0.2	
		Anterior	-0.1	-0.3	-1.9	-0.8	-0.7	-1.2	-0.6	
		Combined	-0.1	-1.7	-0.0	-0.1	-0.1	-0.1	-0.1	
Axial Rotation	Ipsilateral	Intact	4.3	1.6	2.5	2.3	2.1	1.2	3.6	2.6
		PL cut	4.7	1.7	2.5	2.7	2.1	2.2	4.0	3.1
		FC cut	5.3	1.7	2.7	3.0	2.4	2.4	5.0	3.3
		1/2 facet	5.6	1.7	2.7	3.2	2.6	2.5	5.3	3.8
		Full facet	5.7	1.9	2.5	3.5	5.2	3.2	5.7	3.2
		Posterior	0.6	0.9	0.0	1.5	0.8	0.9	0.1	
		Anterior	0.8	1.5	1.2	2.6	6.5	3.6	7.5	
		Combined	0.2	2.9	0.1	0.2	1.3	1.4	0.7	
	Contralateral	Intact	-4.9	-2.7	-6.6	-2.7	-3.4	-3.0	-3.2	-4.0
		PL cut	-5.0	-3.0	-7.3	-2.7	-3.9	-4.1	-5.6	-3.2
		FC cut	-5.6	-3.1	-7.4	-2.7	-4.1	-4.7	-3.7	-3.4
		1/2 facet	-5.6	-3.2	-7.6	-3.5	-4.0	-4.8	-3.8	-3.7
		Full facet	-5.4	-3.4	-9.0	-4.3	-6.1	-6.2	-4.3	-6.1
		Posterior	-0.5	-2.1	-2.8	0.0	-1.1	-1.4	-1.2	
		Anterior	-1.2	-7.0	-6.8	-3.0	-5.6	-5.3	-2.3	
		Combined	-0.3	-2.1	-2.0	-0.4	-1.2	-0.5	-0.2	
Lateral Bending	Contralateral	Intact	2.1	1.7	3.1	1.3	1.0	0.6	0.8	1.8
		PL cut	2.2	1.9	2.9	1.4	1.0	1.2	0.6	2.0
		FC cut	2.7	1.7	2.8	1.6	1.2	1.5	0.5	1.9
		1/2 facet	2.9	1.6	3.2	1.8	1.1	1.4	0.9	2.7
		Full facet	2.2	2.0	2.1	1.5	1.2	1.5	1.0	2.6
		Posterior	0.2	0.1	0.3	0.3	0.0	0.7	0.2	
		Anterior	0.3	6.4	1.9	2.7	1.3	1.1	0.8	
		Combined	0.0	0.2	0.2	0.0	5.1	0.1	0.0	
	Ipsilateral	Intact	-1.4	-1.7	-1.5	-2.1	-0.7	-1.0	-0.4	-2.0
		PL cut	-1.5	-1.9	-1.5	-2.1	-0.7	-1.2	-0.8	-1.9
		FC cut	-1.0	-2.4	-2.0	-2.1	-0.9	-1.5	-1.2	-2.5
		1/2 facet	-0.8	-2.3	-1.8	-2.4	-1.0	-1.5	-1.0	-2.0
		Full facet	-2.1	-2.1	-3.4	-3.1	-1.2	-2.1	-1.0	-2.1
		Posterior	0.0	0.0	-0.6	0.0	0.0	-0.1	-0.1	
		Anterior	-0.2	-6.9	-2.5	-1.3	-9.3	-1.7	-0.8	
		Combined	-0.1	-0.5	-0.2	-0.1	-0.5	0.0	-0.1	

**Table D.3: Chapter 2 Specimens C2-C3 Range of Motion**

Intact C2-C3 ROM data (degrees) in the C3-C4 intact, injured, and instrumented states

Motion	Direction	Condition	Specimen Number							
			1	2	3	4	5	6	7	8
Flexion-Extension	Flexion	Intact	1.6	2.7	1.4	1.6	1.6	1.2	0.8	2.2
		PL cut	1.6	3.0	1.1	1.5	1.7	1.5	0.8	2.2
		FC cut	1.4	2.6	1.0	1.4	1.8	1.5	0.8	2.3
		1/2 facet	1.5	3.1	1.1	1.2	1.8	1.2	0.9	2.1
		Full facet	1.4	2.8	1.1	1.3	1.9	1.4	1.0	2.2
	Extension	Intact	-1.2	-2.4	-0.8	-1.8	-1.6	-1.1	-0.7	-1.9
		PL cut	-1.3	-2.3	-1.0	-1.8	-1.8	-0.9	-0.7	-1.7
		FC cut	-1.5	-2.7	-0.8	-1.8	-1.8	-0.8	-0.6	-1.4
		1/2 facet	-1.5	-2.3	-0.8	-1.9	-1.7	-1.0	-0.9	-1.7
		Full facet	-1.4	-2.8	-0.8	-1.9	-1.6	-0.9	-0.7	-1.5
Axial Rotation	Ipsilateral	Intact	3.8	2.3	1.4	4.2	2.4	2.0	3.1	4.7
		PL cut	4.1	2.4	1.5	4.9	2.6	1.9	3.5	4.9
		FC cut	3.4	2.4	1.5	5.1	2.6	1.9	3.9	5.2
		1/2 facet	3.9	2.5	1.4	4.9	2.7	1.8	4.5	5.0
		Full facet	4.0	2.6	1.6	4.6	2.7	1.9	6.3	5.0
	Contralateral	Intact	-2.8	-2.8	-1.7	-3.5	-1.4	-1.8	-2.5	-6.7
		PL cut	-2.9	-2.9	-1.8	-2.6	-1.6	-1.8	-3.9	-6.7
		FC cut	-3.8	-3.0	-1.8	-2.8	-1.7	-2.0	-4.6	-6.6
		1/2 facet	-3.5	-3.1	-2.0	-3.2	-1.6	-1.8	-5.5	-6.8
		Full facet	-4.1	-3.0	-2.3	-3.8	-1.9	-2.1	-4.3	-7.3
Lateral Bending	Contralateral	Intact	3.4	2.4	1.4	2.6	3.7	3.4	1.9	
		PL cut	3.3	2.8	1.2	2.2	4.6	2.6	2.1	
		FC cut	4.4	2.8	1.2	2.6	4.2	3.0	1.8	
		1/2 facet	4.6	3.1	1.4	2.3	4.6	2.8	2.3	
		Full facet	3.1	2.4	1.1	1.3	4.5	3.0	2.4	
	Ipsilateral	Intact	-3.0	-2.4	-1.2	-2.0	-3.7	-2.3	-1.4	
		PL cut	-2.9	-2.5	-1.6	-2.5	-2.9	-2.9	-1.3	
		FC cut	-1.8	-2.4	-1.5	-2.0	-3.3	-2.5	-1.5	
		1/2 facet	-1.7	-2.3	-1.4	-2.3	-3.0	-2.6	-1.1	
		Full facet	-2.9	-3.1	-1.4	-3.1	-3.1	-2.4	-1.2	

**Table D.4: Chapter 2 Specimens C4-C5 Range of Motion**

Intact C4-C5 ROM data (degrees) in the C3-C4 intact, injured, and instrumented states

Motion	Direction	C3-C4 Condition	Specimen Number							
			1	2	3	4	5	6	7	8
Flexion-Extension	Flexion	Intact	3.5	2.3	0.7	0.4	1.2	1.2	1.5	1.5
		PL cut	3.8	2.8	0.6	0.4	1.1	1.1	1.5	1.4
		FC cut	4.7	2.8	0.5	0.4	1.2	1.2	1.4	1.3
		1/2 facet	4.2	2.6	0.5	0.4	1.2	1.4	1.3	1.6
		Full facet	4.0	2.7	0.5	0.5	1.2	1.3	1.4	1.4
	Extension	Intact	-2.9	-3.1	-0.5	-0.5	-1.4	-1.4	-1.5	-1.4
		PL cut	-3.1	-2.8	-0.6	-0.5	-1.5	-1.7	-1.6	-1.4
		FC cut	-2.5	-2.8	-0.6	-0.5	-1.5	-1.7	-1.6	-1.5
		1/2 facet	-2.7	-3.0	-0.7	-0.5	-1.5	-1.3	-1.8	-1.4
		Full facet	-3.1	-3.2	-0.5	-0.5	-1.5	-1.6	-1.6	-1.6
Axial Rotation	Ipsilateral	Intact	7.1	4.0	4.2	1.5	5.0	2.4	4.2	2.7
		PL cut	8.6	4.0	4.3	1.7	5.5	2.8	4.7	5.1
		FC cut	9.5	4.2	4.4	1.5	5.7	2.8	4.9	2.6
		1/2 facet	11.6	4.4	4.6	1.4	5.6	2.7	6.0	2.8
		Full facet	12.3	4.3	5.0	1.7	5.5	2.8	5.4	2.8
	Contralateral	Intact	-9.4	-5.8	-4.4	-1.6	-5.9	-2.3	-5.1	-2.6
		PL cut	-10.6	-5.8	-4.8	-1.4	-5.9	-1.8	-4.7	-0.7
		FC cut	-11.9	-6.0	-4.7	-1.7	-6.0	-1.9	-4.8	-2.7
		1/2 facet	-12.4	-5.9	-4.6	-1.9	-6.0	-2.1	-5.4	-2.7
		Full facet	-13.2	-6.2	-4.3	-1.9	-6.1	-2.5	-6.7	-2.9
Lateral Bending	Contralateral	Intact	1.7	1.3	0.8	0.4	0.5	0.5	0.8	
		PL cut	1.8	1.7	0.5	0.3	0.5	0.3	0.6	
		FC cut	1.7	1.6	1.1	0.3	0.4	0.4	0.5	
		1/2 facet	1.7	1.9	0.5	0.3	0.5	0.3	0.6	
		Full facet	2.2	2.1	0.8	0.2	0.3	0.3	0.6	
	Ipsilateral	Intact	-1.5	-1.3	-1.3	0.0	-0.3	-0.4	-0.7	
		PL cut	-1.6	-1.1	-1.7	-0.2	-0.3	-0.5	-0.9	
		FC cut	-1.3	-1.6	-1.1	-0.2	-0.3	-0.2	-0.8	
		1/2 facet	-1.5	-1.4	-1.9	-0.2	-0.3	-0.3	-0.9	
		Full facet	-2.5	-1.3	-1.7	-0.3	-0.3	-0.2	-0.7	

**Table D.5: Chapter 2 Specimens C2-C5 Neutral Zone**

Overall C2-C5 NZ data (degrees) in the C3-C4 intact, injured, and instrumented states

Motion	C3-C4 Condition	Specimen Number							
		1	2	3	4	5	6	7	8
Flexion-Extension	Intact	1.1	2.1	1.5	1.1	0.9	1.3	0.9	1.2
	PL cut	1.5	2.0	1.5	1.1	1.1	1.2	0.9	1.3
	FC cut	1.7	2.1	1.5	1.1	1.1	1.1	1.0	1.2
	1/2 facet	1.6	2.1	2.0	1.1	1.2	1.2	1.0	1.3
	Full facet	1.5	2.1	1.7	1.2	1.2	1.3	1.0	1.2
Axial Rotation	Intact	13.4	8.8	8.3	7.5	9.9	4.6	8.6	11.3
	PL cut	15.4	9.7	9.1	7.1	10.9	5.0	8.2	11.4
	FC cut	18.4	9.6	9.4	7.7	11.1	5.7	8.9	12.2
	1/2 facet	20.1	9.5	9.6	8.4	10.6	5.9	10.9	11.9
	Full facet	20.9	9.9	10.0	8.9	11.8	7.4	12.2	12.0
Lateral Bending	Intact	1.2	1.7	1.3	1.0	0.9	1.3	1.0	
	PL cut	1.4	1.8	1.5	1.1	0.9	1.1	0.9	
	FC cut	1.5	1.8	1.3	1.0	1.0	1.1	0.9	
	1/2 facet	1.7	1.8	1.3	1.0	0.9	1.2	0.9	
	Full facet	1.9	1.7	1.4	1.1	0.9	1.1	0.9	

**Table D.6: Chapter 3 – Study 1 Specimens Range of Motion and Neutral Zone**

Single motion segment (C4-C5/C6-C7) ROM (°) and NZ (°) for pre- and post-unilateral facet perch (UFP) injury

Motion	Condition	Specimen Number								
		1	2	3	4	5	6	7	8	9
Flexion ROM	Intact		7.2	7.9	8.5	4.2	5.9	4.1	3.1	3.5
	UFP		5.2	11.9	11.7	6.1	10.3	11.4	5.5	5.6
Extension ROM	Intact		-2.5	-3.5	-3.3	-2.9	-4.1	-4.0	-3.1	-2.7
	UFP		-3.8	-5.5	-2.8	-3.7	-5.7	-4.5	-3.9	-1.5
Flexion-Extension NZ	Intact		1.4	2.2	5.0	0.8	2.6	2.4	0.7	0.9
	UFP		2.8	12.4	3.7	1.4	4.0	3.4	1.9	1.1
Ipsilateral Axial Rotation ROM	Intact		2.9	1.4	3.4	2.9	4.4	3.0	3.0	4.0
	UFP		4.5	0.5	11.7	2.4	5.4	3.1	2.7	2.9
Contralateral Axial Rotation ROM	Intact		-2.9	-1.5	-4.6	-3.2	-4.4	-3.9	-2.4	-4.7
	UFP		-15.5	-10.1	-8.7	-12.0	-18.2	-20.8	-11.2	-13.8
Axial Rotation NZ	Intact		1.7	1.0	2.9	2.1	4.8	3.2	1.3	3.1
	UFP		10.5	3.6	11.6	6.6	12.6	12.5	6.5	7.8
Ipsilateral Lateral Bending ROM	Intact			-3.4	-6.4	-2.9	-7.9	-2.9	-2.0	-2.0
	UFP			-8.5	-14.4	-6.1	-11.4	-7.8	-2.8	0.2
Contralateral Lateral Bending ROM	Intact			4.7	4.1	4.8	5.9	3.3	2.5	3.4
	UFP			5.5	-0.2	6.3	13.0	7.0	6.0	9.4
Lateral Bending NZ	Intact			2.0	1.9	1.5	2.9	2.0	0.7	1.0
	UFP			4.7	2.1	3.4	4.7	3.8	2.1	3.0

**Note:** The kinematic data was not collected for the first specimen or in lateral bending for the second.

**Table D.7: Chapter 3 – Study 2 Specimens Range of Motion and Neutral Zone**

Single motion segment (C4-C5/C5-C6) ROM (°) and NZ (°) for the intact, surgical sectioning injury, and standardized injury model (SIM).

Motion	Condition	Specimen Number									
		1	2	3	4	5	6	7	8	9	10
AR ROM	Intact	14.7	4.5	5.6	12.3	10.3	8.9	9.8	5.9	7.7	7.6
	Surgical Injury	15.5	5.6	6.1	14.2	12.0					
	SIM	17.2	16.2	8.0	15.3	7.5	13.5	16.7	14.6	14.9	9.9
AR NZ	Intact	6.7	0.8	1.5	5.1	2.1	1.3	2.1	1.5	1.6	1.1
	Surgical Injury	11.4	1.0	2.0	7.6	3.9					
	SIM	13.3	8.0	3.6	9.1	2.8	1.7	2.7	1.5	1.9	1.3
FE ROM	Intact	10.4	3.8	6.8	11.8	9.5	8.0	5.9	3.0	4.2	5.3
	Surgical Injury	12.5	5.0	8.8	15.2	12.0					
	SIM	17.3	26.8	14.5	18.2	15.4	14.1	14.7	22.0	10.5	10.5
FE NZ	Intact	4.5	1.2	2.3	6.8	5.0	1.9	0.6	0.3	2.1	0.9
	Surgical Injury	5.9	1.7	3.5	10.0	6.7					
	SIM	12.4	21.1	7.0	11.1	10.2	3.1	1.7	5.5	5.8	1.2
LB ROM	Intact	6.9	2.3	6.7	8.0	7.8	7.2	6.9	2.5	4.7	2.9
	Surgical Injury	8.8	3.7	8.4	10.3	9.1					
	SIM	10.9	4.6	12.2	10.7	11.0	10.0	12.3	10.1	9.8	6.1
LB NZ	Intact	2.0	0.4	1.9	2.3	2.6	2.2	2.0	0.4	1.1	0.5
	Surgical Injury	1.4	0.7	2.6	3.5	3.1					
	SIM	1.6	0.5	4.8	3.1	4.1	2.0	2.5	1.7	1.4	0.3

**Note:** The surgical sectioning injury was completed in only five specimens.



**Table D.8: Chapter 5 Specimens Range of Motion**

C5-C6 ROM (°) for the intact, SIM, and ACDFP instrumented states with varying injury and graft size height.

Motion	Condition	Graft	Specimen Number						
			1	2	3	4	5	6	7
Axial Rotation	Intact		1.6	5.7	2.7	4.6	6.9	5.6	5.0
	SIM		11.4	19.5	10.8	15.5	14.9	14.5	21.5
	ACDFP:SIM	Measured	2.6	5.5	2.4	2.4	3.7	2.2	4.6
		Undersized	2.4	5.1	2.9	3.3	7.5	2.4	3.3
		Oversized	3.0	5.2	3.5	3.1	2.7	3.9	5.0
	ACDFP:SIM+UF#	Measured	3.8	7.9	3.8	4.5	4.6	4.4	4.6
		Undersized	2.9	7.0	2.3	3.5	4.4	2.6	2.3
		Oversized	2.0	6.4	4.3	4.1	3.1	3.7	5.3
	ACDFP:SIM+UF#+BFD	Measured	5.5	14.9	5.7	6.2	4.3	4.7	4.1
		Undersized	4.5	11.2	2.2	2.7	4.0	2.7	2.1
		Oversized	3.2	17.9	4.4	5.6	2.9	5.1	5.7
Flexion-Extension	Intact		9.8	1.8	6.8	9.1	11.3	10.4	8.1
	SIM		20.1	7.0	14.0	20.1	17.4	15.7	18.7
	ACDFP:SIM	Measured	6.8	1.7	2.4	2.8	2.2	3.3	4.3
		Undersized	6.1	1.8	4.7	5.4	6.9	5.4	5.9
		Oversized	4.4	2.0	1.5	2.3	1.7	3.2	3.6
	ACDFP:SIM+UF#	Measured	8.5	2.5	4.7	5.3	3.3	6.4	5.5
		Undersized	6.5	2.9	4.9	6.7	5.0	6.6	4.5
		Oversized	5.0	1.2	2.3	2.7	1.8	3.7	4.0
	ACDFP:SIM+UF#+BFD	Measured	13.0	6.1	7.2	6.8	3.1	7.5	6.1
		Undersized	9.0	7.9	4.1	6.8	4.9	7.3	5.1
		Oversized	19.0	2.5	2.7	4.2	1.8	5.5	5.5
Lateral Bending	Intact		1.2	5.1	4.6	3.9	5.7	8.0	4.5
	SIM		5.2	11.6	10.1	9.5	10.4	12.3	15.5
	ACDFP:SIM	Measured	3.2	8.5	4.6	5.1	4.5	5.5	7.6
		Undersized	2.4	5.4	5.1	4.5	5.8	5.5	4.2
		Oversized	5.1	10.9	3.6	4.0	3.7	5.4	7.2
	ACDFP:SIM+UF#	Measured	7.5	10.5	9.0	9.2	6.1	8.8	9.1
		Undersized	3.9	7.0	5.0	4.7	3.4	4.4	3.4
		Oversized	3.1	12.4	5.2	5.7	4.3	7.8	9.7
	ACDFP:SIM+UF#+BFD	Measured	9.3	12.3	10.5	9.3	6.1	8.7	9.9
		Undersized	7.3	7.8	4.5	3.6	3.5	4.6	2.8
		Oversized	5.6	18.3	5.5	7.5	4.5	8.8	10.8

**Note:** UF# is a unilateral facet fracture. BFD is a simulated bilateral facet dislocation soft tissue injury.

## APPENDIX E – MATLAB CODE FOR ALPHA SHAPES

### E.1 BACKGROUND ON ALPHA SHAPES

Explored in Chapters 4 & 5 as a way to quantify kinematic stability changes using the generated planar intercept points of the FHAs, the alpha shape is a computational geometric technique used to envelop a finite set of points in a series of curves. This technique to describe the shape of a set of points was originally introduced by Edelsbrunner *et al.* (1983).<sup>11</sup> The method requires a set of point data (2D or 3D) and a value of “alpha” as inputs, and uses them to define the level of detail in the outline shape of the point set. A smaller value of alpha will increase the detail of the shape, in so far as creating multiple smaller alpha shapes from the same data set (a value of zero returns no shape).

### E.2 MATLAB CODE FOR GENERATING MULTIPLE ALPHA SHAPES BASED ON FHA INTERCEPT DATA SETS

Two MATLAB programs were required to generate multiple alpha shape plots on the same image plot. The first program is setup to plot two sets of X,Y data. The first program calls the alpha shape function “alphavol”. The alphavol function was downloaded from the MATLAB File Exchange website. The original “alphavol” function was written by Jonas Lundgren in 2010.

```
% The following code runs a data set of FHA intercept points for the
% intact and injured spine (2 loops)
% The Excel file must in CSV format, with the columns representing the
% X,Y data points
% Additional data points can be included following the intact and
% injured columns to display the centroid and digitized bony landmarks
clc;
[filename pathname]=uigetfile('*.csv','select intercept file')
data=csvread([pathname filename],0,0);
hold off
```

---

<sup>11</sup> Edelsbrunner H., Kirkpatrick DG., Seidel R. (1983). On the Shape of a Set of Points in the Plane. IEEE Transactions on Information Theory; 29(4):551-559.

```

colours = ['b' 'r']; % line colours
widths = [5 2]; % line widths
x1=data(:,1);
y1=data(:,2);
X1=[x1,y1];
[V,S]=alphavol(X1,3,1,colours(1),widths(1)); % Calculate & Plot Alpha
Shape (Alpha = 3)
hold on
Area1=V;
x2=data(:,3);
y2=data(:,4);
X2=[x2,y2];
[V,S]=alphavol(X2,3,1,colours(2),widths(2)); % Calculate & Plot Alpha
Shape (Alpha = 3)
hold on
Area2=V;
dig1 = [data(1,9),data(1,10)]; % bony landmark locations in Excel file
dig2 = [data(2,9),data(2,10)];
dig3 = [0,0];
centroid_intact = [data(3,5),data(3,6)]; % centroid locations in Excel
file
centroid_injury = [data(4,5),data(4,6)];
plot(dig1(1),dig1(2),'g*','MarkerSize',12);
plot(dig2(1),dig2(2),'g*','MarkerSize',12);
plot(dig3(1),dig3(2),'g*','MarkerSize',12);
plot(centroid_intact(1),centroid_intact(2),'bo','MarkerSize',10,
'MarkerFaceColor','b');
plot(centroid_injury(1),centroid_injury(2),'ro','MarkerSize',10,
'MarkerFaceColor','r');
axis([-60,10,-20,50]); % Plot Axes Scale
xlabel('X axis (mm)', 'FontSize',16);
ylabel('Z axis (mm)', 'FontSize',16);
title({'Alpha Shapes';'Sagittal Plane Intercept'}, 'FontSize',16);
Area=[Area1 Area2];

print(gcf, '-dpng', 'AlphaShape.png');% Save plot as a PNG graphic file
%-----

function [V,S] = alphavol(X,R,fig,colour,width)
%ALPHAVOL Alpha shape of 2D or 3D point set.
% V = ALPHAVOL(X,R) gives the area or volume V of the basic alpha
shape
% for a 2D or 3D point set. X is a coordinate matrix of size Nx2 or
Nx3.
%
% R is the probe radius with default value R = Inf. In the default
case
% the basic alpha shape (or alpha hull) is the convex hull.
%
% [V,S] = ALPHAVOL(X,R) outputs a structure S with fields:
% S.tri - Triangulation of the alpha shape (Mx3 or Mx4)
% S.vol - Area or volume of simplices in triangulation (Mx1)
% S.rcc - Circumradius of simplices in triangulation (Mx1)
% S.bnd - Boundary facets (Px2 or Px3)
%
% ALPHAVOL(X,R,1) plots the alpha shape.

```

```

%
% % 2D Example - C shape
% t = linspace(0.6,5.7,500)';
% X = 2*[cos(t),sin(t)] + rand(500,2);
% subplot(221), alphavol(X,inf,1);
% subplot(222), alphavol(X,1,1);
% subplot(223), alphavol(X,0.5,1);
% subplot(224), alphavol(X,0.2,1);
%
% % 3D Example - Sphere
% [x,y,z] = sphere;
% [V,S] = alphavol([x(:),y(:),z(:)]);
% trisurf(S.bnd,x,y,z,'FaceColor','blue','FaceAlpha',1)
% axis equal
%
% See also DELAUNAY, TRIREP, TRISURF

% Author: Jonas Lundgren 2010

% 2010-09-27 First version of ALPHAVOL.
% 2010-10-05 DelaunayTri replaced by DELAUNAYN. 3D plots added.
% 2012-03-08 More output added. DELAUNAYN replaced by DELAUNAY.
% 2013-03-01 Change line width and colour on plot (S. McLachlin)

if nargin < 2 || isempty(R), R = inf; end
if nargin < 3, fig = 0; end

% Check coordinates
dim = size(X,2);
if dim < 2 || dim > 3
    error('alphavol:dimension','X must have 2 or 3 columns.')
end

% Check probe radius
if ~isscalar(R) || ~isreal(R) || isnan(R)
    error('alphavol:radius','R must be a real number.')
end

% Unique points
[X,imap] = unique(X,'rows');

% Delaunay triangulation
T = delaunay(X);

% Remove zero volume tetrahedra since
% these can be of arbitrary large circumradius
if dim == 3
    n = size(T,1);
    vol = volumes(T,X);
    epsvol = 1e-12*sum(vol)/n;
    T = T(vol > epsvol,:);
    holes = size(T,1) < n;
end

% Limit circumradius of simplices
[~,rcc] = circumcenters(TriRep(T,X));
T = T(rcc < R,:);

```

```

rcc = rcc(rcc < R);

% Volume/Area of alpha shape
vol = volumes(T,X);
V = sum(vol);
% Return?
if nargout < 2 && ~fig
    return
end
% Turn off TriRep warning
warning('off','MATLAB:TriRep:PtsNotInTriWarnId')

% Alpha shape boundary
if ~isempty(T)
    % Facets referenced by only one simplex
    B = freeBoundary(TriRep(T,X));
    if dim == 3 && holes
        % The removal of zero volume tetrahedra causes false boundary
        % faces in the interior of the volume. Take care of these.
        B = trueboundary(B,X);
    end
else
    B = zeros(0,dim);
end

% Plot alpha shape
if fig
    if dim == 2
        % Plot boundary edges and point set
        x = X(:,1);
        y = X(:,2);
        plot(x(B)',y(B)', colour,'linewidth',width), hold on % MODIFIED
CODE TO CHANGE LINE COLOUR % WIDTH
        %fill (x(B), y(B), colour,'facealpha', 0.5) % CAN USE TO FILL
ALPHA SHAPE WITH COLOUR
        plot(x,y,'k.'), hold off
        str = 'Area';
    elseif ~isempty(B)
        % Plot boundary faces
        trisurf(TriRep(B,X),'FaceColor','red','FaceAlpha',1/3);
        str = 'Volume';
    else
        cla
        str = 'Volume';
    end
    axis equal
    str = sprintf('Radius = %g,    %s = %g',R,str,V);
    title(str,'fontsize',12)
end
% Turn on TriRep warning
warning('on','MATLAB:TriRep:PtsNotInTriWarnId')
% Return structure
if nargout == 2
    S = struct('tri',imap(T),'vol',vol,'rcc',rcc,'bnd',imap(B));
end

%-----

```

## APPENDIX F – PROTOCOL FOR CREATING 3D BONE MODELS

**OVERVIEW:** *One of the original considerations for this thesis work included was the development of a technique to generate 3D computer bone models of vertebrae, with the idea that it would improve visualization of cervical spine bony anatomy and potentially the generated kinematics. While not seen as a specific objective of thesis, this technique was developed using the steps described below. This protocol made use of the image segmentation tools in Mimics 14 software (Materialise, Leuven, Belgium) to isolate individual vertebrae in thresholded DICOM images (captured in CT scans). This technique was used to generate all of the 3D anatomical images in Chapter 1 and throughout the rest of the thesis.*

### Image Segmentation Steps

1. Capture CT images of cadaver cervical spine specimen
2. Export DICOM images to a CD/DVD/USB key
3. Open MIMICS software (Version 14 used in this work)
4. Under File, select Import Images
  - a. Select DICOM images file path
  - b. Click Convert
5. Under Segmentation, select Thresholding
  - a. Use Bone (CT) as value, though adjustments can be made
  - b. A green “mask” will be created for the entire spine

To generate individual bone models, a separate mask is required for each vertebra of interest. To do this, the green mask of the entire spine must be edited to remove any contact between vertebrae (Figure F.1).

6. Under Segmentation, select Edit Masks
  - a. Click on the Erase button and select a circle with a size of 4
  - b. In each plane, cycle through each image and “erase” any connection between adjacent vertebrae (**Note:** *this is a labor intensive process*)
  - c. Areas such as the facet and uncovertebral joints will require the most effort

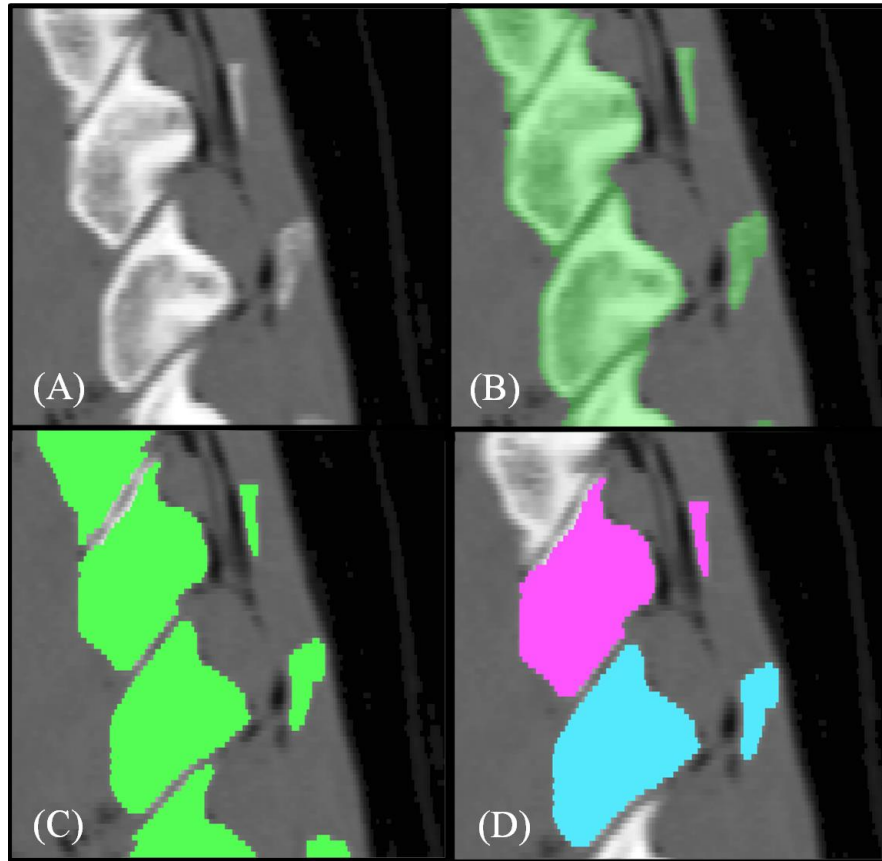


**Figure F.1: Image Segmentation Steps to Isolate Individual Vertebra**

Starting with the original set of DICOM images (A) (sagittal plane view of multiple facet joints in the cervical spine shown), an original mask (*i.e.*, thresholded image) (B) was created based on the Bone (CT) density range. Each threshold image was then altered using the edit mask tool to erase facet joint contact (C). Segmentation was complete when individual masks for adjacent vertebrae were evident (D).

7. To check that separation has been achieved, use the Region Growing tool under Segmentation. Place a point on the isolated vertebra. If it has been successfully isolated, a new mask will appear only on this vertebra. If the new mask connects multiple vertebrae, a connection still exists in the original green mask. The process must be repeated until the mask appears in a single vertebra
8. Under Segmentation, select Calculate 3D
  - a. Select mask of interest, optimal quality, then press calculate to generate a 3D model
  - b. Can smooth model by selecting smoothing/triangle reduction (click “compensate shrinkage” first)

A 3D bone model has now been generated for an individual vertebra. The process can be repeated for adjacent vertebrae. One final option would be to export the 3D model as an STL file.

9. Under Export, select ASCII STL, then click on the appropriate 3D object



## **APPENDIX G – BIAXIAL BEARING STAGE DEVELOPMENT**

### **G.1 PROJECT SUMMARY**

The design and development of the biaxial bearing stage used in Chapter 6 was completed as a 4<sup>th</sup> year undergraduate design project in Mechanical & Materials Engineering by a team of four students (Joshua Bernick, Alex Heroux, Tyler Moores, Paola Soriano). The project was conducted in the Jack McBain Biomechanical Testing Laboratory under the supervision of Dr. Cynthia Dunning and Stewart McLachlin. The title of their project was “Evaluation and Refinement of a Simulator Design for Laboratory Investigations of Spine Motion.” The objective of this project was to assess and develop new techniques to improve the efficiency of the spinal loading simulator to apply pure bending moment loading to the spine in flexion-extension, lateral bend, and axial rotation. This would be accomplished through the design of a testing stage that added translational freedom to the caudal end of the specimen.

The given design requirements included: near frictionless device, a locking mechanism, ability to function as a passive system (without motors) or an active system (with motors), durable, and a minimal cost (<\$1000). The team came up with multiple “free translation” stage prototypes to fit in the simulator, used engineering design principles to assess potential design flaws, and ultimately coordinated with University Machine Services (UMS) to construct the initial biaxial bearing stage. Sections of their final design report have been included below (edited for readability).

### **G.2 CONCEPT GENERATION: LINEAR BEARING SYSTEMS**

Two distinct alternatives for a linear bearing system were generated. The first concept was a two bearing design, using guide block sliders and rails (Figure G.1). This system required only two rails and blocks, but to effectively withstand the applied load, a thicker block and rail would be required. It was uncertain though how this design would

perform in situations requiring large bending or torsional loads. The second concept was a four bearing design, using linear ball bearings and metal shafts (Figure G.2). A

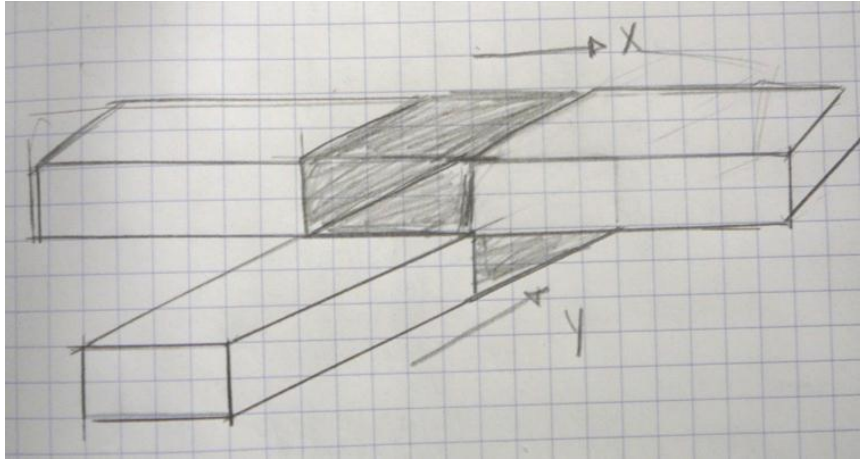


**Figure G.1: Guide Blocks and Rails Design Concept**

The first option used guide blocks and rails arranged in a cross-junction assembly to create linear motion in both the X and Y directions.

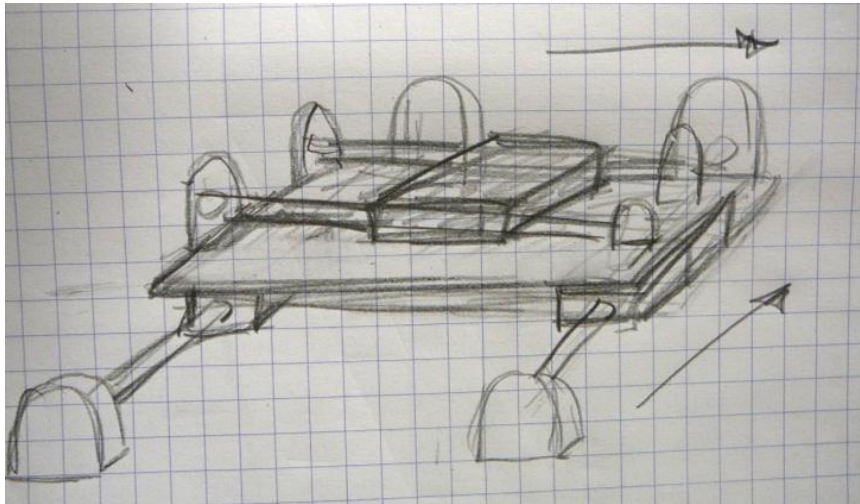


**Figure G.2: Linear Bearing and Shaft Design Concept**

The second design considered parallel sets of linear bearings running along two shafts in both the X and Y directions. This was chosen as the final design.

significant advantage of this setup compared to the guide blocks and rails is that shafts have a lower moment of inertia than the more complicated T-beam cross section of the rails. With circular cross-sections and a lower moment of inertia, the shafts in this design are likely able to withstand higher torques. In addition, with an additional set of bearings to divide the load, these components can be smaller than the guide block and rail design. This reduction in weight would also reduce friction in the bearings.

After discussions with UMS, amongst the design team, and with the project advisors, the shaft and bearing system was selected. The linear guide block and rail system was appealing because it offered stability in a smaller space and had less components leading to an easier assembly. However, this system was heavier, more expensive, had a shorter life expectancy, and had questionable functionality to translate smoothly under an applied torque condition, rendered this concept unsuitable for meeting the design requirements. Therefore, the linear ball bearings and shaft system was chosen as the final design concept.

### **G.3 BEARING STAGE COMPONENTS**

All components were sourced through McMaster-Carr. Closed linear bearings were chosen because they can be mounted in any position without affecting their performance. The closed linear ball bearings are enclosed in housings and paired with hardened precision shafts and shaft supports. Bearings were chosen based on the maximum applied loading and torque the system would need to withstand, with 0.5" inner diameter (ID) closed bearings (part # 8974T1) chosen. Based on the outer diameter (OD) of the bearing, housings were selected with a 7/8" housing bore (part # 9804K3).

Shafts were selected based on the bearing ID and the maximum required translation of the bearing. Shaft lengths had to be at least twice the range of motion needed. Therefore, 0.5" diameter, 203.2mm (8") length, shafts (part # 6061K103) were selected. Shaft supports were selected based on the shaft OD. Thus, shaft supports with a base mount of 0.5" (part # 6068K23) were chosen.

With the framework of the system designed, a locking mechanism now had to be considered. This additional component would allow the specimen to be locked in any offset position of up to 5cm (anterior/posterior or medial/lateral) and tested in that locked position. Although slightly more expensive than a simple set-screw shaft collar, the increase in cost was justified because the quick release option (using snaps rather than set-screws) would enhance ease of use and convenience during testing. Thus, eight quick-release shaft collars were ordered (part # 1511K12) and used in the design.

# APPENDIX H – COPYRIGHT PERMISSION

## H.1 CHAPTER 2 – COPYRIGHT RELEASE

3/11/13


Rightslink Printable License

### ELSEVIER LICENSE TERMS AND CONDITIONS

Mar 11, 2013

This is a License Agreement between Stewart D McLachlin ("You") and Elsevier ("Elsevier") provided by Copyright Clearance Center ("CCC"). The license consists of your order details, the terms and conditions provided by Elsevier, and the payment terms and conditions.

**All payments must be made in full to CCC. For payment instructions, please see information listed at the bottom of this form.**

Supplier	Elsevier Limited The Boulevard, Langford Lane Kidlington, Oxford, OX5 1GB, UK
Registered Company Number	1982084
Customer name	Stewart D McLachlin
Customer address	
License number	3106041158126
License date	Mar 11, 2013
Licensed content publisher	Elsevier
Licensed content publication	The Spine Journal
Licensed content title	The importance of the posterior osteoligamentous complex to subaxial cervical spine stability in relation to a unilateral facet injury
Licensed content author	Parham Rasoulinejad, Stewart D. McLachlin, Stewart I. Bailey, Kevin R. Gurr, Christopher S. Bailey, Cynthia E. Dunning
Licensed content date	July 2012
Licensed content volume number	12
Licensed content issue number	7
Number of pages	6
Start Page	590
End Page	595
Type of Use	reuse in a thesis/dissertation
Portion	full article
Format	both print and electronic
Are you the author of this Elsevier article?	Yes

3/11/13

Rightslink Printable License

Will you be translating? No

Order reference number

Title of your thesis/dissertation An Investigation of Subaxial Cervical Spine Trauma and Surgical Treatment through Biomechanical Simulation and Kinematic Analysis

Expected completion date Apr 2013

Estimated size (number of pages) 250

Elsevier VAT number GB 494 6272 12

Permissions price 0.00 USD

VAT/Local Sales Tax 0.0 USD / 0.0 GBP

Total 0.00 USD

Terms and Conditions

## INTRODUCTION

1. The publisher for this copyrighted material is Elsevier. By clicking "accept" in connection with completing this licensing transaction, you agree that the following terms and conditions apply to this transaction (along with the Billing and Payment terms and conditions established by Copyright Clearance Center, Inc. ("CCC"), at the time that you opened your Rightslink account and that are available at any time at <http://myaccount.copyright.com>).

## GENERAL TERMS

2. Elsevier hereby grants you permission to reproduce the aforementioned material subject to the terms and conditions indicated.

3. Acknowledgement: If any part of the material to be used (for example, figures) has appeared in our publication with credit or acknowledgement to another source, permission must also be sought from that source. If such permission is not obtained then that material may not be included in your publication/copies. Suitable acknowledgement to the source must be made, either as a footnote or in a reference list at the end of your publication, as follows:

"Reprinted from Publication title, Vol /edition number, Author(s), Title of article / title of chapter, Pages No., Copyright (Year), with permission from Elsevier [OR APPLICABLE SOCIETY COPYRIGHT OWNER]." Also Lancet special credit - "Reprinted from The Lancet, Vol number, Author(s), Title of article, Pages No., Copyright (Year), with permission from Elsevier."

4. Reproduction of this material is confined to the purpose and/or media for which permission is hereby given.

5. Altering/Modifying Material: Not Permitted. However figures and illustrations may be altered/adapted minimally to serve your work. Any other abbreviations, additions, deletions and/or any other alterations shall be made only with prior written authorization of Elsevier Ltd. (Please contact Elsevier at [permissions@elsevier.com](mailto:permissions@elsevier.com))

6. If the permission fee for the requested use of our material is waived in this instance, please be

advised that your future requests for Elsevier materials may attract a fee.

7. **Reservation of Rights:** Publisher reserves all rights not specifically granted in the combination of (i) the license details provided by you and accepted in the course of this licensing transaction, (ii) these terms and conditions and (iii) CCC's Billing and Payment terms and conditions.

8. **License Contingent Upon Payment:** While you may exercise the rights licensed immediately upon issuance of the license at the end of the licensing process for the transaction, provided that you have disclosed complete and accurate details of your proposed use, no license is finally effective unless and until full payment is received from you (either by publisher or by CCC) as provided in CCC's Billing and Payment terms and conditions. If full payment is not received on a timely basis, then any license preliminarily granted shall be deemed automatically revoked and shall be void as if never granted. Further, in the event that you breach any of these terms and conditions or any of CCC's Billing and Payment terms and conditions, the license is automatically revoked and shall be void as if never granted. Use of materials as described in a revoked license, as well as any use of the materials beyond the scope of an unrevoked license, may constitute copyright infringement and publisher reserves the right to take any and all action to protect its copyright in the materials.

9. **Warranties:** Publisher makes no representations or warranties with respect to the licensed material.

10. **Indemnity:** You hereby indemnify and agree to hold harmless publisher and CCC, and their respective officers, directors, employees and agents, from and against any and all claims arising out of your use of the licensed material other than as specifically authorized pursuant to this license.

11. **No Transfer of License:** This license is personal to you and may not be sublicensed, assigned, or transferred by you to any other person without publisher's written permission.

12. **No Amendment Except in Writing:** This license may not be amended except in a writing signed by both parties (or, in the case of publisher, by CCC on publisher's behalf).

13. **Objection to Contrary Terms:** Publisher hereby objects to any terms contained in any purchase order, acknowledgment, check endorsement or other writing prepared by you, which terms are inconsistent with these terms and conditions or CCC's Billing and Payment terms and conditions. These terms and conditions, together with CCC's Billing and Payment terms and conditions (which are incorporated herein), comprise the entire agreement between you and publisher (and CCC) concerning this licensing transaction. In the event of any conflict between your obligations established by these terms and conditions and those established by CCC's Billing and Payment terms and conditions, these terms and conditions shall control.

14. **Revocation:** Elsevier or Copyright Clearance Center may deny the permissions described in this License at their sole discretion, for any reason or no reason, with a full refund payable to you. Notice of such denial will be made using the contact information provided by you. Failure to receive such notice will not alter or invalidate the denial. In no event will Elsevier or Copyright Clearance Center be responsible or liable for any costs, expenses or damage incurred by you as a result of a denial of your permission request, other than a refund of the amount(s) paid by you to Elsevier and/or Copyright Clearance Center for denied permissions.



## LIMITED LICENSE

The following terms and conditions apply only to specific license types:

**15. Translation:** This permission is granted for non-exclusive world English rights only unless your license was granted for translation rights. If you licensed translation rights you may only translate this content into the languages you requested. A professional translator must perform all translations and reproduce the content word for word preserving the integrity of the article. If this license is to re-use 1 or 2 figures then permission is granted for non-exclusive world rights in all languages.

**16. Website:** The following terms and conditions apply to electronic reserve and author websites:  
**Electronic reserve:** If licensed material is to be posted to website, the web site is to be password-protected and made available only to bona fide students registered on a relevant course if

This license was made in connection with a course,

This permission is granted for 1 year only. You may obtain a license for future website posting. All content posted to the web site must maintain the copyright information line on the bottom of each image,

A hyper-text must be included to the Homepage of the journal from which you are licensing at <http://www.sciencedirect.com/science/journal/xxxxx> or the Elsevier homepage for books at <http://www.elsevier.com>, and

Central Storage: This license does not include permission for a scanned version of the material to be stored in a central repository such as that provided by Heron/XanEdu.

**17. Author website** for journals with the following additional clauses:

All content posted to the web site must maintain the copyright information line on the bottom of each image, and the permission granted is limited to the personal version of your paper. You are not allowed to download and post the published electronic version of your article (whether PDF or HTML, proof or final version), nor may you scan the printed edition to create an electronic version. A hyper-text must be included to the Homepage of the journal from which you are licensing at <http://www.sciencedirect.com/science/journal/xxxxx>. As part of our normal production process, you will receive an e-mail notice when your article appears on Elsevier's online service ScienceDirect ([www.sciencedirect.com](http://www.sciencedirect.com)). That e-mail will include the article's Digital Object Identifier (DOI). This number provides the electronic link to the published article and should be included in the posting of your personal version. We ask that you wait until you receive this e-mail and have the DOI to do any posting.

Central Storage: This license does not include permission for a scanned version of the material to be stored in a central repository such as that provided by Heron/XanEdu.

**18. Author website** for books with the following additional clauses:

Authors are permitted to place a brief summary of their work online only.

A hyper-text must be included to the Elsevier homepage at <http://www.elsevier.com>. All content posted to the web site must maintain the copyright information line on the bottom of each image.

You are not allowed to download and post the published electronic version of your chapter, nor



3/11/13

Rightslink Printable License

may you scan the printed edition to create an electronic version.

Central Storage: This license does not include permission for a scanned version of the material to be stored in a central repository such as that provided by Heron/XanEdu.

19. **Website (regular and for author):** A hyper-text must be included to the Homepage of the journal from which you are licensing at <http://www.sciencedirect.com/science/journal/xxxxx> or for books to the Elsevier homepage at <http://www.elsevier.com>

20. **Thesis/Dissertation:** If your license is for use in a thesis/dissertation your thesis may be submitted to your institution in either print or electronic form. Should your thesis be published commercially, please reapply for permission. These requirements include permission for the Library and Archives of Canada to supply single copies, on demand, of the complete thesis and include permission for UMI to supply single copies, on demand, of the complete thesis. Should your thesis be published commercially, please reapply for permission.

21. **Other Conditions:**

v1.6

If you would like to pay for this license now, please remit this license along with your payment made payable to "COPYRIGHT CLEARANCE CENTER" otherwise you will be invoiced within 48 hours of the license date. Payment should be in the form of a check or money order referencing your account number and this invoice number RLNK500974747. Once you receive your invoice for this order, you may pay your invoice by credit card. Please follow instructions provided at that time.

**Make Payment To:**  
Copyright Clearance Center  
Dept 001  
P.O. Box 843006  
Boston, MA 02284-3006

For suggestions or comments regarding this order, contact RightsLink Customer Support: [customercare@copyright.com](mailto:customercare@copyright.com) or +1-877-622-5543 (toll free in the US) or +1-978-646-2777.

Gratis licenses (referencing \$0 in the Total field) are free. Please retain this printable license for your reference. No payment is required.

## H.2 CHAPTER 3 – COPYRIGHT RELEASE

### PERMISSION LICENSE AGREEMENT

P4353.JBJSInc.JBJS Am.Nadeau.2599.University of Western Ontario.McLachlin

JBJSInc.JBJS Am.Nadeau.2599

3/13/2013

Mr. Stewart McLachlin

INVOICE  
ATTACHED

University of Western Ontario  
, Canada

Dear Mr. McLachlin,

Thank you for your interest in JBJS [Am] material. Please note: This permission does not apply to any figure or other material that is credited to any source other than JBJS. It is your responsibility to validate that the material is in fact owned by JBJS. If material within JBJS material is credited to another source (in a figure legend, for example) then any permission extended by JBJS is invalid. We encourage you to view the actual material at [www.ejbs.org](http://www.ejbs.org) or a library or other source. Information provided by third parties as to credits that may or may not be associated with the material may be unreliable.

We are pleased to grant you non-exclusive, nontransferable permission, limited to the format described below, and provided you meet the criteria below. Such permission is for one-time use and does not include permission for future editions, revisions, additional printings, updates, ancillaries, customized forms, any electronic forms, Braille editions, translations or promotional pieces unless otherwise specified below. We must be contacted for permission each time such use is planned. This permission does not include the right to modify the material. Use of the material must not imply any endorsement by the copyright owner. This permission is not valid for the use of JBJS logos or other collateral material, and may not be resold.

Abstracts or collections of abstracts and all translations must be approved by publisher's agent in advance, and in the case of translations, before printing. No financial liability for the project will devolve upon JBJS, Inc. or on Rockwater, Inc.. All expenses for translation, validation of translation accuracy, publication costs and reproduction costs are the sole responsibility of the foreign language sponsor. The new work must be reprinted and delivered as a stand-alone piece and may not be integrated or bound with other material. JBJS does not supply photos or artwork; these may be downloaded from the JBJS website, scanned, or (if available) obtained from the author of the article.

#### PERMISSION IS VALID FOR THE FOLLOWING MATERIAL ONLY: article

Journal of Bone and Joint Surgery American, November, 2012, 94, 21, A biomechanical assessment of soft-tissue damage in the cervical spine following a unilateral facet injury, Nadeau, e156

#### IN THE FOLLOWING WORK ONLY:

electronic and/or print copies of article to be included with Doctoral thesis titled: "An Investigation of Subaxial Cervical Spine Trauma and Surgical Treatment through Biomechanical Simulation and Kinematic Analysis" where article and thesis share common author

CREDIT LINE(S) must be published next to any figure, and/or if permission is granted for electronic form, visible at the same time as the content republished with a hyperlink to the publisher's home page.

WITH PAYMENT OF PERMISSIONS FEE. License, once paid, is good for one year from your anticipated publication date unless otherwise specified above. Failure to pay the fee(s) or to follow instructions here upon use of the work as described here, will result in automatic termination of the license or permission granted. All information is required.

Payment should be made to Rockwater, Inc. by check or credit card, via mail

Please contact Beth Ann Rocheleau at [jbjs@rockwaterinc.com](mailto:jbjs@rockwaterinc.com) or 1-803-359-4578 with questions.

## **CURRICULUM VITAE**

**NAME:** Stewart David McLachlin, BEng, MEng

**PLACE OF BIRTH:** St. Thomas, Ontario, Canada

**YEAR OF BIRTH:** 1983

**EDUCATION:**

2009 – Present	Doctor of Philosophy Candidate, Mechanical & Materials Engineering University of Western Ontario, London, Ontario
2006 – 2008	Master of Engineering Science, Mechanical & Materials Engineering University of Western Ontario, London, Ontario
2002 – 2006	Bachelor of Engineering Science, Mechanical & Materials Engineering University of Western Ontario, London, Ontario

**EMPLOYMENT HISTORY:**

2008 – 2009	Research Associate, Jack McBain Biomechanical Testing Laboratory Department of Mechanical & Materials Engineering University of Western Ontario, London, Ontario
-------------	--

**ACADEMIC HONOURS AND AWARDS:**

*Awards and Scholarships (primary recipient)*

2010	Graduate Thesis Research Award, University of Western Ontario
2010 – 2013	Canadian Institutes of Health Research (CIHR) Graduate Fellow in Musculoskeletal Health Research, Joint Motion Program (JuMP) – A CIHR Training Program in Musculoskeletal Health Research and Leadership
2009	Graduate Thesis Research Award, University of Western Ontario
2009 – 2012	NSERC Alexander Graham Bell Canada Graduate Scholarship (CGS-D)
2008	Canadian Society of Biomechanics (CSB) Congress Travel Grant
2007 – 2008	Ontario Graduate Scholarship (OGS)
2006	Western Engineering Graduate Entrance Scholarship
2002 – 2006	Engineering Dean's Honour List

***Awards and Scholarships (co-author)***

2012	Canadian Society for Biomechanics Doctoral Student Award (Finalist), Ontario Biomechanics Conference, Barrie, ON.
2011	1 <sup>st</sup> Place Basic Science Research Award, Cervical Spine Research Society Annual Meeting, Phoenix, AZ, USA
2011	Top 20 Poster, Cervical Spine Research Society Annual Meeting, Phoenix, AZ, USA
2010	Best Basic Science Paper Award, 38 <sup>th</sup> Clinical Seminar in Orthopaedic Surgery, University of Western Ontario
2008	Best Paper, Canadian Orthopaedic Residents Association, Quebec City, PQ

**TEACHING EXPERIENCE:**

***Undergraduate Teaching***

2011	Guest Lecturer – “Finite Element Modeling using Solid Works” MME 3360b: Finite Element Methods for Mechanical Engineering Department of Mechanical & Materials Engineering University of Western Ontario
------	---

***Graduate Teaching***

2010 – 2011	Guest Lecturer – “Kinematic Methods – Screw Displacement Axis” MME 9615: Biomechanics of Human Joint Motion Department of Mechanical & Materials Engineering University of Western Ontario
-------------	---

***Teaching Assistantships***

2007 – 2012	Teaching Assistant: Finite Element Methods for Mechanical Engineering Department of Mechanical & Materials Engineering <i>Supervisors: Dr. Cynthia Dunning (07), Dr. Paul Kurowski (08-11)</i>
2009 – 2011	Teaching Assistant: Biomechanics of Human Joint Motion Department of Mechanical & Materials Engineering <i>Supervisors: Dr. Cynthia Dunning &amp; Dr. Thomas Jenkyn</i>
2006 – 2007	Teaching Assistant: Mechanical Properties of Materials Department of Mechanical & Materials Engineering <i>Supervisor: Dr. John Dryden</i>

### ***Student Supervision***

#### ***Summer Research Students (co-supervised)***

- 2011 Jacob Reeves: Third Year Undergraduate, Mechanical & Materials Engineering, University of Western Ontario  
Project: Re-design of an Impact Loading System (NSERC USRA)
- 2010 Meghan Clynick: First Year Undergraduate, Engineering, University of Western Ontario  
Project: The Role of Implant Stem Curvature on Loosening (NSERC USRA)

#### ***Undergraduate Projects (co-supervised)***

- 2010 – 2011 Joshua Bernick, Alexander Heroux, Tyler Moores, Paola Soriano  
Project: Evaluation and Refinement of a Simulator Design for Laboratory Investigation of the Spine  
Program: MME 4499, Mechanical Engineering Project, University of Western Ontario

#### ***Orthopaedic Resident's Research Blocks (laboratory supervisor)***

- 2012 Reina Yao  
Project: Influence of graft size on spinal stability for unilateral facet dislocation with and without facet fracture treated with anterior plate stabilization  
Program: PGY-3, Orthopaedic Surgery, University of Western Ontario
- 2011 C. Maxwell McCabe  
Project: The Role of Soft Tissue Restraints Following Type II Odontoid Fractures in the Elderly  
Program: PGY-3, Orthopaedic Surgery, University of Western Ontario
- 2010 Melissa Nadeau  
Project: Qualitative and Quantitative Assessment of Soft Tissue Damage in the Cervical Spine Following a Unilateral Facet Injury  
Program: PGY-3, Orthopaedic Surgery, University of Western Ontario
- 2009 Parham Rasoulinejad  
Project: The Importance of the Posterior Osteoligamentous Complex to Subaxial Cervical Spine Stability in Relation to a Unilateral Facet Injury  
Program: PGY-3, Orthopaedic Surgery, University of Western Ontario

#### **PUBLICATIONS IN REFEREED JOURNALS:**

1. **McLachlin SD**, Beaton BJB, Sabo MT, Gurr KR, Bailey SI, Bailey CS, Dunning CE. (2008). Comparing the Fixation of a Novel Hollow Screw and a Conventional Solid Screw in the Human Sacra under Cyclic Loading. *Spine* 33(17):1870-1875.
2. Quenneville CE, **McLachlin SD**, Fraser GS, Dunning CE. (2011). Injury Tolerance Criteria for Short-Duration Axial Impulse Loading of the Isolated Tibia, *Journal of Trauma*, 70(1):E13-E18.
3. **McLachlin SD**, Al Saleh K, Gurr KR, Bailey SI, Bailey CS, Dunning CE. (2011). Comparative Assessment of Sacral Screw Loosening Augmented with PMMA versus a Calcium Triglyceride Bone Cement, *Spine* 36(11): E699-704.
4. McCabe CMJ, **McLachlin SD**, Bailey SI, Gurr KR, Bailey CS, Dunning CE. (2012). The Role of Soft Tissue Restraints Following Type II Odontoid Fractures in the Elderly – A Biomechanical Study, *Spine* 37(12): 1030-1035.
5. Hosein YK, Clynick MP, **McLachlin SD**, King GJW, Dunning CE. (in press). The Effect of Intramedullary Stem Curvature on the Torsional Stability of Cemented Joint Replacement Systems. *Journal of Applied Biomechanics and Biomaterials*, accepted March 20, 2012.
6. Nadeau M, **McLachlin SD**, Bailey SI, Gurr KR, Dunning CE, Bailey CS. (in press). A Biomechanical Assessment of Soft Tissue Damage in the Cervical Spine Following a Unilateral Facet Injury. *Journal of Bone and Joint Surgery (Am.)*, accepted May 7, 2012.
7. Rasoulinejad P, **McLachlin SD**, Bailey SI, Gurr KR, Bailey CS, Dunning CE. (in press) The Importance of the Posterior Osteoligamentous Complex to Subaxial Cervical Spine Stability in Relation to a Unilateral Facet Injury. *The Spine Journal*, accepted July 9, 2012.

#### **SUBMITTED MANUSCRIPTS FOR PUBLICATION UNDER REVIEW:**

1. **McLachlin SD**, Rasoulinejad P, Bailey SI, Gurr KR, Bailey CS, Dunning CE. Anterior versus Posterior Fixation for an Isolated Posterior Facet Complex Injury in the Sub-axial Cervical Spine, *Journal of Neurosurgery Spine*. In Revision 2013.
2. **McLachlin SD**, Nadeau M, Bailey SI, Gurr KR, Bailey CS, Dunning CE. Validation of an Injury Model for a Unilateral Facet Perch in the Cervical Spine. *The Spine Journal*. Under Review 2012.
3. **McLachlin SD**, Ferreira LF, Dunning CE. A refined technique to calculate helical axes from six-DOF tracker output. *Journal of Biomechanics*. Under Review 2013.

#### **MANUSCRIPTS IN PREPARATION FOR SUBMISSION:**

1. Yao R, **McLachlin SD**, Rasoulinejad P, Gurr KR, Dunning CE, Bailey CS. Influence of graft size on anterior cervical plate fixation following in vitro flexion-distraction injuries. 2013.

**PUBLISHED REFEREED ABSTRACTS:**

1. **McLachlin SD**, Beaton BJB, Sabo MT, Gurr KR, Bailey SI, Bailey CS, Dunning CE. Comparing the Fixation of a Novel Hollow Screw and a Conventional Solid Screw in the Human Sacra under Cyclic Loading. 54<sup>th</sup> Annual Meeting of the Orthopaedic Research Society, San Francisco, California, March 2008. Poster Presentation.
2. **McLachlin SD**, Beaton BJB, Sabo MT, Gurr KR, Bailey SI, Bailey CS, Dunning CE. Comparing the Fixation of a Novel Hollow Screw and a Conventional Solid Screw in the Human Sacra under Cyclic Loading. 8<sup>th</sup> Annual Scientific Conference of the Canadian Spine Society, Sun Peaks Resort, BC, March 12, 2008. Poster Presentation.
3. **McLachlin SD**, Beaton BJB, Sabo MT, Gurr KR, Bailey SI, Bailey CS, Dunning CE. Comparing the Fixation of a Novel Hollow Screw and a Conventional Solid Screw in the Human Sacra under Cyclic Loading. 42<sup>nd</sup> Annual Canadian Orthopaedic Research Society Meeting, Quebec City, Quebec, June 4-7, 2008. Poster Presentation.
4. Sabo MT, **McLachlin SD**, Beaton BJB, Gurr KR, Bailey SI, Holdsworth DW, Dunning CE, Bailey CS. Comparing the Fixation of a Novel Hollow Screw and a Conventional Solid Screw in the Human Sacra under Cyclic Loading, 34<sup>th</sup> Annual Canadian Orthopaedic Residents Association Meeting, Quebec City, Quebec, June 4-7, 2008. Podium Presentation.
5. **McLachlin SD**, Beaton BJB, Sabo MT, Gurr KR, Bailey SI, Bailey CS, Dunning CE. Comparing the Fixation of a Novel Hollow Screw and a Conventional Solid Screw in the Human Sacra under Cyclic Loading. 2008 North American Congress on Biomechanics, Ann Arbor, Michigan, August 5-9, 2008. Podium Presentation.
6. Quenneville CE, **McLachlin SD**, Fraser GS, Dunning CE. Injury Tolerance Criteria for Short-Duration Axial Loading of the Tibia. 2009 American Society of Biomechanics, University Park, Pennsylvania, August 26-29, 2009. Poster Presentation.
7. **McLachlin SD**, Bailey CS, Al Saleh K, Bailey SI, Gurr KR, Dunning CE. Cement Augmentation of Sacral Pedicle Screw Fixation. 56<sup>th</sup> Annual Meeting of the Orthopaedic Research Society, New Orleans, Louisiana, March 6-9, 2010. Poster Presentation.
8. Quenneville CE, **McLachlin SD**, Fraser GS, Dunning CE. Injury Tolerance Criteria for Short-Duration Axial Loading of the Tibia. 56<sup>th</sup> Annual Meeting of the Orthopaedic Research Society, New Orleans, Louisiana, March 6-9, 2010. Poster Presentation.
9. Rasoulinejad P, **McLachlin SD**, Bailey CS, Bailey SI, Gurr KR, Dunning CE. Sub-axial Cervical Spine Instability following Unilateral Facet Injury: A Biomechanical Analysis. 10<sup>th</sup> Annual Scientific Conference of the Canadian Spine Society, Lake Louise, Alberta, March 10-13, 2010. Podium Presentation.

10. Rasoulinejad P, **McLachlin SD**, Bailey CS, Bailey SI, Gurr KR, Dunning CE. Sub-axial Cervical Spine Instability following Unilateral Facet Injury: A Biomechanical Analysis. 44<sup>th</sup> Annual Canadian Orthopaedic Research Society Meeting, Edmonton, Alberta, June 17-20, 2010. Poster Presentation.
11. **McLachlin SD**, Al Saleh K, Gurr KR, Bailey SI, Bailey CS, Dunning CE. Comparative Assessment of Sacral Screw Loosening Augmented with PMMA versus a Calcium Triglyceride Bone Cement. ASME 2010 Summer Bioengineering Conference, Naples, Florida, June 16-19, 2010. Poster Presentation.
12. **McLachlin SD**, Rasoulinejad P, Gurr KR, Bailey SI, Bailey CS, Dunning CE. Sub-axial Cervical Spine Instability following Unilateral Facet Injury: A Biomechanical Analysis. ASME 2010 Summer Bioengineering Conference, Naples, Florida, June 16-19, 2010. Podium Presentation.
13. Hosein YK, **McLachlin SD**, King GJW, Dunning CE. Development of Methodology to Assess Stem Surface Finish in Cemented Implant Loosening. ASME 2010 Summer Bioengineering Conference, Naples, Florida, June 16-19, 2010. Poster Presentation.
14. Quenneville CE, **McLachlin SD**, Fraser GS, Dunning CE. Injury Tolerance Criteria for Short-Duration Axial Loading of the Tibia. ASME 2010 Summer Bioengineering Conference, Naples, Florida, June 16-19, 2010. Podium Presentation.
15. Hosein YK, Clynick MP, Takaki SE, **McLachlin SD**, Dunning CE. The Effect of Intramedullary Stem Curvature on the Torsional Stability of Cemented Joint Replacement Systems. 57<sup>th</sup> Annual Meeting of the Orthopedic Research Society, Long Beach, California, January 13-16, 2011. Poster Presentation.
16. Rasoulinejad P, **McLachlin SD**, Bailey SI, Gurr KR, Bailey CS, Dunning CE. The Importance of the Posterior Osteoligamentous Complex to Sub-axial Cervical Spine Stability in Relation to a Unilateral Facet Injury. 57<sup>th</sup> Annual Meeting of the Orthopedic Research Society, Long Beach, California, January 13-16, 2011. Poster Presentation.
17. **McLachlin SD**, Rasoulinejad P, Bailey SI, Gurr KR, Bailey CS, Dunning CE. Anterior versus Posterior Fixation for an Isolated Posterior Facet Complex Injury in the Sub-axial Cervical Spine. 57<sup>th</sup> Annual Meeting of the Orthopedic Research Society, Long Beach, California, January 13-16, 2011. Poster Presentation.
18. Nadeau M, **McLachlin SD**, Bailey SI, Gurr KR, Bailey CS, Dunning CE. Qualitative and Quantitative Assessment of Soft Tissue Damage in the Cervical Spine Following a Unilateral Facet Injury. 57<sup>th</sup> Annual Meeting of the Orthopedic Research Society, Long Beach, California, January 13-16, 2011. Poster Presentation.
19. Nadeau M, **McLachlin SD**, Bailey SI, Gurr KR, Bailey CS, Dunning CE. Qualitative and Quantitative Assessment of Soft Tissue Damage in the Cervical Spine Following a Unilateral Facet Injury. 11<sup>th</sup> Annual Scientific Conference of the Canadian Spine Society, Quebec City, Quebec, March 9-12, 2011. Poster Presentation.



20. **McLachlin SD**, Rasoulinejad P, Bailey SI, Gurr KR, Bailey CS, Dunning CE. Anterior versus Posterior Fixation for an Isolated Posterior Facet Complex Injury in the Sub-axial Cervical Spine. 11<sup>th</sup> Annual Scientific Conference of the Canadian Spine Society, Quebec City, Quebec, March 9-12, 2011. Poster Presentation.
21. **McLachlin SD**, Rasoulinejad P, Bailey SI, Gurr KR, Bailey CS, Dunning CE. Anterior versus Posterior Fixation for an Isolated Posterior Facet Complex Injury in the Sub-axial Cervical Spine. ASME 2011 Summer Bioengineering Conference, Farmington, Pennsylvania, June 22-25, 2011. Poster Presentation.
22. Hosein YK, Clynick MP, Takaki SE, **McLachlin SD**, Dunning CE. The Effect of Intramedullary Stem Curvature on the Torsional Stability of Cemented Joint Replacement Systems. ASME 2011 Summer Bioengineering Conference, Farmington, Pennsylvania, June 22-25, 2011. Poster Presentation.
23. **McLachlin SD**, Rasoulinejad P, Bailey SI, Gurr KR, Bailey CS, Dunning CE. Anterior versus Posterior Fixation for an Isolated Posterior Facet Complex Injury in the Sub-axial Cervical Spine. 45<sup>th</sup> Annual Canadian Orthopaedic Research Society Meeting, St. John's, Newfoundland, July 7-9, 2011. Poster Presentation.
24. Nadeau M, **McLachlin SD**, Bailey SI, Gurr KR, Bailey CS, Dunning CE. Qualitative and Quantitative Assessment of Soft Tissue Damage in the Cervical Spine Following a Unilateral Facet Injury. 45<sup>th</sup> Annual Canadian Orthopaedic Research Society Meeting, St. John's, Newfoundland, July 7-9, 2011. Poster Presentation.
25. Nadeau M, **McLachlin SD**, Bailey SI, Gurr KR, Bailey CS, Dunning CE. Qualitative and Quantitative Assessment of Soft Tissue Damage in the Cervical Spine Following a Unilateral Facet Injury. 26<sup>th</sup> Annual North American Spine Society Meeting, Chicago, Illinois, November 2-5, 2011. Podium Presentation.
26. **McLachlin SD**, Rasoulinejad P, Bailey SI, Gurr KR, Dunning CE, Bailey CS. Anterior versus Posterior Fixation for an Isolated Posterior Facet Complex Injury in the Sub-axial Cervical Spine. 39<sup>th</sup> Annual Cervical Spine Research Society Meeting, Scottsdale, Arizona, December 7-10, 2011. Podium Presentation.
27. Rasoulinejad P, **McLachlin SD**, Bailey SI, Gurr KR, Dunning CE, Bailey CS. The Importance of the Posterior Osteoligamentous Complex to Sub-axial Cervical Spine Stability in Relation to a Unilateral Facet Injury. 39<sup>th</sup> Annual Cervical Spine Research Society Meeting, Scottsdale, Arizona, December 7-10, 2011. Poster Presentation.
28. McCabe CMJ, **McLachlin SD**, Bailey SI, Gurr KR, Dunning CE, Bailey CS. The Role of Soft Tissue Restraints Following Type II Odontoid Fractures in the Elderly – A Biomechanical Study. 39<sup>th</sup> Annual Cervical Spine Research Society Meeting, Scottsdale, Arizona, December 7-10, 2011. Podium Presentation.
29. McCabe CMJ, **McLachlin SD**, Bailey SI, Gurr KR, Bailey CS, Dunning CE. The Role of Soft Tissue Restraints Following Type II Odontoid Fractures in the Elderly – A Biomechanical Study, 58th Annual Meeting of the Orthopaedic Research Society, San Francisco, California, February 4-7, 2012. Poster Presentation.

30. Nadeau M, **McLachlin SD**, Bailey SI, Gurr KR, Dunning CE, Bailey CS. Evaluation of Instrumentation Techniques for a Unilateral Facet Fracture Dislocation Using a Validated Soft Tissue Injury Model, 12<sup>th</sup> Annual Scientific Conference of the Canadian Spine Society, Sun Peaks, BC, February 29 - March 3, 2012. Poster Presentation.
31. **McLachlin SD**, Nadeau M, Bailey SI, Gurr KR, Dunning CE, Bailey CS. Evaluation of Instrumentation Techniques for a Unilateral Facet Fracture Dislocation Using a Validated Soft Tissue Injury Model, 9<sup>th</sup> Annual Ontario Biomechanics Conference, Barrie, ON, March 16-18, 2012. Podium Presentation.
32. McCabe CMJ, **McLachlin SD**, Bailey SI, Gurr KR, Bailey CS, Dunning CE. The Role of Soft Tissue Restraints Following Type II Odontoid Fractures in the Elderly – A Biomechanical Study, 46<sup>th</sup> Annual Meeting of the Canadian Orthopaedic Research Society, Ottawa, ON, June 8-10, 2012. Podium Presentation.
33. **McLachlin SD**, Nadeau M, Bailey SI, Gurr KR, Dunning CE, Bailey CS. Evaluation of Instrumentation Techniques for a Unilateral Facet Fracture Using a Validated Soft Tissue Injury Model, 46<sup>th</sup> Annual Meeting of the Canadian Orthopaedic Research Society, Ottawa, ON, June 8-10, 2012. Podium Presentation.
34. **McLachlin SD**, Nadeau M, Bailey SI, Gurr KR, Dunning CE, Bailey CS. Development of a Soft Tissue Injury Model for a Unilateral Facet Perch in the Cervical Spine, 46<sup>th</sup> Annual Meeting of the Canadian Orthopaedic Research Society, Ottawa, ON, June 8-10, 2012. Poster Presentation.

#### **OTHER ABSTRACTS AND PRESENTATIONS**

1. Sabo MT, **McLachlin SD**, Beaton BJB, Gurr KR, Bailey SI, Holdsworth DW, Dunning CE, Bailey CS. Comparing the Fixation of a Novel Hollow Screw and a Conventional Solid Screw in the Human Sacra under Cyclic Loading, 35<sup>th</sup> Clinical Seminar in Orthopaedic Surgery, University of Western Ontario, London, Ontario, September 2007. Podium Presentation.
2. Rasoulinejad P, **McLachlin SD**, Bailey SI, Gurr KR, Bailey CS, Dunning CE. Sub-axial Cervical Spine Instability following Unilateral Facet Injury: A Biomechanical Analysis. 37<sup>th</sup> Clinical Seminar in Orthopaedic Surgery, University of Western Ontario, London, Ontario, September 2009. Podium Presentation.
3. Rasoulinejad P, **McLachlin SD**, Bailey SI, Gurr KR, Dunning CE, Bailey CS. Anterior versus Posterior Fixation for an Isolated Posterior Facet Complex Injury in the Sub-axial Cervical Spine. 38<sup>th</sup> Clinical Seminar in Orthopaedic Surgery, University of Western Ontario, London, Ontario, September 2010. Podium Presentation.
4. Nadeau M, **McLachlin SD**, Bailey SI, Gurr KR, Dunning CE, Bailey CS. Qualitative and Quantitative Assessment of Soft Tissue Damage in the Cervical Spine Following

- a Unilateral Facet Injury. 38<sup>th</sup> Clinical Seminar in Orthopaedic Surgery, University of Western Ontario, London, Ontario, September 2010. Podium Presentation.
5. **McLachlin SD**. Cervical Spine Unilateral Facet Injuries: Simulation, Quantification, and Visualization of Mechanisms and Treatment, Seminar Series in Mechanical & Materials Engineering, University of Western Ontario, January 2011. Podium Presentation.
  6. **McLachlin SD**, Rasoulinejad P, Bailey SI, Gurr KR, Dunning CE, Bailey CS. Anterior versus Posterior Fixation for an Isolated Posterior Facet Complex Injury in the Sub-axial Cervical Spine. CIHR Joint Motion Training Program in Musculoskeletal Health Research and Leadership: Annual Retreat, University of Western Ontario. London, Ont. May 2011. Poster Presentation.
  7. Nadeau M, **McLachlin SD**, Bailey SI, Gurr KR, Bailey CS, Dunning CE. Evaluation of Instrumentation Techniques for a Unilateral Facet Fracture Dislocation Using a Validated Soft Tissue Injury Model. 39<sup>th</sup> Clinical Seminar in Orthopaedic Surgery, University of Western Ontario, London, Ontario, September 2011. Podium Presentation.
  8. McCabe CMJ, **McLachlin SD**, Bailey SI, Gurr KR, Dunning CE, Bailey CS. The Role of Soft Tissue Restraints Following Type II Odontoid Fractures in the Elderly – A Biomechanical Study. 39<sup>th</sup> Clinical Seminar in Orthopaedic Surgery, University of Western Ontario, London, Ontario, September 2011. Podium Presentation.
  9. **McLachlin SD**. Cervical Spine Unilateral Facet Injuries: Simulation, Quantification, and Visualization of Mechanisms and Treatment, Seminar Series in Mechanical & Materials Engineering, University of Western Ontario, December 2011. Podium Presentation.

#### **OTHER SCHOLARLY AND PROFESSIONAL ACTIVITIES:**

##### ***Professional Development***

1. Health Sector 1 Course, Master of Business Administration (Health Sector Stream), Richard Ivey School of Business, October – December, 2011.
2. Statistics Workshop, Robarts Research Institute, December 2011.
3. Leaders in the Lab, Joint Motion Program & Richard Ivey School of Business, 2010-2011.
4. Fairness in grading group projects?, Teaching Support Centre, University of Western Ontario, November 2010.
5. Research Lab Managers Boot Camp, The University of Guelph, October 2008.

##### ***Professional Meetings Attended***

1. 41<sup>st</sup> Annual Meeting of the Canadian Orthopaedic Research Society, Halifax, Nova Scotia, June 2007.

2. 54<sup>th</sup> Annual Meeting of the Orthopaedic Research Society, San Francisco, California, March 2008.
3. 42<sup>nd</sup> Annual Canadian Orthopaedic Research Society Meeting, Quebec City, Quebec, June 2008.
4. American Society of Mechanical Engineers – Summer Bioengineering Conference, Marco Island, Florida, June 2008.
5. North American Congress on Biomechanics, Ann Arbor, Michigan, August 2008.
6. 55<sup>th</sup> Annual Meeting of the Orthopedic Research Society, Las Vegas, Nevada, February 2009.
7. 56<sup>th</sup> Annual Meeting of the Orthopedic Research Society, New Orleans, Louisiana, March 2010.
8. American Society of Mechanical Engineers – Summer Bioengineering Conference, Naples, Florida, June 2010.
9. Ivey Global Health Conference, Toronto, Ontario, November 2010.
10. 57<sup>th</sup> Annual Meeting of the Orthopedic Research Society, Long Beach, California, January 2011.
11. Medical Technology Innovation Symposium, London, Ontario, June 2011.
12. American Society of Mechanical Engineers – Summer Bioengineering Conference, Farmington, Pennsylvania, June 2011.
13. 45<sup>th</sup> Annual Meeting of the Canadian Orthopaedic Research Society, St. John's, Newfoundland, July 2011.
14. 26<sup>th</sup> Annual Meeting of the North American Spine Society, Chicago, Illinois, November 2011.
15. 39<sup>th</sup> Annual Meeting of the Cervical Spine Research Society, Scottsdale, Arizona, December 2011.
16. 9<sup>th</sup> Annual Ontario Biomechanics Conference, Barrie, ON, March 16-18, 2012.
17. 46<sup>th</sup> Annual Meeting of the Canadian Orthopaedic Research Society, Ottawa, ON, June 8-10, 2012.

#### ***University Service & Committee Work***

2011 – Present	Program Operations Committee Student Representative, Joint Motion Program
2010 – 2011	Seminar Series Coordinator, Joint Motion Program
2009 – 2011	Graduate Representative, Mechanical & Materials Department Council

#### ***Professional Society Memberships***

2010 – Present	Engineering-Intern-Training (EIT), Professional Engineers Ontario
2009 – Present	Canadian Society of Biomechanics